Determining the Native and Nonnative Effects of Myristoylation on the Folding and Switching of Hisactophilin

by

Martin Thomas James Smith

A thesis

presented to the University of Waterloo

in fulfilment of the

thesis requirement for the degree of

Doctor of Philosophy

in

Chemistry

Waterloo, Ontario, Canada, 2012

Author's Declaration

I hereby declare that I am the sole author of this thesis. This is a true copy of the thesis, including any required final revisions, as accepted by my examiners.

I understand that my thesis may be made electronically available to the public.

Abstract

Myristoylation, the covalent linkage of a C14 saturated fatty acyl chain to the N-terminal glycine in a protein, plays an important role in reversible membrane and protein binding in cellular signaling by the modified proteins. Little is known about the effects of myristoylation on the energetics and molecular mechanisms of folding and switching between functional states of the myristoyl group. Here, hisactophilin, a small naturally myristoylated histidine-rich β-trefoil protein which binds cell membranes and actin in a pH-dependent manner, is used as a model system to study the effects of myristoylation on the folding and switching behaviour in proteins. The combination of equilibrium denaturation, kinetic folding, kinetic unfolding, NMR chemical shift analysis, NMR lineshape analysis, and NH/D exchange provide insight into energetic and dynamic mechanisms that govern the folding and switching function of hisactophilin. Equilibrium denaturation measurements show that myristoylation significantly increases hisactophilin stability. From a comparison to other proteins, it is concluded that an increase in protein stability upon modification and burial of the attached group is likely to occur in numerous proteins modified with fatty acyl or other hydrophobic groups, and that the biophysical effects of such modification are likely to play an important role in their functional switches. Interestingly, the global protein folding and unfolding rates for hisactophilin are both markedly increased upon myristoylation. In addition, the increased global dynamics caused by myristoylation of hisactophilin reveals a general mechanism whereby hydrophobic moieties can make nonnative interactions or relieve strain in transition states, thereby increasing the rates of interconversion between different conformational states. To test this general mechanism

various mutations were introduced into hisactophilin to alter the nonnative interactions surrounding the myristoyl binding pocket. The folding rates of these mutants suggest that the myristoyl group makes robust interactions that vary in the transition state. Myristoylation is also fundamental to the pH-dependent conformational switch function of hisactophilin, which involves the uptake of ~1.5 protons, likely by a few key histidines, the myristoyl group switches from a sequestered state in the protein core to an accessible state where the myristoyl may bind to the inside of the membrane. Using thermodynamic cycle analysis of stability data *vs.* pH an apparent conformational switch pK_a, the pK_{switch}, of 6.95 and an apparent coupling energy, ΔG_{switch}, of 2.0 kcal·mol^{-1} is obtained. The equations used to analyze H^+-binding induced switching in hisactophilin are then recast to analyze the thermodynamic interactions in any ligand-binding induced switching system. This approach is applied to other ligand-binding induced switching systems and several hisactophilin mutants, in which switching is broken. The results show that the magnitude of ΔG_{switch} provides a good measure for the extent of conformational change in a switching system. For a series of hisactophilin mutants, including mutants in which the switching is broken, the folding rates vary between mutants. However, all mutant forms of hisactophilin show a consistent increase in the folding rate acquired upon myristoylation. The fact that switching can be broken in some mutants but the effect of myristoylation on the folding rate is consistent suggests that while the folding transition state myristoyl interactions are robust, the interactions that govern equilibrium myristoyl switching are quite sensitive to change. NMR measurements also indicate that myristoyl switching exhibits fast dynamics. NH/D exchange experiments reveal that while many amides show increased stability upon myristoylation there are local areas of structure that are destabilized upon myristoylation

which may facilitate the fast pH switch. Thus, the energetic and dynamic effects of myristoylation characterized *in vitro* using biophysical methods provide insight into the molecular mechanism that underlies myristoyl switching that occurs *in vivo*.

Acknowledgements

I am fortunate to have many great people in my life that support my personal and scientific endeavours. Above all else, I would like to acknowledge my family. I could not have succeeded in my studies without the support of my parents, Susan and Andrew, and partner Jen. I would like to thank Dr. Elizabeth Meiering for her guidance, in science and in life, through the years of my PhD. To my advisory committee, thank you for your lively discussions of my research. I would like to acknowledge Dr. Yaakov Levy, Dr. Dalit Shental-Bechor, Dr. John Dawson and Paul McRorie for their interesting and challenging collaborations. To my lab mates, I thank you for your friendship and support throughout the years of my graduate work. You have provided a stimulating and fun environment for study. In particular, I would like to acknowledge Duncan MacKenzie, Fernando Bralha, Chris Go, Sam Reaume and Hannah Jantzi who were the undergraduate students that have helped with my research.

Dedication

I dedicate this thesis to my parents, Andrew and Susan Smith, and my amazing partner Jennifer Kurz.

Table of Contents

List of Figures

List of Tables

List of Abbreviations

1D	one-dimensional
3D	three-dimensional
Φ	folding phi-value
δ	chemical shift
‡	transition state
A	area
Å	angstrom
ADA2h	procarboxypeptidase A2
ADP	adenosine-5'-diphosphate
ARF	ADP ribosylation factor
ATP	adenosine-5'-triphosphate
a.u.	arbitrary units
BEM	binomial extrapolation method
β_T	Tanford β-value
cAMP	cyclic 5-adenosine monophosphate
CD	circular dicroism
CHAPS	[3-(3-Chloramidopropyl)] dimethylammonio-1-propanesulfonate
ChTnC	calcium binding troponin C
C_{mid}	folding midpoint
CoA	coenzyme A

CPMG	Carr Purcell Meibroom Gill
D	deuterium, ^2H
Da	dalton
D. discoideum	*Dictyostelium discoideum*
DES	diethylsilbesterol
DEAE	diethylaminoethyl
DNA	deoxyribonucleic acid
E. coli	*Escherichia coli*
EDTA	ethylene diamine tetra acetic acid
F	folded
ΔG	change in Gibbs free energy, stability
$\Delta\Delta G$	difference energy, change in stability
ΔG_{switch}	switch coupling energy
GCAP	guanylate cyclase activating protein
GDP	guanosine-5'-diphosphate
GFP	green fluorescent protein
GTP	guanosine-5'-triphosphate
ΔH	change in enthalpy
$\Delta\Delta H$	differences in enthalpy
HIV	human immuno deficiency
HSQC	heteronuclear single quantum correlation
k_B	Boltzmann constant
k_f	folding rate

k_{in}	rate constant for sequestering the myristoyl group
k_{int}	intrinsic solvent exchange rate constant
k_{out}	rate constant for the myristoyl group becoming accessible
k_{obs}	observed rate constant
k_u	unfolding rate
kcal	kilocalorie
kDa	kilodalton
LLL	F6L/I85L/I93L
m	urea dependence of Gibbs free energy
MARCKS	myristoylated alanine rich protein kinase C
MD	molecular dynamics
MES	2-morpholino-ethanesulfonic acid
myr_{seq}	myristoyl sequestered state
myr_{acc}	myristoyl accessible state
myr	myristoylated
NCS	neuronal calcium sensor
NH/D	amide deuterium exchange
NMR	nuclear magnetic resonance
NOE	nuclear overhauser effect
NOESY	nuclear overhauser effect spectroscopy
nonmyr	nonmyristoylated
P	protection factor
ΔP	change in protection factor

ΔΔP	difference in protection factor
PDB	protein data bank
pI	isoelectric point
PKCα	protein kinase C α
Q_{acc}	net protein charge the accessible state
$Q_{Folding}$	simulated folding interactions within the protein
$Q_{Prot\text{-}Myristoyl}$	simulated folding interactions for the myristoyl group
Q_{seq}	net protein charge the sequestered state
r	radius
R	universal gas constant
R_g	radius of gyration
RNA	ribonucleic acid
RP-HPLC	reverse phase high performance liquid chromatography
ΔS	change in entropy
ΔΔ	differences in entropy
SEM	single extrapolation method
T	temperature
T_F	folding temperature
TOCSY	total correlation spectroscopy
Tris	2-Amino-2-hydroxymethyl-propane-1,3-diol
TS	transition state
U	unfolded
WT	wildtype

NOTE: Standard amino acid and nucleotide residue abbreviations have been used

Chapter 1 – Introduction

Proteins are the major workhorses of the biological cell and carry out a wide range of functions that allow life to exist. The diverse physical and chemical functions carried out by proteins are largely bestowed by their secondary and tertiary structure elements. From the diverse structures and functions of proteins it is easy to imagine that the process that allows these proteins to fold - that is, to adopt their secondary and tertiary structure - might require some complex pathway and complicated cellular machinery. Amazingly, many proteins spontaneously adopt a structure encoded only by their primary sequence. Furthermore, the fold and function of a protein can be altered by post-translational modifications. One common modification found on proteins is the N-terminal lipid anchor. However, there is a scarcity of information pertaining to the effects of myristoylation on the energetics and molecular mechanisms of folding and switching between functional states of the myristoyl group. Therefore, the purpose of this thesis is to investigate effects of N-terminal myristoylation on protein folding and function using hisactophilin, a small naturally myristoylated histidine-rich β-trefoil protein which binds cell membranes and actin in a pH-dependent manner, as a model system to study the effects of myristoylation on the folding and myristoyl switching behaviour in proteins. The combination of biophysical techniques used to characterize myristoylated hisactophilin will provide insight into native and nonnative energetic and dynamic processes that govern the folding and switching function of hisactophilin.

The thesis structure is composed of an introductory chapter that reviews some of the important aspects of the understanding of myristoylated proteins. The introduction is

followed by several chapters that highlight my research and how it fills the need for a better quantitative understanding of the thermodynamic and kinetic effects of myristoylation on proteins. Chapters 2 through 4 begin with a preamble that explains how the chapter fits into other research being conducted at this time. Chapter 5 represents unpublished work that is currently being prepared for publication. The final chapter reviews the main focus of my thesis and draws together some of the main conclusions that arise from the project. The thesis is concluded with a brief summary of future studies that may be conducted to expand on what has been learned about myristoylation. Let us begin our discussion with a general introduction of protein folding.

Protein stability. In his 1972 Nobel lecture, Christian Anfinsen outlines the "thermodynamic hypothesis" of protein folding. This hypothesis suggests that the folded state of a protein exists because it represents the most thermodynamically stable structure. Generally, the stability is described by:

$$\Delta G = \Delta H - T\Delta S \qquad [1.1]$$

where ΔG, ΔH and ΔS represent the change in Gibbs free energy, enthalpy and entropy upon folding of the system at a given temperature, T, respectively. The ΔG between the folded and unfolded states is used as a measure of the stability of a protein. The driving forces behind this stability involve balance of electrostatic, hydrophobic and hydrogen bonding interactions that differ between the folded and unfolded states. Even though stability

involves the balance of hundreds or even thousands of interactions, the stability of proteins typically range from -5 to -12 kcal·mol^{-1} (Dill, 1990). As equation 1.1 suggests, the folded state stability is achieved through the balance of enthalpic and entropic terms that are established within the system. Favourable enthalpic interactions in the folded state that offset the entropy lost from the unfolded state cause proteins to remain folded. Another important driving force for protein folding is the interactions made with the solvent. In aqueous solution, the unfolded state is enthalpically stabilized by the formation of clathrate cages; however, the water molecules lose entropy in the process of forming such cages. Clathrate formation illustrates that proteins make important protein-protein and protein-solvent interactions in all states that influence folding and function. Therefore, it is important to characterize all states in the folding pathway to understand the mechanisms that govern folding (Daggett*, et al.*, 1996). As such, when determining the effects of myristoylation on the protein folding pathway of hisactophilin all states must be considered. In the next section a discussion of protein folding pathways will show how native- and nonnative-interactions have led to the current model for protein folding.

Protein Folding Pathways. Classically, protein folding is viewed as the transition from the unfolded to folded state through a series of discrete intermediates separated by an energetic barrier. This reaction can be represented along a simplified reaction trajectory (Fig. 1.1). Many small single domain proteins (< 110 amino acids) have been shown to have a simple empirical folding transition that occurs between the folded and unfolded states through a single, high energy transition state (Fersht*, et al.*, 1992). This mechanism, which

contains no stable intermediates along the folding pathway, is described as a two-state folding system.

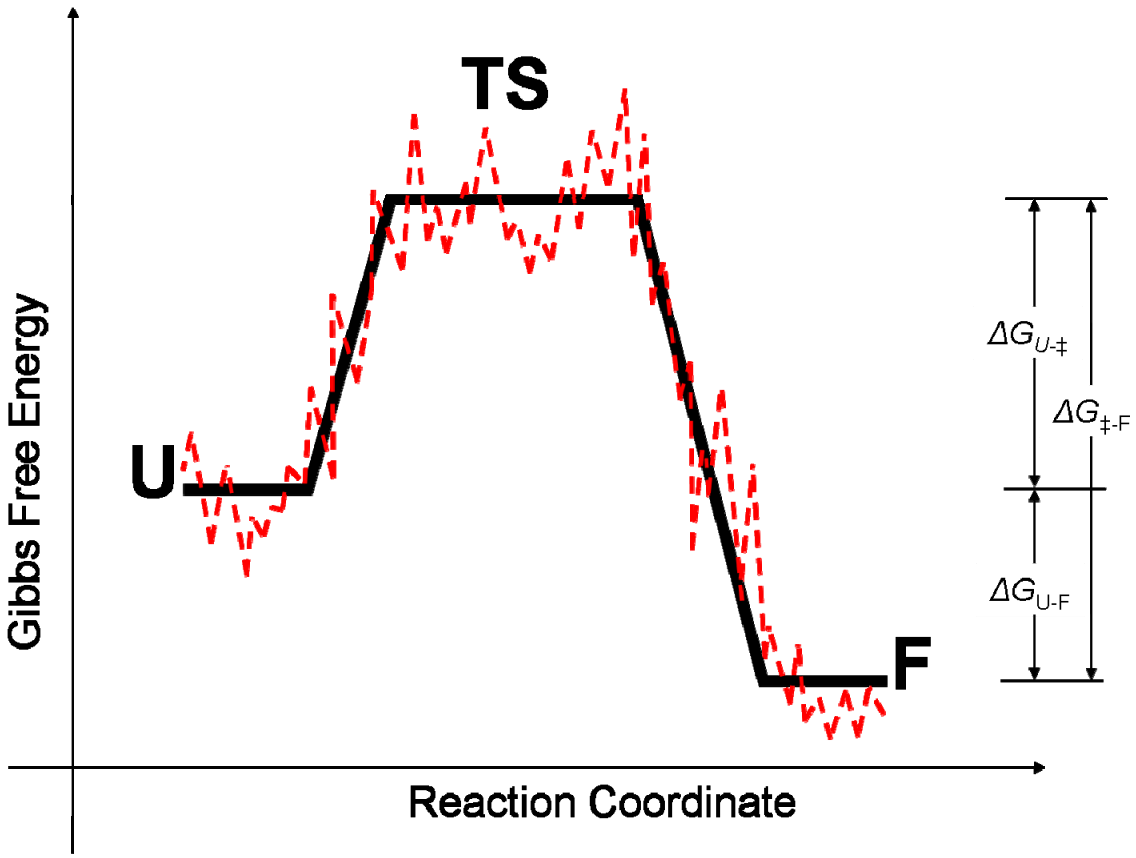

Fig. 1.1. The classic folding model of a two-state protein. In this model of protein folding the reaction coordinate is represented along the x-axis and the Gibbs free energy, *G*, is represented along the y-axis. For a two-state folding process, there is a single energy barrier through a transition state (TS) that separates the folded (F) and unfolded (U) states. The free energy of unfolding, $\Delta G_{U\text{-}F}$, represents the stability of the protein. The energy barrier for folding, $\Delta G_{U\text{-}\ddagger}$, and unfolding, $\Delta G_{F\text{-}\ddagger}$, are defined by folding (k_f) and unfolding (k_u) rates, respectively. While a realistic view of the folding reaction (---) is pitted with many local minima (i.e. frustrated, see text) it is often represented by the simplified black reaction trajectory.

In the classical model, the folded state of the protein represents the fully structured form of the protein that is normally the most stable under physiological conditions (Daggett and Fersht, 2002). The unfolded state represents the unstructured protein that was once

thought to consist primarily of a random coil structure. It is now accepted that random coil structures tend to exist only in very harsh denaturants (Bowler, 2012). In general, the unfolded state has been shown to contain brief elements of structure that act as nuclei for the folding process. As the folded and unfolded states are ground states, they can be readily studied by perturbing one of several physiological variables such as temperature, salt, pH, or adding denaturant. Unlike the folded or unfolded states, the transition state represents a high energy state that is not highly populated. The transition state of a protein folding reaction can be thought of as an expanded and distorted ensemble of structures where the specific non-covalent interactions in the folded state are being formed or broken (Daggett*, et al.*, 1996). Under this scheme, interactions between amino acids may occur in the unfolded-, folded- and transition-states that affect the folding pathway. When interactions can be defined in the folded structure (usually by x-ray crystallography or NMR spectroscopy), they are referred to as folded state interactions. Alternatively, interactions that occur in either the unfolded or transition states are referred to as nonnative interactions (Yoo*, et al.*, 2012). In the classic view, native interactions can be thought of as being incrementally formed along the folding pathway, whereas nonnative interactions that occur during folding do not persist into the folded state of the protein and therefore decrease as folding occurs. Recent research has shown that nonnative interactions can compete with native interactions, thereby affecting the folding of the protein. Nonnative interactions are often thought to interfere with and slow folding. However, evidence (including research presented in this thesis) also suggests that nonnative interactions can accelerate folding (Zarrine-Afsar*, et al.*, 2008). Both native and nonnative effects can be monitored using protein folding kinetics and protein stability measurements. Therefore, the classical protein folding view provides one model to explore

the events in protein folding through experiment. However, computer simulations of protein folding events have provided an alternate view of protein folding known as the landscape view.

The landscape view visualizes the protein folding pathway as a funnel-shaped energy surface (Fig. 1.2)(Onuchic and Wolynes, 2004, Fersht, 1999). Often these coordinates represent some measure of protein conformation obtained from simulation (i.e. root-mean-squared-distance between atoms). The vertical z-coordinate represents an energy calculated for that particular conformation based upon a given force field. At any given vertical position the width of the funnel represents the number of conformations (and therefore the entropy) at a given energy. The folded state is represented at the global minimum of this funnel. The landscape model therefore suggests that the folded state is attained by a folding process such that an ensemble of protein molecules transition through a series of conformational adjustments that reduce their entropy and free energy (Baker, 2000). A realistic view supported by the presence of rapid folded like structures in the folding process is a funnel where every point is sloped down towards the final folded state. However, the funnel may be pitted with non-global wells that represent intermediate states along the folding pathway, and populating the landscape with these wells will slow folding as in the classical model (Sutto*, et al.*, 2007, Capaldi*, et al.*, 2002). The ruggedness of a landscape has been formalized by Wolynes and Onuchic as topological frustration (Bryngelson*, et al.*, 1995). Highly pitted protein landscapes that contain many intermediates are said to be frustrated.

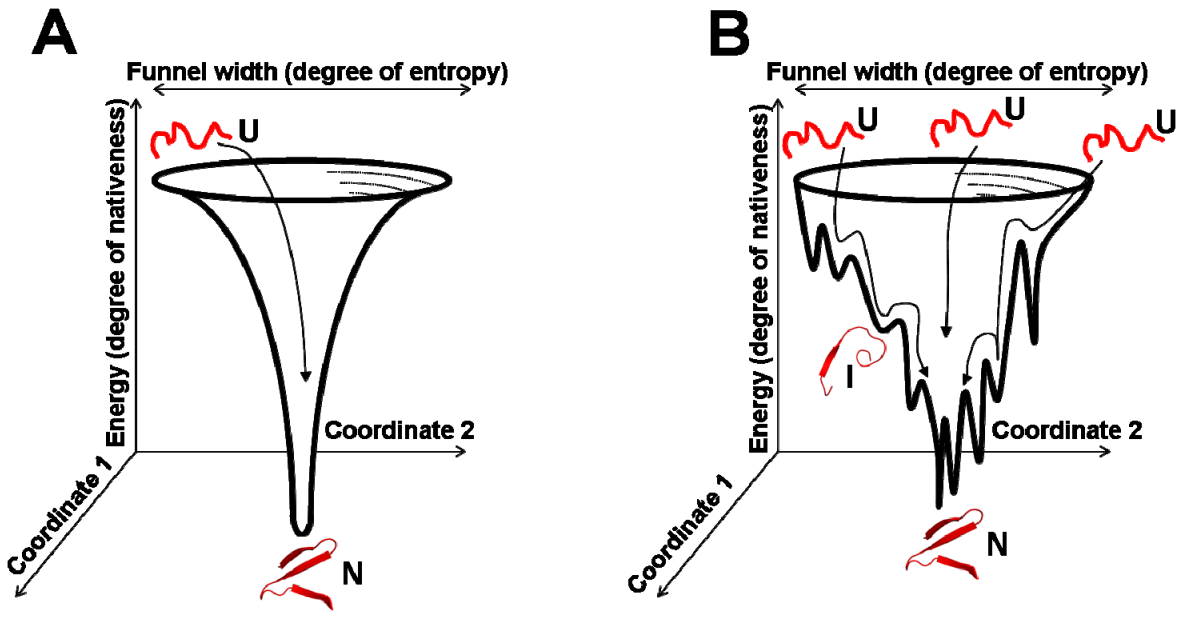

Fig. 1.2. A 3D representation of a protein folding landscape funnel. (A) Depiction of an ideal folding funnel. In the unfolded state, U, a protein exists at the top of the funnel with the most configurational entropy. As the protein folds it traverses the funnel and becomes more native-like, ultimately reaching the most stable native, N, energy well. As folding progresses the width of the funnel narrows and the protein becomes more stable. (B) The folding funnel of a frustrated protein depicting three possible folding routes along the funnel. The folding progresses as in panel A, however, the energy landscape is pitted with smaller energy wells that represent local intermediates, I, that may become populated and slow folding. The overall ruggedness gives an impression of the degree of frustration (see discussion of frustration in the text).

Frustrated sites in proteins arise because some residues can make multiple equally stable interactions with the surrounding protein that compete with and slow the folding process. Research suggests that frustrated sites may be linked to important physiological functions (Ferreiro*, et al.*, 2011, Gosavi*, et al.*, 2008). While the landscape model provides new insight into folding pathways, it is difficult to apply these computer based models to empirical folding methods. Therefore, both the landscape view and the previously mentioned classical view of protein folding provide unique and interesting ways to explore the mechanisms of protein folding. The prevailing folding mechanisms are described next.

Protein Folding Mechanisms. The classic and landscape models of protein folding have led to several general mechanisms that describe protein folding (Gianni*, et al.*, 2003). The framework model describes protein folding as beginning with α-helical and β-sheet elements forming a framework of secondary structure. This is followed by these elements diffusing together to form the higher order structures on the folded state. There are several studies on the chymotrypsin inhibitor 2 (CI2) that support this model of folding (Jackson*, et al.*, 1993, Jackson*, et al.*, 1993). The existence of fleeting secondary structure that remains in the unfolded state supports this mechanism, but usually small segments of protein do not exhibit strong conformational preferences. Furthermore, evidence of two-state folding proteins suggested that discrete, kinetically stable, intermediates of formed secondary structure are not necessary (Fersht, 1999).

The lack of kinetically stable intermediates observed in two-state folding is captured in the hydrophobic collapse model. In the hydrophobic collapse model, protein folding is driven by the hydrophobic effect, which drives the general collapse of the protein because the hydrophobic residues are more stable when they collapse together to avoid interactions with the aqueous medium. This hydrophobic collapse would reduce the degrees of freedom that a protein chain must sample to find the folded state. This collapsed state is often depicted to resemble the molten globule state where elements of secondary structure may be formed in a loosely packed, ill-defined tertiary structure. Recent studies suggest that there are nonspecific hydrophobic interactions that form in the transition state that drive protein folding (Viguera*, et al.*, 2002). However, even if the degrees of freedom are reduced, these

nonspecific interactions would not be enough to explain the rapid folding observed in many proteins.

The nucleation-condensation model combines elements of both the framework and hydrophobic-collapse model to provide a better explanation of observed protein folding behaviour. Here, fleeting nuclei of structure that remain in the unfolded state provide the starting point for protein folding. The structure condenses around these nuclei aided by the hydrophobic collapse. Therefore, a realistic protein folding mechanism most likely exists where elements of secondary and tertiary structure are formed in parallel as the protein collapses to a molten globule and ultimately the folded state.

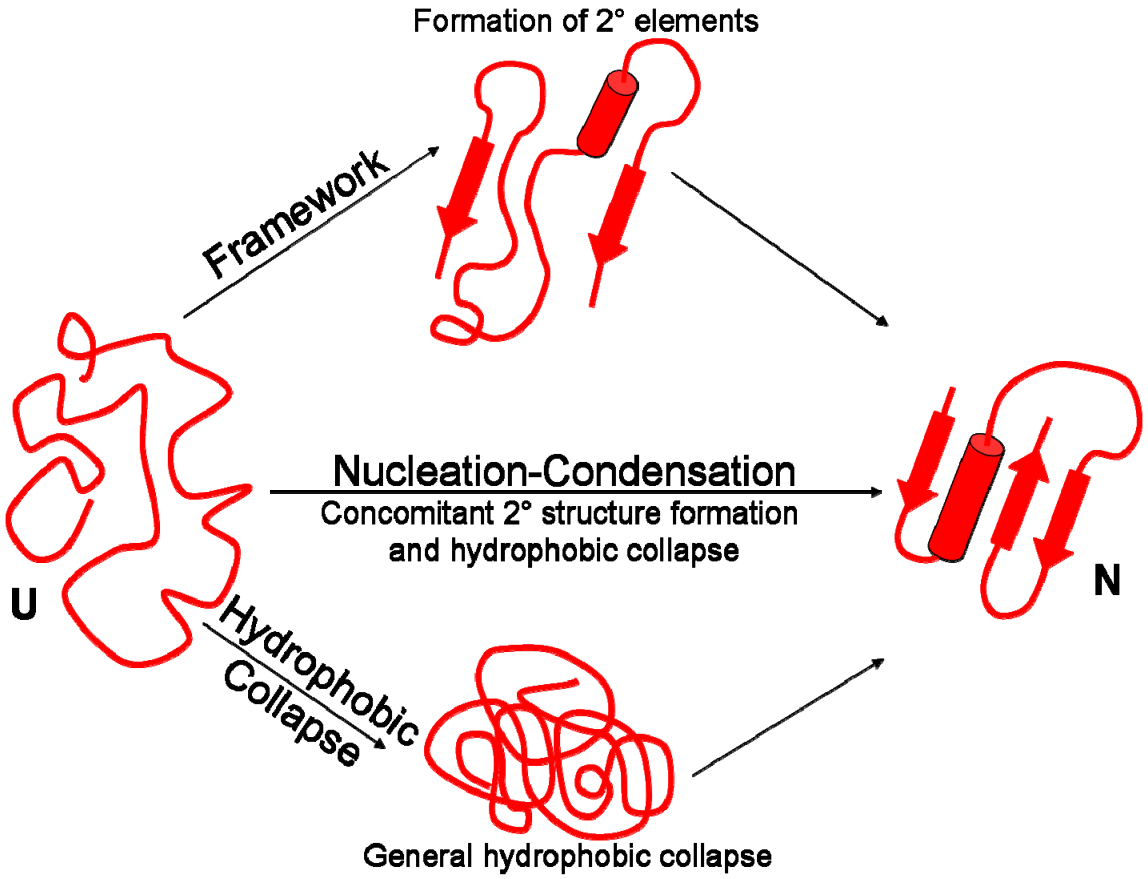

Fig. 1.3. Overview of proposed protein folding mechanisms. The framework model (top) suggests that elements of secondary structure provide the framework to build increasing elements of tertiary structure. Alternatively, the hydrophobic collapse model (bottom) suggests the first step to attaining the folded state is the collapse to the molten globule state, driven by the hydrophobic effect. This is followed by the formation of secondary structure within the collapsed molten globule. The nucleation-condensation model (middle) postulates that secondary structure formation and hydrophobic collapse occur at the same time in a logical parallel progression.

Co- and post-translational modifications can have a profound effect on protein folding and function. The various folding models described above provide the foundation to describe the forces that underlay the effects of protein modification. Myristoylation is one such co-translational modification where little is known about its effects on protein. Therefore, one aim of this thesis is to determine the native and nonnative effects of

myristoylation on the folding and function of the model protein, hisactophilin, and place it in the general context of these protein folding models. As such let us now discuss the process of N-terminal protein myristoylation.

Myristoylation. Myristoylation is a common acyl modification to proteins where a saturated 14 carbon fatty acid, myristic acid, is irreversibly added to the N-terminus of the protein. While myristate comprises less than 1% of the cellular fatty acid content, myristoylation is one of the most common acyl modifications to proteins; 0.5-1% of all proteins in eukaryotic cells are myristoylated (Resh, 1999). The high percentage of incorporation of myristic acid over other cellular fatty acids is due to the activity of N-myristoyl transferase (NMT)(Gordon*, et al.*, 1991). Numerous NMTs have been isolated from different organisms, including several fungal and mammalian sources. NMT is a 50-60 kilodalton (kDa) enzyme that catalyzes the transfer of a myristoyl group from myristoyl-CoA to the N-terminal glycine of a protein substrate (Raju*, et al.*, 1995). However, not all proteins with an N-terminal glycine are myristoylated, indicating that there are several requirements for this acylation to occur. One requirement is the N-terminal consensus sequence: Met-Gly-X-X-X-Ser/Thr-Lys/Arg (Gordon*, et al.*, 1991). Initially, the N-terminal methionine is cleaved from the protein substrate via the enzyme methionine amino-peptidase (MAP) (Resh, 1999), exposing the Gly-2 as the N-terminal amino acid. N-terminal myristoylation occurs co-translationally while the protein is being translated on the ribosome (Gordon*, et al.*, 1991). The myristoylation of proteins has been shown to have several effects on both the structure and functionality of the protein substrate, described below.

Subcellular Function and Localization of Myristoylated Proteins. N-terminal myristoyl groups have been shown to play a role in protein-membrane interactions as well as protein-protein interactions (Taniguchi and Manenti, 1993). Because the C_{14} chain of the myristoyl tail is less hydrophobic relative to palmitate, it has been suggested that myristoylation is involved in reversible membrane binding (Resh, 1999). Although the myristoyl group increases the overall hydrophobicity of a protein, it typically contributes only ~8 kcal·mol^{-1} of energy towards membrane binding (McLaughlin and Aderem, 1995). Energy totalling 8 kcal·mol^{-1} is small relative to other forces of protein-membrane interaction and consequently, myristoylation has been proposed to act in concert with additional mechanisms in membrane binding (Blenis and Resh, 1993). For example, an electrostatic interaction between positively charged basic residues on the protein with the negatively charged acidic phospholipids of the inner membrane leaflet play a large role in providing a favourable interaction between membrane and protein (Taniguchi and Manenti, 1993, Blenis and Resh, 1993). This is supported by the observations that membrane association of myristoylated proteins increases with: 1) increasing concentrations of acidic phospholipids; 2) increasing basic residues in the protein; and 3) a reduction in the ionic strength of the solution (McLaughlin and Aderem, 1995).

Another important mechanism of electrostatic control is phosphorylation. Phosphorylation of specific serine residues on the myristoylated protein has been shown to cause the dissociation of the protein from the membrane (McLaughlin and Aderem, 1995). The negative charge imparted by the phosphate group weakens the electrostatic interaction with the membrane. An example of this mechanism is the membrane binding of MARCKS. This myristoylated protein is a natively unfolded protein that is a substrate for PKCα.

Research has shown that in order for MARCKS to be membrane bound it must be myristoylated at the N-terminus and in the unphosphorylated state (Arbuzova*, et al.*, 2002).

It is interesting to note that myristoylation in general has been shown to stabilize the structure of a protein, which may suggest that the myristoyl tail interacts with the protein itself (Resh, 1999). This fact, coupled with observation that myristoylated proteins have been found both localized at the membrane and free in the cytosol, has led to a more dynamic view of myristoylated protein regulation. It is now believed that some myristoylated proteins exhibit a *myristoyl switch* that causes them to flip back and forth between membrane-bound and cytosolic state (McLaughlin and Aderem, 1995).

Myristoyl Switches. The orientation of the myristoyl moiety on a protein is not always constant. Some myristoylated proteins exhibit two conformational states. In one state, the myristoyl tail is sequestered within a hydrophobic binding pocket of the protein. In the second conformation the myristoyl group is exposed to the solvent and is capable of inserting into the cell membrane (McLaughlin and Aderem, 1995). The transition between these two states is known as a myristoyl switch. These switches are categorized into three main groups: ligand binding switch mechanisms, electrostatic mechanisms and proteolytic mechanisms (Fig. 1.4) (Resh, 1999).

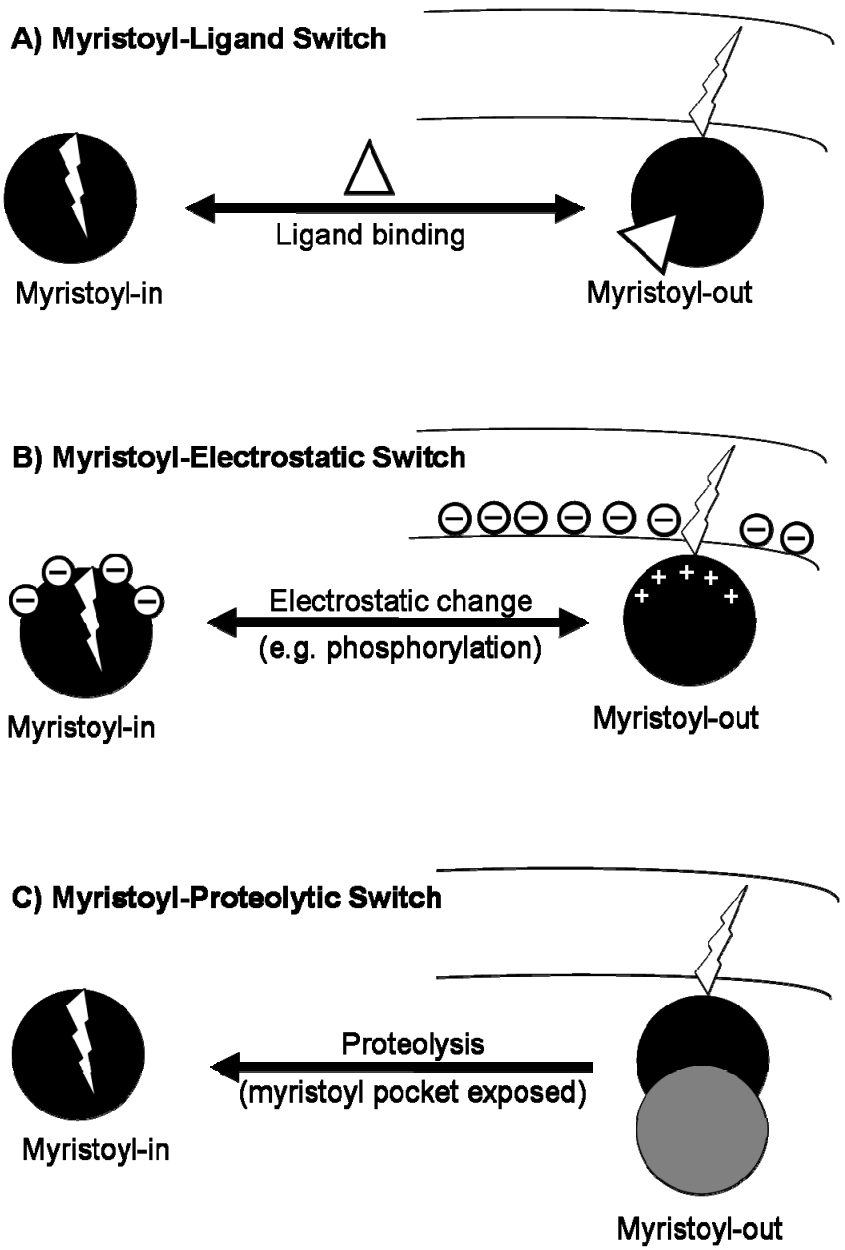

Fig. 1.4. General mechanisms proposed for myristoyl switches. The myristoyl tail may be extruded by several possible mechanisms. (A) Ligand (Δ), such as H^+, Ca^{2+}, GTP, DNA or other proteins, bind to the protein, which elicits the myristoyl-ligand switch. (B) The myristoyl-electrostatic switch illustrating the involvement in membrane association. Modification of a protein changes the charge of the protein and causes membrane association that is facilitated by favourable electrostatic interactions with the negatively charged lipid heads in the membrane. Note, that the myristoyl group may become sequestered in the protein upon dissociation. (C) Myristoyl proteolytic switch that illustrates how proteolysis can expose a myristoyl binding pocket that facilitates the sequestration of the myristoyl group.

In the ligand binding mechanism, a myristoylated protein has a specific binding site for a ligand (Fig. 1.4A). When the ligand is not bound, the overall structure of the protein accommodates the myristoyl tail at some site within the protein. When the ligand binds to the protein, this new association causes the myristoyl tail to become exposed. It is also possible that ligand binding may have the reverse effect, causing the myristoyl tail to become sequestered in the protein (Resh, 1999). A well characterized protein that exhibits ligand binding myristoyl switch is recoverin.

Recoverin is a 23 kDa protein that is found in the retina (Zozulya and Stryer, 1992). The overall function of recoverin has been implicated in Ca^{2+}-dependent photoresponse (Ames*, et al.*, 1995). At low concentrations of calcium, the protein remains unbound to the membrane; as calcium concentrations increase, cooperative binding of 2 Ca^{2+} ions causes recoverin to become membrane bound (Zozulya and Stryer, 1992). Initial ^{1}H-^{15}N Heteronuclear-Single Quantum Correlation (HSQC) nuclear magnetic resonance (NMR) experiments showed dramatic changes in the chemical shift between myristoylated and nonmyristoylated recoverin (Ames*, et al.*, 1995). These changes motivated further NMR studies, which indicated that, in the calcium unbound state, the myristoyl group is sequestered deep in the protein (Ames*, et al.*, 1995). Close interactions were noted between 5 helices in the protein. Upon calcium binding, dramatic changes in the N-terminal region caused the N-terminal helix to melt, allowing for flexible extension of the myristoyl group into the solvent (Fig. 1.5). Several of the other helical domains change their geometry and disrupt the myristoyl binding site (Fig. 1.5, (Tanaka*, et al.*, 1995)).

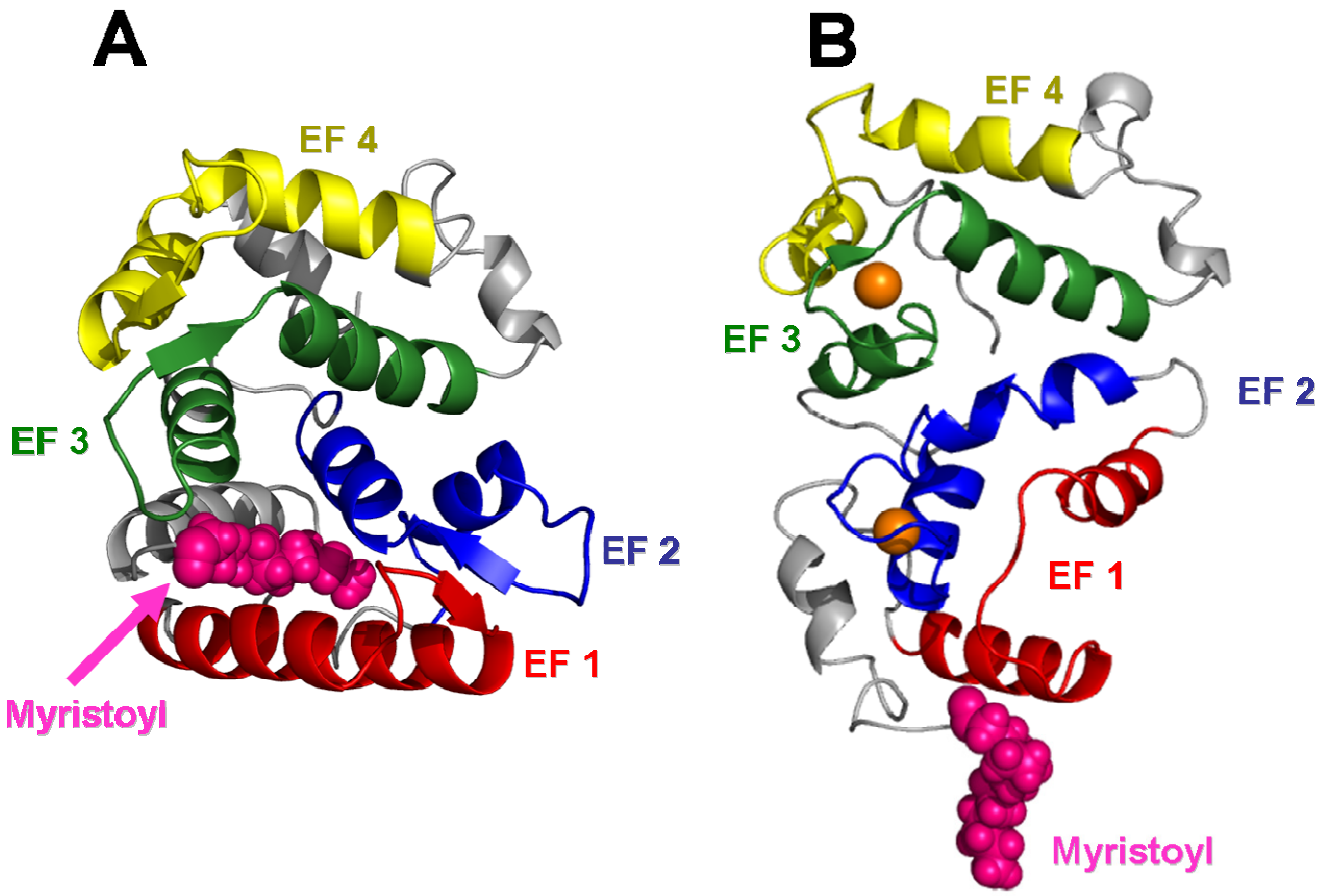

Fig. 1.5. Ribbon diagrams of the two conformations of recoverin. The conformational state of the myristoyl group (pink spheres) switches between sequestered and exposed states depending upon the binding of two Ca^{2+} ions (orange spheres). EF hand motifs 1 – 4 found within recoverin are shown in red, blue, green and yellow, respectively. (A) The sequestered myristoyl conformation where the myristoyl group is bound within a hydrophobic binding pocket. (B) The exposed myristoyl conformation where the myristoyl group is found exposed to solvent when a Ca^{2+} binds to EF hand 2 and EF hand 3.

Solid state NMR experiments that accompanied these experiments show that the myristoyl group inserts into the plasma membrane without disrupting the overall protein structure (Valentine, *et al.*, 2003). Structural studies done on the membrane-bound recoverin revealed several basic residues that are within 5 Å of the membrane and may aid in membrane binding (Valentine, *et al.*, 2003). Thus, the studies performed on recoverin

indicate that the myristoyl group is not a simple hydrophobic protein modification but a more dynamic entity.

The type of myristoyl switch illustrated in Fig. 1.4C is the proteolytic switch. The general idea behind this switch mechanism is that the initial state of the myristoyl group (either "in" or "out") is converted to the opposite conformation by proteolysis of the protein (Resh, 1999). An example of this mechanism is found in the Human Immunodeficiency Virus-1 Gag (HIV1 Gag) protein. The HIV1 Gag protein is found as a myristoylated 55 kea protein schematically depicted in Fig. 1.6A (Resh, 2004).

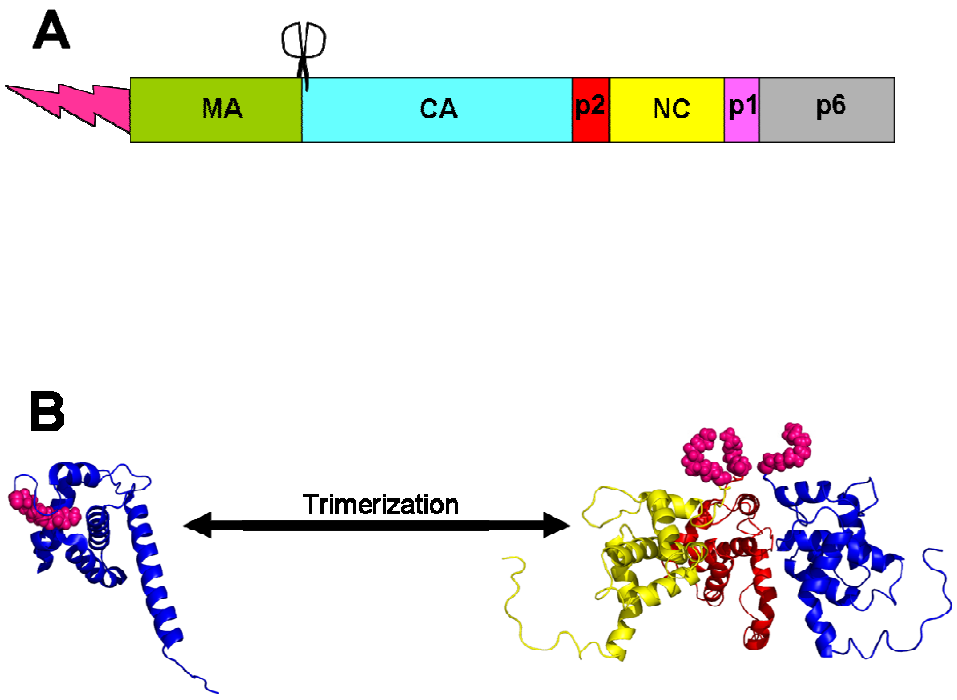

Fig. 1.6. The different domains of the HIV1 Gag protein. (A) A simplified representation of one subunit of the full length trimeric HIV-1 Gag protein with N-terminal myristoyl group (pink). The MA, CA, p2, NC, p1, p6 domains have been coloured as green, cyan, red, yellow, purple and grey, respectively. Scissors denote the location where proteolysis occurs. (B) Proteolysis of the matrix domain, MA (blue, red and yellow), in the trimeric Gag protein from the rest of the protein exposes a myristoyl binding pocket where the myristoyl group (pink spheres) binds.

In the full form, the Gag protein has the myristoyl tail in the "out" position. The myristoyl tail, in concert with several basic residues found near the protein-membrane interaction site, causes the Gag protein to remain membrane bound (Resh, 2004). Subsequently, the viral protease cleaves the N-terminal domain of Gag, releasing the MA protein. This exposes a myristoyl binding site and causes the myristoyl group to switch to the "in" position (Resh, 2004). NMR data has been used to determine the structure of the 17 kDa cleaved Gag protein with the myristoyl group in the sequestered position (Tang, *et al.*,

2004). Further studies have indicated that the HIV1 Gag protein-myristoyl switch is actually more complicated than originally believed. The cleaved 17 kDa MA Gag protein exists in both monomeric and trimeric states (Fig. 1.6B). The striking result is that in the monomeric state the myristoyl group remains sequestered, but it adopts the "out position" in the trimeric complex (Tang, *et al.*, 2004). Thus, as the protein favours the trimeric state, the myristoyl group once again becomes exposed. This additional complication to the HIV1 Gag myristoyl switch has led to it also been referred to as an *entropic* switch. It nevertheless serves to illustrate the involvement of proteolytic cleavage in myristoyl switching mechanisms. This example also provides further evidence that the addition of a simple myristoyl moiety can have extensive impacts on both the structure and function of a protein.

The final type of myristoyl switch to be examined is the electrostatic myristoyl switch. As mentioned previously, the myristoyl group alone does not supply enough binding energy to drive membrane binding, and membrane binding of a myristoylated protein is often a synergistic effort between a myristoyl moiety and the electrostatic interaction of several "well-placed" basic residues that interact favourably with acidic phospholipids. As such, by modifying the protein to remove these favourable electrostatic interactions it loses the ability to bind and subsequently locates to the cytoplasm. This charge manipulation can happen by many means and a good example illustrating this is hisactophilin.

Hisactophilin. In 2000, Ponting and Russell published a paper that illustrated that fascins and hisactophilin belong to the same family of proteins (Ponting and Russell, 2000). When the protein sequences were aligned both the fascins and hisactophilin showed highly conserved structural similarities that linked these proteins as homologues (Ponting and

Russell, 2000). This homology in part suggested that the evolution of β-trefoil proteins occurred though genetic duplications of a single trefoil element (Fig. 1.7).

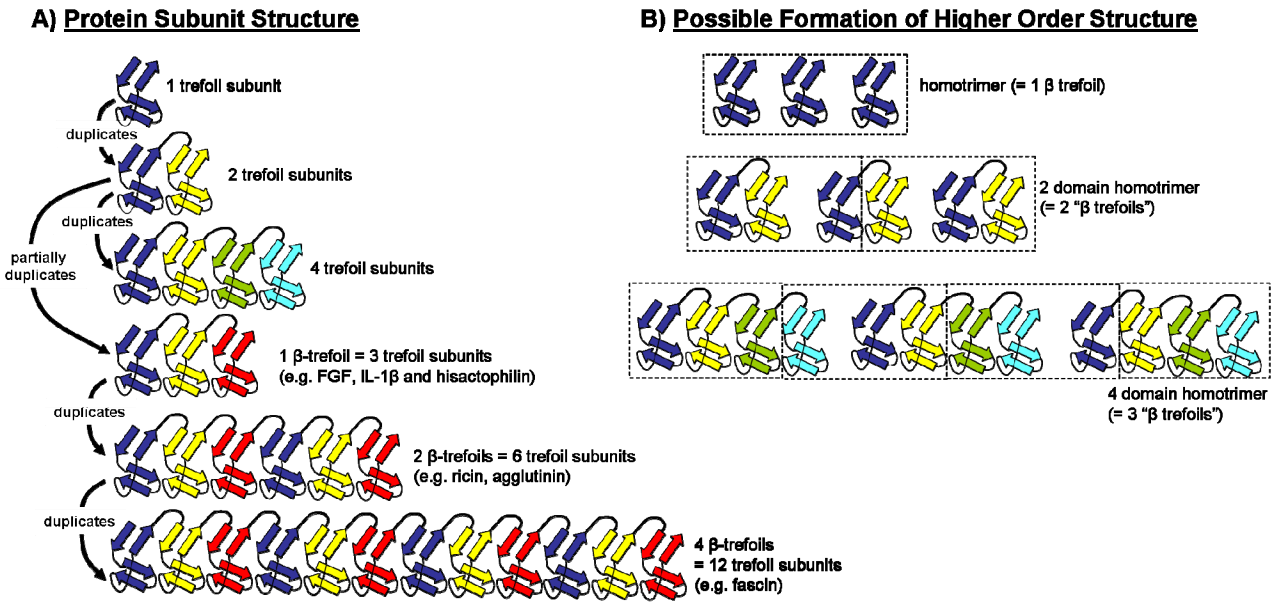

Fig. 1.7. The evolutionary link between β-trefoils. (A) Evolutionary duplication events that may have led to the formation of various β-trefoil proteins. Each trefoil subunit (i.e. building block) represents a 4β-stranded structural subunit of the β-trefoil, which contains 3 trefoil subunits. Coloured subunits emphasize the evolutionary origin of that particular trefoil subunit. Black arrows depict the evolutionary events that would lead to the formation of that particular structure. (B) The possible formation of whole β-trefoil proteins from incomplete trefoil subunits. Dashed lines outline the subunits that would oligomerize to form each whole "β-trefoil" protein.

The fascins contain highly conserved sequence features across all isoforms. These include actin binding domains and a phosphorylation site (Pollard*, et al.*, 1994). Both of these characteristics have been related to physiological function and it is interesting to note that these elements are common with hisactophilin. Within the fascins, the most highly conserved sequence is the region between amino acids 11- 50 (Adams, 2004). This sequence

has been shown to be a site for phosphorylation by protein kinase C (PKCα) at Ser39, which is exposed on an external loop of the protein. Mutational analysis has shown that phosphorylation diminishes actin binding *in vitro* (Adams, 2004). One of the actin binding sites found within the β-trefoil has been mapped by limited proteolytic analysis (Edwards and Bryan, 1995, Kureishy*, et al.*, 2002). A second actin binding site in fascin has been proposed that closely resembles the actin binding domain of another actin associated protein, MARCKS (Kureishy*, et al.*, 2002). This suggested binding site overlaps with the phosphorylation site in the same region and could most likely contribute to the dynamic interaction between phosphorylation and actin bundling. With these structural elements in mind it is interesting to look at the physiological role of the fascins.

Fascin-1 is highly expressed in neural cells, glial cells, skeletal smooth muscle cells and is upregulated in tumour cells (Kureishy*, et al.*, 2002). In these cells it is known to be the core actin bundling protein of dendrites, filopodia and lamellipodial ribs. Fascin-1 is also located in cellular protrusions in motile cells (Fig. 1.8) (Adams, 2004).

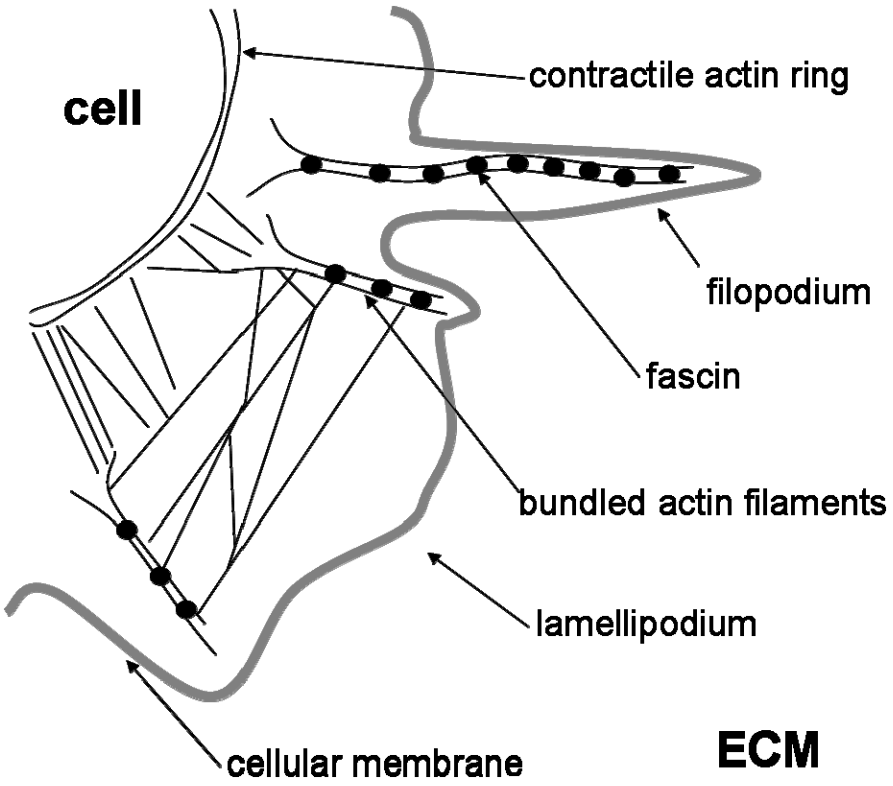

Fig. 1.8. The involvement of actin filaments in the formation of cellular protrusions. Fascin (black circles) bundle together actin filaments into actin spikes that provide the structural support for features of the cellular membrane used for chemotaxis such as filopodia and lamellipodia.

This role in cellular mobility is supported by immunoblocking studies conducted in breast epithelial cells, where the introduction of antibodies into cells that bind to the actin binding domain of fascin completely abolished the ability to move (Kureishy*, et al.*, 2002, Adams and Schwartz, 2000). Another intriguing role of fascin has been uncovered in cell-to-cell contact in mesenchymal cells. The localization of fascin in these cells is highly responsive to extracellular matrix adhesions. Mesenchymal cells adhere to fibronectin by recruiting integrins to form focal adhesions (Adams, 2004). Focal adhesion formation

involves PKCα, implicating a high concentration of phosphorylated fascin, which in turn would abolish actin-fascin association. In contrast, cell adhesion to thrombospondin does not involve PKCα. Zones of adhesion have highly localized fascin-actin associated structures concentrated within them (Adams, 2004). The similarities between fascins and hisactophilin in structure, function and actin interaction among the fascins and hisactophilin are well established. By studying the structure and actin associated function of hisactophilin the fascin family can be better understood. However, the two differ in that the N-terminal myristoyl group is involved in the cellular function of hisactophilin but not the fascins.

As with the fascins and other actin-associated proteins, the function of hisactophilin is centered on the dynamics of actin networks. Hisactophilin binds actin in a pH-dependent manner (Hanakam*, et al.*, 1996). At pH 6.5, hisactophilin co-sediments quite strongly with actin, but this association is abolished at a higher pH of 7.5 (Hanakam*, et al.*, 1996). Studies conducted at pH 6 indicated a K_d between actin and hisactophilin of 0.1μM (Scheel*, et al.*, 1989). At pH 6 actin (pI = 5.6) will be negatively charged and hisactophilin (pI = 7.2) will be positively charged, suggesting that their association involves some electrostatic interaction. However, it is interesting that when the ionic strength is increased by the addition of 100 mM KCl at pH 6, the binding is almost unaffected (Scheel*, et al.*, 1989). In the presence of hisactophilin, G-actin can be polymerized into F-actin using Mg^{2+}. Furthermore, the ratio of hisactophilin to actin monomers appears to be ~1:1 (Behrisch*, et al.*, 1995). These two facts would suggest that hisactophilin associates with the sides of F-actin rather than capping it. Little else is known about the site specific interactions between actin and hisactophilin. Like other fascins and myristoylated proteins such as MARCKS, hisactophilin is also a substrate for phosphorylation. Using ^{32}P-labeled hisactophilin from *D.*

discoideum, both Ser and Thr were suggested as target sites for phosphorylation (Hanakam*, et al.*, 1995). There have been no conclusive studies done to determine the exact role of phosphorylation with respect to hisactophilin. However, it was found that under hypertonic conditions and also elevated cAMP, there was a spike in the concentration of phosphorylated hisactophilin that remained for approximately an hour after the stimulus began (Pintsch*, et al.*, 2002).

Hisactophilin associates with the membrane in a pH-dependent manner. Membrane binding measurements using negatively charged vesicles indicated that at pH 6, where hisactophilin has a charge of +3.5, the protein binds strongly to the membrane, whereas at pH 7.5, where the net charge of hisactophilin is -1.3, no binding was observed (Hanakam*, et al.*, 1996). Membrane binding energy calculations gave a ΔG contribution from the myristoyl group of 7.8 kcal/mol, and an electrostatic binding energy of 2.7 kcal·mol^{-1}, indicating that the majority of the binding energy comes from the insertion of the myristoyl group (Hanakam*, et al.*, 1996). These *in vitro* experiments were complemented with clever *in vivo* experiments. Using a Green Fluorescent Protein, GFP, labelled form of hisactophilin, it was shown that GFP-hisactophilin relocated to the membrane upon localized acidification of the cytosol at the membrane. At a higher pH of ~7.3, hisactophilin remained in the cytosol (Hanakam and Gerisch, 1999). In a similar fashion, when exposed to diethylsilbesterol (DES), a chemical known to inhibit H^+/ATPase, *D. discoideum* cells showed membrane blebbing and altered actin networks. Highly pH-dependent membrane- and actin-binding are consistent with the idea that hisactophilin acts in the cell as a pH-dependent shuttle between the actin cytoskeleton and the inner leaf of the cellular membrane (Stoeckelhuber*, et al.*, 1996).

Hisactophilin Structural Features. Named after the histidine-rich actin loving nature of the protein, hisactophilin is a relatively small 118 amino acid protein isolated from *Dictyostelium discoideum* in two homologous isoforms that are both myristoylated *in vivo*. Hisactophilin I has a molecular weight of 13 536 Da and is the form to be expressed in all of the proposed experimental procedures. Hisactophilin II has a molecular weight of 13 715 Da (Hanakam*, et al.*, 1995). Fig. 1.9 illustrates the three dimensional structure of hisactophilin I, as determined by NMR, which belongs to the β-trefoil structural family (Habazettl*, et al.*, 1992). The β-trefoil of hisactophilin I has a three-fold symmetric structure. The structure consists of three 4-stranded β-trefoil structural units. The first and fourth β strands of each trefoil unit form an anti-parallel β-sheet which combines with similar elements from the other two trefoil units to form a β barrel. The three remaining pairs of β strands come together to form a triangular substructure that covers the barrel in a β-hairpin triplet. The trefoil structure has been described as a β-β-β-loop-β motif (Habazettl*, et al.*, 1992). The protein contains one cysteine at position 49 that is not palmitoylated. The most striking structural feature of hisactophilin is the high histidine content. Hisactophilin contains 31 histidine residues, 28 of which are found exposed on the surface of the protein (Hammond*, et al.*, 1998). The average apparent pK_a values for the histidines in hisactophilin are ~6.8. This falls in the physiologically important range found *in vivo*. Because of the high histidine content, small pH changes in this range will have dramatic effects on the charge of the protein and thus its actin/membrane binding properties of the protein. Indeed, these membrane binding predictions based on the structural properties are what have been

observed in functional studies of the protein. Fig. 1.10 illustrates a conceptual view of this physiological switch (Hanakam*, et al.*, 1996).

A

Hisactophilin I

MGNRAFKSHHGHFLSAEGEAVKTHHGHHDHHTHFHVENHGGKVALKTHCGKYLSIGDHKQVYLSHHLHGDHS
LFHLEHHGGKVSIKGHHHHYISADHHGHVSTKEHHDHDTTFEEIII

Hisactophilin II

MGNRAFKAHNGHYLSAEHDHVKTHHGHHDHHTHFHIENHGSKVALRTHCGKYVSIGDHKQVYLSHHLHGDHS
LFHLEHHHGKVSIKGHHHHYISVDGHGHVSTSHHHDHHATFEEHIL

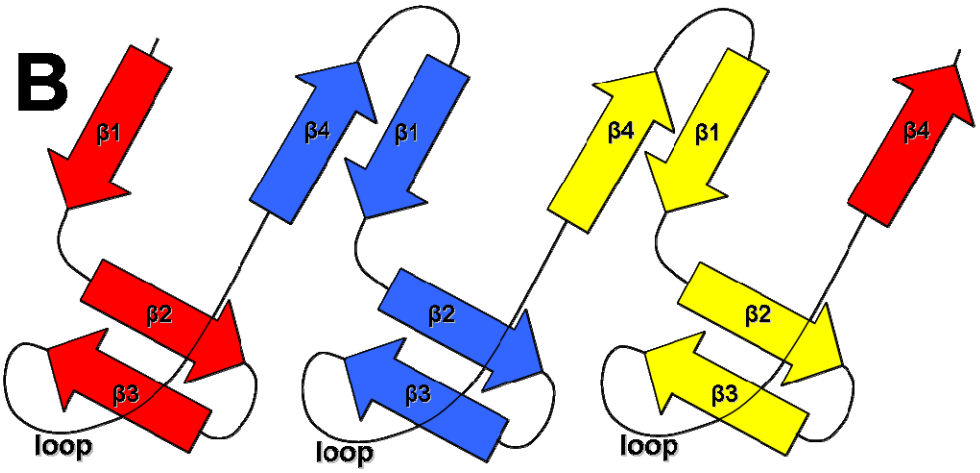

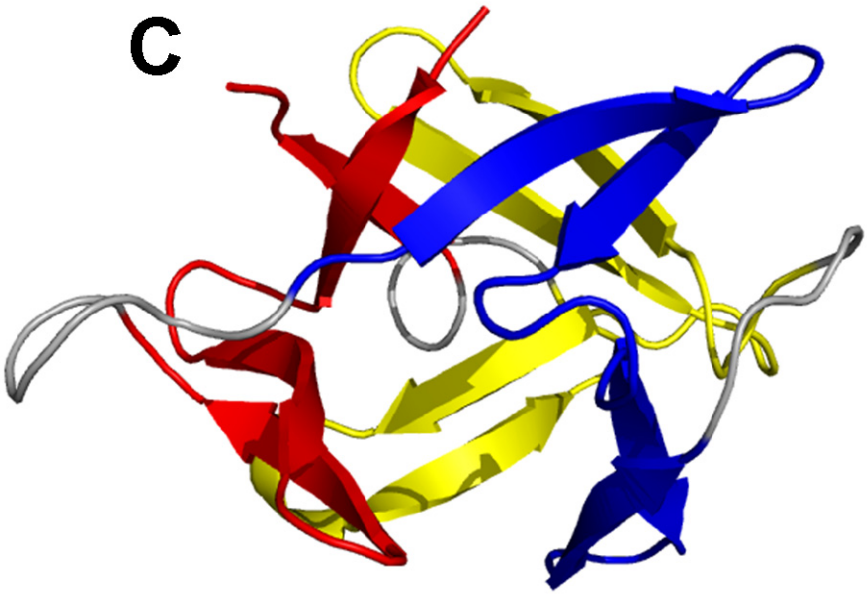

(figure legend on following page)

Fig. 1.9. The varying levels of structure in hisactophilin. (A) The primary sequence of amino acids found in hisactophilin I and hisactophilin II (NCBI Protein Databank). (B) Secondary structure of hisactophilin I illustrating the β1-β2-β3-loop-β4 motif found in each β-trefoil subunit. The β-strands that form each lobe of the trefoil have been coloured red, blue and yellow, respectively. (C) The 3D structure of hisactophilin I as solved by NMR (PDB: 1HCD). The trefoil strands have been coloured as in panel B.

Hisactophilin Myristoyl Switch. What is the conformation of the myristoyl group in this membrane binding scheme (Fig. 1.10)? Research on other proteins such as recoverin, MARCKS, or HIV1 Gag (see above) have shown that regulation of function in myristoylated proteins is a complicated process and involves dynamic structural changes that alter the location of the myristoyl tail. These observations have led to the belief that the physiological role of hisactophilin is actually regulated by a myristoyl switch involving a conformational change of the myristoyl tail from an exposed position to one sequestered in the protein (Meissner, 2007). In the cytosolic state, above pH 7.5, the myristoyl tail would remain sequestered in the protein. As physiological signals cause a decrease in pH, some structural changes would occur in the protein causing the myristoyl tail to become exposed to the solvent.

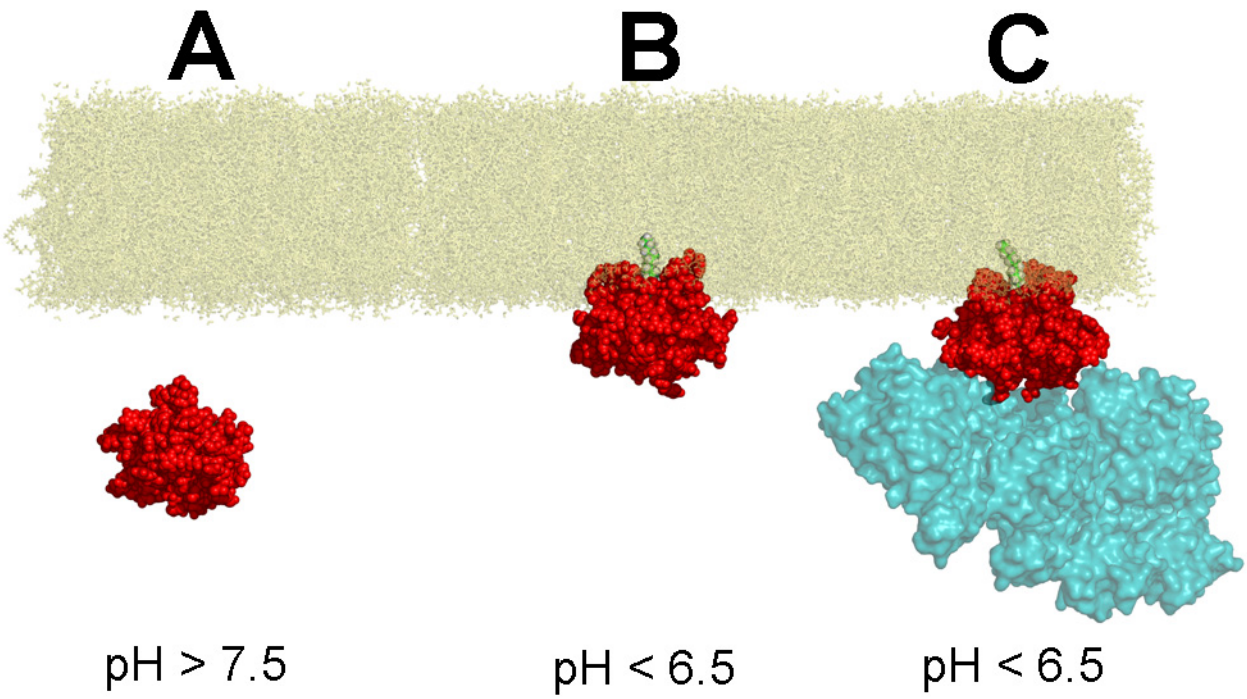

Fig. 1.10. Illustrating the pH-dependent switch of hisactophilin. (A) At pH >7.5 hisactophilin (red surface) is located in the cytosol. The myristoyl group is depicted in the core of hisactophilin, hence, in the "sequestered" state where the myristoyl group is not available for membrane binding. Note that before the research conducted in this thesis the conformation of the myristoyl group in the cytosolic form of hisactophilin was unknown. (B) At pH < 6.5, histidine residues in hisactophilin (red surface) become protonated and hisactophilin undergoes a myristoyl-electrostatic switch to the accessible myristoyl state where the myristoyl group becomes accessible to the solvent. Upon switching to the accessible state hisactophilin becomes membrane bound due to the insertion of the myristoyl group (green) and favourable electrostatic interactions with the negatively charged membrane phospholipids (yellow). (C) At pH < 6.5 hisactophilin also binds to actin (cyan, PDB: 1J6Z) and recruits actin filaments to the cellular membrane. This illustrative model was created using PyMol modelling software (Delano Scientific).

As this change in pH coincides with the protonation of the numerous histidines, it is believed that the histidine residues play a crucial role in the conformational switch; hence, the switch mechanism has been proposed as a histidine-myristoyl electrostatic switch mechanism. Despite past studies on other myristoylated proteins, surprisingly little is known about the molecular basis of this type of myristoyl switch. Furthermore, there is still little

structural information on the cytosolic and membrane-bound states of the myristoyl group in any particular protein. Therefore, another focus of this thesis is study of the mechanisms that govern the pH-dependent myristoyl switch in hisactophilin and gathering structural information about the different switch states observed for myristoylated hisactophilin. Much research has already been conducted on nonmyristoylated hisactophilin and a brief outline of the results now follows.

Structure and Stability Studies on Hisactophilin. Previous extensive studies have characterized the equilibrium stability and kinetic folding/unfolding rates of nonmyristoylated hisactophilin (Hammond*, et al.*, 1998, Liu*, et al.*, 2001, Wong*, et al.*, 2004). Equilibrium and kinetic denaturation of nonmyristoylated hisactophilin using urea as the chaotrope is highly reversible. The equilibrium and kinetic folding/unfolding of hisactophilin has been characterized at pH 5.7, 6.7, 7.7, 8.7 and 9.7 using fluorescence and circular dichroism (CD) and fit well to a two-state unimolecular model of unfolding. In the pH range of 5.7 to 9.7 hisactophilin has moderate stability that ranges from ~2.4 kcal·mol^{-1} to ~10.1 kcal·mol^{-1}. From the stability measurements, it was shown that above pH 7.7 the stability of hisactophilin is fairly constant. However, below pH 7.7 stability decreases in a non-linear fashion due to the protonation of the histidine residues as seen by denaturation curves in Fig. 1.11. This trend is interesting because it further implicates the pH-driven histidine-myristoyl electrostatic switch by placing emphasis on the central role of the histidine residues in protein stability.

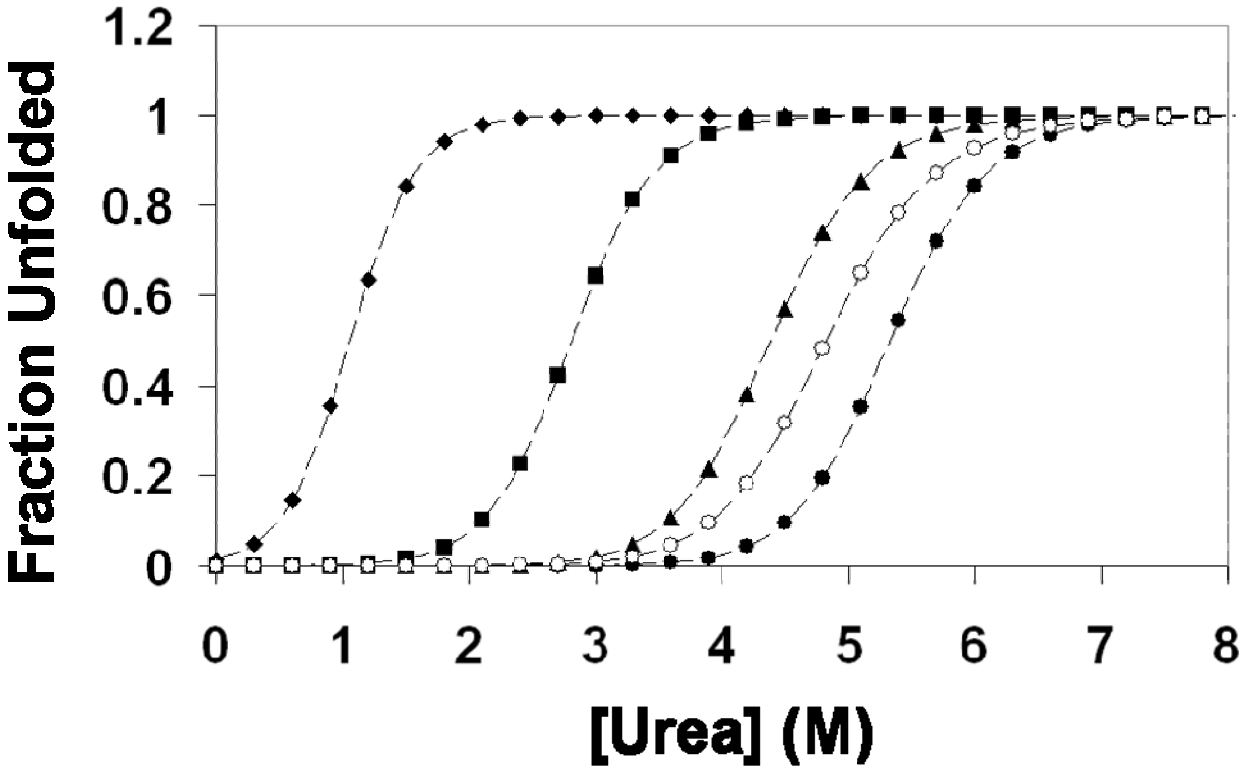

Fig. 1.11. Denaturation curves acquired for nonmyristoylated hisactophilin with 4 additional amino acids at the N-terminus. Simulated fraction of unfolded hisactophilin *vs.* urea denaturant concentration at 20˚C for: pH 5.7(♦), pH 6.7(■), pH 7.7(▲), pH 9.7(○), pH 8.7(●). Equilibrium unfolding data was simulated using parameters from previously published data using the binomial extrapolation method (Liu*, et al.*, 2001).

Previous structural studies in this lab on nonmyristoylated hisactophilin have shown the overall secondary structure of nonmyristoylated hisactophilin to be similar to naturally isolated hisactophilin found by Hanakam *et al.* by CD (Hanakam*, et al.*, 1996, Liu*, et al.*, 2001). NMR studies from this lab performed by Hammond *et al.* utilized ^{1}H-^{15}N HSQC pH titrations to characterize the apparent pK_as for the chemical shift of specific amide, NH, backbone protons (Hammond*, et al.*, 1998). Furthermore, the NH/D exchange for nonmyristoylated hisactophilin has been characterized as a function of pH, urea and temperature (Houliston, 2004). NH/D exchange experiments yielded site-specific information on the kinetics and stability of local and global structural fluctuations in

hisactophilin. Therefore, the combination of NMR with other techniques to monitor the equilibrium and kinetics of folding provides a significant knowledge base to study the effects of myristoylation on the folding and function of hisactophilin.

As explained throughout the introduction, the goals of this thesis include: 1) characterizing the thermodynamic and kinetic effects of myristoylation on the native and nonnative states in the folding pathway of hisactophilin, 2) understanding the effects of myristoylation on folding in the context of existing folding models, 3) obtaining structural information on the conformation of the myristoyl group in the different states involved in the myristoyl switch, and 4) gaining insight into the energetic and dynamic processes that govern the myristoyl switching function. In order to do this a combination of techniques including: equilibrium stability, kinetic folding/unfolding, ^{1}H-^{15}N HSQC pH titrations, mutagenesis and NH/D exchange are be applied to recombinantly expressed myristoylated and nonmyristoylated hisactophilin and compared the previous studies on nonmyristoylated hisactophilin (described above). Information obtained from 3D ^{15}N-editted NOESY-HSQC and TOCSY-HSQC experiments performed on myristoylated hisactophilin yields a structural model of hisactophilin with the myristoyl group in the sequestered state (chapter 2). Modelling the sequestered state provides critical structural information that supports all of the other energetic and structural analyses performed on myristoylated hisactophilin. The equilibrium stability of myristoylated hisactophilin is measured as a function of pH for wildtype and several hisactophilin mutants (chapter 2, 3 and 4). Comparison to the previous work on nonmyristoylated hisactophilin yields fundamental information about the effects of myristoylation on the stability and energetics of myristoyl switching in hisactophilin (chapter 2). The kinetics of folding and unfolding for myristoylated hisactophilin is also determined

at several pHs for wildtype hisactophilin and several hisactophilin mutants. Determining the folding and unfolding rates for both wildtype and mutant hisactophilin will yields insights into the nonnative effects of myristoylation on the kinetic folding pathway of proteins (chapter 4). ^{1}H-^{15}N HSQC will be acquired *vs.* pH are used to determine site-specific apparent pK_as for myristoylated hisactophilin. Changes upon myristoylation in the apparent amide pK_as will be used model site-specific information about the pH-dependent myristoyl switch that governs the function of hisactophilin (chapter 2). NH/D exchange for myristoylated hisactophilin is acquired at several temperatures and pH. NH/D exchange data acquired as a function of pH for myristoylated hisactophilin are compared to data obtained previously for nonmyristoylated hisactophilin and used to provide site-specific information reporting on changes in stability, $\Delta\Delta G$, upon myristoylation. NH/D exchange for myristoylated hisactophilin acquired at several temperatures is compared to previous studies on nonmyristoylated hisactophilin and used to determine site-specific effects of myristoylation on enthalpy, $\Delta\Delta H$, and entropy, $\Delta\Delta S$ (chapter 5). Together the results from all of these techniques will provide critical information on the energetic effects of myristoylation on protein folding and function.

Preamble

As outlined in the introduction, significant efforts have been made to understand the structure and membrane binding function of myristoylated proteins because of their vital role in biology. However, at the time when this research was conducted the scientific community lacked a quantitative understanding of the energetics effects of myristoylation on the folding a switching function of various myristoylated proteins. Therefore, the experiments in chapter 2 were conducted to quantify the thermodynamic and kinetic effects that myristoylation has on folding and myristoyl switching on the model protein, hisactophilin.

The research conducted on hisactophilin in chapter 2 contain quantitative indications about the native and nonnative effects that myristoylation has on proteins that underlay the biological folding and switching function of hisactophilin. In chapter 2 the energetic mechanisms identified in hisactophilin are compared to other switching systems, including myristoylated proteins, to help understand the mechanisms that underlay the folding and switching function of myristoylated proteins. The content represents the main body and supplementary information that was published in the article:

Smith, MTJ., Meissner, J., Esmonde, S., Wong, HJ., Meiering, EM. (2010) Energetics and mechanisms of folding and flipping the myristoyl switch in the beta-trefoil protein, hisactophilin. *Proc. Natl. Acad. Sci*. 107(49), pp. 20952-7

This work has been reproduced here in accordance with the journal publication policy (also see letter of permission section). All of the data presented in this chapter were obtained by Martin Smith. These experiments were a continuation on the work of two M.Sc. students: Joe Meissner and Hannah Wong, who developed the expression system and purification protocol for recombinantly expressing and purifying myristoylated hisactophilin in *E. coli* bacteria. The supplementary materials and methods section from the published article has been incorporated into the main text of this chapter with additional details regarding hisactophilin expression and purification. The supplementary results section has been placed before the discussion section to form a continuous results section in chapter 2 of this thesis.

Chapter 2 – The Effects of Myristoylation on the Flipping and Folding of Hisactophilin

Introduction

Myristoylation is a common co-translational modification found in ~0.5–0.8% of eukaryotic proteins (Resh, 2006). This modification involves the covalent linkage of a saturated C_{14} fatty acyl chain to the N-terminal glycine residue in a protein (Resh, 2006). Myristoylated proteins play vital roles in many biological processes and commonly undergo reversible switches. The "flipping" of myristoyl switches typically involves inter-conversion between a myristoyl-sequestered state, myr_{seq}, where the myristoyl group is located in a hydrophobic binding pocket within the protein, and a myristoyl-accessible state, myr_{acc}, where the myristoyl group is available for binding to membranes or other proteins. Switching may be associated with relatively large or subtle structural and/or dynamic changes in the myristoylated protein (Orban*, et al.*, 2010, Ames*, et al.*, 1997). It can also be regulated by binding of various ligands (e.g. H^+, Ca^{2+}, GTP, or regulatory protein) (Resh, 2004, Ames*, et al.*, 1997, Kahn*, et al.*, 1992). Some examples of proteins that undergo myristoyl switching include: Ca^{2+}-dependent recoverin, which mediates photo-responses in the retina (Ames*, et al.*, 1997); Ca^{2+}-dependent guanylate cyclase activating protein (GCAP), which regulates the function of guanylate cyclase (Orban*, et al.*, 2010, Lim*, et al.*, 2009); oligomerization-dependent HIV-1 Gag, which orchestrates HIV-1 viral proliferation (Resh, 2004); GTP-dependent ADP ribosylation factor (ARF) proteins, which are involved in membrane trafficking (Randazzo*, et al.*, 1995), and pH-dependent hisactophilin, involved in controlling cytoskeletal changes during cellular movement and osmotic stress (Hanakam*, et*

al., 1996, Pintsch*, et al.*, 2002). Thus, ligand-regulated myristoyl switching is a versatile mechanism for controlling a wide range of biologically important processes. Myristoyl switches have been characterized extensively at the functional level, but remain poorly understood at the energetic and molecular levels (Resh, 2006). Furthermore, there is a paucity of data on the effects of myristoylation on protein folding and stability.

In this study we use hisactophilin as a model to analyze the effects of myristoylation. Hisactophilin is a pH-dependent, myristoylated, histidine-rich actin- and membrane-binding protein from the model organism, *Dictyostelium discoideum*. This small (13.5 kDa) protein facilitates cell shape changes and movements in response to chemotactic signals and osmotic stress, which result in cellular pH changes. *In vivo*, hisactophilin reversibly switches between a cytoplasmic form at pH 7.5 to a membrane-bound form at pH 6.5, which also anchors actin filaments to the inner leaflet of the cellular membrane. *In vitro*, hisactophilin undergoes a reversible myristoyl switch driven by pH. Hisactophilin contains an unusually large proportion of histidines (31 of 118 residues), with average apparent pK_a values of ~6.8 (Hammond*, et al.*, 1998). Reversible proton binding/release by histidines has been implicated in regulating the equilibrium between the cytosolic and membrane-bound forms (Hanakam*, et al.*, 1996). In-depth biophysical analyses have been conducted for the nonmyristoylated form of the protein (Liu*, et al.*, 2001, Wong*, et al.*, 2004); the myristoylated form is amenable to similar analyses, as described in this report. We describe the first quantitative analyses of thermodynamic stability and kinetics of folding/unfolding for a myristoylated protein, combined with NMR analyses of switching. Our results reveal dramatic effects of myristoylation on folding, which are mediated by nonnative interactions, and provide novel insights into the energetics and mechanism of pH-dependent myristoyl

switching in hisactophilin. The results and methodology have important implications for understanding the interplay between ligand binding and interactions of hydrophobic moieties in many other switching systems.

Materials and Methods

Chemicals. Chemical were analytical grade and obtained from Bioshops Inc., Canada, unless otherwise specified. Urea concentrations were confirmed by refractometry (Pace, 1986).

Recombinant hisactophilin expression and purification. Wild-type hisactophilin was expressed as described previously (Liu*, et al.*, 2001), after performing site-directed mutagenesis (QuickChange, Stratagene) to remove extraneous N-terminal GEFG residues (Wong, 2002). Briefly, to express N-myristoylated hisactophilin, *E.coli* was simultaneously co-transformed with the pHV738 plasmid and the pHW plasmid. The pHV738 contains the human N-myristoyltransferase 1 gene under the IPTG inducible Ptac promoter, kanamycin resistance gene and the *E. coli* methionine aminopeptidase gene. The pHW plasmid contains the hisactophilin gene under the IPTG inducible Ptac promoter and an ampicillin resistance gene. *E.coli* cells were selected for resistance to both ampicillin and kanamycin. Cells that exhibited resistance to both ampicillin and kanamycin were grown in LB media with 100 $\mu g \cdot mL^{-1}$ ampicillin and 30 $\mu g \cdot mL^{-1}$ kanamycin at 37˚C to an optical density at 600nm (OD_{600}) = 0.3 where 1 mM sodium myristate is added at OD_{600} = 0.3 (~1

hour before induction). At OD_{600} = 0.7 cells were induced by adding 1 mM IPTG and incubated at 37˚C. *E.coli* cells were harvested using centrifugation ~6 hours after induction. Harvested cells containing hisactophilin were flash frozen and stored at -80˚C for purification at a later date.

Protein purification. Myristoylated hisactophilin was purified, as described previously (Liu*, et al.*, 2001), with an additional separation by acetonitrile gradient RP-HPLC. Briefly, cells containing myristoylated hisactophilin were resuspended in Tris buffer pH 8 and lysed using an Emulsiflex C-5 emulsifier (Avestin Inc.). Next, 0.5% (w/v) [3-(3-Chloramidopropyl)] dimethylammonio-1-propanesulfonate (CHAPS) was added to the crude cell lysate which was then incubated for 2 hours at 4˚C to facilitate solubilization of membrane bound hisactophilin. Hisactophilin was purified using DEAE (Biorad Inc.) anion exchange chromatography, followed by gel filtration using a HiLoad 26/60 Superdex 75 column (GE Healthcare). Myristoylated and nonmyristoylated hisactophilin eluted in well separated peaks in RP-HPLC chromatography using a C_{18} column (Waters Inc.) and an acetonitrile gradient. The level of myristoylation of hisactophilin was typically ~80%. Purified protein was exchanged into 25 mM ammonium carbonate, lyophilized and stored at -80˚C. The percentage of myristoylation in the purified protein was verified by mass spectrometry (Appendix 1)(Scheel*, et al.*, 1989, Meissner, 2007).

Equilibrium, folding and unfolding measurements. Equilibrium denaturation curves were measured as described previously (Wong*, et al.*, 2004). Stock protein solution was prepared by dissolving lyophilized hisactophilin to a concentration of 2 $mg \cdot mL^{-1}$ in

either 500 mM 2-morpholino-ethanesulfonic acid (MES), 500 mM potassium phosphate or 500 mM glycine at the appropriate pH. Protein stocks were diluted ten-fold in water and stock urea to the desired final concentration of urea. Samples were equilibrated at 25.0°C in a water bath for at least ten half-lives as measured for kinetic folding/unfolding transitions. Samples were monitored by fluorescence using a Fluorolog3-22 spectrofluorometer (Horiba-Jobin-Yvon Spex Inc.) as described previously with excitation and emission wavelengths of 277 nm and 306 nm, respectively (Wong*, et al.*, 2004, Liu*, et al.*, 2002). Equilibrium denaturation and renaturation curves were also monitored by circular dichroism at 227 nm using a J715 spectropolarimeter (Jasco Inc.) as described previously (Liu*, et al.*, 2001). Curves can be fit to the linear extrapolation model (LEM) using the equation:

$$Y = \frac{(Y_N + S_N \cdot [urea]) - \{(Y_N + S_N \cdot [urea]) - ((Y_U + S_U \cdot [urea])\} \cdot (e^{\frac{\Delta G_{U-F} - meq[urea]}{RT}})}{1 + (e^{\frac{\Delta G_{U-F} - meq[urea]}{RT}})} \quad [2.1]$$

where $\Delta G_{U\text{-}F}$ represents the free energy of folding in H_2O, m_{eq} represents the dependence of $\Delta G_{U\text{-}F}$ on the [urea], Y and S represent the optical signal and urea dependence of the native, N, and unfolded, U, protein. Denaturation curves were also fit to the binomial extrapolation method using the equation:

$$Y = \frac{(Y_N + S_N \cdot [urea]) - \{(Y_N + S_N \cdot [urea]) - ((Y_U + S_U \cdot [urea])\} \cdot (e^{\frac{\Delta G_{U-F} - meq[urea] + m_2[urea]^2}{RT}})}{1 + (e^{\frac{\Delta G_{U-F} - meq[urea] + m_2[urea]^2}{RT}})} \quad [2.2]$$

where the additional parameter, m_2, describes the second order curvature observed in the urea dependence of the folding stability.

Kinetic folding/unfolding reactions with half lives greater than ~15 seconds were measured by manual mixing using the Fluorolog3-22. Faster folding/unfolding rates were measured using the Fluorolog3-22 interfaced with a SFM4/Q (Molecular Kinetics Inc.). Kinetic data were fit using the Biokine 2.1 software (Molecular Kinetics Inc.). Data were then fit to a 2-state unfolding model (Table 2.S1) using the binomial extrapolation method (BEM) as described previously (Liu*, et al.*, 2002). The two-state observed kinetic rate, k_{obs}, can be fit *vs.* [urea] to the two-state BEM using the equation:

$$\ln(k_{obs}) = \ln\left(k_f^o \cdot e^{m_f^{\ddagger}\cdot[urea]-m_{2ref}\cdot[urea]^2} + k_u^o \cdot e^{m_u^{\ddagger}\cdot[urea]-m_{2unf}\cdot[urea]^2}\right) \qquad [2.3]$$

where k_f° and k_u° are the folding and unfolding rate constants in 0M urea. $m_u^{\ddagger}$ and m_{2unf} present the quadratic denaturant dependence on the natural logarithm of the unfolding rates. $m_f^{\ddagger}$ and m_{2ref} describe the quadratic denaturant dependence of the natural logarithm of the refolding rate.

Applicability of the 2-state model is supported by the agreement of kinetic and equilibrium data (Table 2.S1) and by agreement between fluorescence and circular dichroism results (Table 2.S2). Due to long extrapolations to folding conditions at 0 M urea, the *m* values of some kinetic data show systematic deviations from equilibrium data. However, C_{mid} values from equilibrium and kinetic experiments are similar, which supports the 2-state

folding model (Fersht, 1999). To determine pK_{switch} and ΔG_{switch} (= $\Delta\Delta G_{U\text{-}F,low\ pH} - \Delta\Delta G_{U\text{-}F,high\ pH}$), the dependence of $\Delta\Delta G_{U\text{-}F}$ on pH was fit to a general titration equation:

$$\Delta\Delta G_{U-F}(pH) = \frac{\Delta\Delta G_{U-F,highpH} + \Delta\Delta G_{U-F,lowpH} \cdot \left(10^{pKswitch-pH}\right)}{1 + \left(10^{pKswitch-pH}\right)} \qquad [2.4]$$

NMR Experiments. ^{15}N-labeled hisactophilin was prepared by growing *E. coli* in M9 minimal media with $^{15}NH_4Cl$ (Cambridge Isotopes) as the sole nitrogen source as described previously (Houliston, *et al.*, 2002). Resonance assignments were made using 2D homonuclear NOESY and TOCSY as well as 3D ^{15}N-edited HSQC-NOESY and HSQC TOCSY spectra of myristoylated hisactophilin at pH 6.8 (Appendix 2). Assignments for nonmyristoylated hisactophilin were used as a starting point for making assignments of the myristoylated protein, followed by confirmation and extension using standard procedures (Wuthrich, 1986). Assignments were obtained for the α-proton and amide nitrogen/proton resonances of 96 of 118 residues; the majority of unassigned residues are in the loop consisting of residues 25 – 32. ^{1}H spectra for lineshape analysis were acquired at pH 6.1 at temperatures ranging from 1-25˚C. Lineshapes were simulated using the following equations to follow the two-state exchange defined by the equilibrium:

$$Accessible \underset{k_{acc}}{\overset{k_{seq}}{\rightleftharpoons}} Sequestered$$

where k_{seq} and k_{acc} represent the rates of exchange between the sequestered and accessible state. The intensity of the NMR spectrum, I, is fit as a function of frequency, ν, to the following equations as referenced from Duggan and Craik, 1997:

$$I(\nu) = C \frac{\left(H \left(1 + \tau \left(\frac{P_{seq}}{T_{2\,acc}} + \frac{P_{acc}}{T_{2\,seq}} \right) \right) + Q \cdot R \right)}{H^2 + R^2} \qquad [2.5]$$

where C represents an all-purpose scaling factor, P_{seq} and P_{acc} represent the populations of the sequestered and accessible states, respectively, and, T_{2seq} and T_{2acc} represent the transverse relaxation times of the sequestered and accessible states, respectively. H, Q and R represent the following:

$$H = \tau\left(\frac{1}{T_{2acc} \cdot T_{2seq}} - 4\pi \cdot \Delta\nu^2 + \pi^2 \cdot \delta\nu^2 \right) + \frac{P_{acc}}{T_{2acc}} + \frac{P_{seq}}{T_{2seq}}, \qquad [2.6]$$

$$Q = \tau\left(2\pi \cdot \Delta\nu - \pi \cdot \delta\nu\left(P_{acc} - P_{seq}\right)\right), \qquad [2.7]$$

$$R = 2\pi \cdot \Delta\nu\left(1 + \tau\left(\frac{1}{T_{2seq}} + \frac{1}{T_{2acc}}\right)\right) + \pi \cdot \delta\nu \cdot \tau\left(\frac{1}{T_{2seq}} - \frac{1}{T_{2acc}}\right) + \pi \cdot \delta\nu\left(P_{acc} - P_{seq}\right) \qquad [2.8]$$

where,

$$\tau = \frac{P_{acc}}{k_{seq}} = \frac{P_{seq}}{k_{acc}} \quad [2.9]$$

$$\delta\nu = \nu_{acc} - \nu_{seq} \quad [2.10]$$

$$\Delta\nu = \frac{\nu_{acc} + \nu_{seq}}{2} - \nu \quad [2.11]$$

such that ν_{seq} and ν_{acc} represent the limiting frequencies of the sequestered and accessible state, respectively.

Results

pH-dependent increase in protein stability upon myristoylation and the energetics of the myristoyl switch. The equilibrium stabilities of myristoylated and nonmyristoylated hisactophilin were measured by CD- and fluorescence-monitored urea denaturation curves at pH 5.7-9.7. The data can be well fit by a reversible 2-state folding transition between folded (F) and unfolded (U) states of the protein (see SI Methods) to determine the Gibbs free energy of unfolding, $\Delta G_{U\text{-}F}$ (= $G_U - G_F$), and the denaturant-dependence of $\Delta G_{U\text{-}F}$ or *m* value (Fig. 2.1A; Tables 2.S1 and 2.S2). There is good agreement

between fitted values determined by CD and fluorescence, and between equilibrium and kinetic (see below) measurements; this supports the applicability of the 2-state folding model (Fersht, 1999). The lack of observable 3-state behaviour in the equilibrium curves indicates that there is rapid interchange between the two folded states, myr_{seq} and myr_{acc}, which was confirmed by NMR lineshape analysis (Fig. 2.S7C, see below).

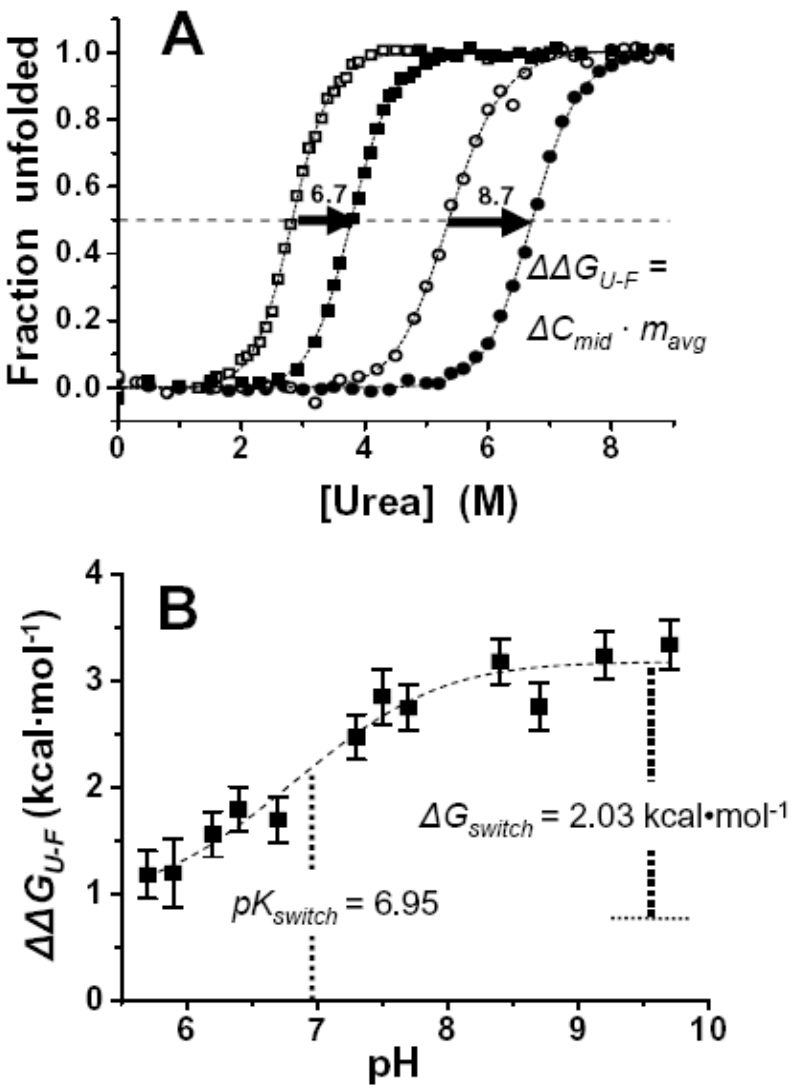

Fig. 2.1. Effects of myristoylation on protein stability. (A) Fluorescence-monitored equilibrium denaturation curves showing fraction of unfolded protein as a function of urea concentration for nonmyristoylated (open symbols) and myristoylated (filled symbols) hisactophilin at pH 6.7 (squares) and pH 8.7 (circles). Dashed lines represent fits of the data using the BEM 2-state model (Liu*, et al.*, 2001). The horizontal dotted line is at the transition midpoint, C_{mid}, where half of the protein is unfolded. (B) $\Delta\Delta G_{U\text{-}F}$ as a function of pH. The magnitude of the change in $\Delta\Delta G_{U\text{-}F}$ at limiting pHs corresponds to the ΔG_{switch} of 2.03 ± 0.17 kcal·mol^{-1} (Figs 2.S1, 2.S2). The pK_{switch} of 6.95 ± 0.15 is the pH at the midpoint of the switch. The dashed line represents the fit of the data to Eq. 2.1.

Myristoylated hisactophilin is more stable than the nonmyristoylated protein at all pHs (Fig. 2.1). Notably, the increase in stability upon myristoylation, $\Delta\Delta G_{U\text{-}F}$ (= $\Delta G_{U\text{-}F,myr} - \Delta G_{U\text{-}F,nonmyr}$), varies significantly with pH in the physiological range, from 3.15 kcal·mol^{-1} to 1.13 kcal·mol^{-1}, corresponding to predominantly myr_{seq} at high pH and myr_{acc} at low pH, respectively. These changes in energetics can be interpreted using thermodynamic cycles (Fig. 2.S1 and SI Results) (Hanakam*, et al.*, 1996). The pH-dependence of $\Delta\Delta G_{U\text{-}F}$ fits an apparent pK_{switch} of 6.95 ± 0.15 (Eq. 2.1, Fig. 2.1B), and has an apparent switch energy for flipping from the sequestered to the accessible state, ΔG_{switch} (= $\Delta\Delta G_{U\text{-}F,low\ pH} - \Delta\Delta G_{U\text{-}F,high\ pH}$), of 2.03 ± 0.17 kcal·mol^{-1} (Eq. 2.1, Fig. 2.1B). The pK_{switch} is in the typical range of pK_a values for histidine residues in proteins, further supporting involvement of these residues in controlling the switch (Hammond*, et al.*, 1998), which is also supported by NMR data (see below).

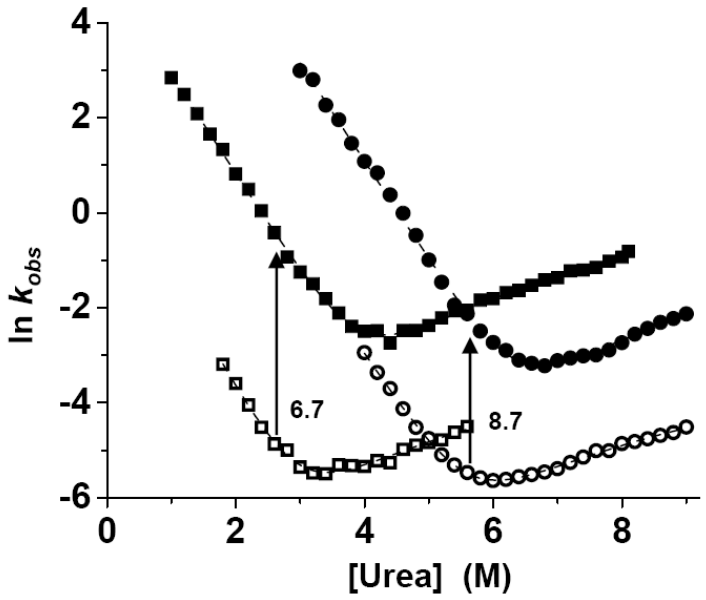

Fig. 2.2. Chevron plots of the natural logarithm of the observed rate constants, k_{obs}, as a function of urea concentration. For nonmyristoylated (open symbols) and myristoylated (closed symbols) hisactophilin at pH 6.7 (squares) and pH 8.7 (circles). Dashed lines represent fits of the data to a 2-state binomial extrapolation model (Wong*, et al.*, 2004) and fitted values are given in Table 2.S1.

The pH-dependence of $\Delta\Delta G_{U\text{-}F}$ can also be fit in terms of the number of ionizable groups involved in controlling the switch and the associated pK_a values in the myr_{seq} and myr_{acc} states (Cho*, et al.*, 2004) (Figs 2.1B and 2.S1). This fitting reveals that the apparent pK_a of ionizable groups increases from $pK_{a,seq}$ of ~6-6.5 to $pK_{a,acc}$ ~7.6-7.0 when the myristoyl group switches from myr_{seq} to myr_{acc}, respectively. This means that decreasing pH favours increased population of myr_{acc} because this state more readily binds protons owing to its higher pK_a value (Figs 2.S1 and 2.S2). There is a net uptake of ~1.5 protons associated with the switch from myr_{seq} to myr_{acc} and the quality of the fits is slightly better for smaller numbers of ionizable groups (Fig. 2.S2, SI Results).

Myristoylation stabilizes the transition state of folding and increases global dynamics. The kinetics of protein folding and unfolding for myristoylated and nonmyristoylated hisactophilin were also measured at various pHs (Fig. 2.2, Table 2.S1), and these data are also well fit by the 2-state model. Surprisingly, despite its higher stability, myristoylated hisactophilin unfolds ~10 times faster than the nonmyristoylated protein, at all pHs. However, the folding rates are also increased within error, to a larger extent than the unfolding rates, resulting in increased stability. The effects of myristoylation on protein energetics can be understood using free energy diagrams and Φ-value analysis (Fersht, 1999) (Fig. 2.3). Φ is defined as $\Delta\Delta G_{\ddagger\text{-}U} / \Delta\Delta G_{F\text{-}U}$, where $\Delta\Delta G_{\ddagger\text{-}U}$ and $\Delta\Delta G_{F\text{-}U}$ represent the free energy change upon myristoylation (analogous to mutation) of the transition state and folded state, respectively, relative to the unfolded state. Classical Φ-values range from 0 to 1, corresponding to the energetic effects of the myristoyl group in the transition state being the same as in the folded state or unfolded state, respectively. Strikingly, the Φ-value for myristoylation is larger than 1. This unusual, non-classical Φ-value suggests that the myristoyl group stabilizes the transition state more than the folded and unfolded states (Fig. 2.3) (Li*, et al.*, 2000).

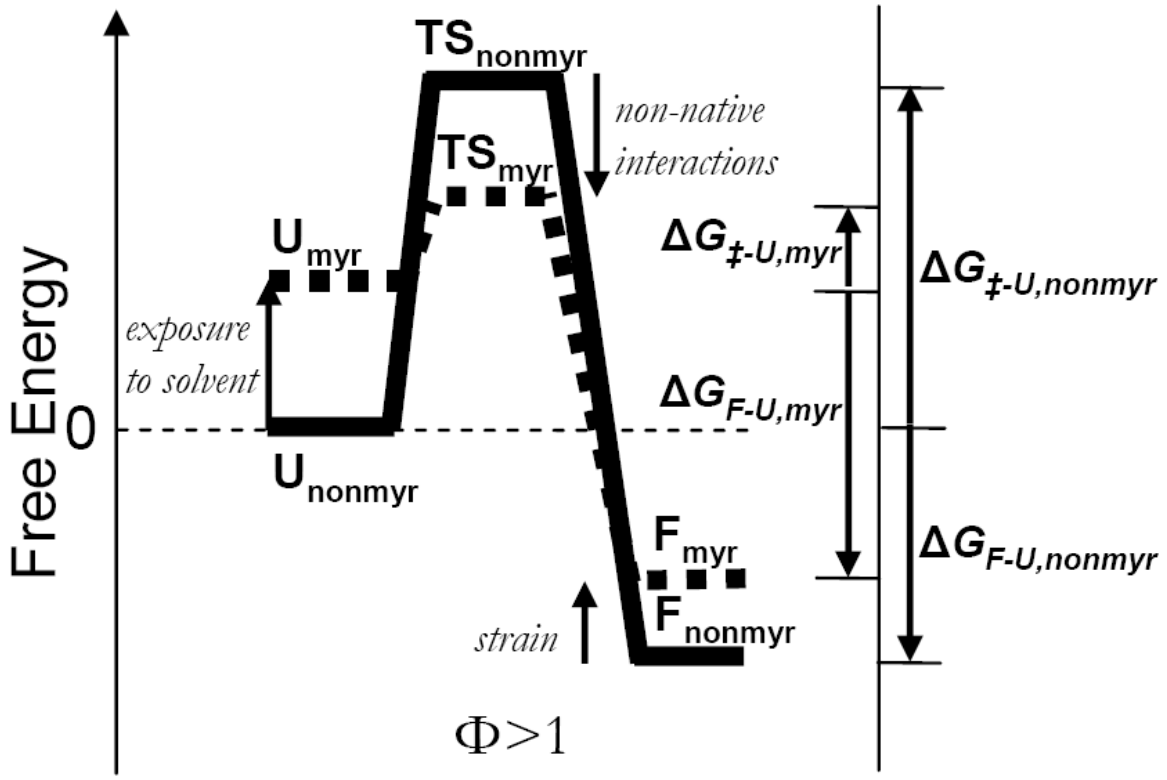

Fig. 2.3. Gibbs free energy diagram for myristoylated (--) and nonmyristoylated (—) hisactophilin. $\Delta G_{\ddagger\text{-}U}$ and $\Delta G_{F\text{-}U}$ represent the measured kinetic folding barriers and free energies of folding, respectively (Fersht, 1999). The free energy of the unfolded state, U, is proposed to be increased upon myristoylation, as generally occurs upon increased exposure of hydrophobic groups to aqueous solution (Tanford, 1978). The free energy of the folded state, F, and transition state, TS, are defined relative to the unfolded state, based on $\Delta G_{F\text{-}U}$ and $\Delta G_{\ddagger\text{-}U}$, respectively. The energies for various states are not drawn to scale, but are consistent with the experimentally determined equilibrium stabilities and kinetic data. Because only relative energy levels can be determined experimentally, the entire profiles for myristoylated and nonmyristoylated hisactophilin may be shifted relative to each other.

Such non-classical Φ-values have often been interpreted as evidence for the formation of non-native interactions in the transition state, which can decrease kinetic energy barriers and so contribute to increased folding and unfolding rates. Additional factors to consider when interpreting energy changes are possible structural reorganization in the protein or solvent. Structural changes in folded hisactophilin appear to be small based on no substantial changes in CD spectrum (Liu*, et al.*, 2001) or protein NOEs upon myristoylation

(*vide infra*). Further details regarding interpretation of energetic changes are considered in the Discussion.

Localization of the myristoyl group in the major hydrophobic core. The structure of myristoylated hisactophilin was investigated as a function of pH using NMR, and compared with data obtained for the nonmyristoylated protein. The myristoyl group exhibits just one set of resonances in NMR spectra (Fig. 2.S3), indicating that exchange between the myr_{seq} and myr_{acc} states is fast on the NMR time scale. A lower limit for the rates of exchange between the myr_{seq} and myr_{acc} states was estimated from lineshape analysis to be on the order of ~1 x 10^5 s^{-1} (Fig. 2.S7C and SI Results). This is consistent with the apparent 2-state transitions in denaturant (Figs 2.1 and 2.2). NOE and chemical shift data show that the myristoyl group is buried in the major hydrophobic core of the protein in the myr_{seq} state. The amide protons of F6, I85, I93 and F113 exhibit NOEs with the terminal methyl of the myristoyl moiety (Figs 2.4A and B). Thus, the myristoyl reaches the interface between the hydrophobic bottom layer of the β-barrel (where F6, I85 and F113 are situated) and the upper β-hairpin layer (where I93 is situated). The observation of the largest chemical shift changes upon myristoylation, $\Delta\delta_{myr}$ (= $\delta_{myr} - \delta_{nonmyr}$), in this region is consistent with the location of the myristoyl group near these residues, although the NOEs for the residues with perturbed chemical shifts are very similar to those in the nonmyristoylated protein, indicating no major structural reorganization. Nevertheless, myristoylation causes extensive chemical shift changes through the protein structure (Figs 2.4C and 2.S4).

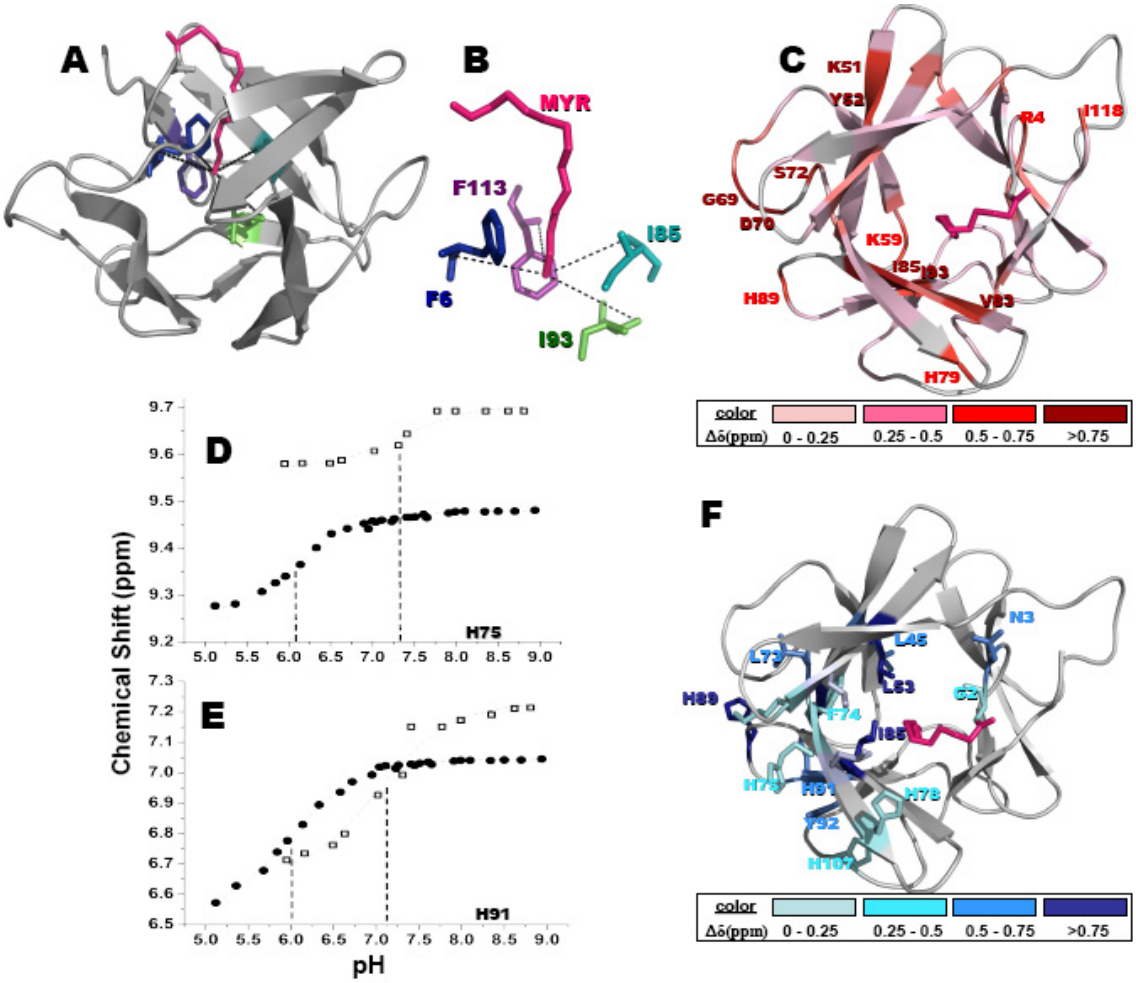

Fig. 2.4. NMR analysis of structure and localization of ionizable groups involved in controlling switching in myristoylated hisactophilin. The structure of the protein was modeled based on the structure of nonmyristoylated hisactophilin (PDB 1HCD) and NOEs observed for the myristoyl group (see SI Results for details). The protein backbone is shown as a ribbon; the myristoyl group (pink) and selected residues are colored (see panel legend) and labeled with single letter code and residue number. (A) The myristoyl group is buried in the hydrophobic core of the protein in the myr_{seq} state. Residues exhibiting NOEs between their amide proton and the terminal methyl of the myristoyl group are shown in stick representation (F6 in blue, I85 in cyan, I93 in green and F113 in purple). (B) Close-up view of myristoyl group illustrating NOEs (dotted lines) from (A). (C) Structure of hisactophilin showing chemical shift changes upon myristoylation, $\Delta\delta_{myr}$ (= $\delta_{myr} - \delta_{nonmyr}$), calculated using Eq. 2.S1 at pH 8.7. (D, E) pH-dependence of chemical shifts for backbone amide ^{1}H resonances of H75 (D) and H91 (E) in nonmyristoylated (□) and myristoylated (●) hisactophilin. Fits of the observed chemical shifts to a single apparent pK_a correspond to those determined from fitting the pH-dependence of $\Delta\Delta G_{U\text{-}F}$ (Fig. 2.S2). Similar pH-dependencies are observed for additional amides in the vicinity of H75 and H91 (Fig. 2.S5), with the magnitude of the chemical shift changes tending to be largest for groups closest to H75 and H91. (F) Structure of hisactophilin color coded according to the magnitude of chemical shift changes associated with a $pK_{a,seq}$ ~6 in myristoylated hisactophilin. The colored amides show a decrease in apparent pK_a from ~7-7.5 to ~6 for ^{1}H and ^{15}N upon myristoylation. $\Delta\delta$ values were calculated similar to previous studies and limiting chemical shift values at low and high pH associated with $pK_{a,seq}$ ~6 (Hammond, *et al.*, 1998).

Role of histidines in flipping the myristoyl switch via proton uptake/release. Further insight into the molecular mechanism of switching was obtained by analyzing the changes in chemical shifts as a function of pH (Figs 2.4D-F). For many NH groups, the apparent pK_a values for pH-dependent changes in chemical shift change from pH~7-7.5 in nonmyristoylated hisactophilin to ~6 in the myristoylated protein (Figs 2.4D, E). These apparent pK_a values are very similar to the values of $pK_{a,acc}$ and $pK_{a,seq}$ for the ionizable groups that govern switching obtained from fitting the pH-dependence of $\Delta\Delta G_{U\text{-}F}$ (Fig. 2.S2). A prominent group of such NHs is clustered on one side of the protein (Fig. 2.4F) in the vicinity of various ionizable groups, including H75 (Fig. 2.4D), H91 (Fig. 2.4E), H78 and H107 (Fig. 2.4F). It is not possible from the available data to determine the exact contributions of each of these groups to switching (see SI Results); however, H75 and H91 are likely to play significant roles since the largest changes in chemical shift occur near these residues. Further inspection of the pattern of chemical shift changes reveals a likely pathway for communication between the ionizable groups and the myristoyl group via hydrophobic residues (L45, L53, F74, I85) that pack near the myristoyl group in the protein core (Fig. 2.4F). Thus, the combined results from fitting the pH-dependence of the switch energetics and the pH-dependence of chemical shift changes provides an intriguing model for the molecular basis of the pH-dependence of the myristoyl switch controlled by histidine ionizations and propagated by hydrophobic residues.

Supplementary Results

Analysis of switch energetics using thermodynamic cycles. The pH-dependence of $\Delta\Delta G_{U\text{-}F}$ can be understood using thermodynamic cycles (Fig. 2.S1) (Fersht, 1999). $\Delta\Delta G_{U\text{-}F}$ is the change in the Gibbs free energy of unfolding upon myristoylation:

$$\Delta\Delta G_{U-F} = \Delta G_{U-F,myr} - \Delta G_{U-F,nonmyr} \quad [2.S1]$$

where the subscripts myr and nonmyr represent myristoylated and nonmyristoylated hisactophilin, respectively. $\Delta\Delta G_{U\text{-}F}$ varies with pH from 3.15 kcal·mol^{-1} at high pH where the myristoyl group is sequestered inside the protein (myr_{seq}) to 1.13 kcal·mol^{-1} at lower pH where the myristoyl group is accessible (myr_{acc}). The apparent free energy change for switching from the sequestered to the accessible state for the myristoylated protein relative to the nonmyristoylated protein, ΔG_{switch}, can be expressed in terms of the change in $\Delta\Delta G_{U\text{-}F}$ from low to high pH:

$$\Delta G_{switch} = \Delta\Delta G_{U-F,highpH} - \Delta\Delta G_{U-F,lowpH} \quad [2.S2]$$

Substituting Eq. 2.S1 into Eq. 2.S2 gives (Fig. 2.S1):

$$\Delta G_{switch} = \Delta G_{U-F,myr,highpH} - \Delta G_{U-F,nonmyr,highpH} - \left(\Delta G_{U-F,myr,lowpH} - \Delta G_{U-F,nonmyr,lowpH}\right) \quad [2.S3]$$

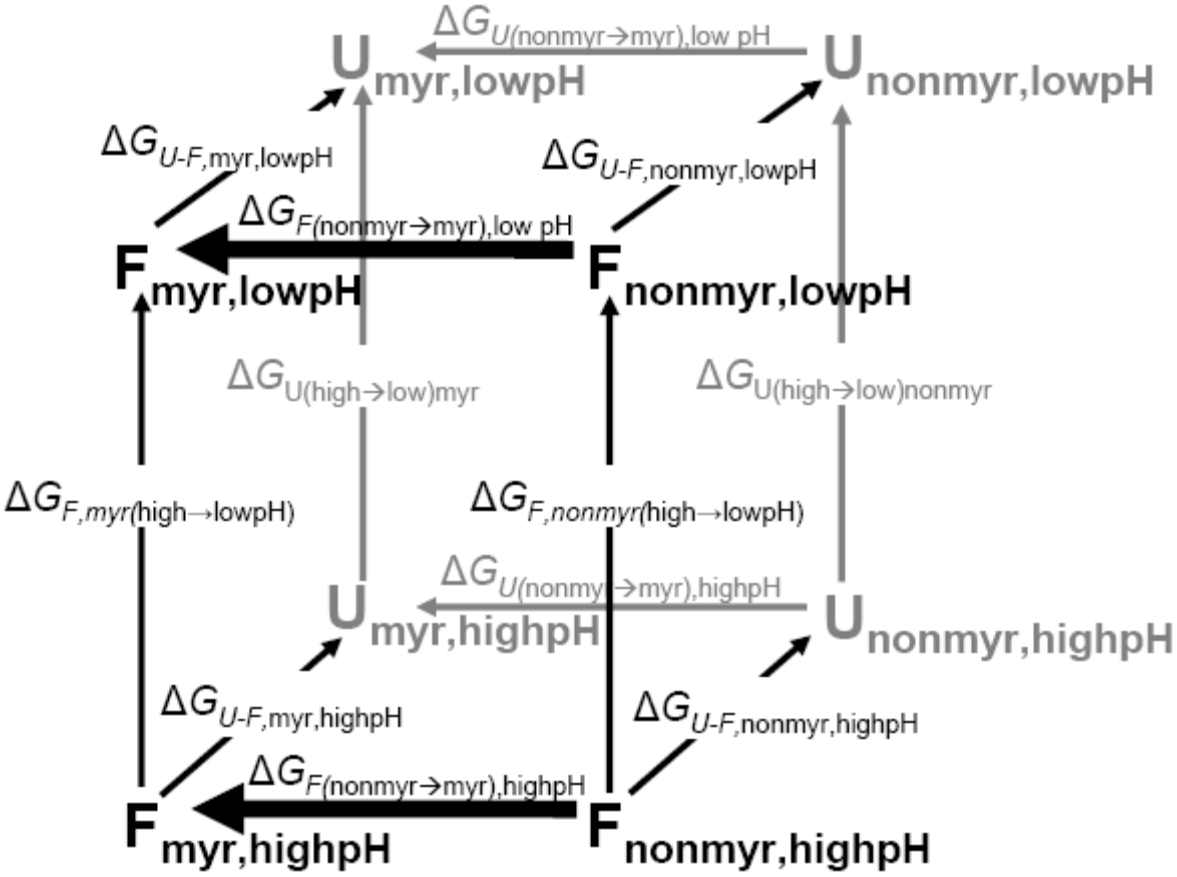

Fig. 2.S1. Thermodynamic cycles for measuring ΔG_{switch}. Arrows define the direction from initial to final states. Each arrow is associated with a change in Gibbs free energy (ΔG) that is defined with a subscript. *U* and *F* refer to the unfolded and folded protein, respectively, subscripts lowpH and highpH represent terms corresponding to myr_{acc} and myr_{seq} states, respectively, and subscripts myr and nonmyr represent the myristoylated and nonmyristoylated forms of hisactophilin, respectively. The derivation for ΔG_{switch} is analogous to the coupling energy derivation described by Fersht (Fersht, 1999). ΔG_{switch} is defined as $\Delta G_{switch} = \Delta G_{F(\text{nonmyr}\rightarrow\text{myr})\text{low pH}} - \Delta G_{F(\text{nonmyr}\rightarrow\text{myr})\text{highpH}} = \Delta G_{F,\text{myr}(\text{high}\rightarrow\text{lowpH})} - \Delta G_{F,\text{nonmyr}(\text{high}\rightarrow\text{lowpH})} = \Delta G_{U\text{-}F,\text{myr,lowpH}} - \Delta G_{U\text{-}F,\text{nonmyr,lowpH}} - (\Delta G_{U\text{-}F,,\text{myr,highpH}} - \Delta G_{U\text{-}F,,\text{nonmyr,highpH}})]$, assuming $\Delta G_{U(\text{high}\rightarrow\text{low})\text{myr}} = \Delta G_{U(\text{high}\rightarrow\text{low})\text{nonmyr}}$, i.e. myristoylation has no effect on the pH-dependence of the free energy of the unfolded state and so these terms cancel out. Bold arrows illustrate $\Delta G_{F(\text{nonmyr}\rightarrow\text{myr})\text{low pH}}$ and $\Delta G_{F(\text{nonmyr}\rightarrow\text{myr})\text{highpH}}$

We assume that the change in the free energy of the unfolded state with pH is not altered upon myristoylation, i.e. $\Delta G_{U\,(\text{low}\rightarrow\text{high})\text{myr}} = G_{U\,\text{high,myr}} - G_{U\,\text{low,myr}} = \Delta G_{U\,(\text{low}\rightarrow\text{high})\text{nonmyr}} = G_{U\,\text{high,nonmyr}} - G_{U\,\text{low,nonmyr}}$, excluding energy contributions for the free amino terminal group in the nonmyristoylated protein, which is not present in the myristoylated protein. In addition, we assume that the contribution of the amino terminal ionizable group does not contribute to protein stability because it is highly exposed to solvent in the folded protein (Fersht, 1999, Habazettl*, et al.*, 1992). Thus, the amino terminal group makes the same contributions to pH dependence of the energy for folded and unfolded states of nonmyristoylated hisactophilin, and these terms cancel out in the analysis. These are reasonable assumptions because the stability and kinetics are the same for the nonmyristoylated hisactophilin characterized herein and another nonmyristoylated variant hisactophilin containing 4 additional random coil residues, GEFG, at the N-terminus (Habazettl*, et al.*, 1992, Wong*, et al.*, 2004) (Table 2.S1). Using the above assumptions, Eq. S2.3 can be simplified as:

$$\Delta G_{switch} = \Delta G_{F,myr(high\rightarrow lowpH)} - \Delta G_{F,nonmuyr(high\rightarrow lowpH)} = \Delta G_{F(nonmyr\rightarrow myr)lowpH} - \Delta G_{F(nonmyr\rightarrow myr)highpH} \qquad [2.S4]$$

Thus, ΔG_{switch} can be interpreted as the coupling energy between the myristoyl group and the sites of protonation involved in switching from the sequestered to the accessible state with decreasing pH for the myristoylated protein relative to the nonmyristoylated protein (Fersht, 1999). Note that the myristoyl group and protonation sites need not interact directly, but may

be coupled indirectly through the protein structure (Horovitz and Fersht, 1990). The switch energy includes various contributions from inter- and intramolecular interactions, including energy terms due to ionization as well as interactions associated with changes in the myristoyl group environment.

Table 2.S1. Thermodynamic parameters for myristoylated and nonmyristoylated hisactophilin

		Myristoylated Hisactophilin							Non-myristoylated Hisactophilin						
pH	**Kinetic/**	C_{mid}	m_1[¶]	$\Delta G_{U\text{-}F}$[¶]	k_u	k_f	$m_{u‡}$	$m_{f‡}$	C_{mid}	m_1[¶]	$\Delta G_{U\text{-}F}$[¶]	k_u	k_f	m_u[§]	m_f[‡]
	Equilibrium	(M)	(kcal·mol^{-1}·M^{-1})	(kcal·mol^{-1})	(s^{-1}x10^{-5})	(s^{-1} x10^{3})	(s^{-1}·M^{-1})	(s^{-1}·M^{-1})	(M)	(kcal·mol^{-1}·M^{-1})	(kcal·mol^{-1})	(s^{-1}x10^{-5})	(s^{-1})	(s^{-1}·M^{-1})	(s^{-1}·M^{-1})
5.7	equilibrium	1.44 ± .07	2.34 ± .22	3.22 ± .38	-------	-------	-------	-------	.91 ± .03	2.63 ± .29	2.34 = .29	-------	-------	-------	-------
5.9	equilibrium	2.05 ± .23	2.40 ± .17	4.85 ± .42	-------	-------	-------	-------	1.49 ± .06	2.20 ± .24	3.09 = .83	-------	-------	-------	-------
6.2	equilibrium	2.62 + .41	2.43 + .13	6.62 + .41	-------	-------	-------	-------	2.27 + .03	2.64 + .05	5.67 − .76	-------	-------	-------	-------
6.4	equilibrium	3.69 ± .03	2.09 ±.11	6.78 ± .42	-------	-------	-------	-------	2.85 ± .02	2.32 ± .12	6.03 ±.36	-------	-------	-------	-------
6.7	equilibrium	3.71 ± .02	2.19 ± .11	7.19 ± .43	-------	-------	-------	-------	2.89 ± .03	2.43 ± .21	6.39 = .67	-------	-------	-------	-------
6.7	kinetics	3.90 ± .22	1.91 ± .007	6.75 ± .22	201 ± 9	.180 ± 006	.607 ± .01	-1.30 ± .001	2.93 ± .30	1.91 ± .071	5.59 = .29	16.0 ± 4.00	2.03 ± 0.797	.607 ± .019	-1.30 ± .07
7.3	equilibrium	5.11 ± .02	2.31 ± .16	9.92 ± .82	-------	-------	-------	-------	3.93 ± .02	2.31 ± .11	7.98 = .45	-------	-------	-------	-------
7.5	equilibrium	5.30 ± .06	2.06 ± .16	8.93 ±.96	-------	-------	-------	-------	3.96 ± .13	3.32 ± .39	7.88 ± 1.52	-------	-------	-------	-------
7.6	equilibrium	5.53 ± .04	1.97 ± .08	8.76 ± .40	-------	-------	-------	-------	3.86 ± .06	1.83 ± .03	8.40 = .92	-------	-------	-------	-------
7.7	equilibrium	5.68 ± .03	2.30 ± .12	11.34 ± .67	-------	-------	-------	-------	4.38 ± .02	2.18 ± .11	8.16 = .32	-------	-------	-------	-------
7.7	kinetics	5.65 ± .13	1.87 ± .063	9.53 ± 1.1	13.0 ± 4	1.27 ± .098	.684 ± .054	-1.18 ± .015	4.68 ± .15	1.87 ± .027	8.25 = .15	2.00 ± .380	22.5 ±2.13	.684 ± .011	-1.18 ± .01
8.4	equilibrium	6.14 ± .03	2.22 ± .18	10.96 ± 1.07	-------	-------	-------	-------	4.64 ± .02	2.13 ± .11	8.37 = .53	-------	-------	-------	-------
8.7	equilibrium	6.72 ± .02	2.47 ± .21	13.44 ± 1.38	-------	-------	-------	-------	5.38 ± .07	2.20 ± .27	9.45 ± 1.24	-------	-------	-------	-------
8.7	kinetics	6.83 ± .17	1.96 ± .032	11.65 ± .3	.200 ± .091	6.99 ± .466	.820 ± .027	-1.13 ± .012	5.59 ± .17	1.95 ± .029	10.44 ± .16	.254 ± .100	116 ±19.4	.820 = .01	-1.13 ± .02
9.2	equilibrium	6.57 ± .04	2.43 ± .34	12.93 ± 2.25	-------	-------	-------	-------	5.04 ± .06	2.39 ± .55	10.21 = 2.75	-------	-------	-------	-------
9.7	equilibrium	6.44 ± .06	2.12 ± .19	11.52 ± 1.18	-------	-------	-------	-------	4.77 ± .07	2.17 ± .35	8.99 ± 1.77	-------	-------	-------	-------

*errors reported are s.d.
†equilibrium values were fit using a binomial extrapolation with $m_2 = 0.072$.
‡kinetic data were also fit using the binomial extrapolation with $m_{2rel} = 0$ and $m_{2unf} = 0.028$.
§protein concentrations were all ~0.3mg/mL.
¶$\Delta G_{U\text{-}F}$ were calculated as described in the Methods section.

Table 2.S2. Comparison of CD and fluorescence data

pH	$C_{mid,CD}$ (M)	$C_{mid,Fl}$ (M)	m_{1CD}†† (kcal·mol^{-1}·M^{-1})	m_{1Fl}†† (kcal·mol^{-1}·M^{-1})	$\Delta G_{U\text{-}F,\ CD}$‡‡ (kcal·mol^{-1})	$\Delta G_{U\text{-}F\ ,Fl}$‡‡ (kcal·mol^{-1})
5.7	1.53±.03	1.44±.07	2.63±.19	2.34 ± .22	3.86 ± .35	3.22 ± .38
5.9	2.07 ± .05	2.05± .23	2.42 ± .15	2.40 ± .17	4.88 ± .32	4.85 ± .42
6.7	3.66 ± .02	3.71± .02	2.69 ± .19	2.19 ± .11	8.30 ± .83	7.19 ± .43
7.7	5.66± .03	5.68± .03	2.23 ± .11	2.30 ± .12	10.35± .58	11.34± .67
9.2	6.64± .04	6.57± .04	2.28 ± .23	2.43 ± .34	13.01± 3.73	12.93 ± 2.25

**errors reported are standard deviation.
††equilibrium values were fit using a binomial extrapolation with $m_2 = 0.072$.
‡‡$\Delta G_{U\text{-}F}$ values were calculated as described in the Methods section.

Fitting the pH-dependence of stability changes to a pKa-change model.

Changes in protein stability as a function of pH can be expressed in terms of the Wyman linkage equation:

$$\frac{d}{dpH}\left(\Delta G_{U-F}\right) = 2.303 \cdot R \cdot T \cdot \left[Q_U\left(pH\right) - Q_F\left(pH\right)\right] \qquad [2.S5]$$

where $Q_U(pH)$ and $Q_F(pH)$ represent the number of protons bound at a given pH to the unfolded and folded protein, respectively, and R and T are the universal gas constant and temperature (in K), respectively (Cho*, et al.*, 2004, Tanford, 1968). For hisactophilin, an analogous equation for the pH-dependence of $\Delta\Delta G_{U\text{-}F}$ can be written in terms of the number of protons bound to the accessible ($Q_{acc}(pH)$) and sequestered ($Q_{seq}(pH)$) states, which may be expressed in terms of the pK_a of residues affected by myristoyl switching, using the nonmyristoylated protein as a reference:

$$\frac{d}{dpH}\left(\Delta\Delta G_{U-F}\right) = 2.303 \cdot R \cdot T \cdot \left[Q_{acc}\left(pH\right) - Q_{seq}\left(pH\right)\right] \quad + \quad C \qquad [2.S6]$$

The constant, *C*, represents the effect of myristoylation on stability at limiting low pH. Integration of Eq. S2.6 from a reference pH (pH =1) chosen outside the range of the myristoyl switch gives:

$$\Delta\Delta G_{U-F}\left(pH\right) = -R \cdot T \cdot n \cdot \ln\left(\frac{(1+10^{pH-pKa,acc}) \cdot (1+10^{1-pKa,seq})}{(1+10^{1-pKa,acc}) \cdot (1+10^{pH-pKa,seq})}\right) \quad + \quad C \qquad [2.S7]$$

where *n* represents the number of ionizable groups whose apparent pK_a values are perturbed upon myristoyl switching and $pK_{a,acc}$ and $pK_{a,seq}$ represent the average apparent pK_a values for these groups in the myr_{acc} and myr_{seq} states, respectively. This derivation assumes that perturbations occur only in folded and not in unfolded hisactophilin. This is supported by differences in the pH-dependence of membrane binding measured for folded myristoylated and nonmyristoylated hisactophilin (Hanakam*, et al.*, 1996), and the reasonable assumption that there are no residual interactions of the myristoyl group in the unfolded protein that alter pK_a values. Also, comparison of the two nonmyristoylated constructs (the construct used herein of the wild type sequence, and the construct with additional GEFG, at the N-terminus (Habazettl*, et al.*, 1992, Wong*, et al.*, 2004)) shows that the N-terminal amino group does not contribute to myristoyl switching (see above). In addition, isoelectric focusing shows that the pI of hisactophilin changes very little (~0.1 pH unit) upon myristoylation or addition of four N-terminal amino acids (Fig. 2.S2C). The addition of GEFG to the N-terminus changes

the pI in a similar way as the myristoyl group but does not affect the pH-dependence of global protein stability. This suggests that the measured pH-dependence of $\Delta\Delta G_{U\text{-}F}$ is not caused by global changes in pI upon myristoylation but rather arises from changes in pK_a of specific residues accompanying switching from the myr_{acc} to the myr_{seq} state.

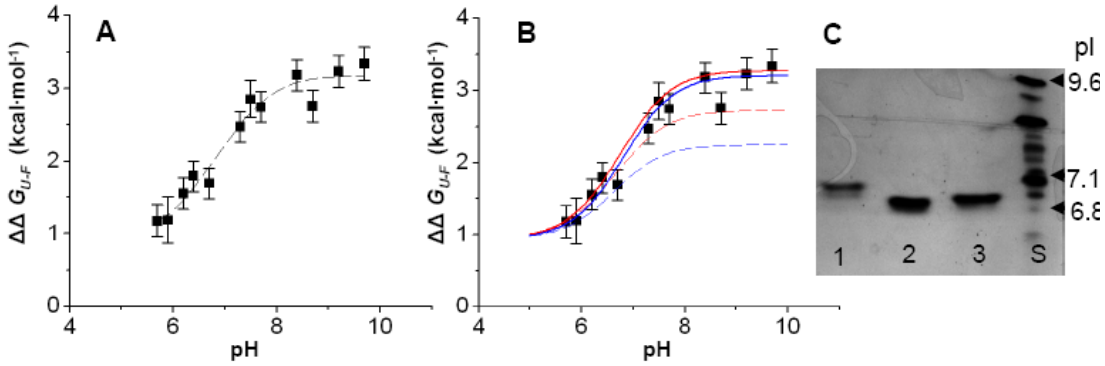

n	1	2	5	15	31
$pK_{a,acc}$	7.66	7.31	7.10	7.00	6.98
$pK_{a,seq}$	6.04	6.55	6.80	6.90	6.93
$\Delta pK_{a(seq-acc)}$	-1.62	-0.74	-0.30	-0.10	-0.05
C (kcal·mol^{-1})	0.96	1.09	1.13	1.13	1.13
χ^2	0.034	0.035	0.036	0.036	0.036
H^+ uptake/release	1.62	1.51	1.49	1.47	1.45

Fig. 2.S2. Change in stability upon myristoylation as a function of pH fit to pK_a-change model. (A) In the graph, the dashed line represents the fit of the data to Eq. 2.S7, allowing all parameters (*n*, $pK_{a,acc}$, $pK_{a,seq}$) to vary. This converged to a best-fit *n*-value of 0.98 ± 0.68 (error estimate is from the fitting program, Origin 5.0). Integration of the curve gives the total number of protons involved in the switch, ~1.5. The data were also fit by fixing *n* to various values, with the values for the remaining fitted parameters summarized in the table. For these, the fitted lines for different values of *n* are extremely similar visually. As *n* increases, the differences in pK_a of the ionizable groups, $\Delta pK_{a(seq-acc)}$, decreases and the χ^2 increases slightly, suggesting that a small number of ionizable groups controls the switch. (B) Based on analysis of the pH-dependence of chemical shift changes (Figs 2.4D-F), data were also simulated assuming only two independent ionizable groups controlling the switch using Eq. 2.S8. Values of $pK_{a,acc}$ and $pK_{a,seq}$ for one group were fixed to 6.1 and 7.1 (corresponding to the data for H91 in Fig. 2.4E) and the corresponding values for the second ionizable group were allowed to vary. This gave fitted values for the second $pK_{a,acc}$ and $pK_{a,seq}$ of 7.4 and 6.7, respectively (solid red line). When values for $pK_{a,acc}$ and $pK_{a,seq}$ were fixed to 6.0 and 7.3 (based on data for H75 in Fig. 2.4D), this gave values of $pK_{a,acc}$ and $pK_{a,seq}$ for the second ionizable group of 7.2 and 6.8, respectively (solid blue line). Dashed lines show data simulations assuming a single ionizable group with $pK_{a,acc}$ and $pK_{a,seq}$ corresponding to the values for H91 (blue) or H75 (red). (C) IEF gel electrophoresis of hisactophilin variants. Lane 1 contains nonmyristoylated wild-type hisactophilin, lane 2 contains myristoylated myristoylated hisactophilin and lane 3 contains nonmyristoylated hisactophilin with additional N-terminal GEFG residues. Lane S contains protein standards with pI values labeled. Weak bands at slightly lower pI values for hisactophilin samples correspond to hisactophilin dimers, likely formed by oxidation of Cys 49 during electrophoresis. Dimerization does not affect the stability of hisactophilin (Liu, *et al.*, 2001).

Fitting of the pH-dependence of $\Delta\Delta G_{U\text{-}F}$ to Eq. S2.7 indicates that the total number of protons taken up upon switching is ~1.5 (Fig. 2.S2). However, the exact number of histidines involved in taking up these protons is not well defined by the data. The quality of the fit is slightly better for low values of *n* based on χ^2 values. The data can alternatively be fit in terms of two histidines with different values of $pK_{a,acc}$ and $pK_{a,seq}$ according to:

$$\Delta\Delta G_{U-F}(pH) = -R \cdot T \cdot \sum_{n=1}^{2} \ln\left(\frac{(1+10^{pH-pKa,acc(n)}) \cdot (1+10^{1-pKa,seq(n)})}{(1+10^{1-pKa,acc(n)}) \cdot (1+10^{pH-pKa,seq(n)})} \right) \quad + \quad C$$

[2.S8]

where *n* represents the index of the ionizable group. The fits did not converge when all parameters were allowed to vary. However, by fixing values of $pK_{a,acc}$ and $pK_{a,seq}$ for one ionizable group based on apparent pK_a values observed by NMR (e.g. for H91 and H75, see main text, Figs 2.S4D, E and following section), values of $pK_{a,acc}$ and $pK_{a,seq}$ could be fit for the second ionisable group, and the fitted lines accounted well for the observed data; the data were not well fit by a single ionizable group (Fig. 2.S2B). These results show that a single ionizable group with $pK_{a,acc}$ and $pK_{a,seq}$ corresponding to apparent pK_a values observed in the NMR data can account for most but not all of the observed pH dependence of $\Delta\Delta G_{U\text{-}F}$. The data can be well fit using just 2 ionizable groups with $pK_{a,acc}$ and $pK_{a,seq}$ in the range of values observed in the NMR data. This does not exclude that more than 2 ionizable groups may be involved, but it supports the conclusion that at least one histidine with a $pK_{a,seq}$ value of ~6 (see also Fig. 2.S5) and a higher value of $pK_{a,acc}$ of ~7 likely plays a key role in

switching. The identity of the ionizable groups involved in switching was further investigated from the patterns in observed chemical shift changes, described below.

NMR data analyses. *Chemical shift changes upon myristoylation*. There are extensive chemical shift changes upon myristoylation ($\Delta\delta_{myr}$). This is illustrated in the 1D ^{1}H spectrum in the changes observed for various downfield amide resonances that are well resolved in the spectrum of nonmyristoylated hisactophilin but not in the spectrum of the myristoylated protein (Fig. 2.S3A). Another obvious change is an additional peak in the upfield region of the spectrum for myristoylated hisactophilin (Fig. 2.S3A). The chemical shift for I85 δCH_3 is -0.800 ppm and -0.732 ppm in nonmyristoylated and myristoylated hisactophilin, respectively, and there is a new peak for the latter at -0.824 ppm, corresponding to the terminal CH_3 of the myristoyl group (2.S3B and C). The upfield shift for the myristoyl resonance likely occurs due to the close proximity of the terminal methyl to the aromatic rings of F6 and F113 in the model of myristoylated hisactophilin (Figs 2.4A, B, see also below). The myristoyl methyl chemical shift was observed to change from pH 7.7 to pH 5.7, where the myristoyl resonance becomes overlapped with other peaks (Fig. 2.S7B).

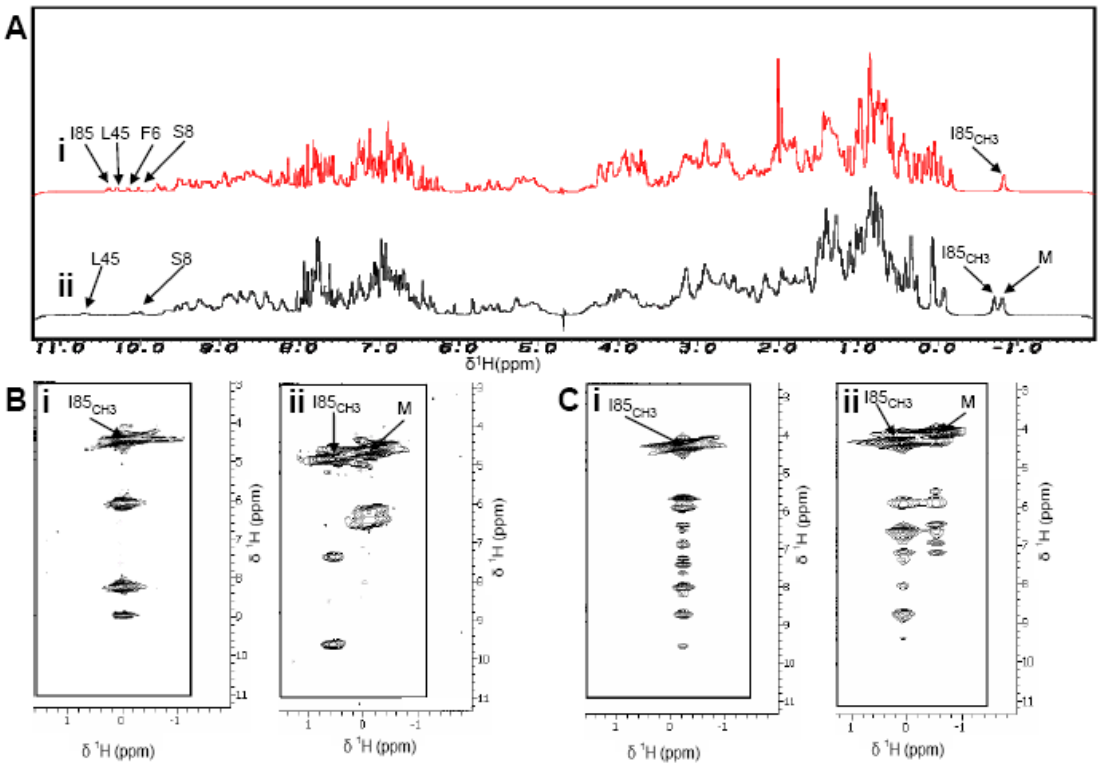

Fig. 2.S3. NMR spectral changes upon myristoylation. Spectra in A, B and C show corresponding regions for nonmyristoylated (i) and myristoylated (ii) hisactophilin. M indicates the resonance for the terminal methyl of the myristoyl group and $I85_{CH3}$ indicates the resonance for the δCH_3 of I85. (A) 1D ^1H spectra. Various residues exhibiting significant changes (F6, S8, L45, I85) are labeled. (B) 2D ^1H-^1H TOCSY and (C) 2D ^1H-^1H NOESY strips, showing new peaks observed for the terminal methyl of the myristoyl.

This pH-dependence most likely reflects a combination of the myristoyl switch and $pK_{a,seq}$ of ~6 (see main text). A single peak was observed for the myristoyl group at all pHs at 25°C, indicating fast exchange between myr_{seq} and myr_{acc} states. Evidence of line broadening was observed at lower temperatures, where rates were slowed to the intermediate exchange rate regime (see below).

Model of myristoylated hisactophilin. The position of the sequestered myristoyl group in the hisactophilin core was modelled based on the NMR structure of nonmyristoylated protein (PDB code 1HCD) since no substantial changes in NOEs were observed in ^{15}N-edited NOESY-HSQC spectra upon myristoylation. Using the UCSF program Chimera (Pettersen*, et al.*, 2004), the myristoyl group was modelled into the core of the structure of nonmyristoylated hisactophilin using the observed NOEs between the myristoyl methyl group and the amide protons of F6, I85, I93 and F113 as distance restraints. Subsequently, using the NAMD and VMD software, the structure was energy minimized and then subjected to a brief molecular mechanics simulation using the CHARMM force field to reduce steric clashes (Humphrey*, et al.*, 1996, Phillips*, et al.*, 2005).

Identification of ionizable groups that control the myristoyl switch from changes in chemical shift as a function of pH. Chemical shifts are sensitive to changes in electrostatic environment caused by pH (Wuthrich, 1986). Thus, amide groups in close proximity to an ionizable group can exhibit pH-dependent changes in chemical shift that reflect the pK_a of that ionizable group. If a given amide group is in rapid exchange on the NMR timescale between states that differ in electrostatic environment (i.e. myr_{seq} and myr_{acc} states, in which ionizable groups have different apparent pK_a values and hence different partial charges), its

observed chemical shift will be a population weighted average of its chemical shifts in the different states (Cavanagh, 2007, Korzhnev, *et al.*, 2004). We focus here on identifying ionizable groups exhibiting pK_a changes that could account for the fits of the pH-dependence of the switch energetic (Fig. 2.S2).

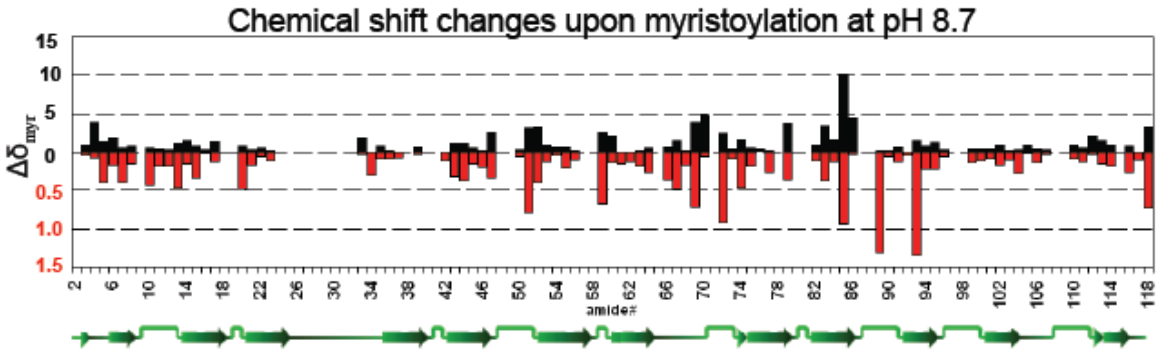

Fig. 2.S4. Absolute value of changes in chemical shift, Δδ, upon myristoylation for ^{1}H (red) and ^{15}N (black) of backbone amide groups *versus* residue number at pH 8.7. The protein secondary structure is shown below the graphs as a green ribbon with β-strands shown as arrows.

These may be expected to exhibit $pK_{a,acc}$ of ~7-7.5 and $pK_{a,seq}$ of ~6 in the myr_{acc} and myr_{seq} states, respectively (Figs 2.S2, 2.4F and 2.S5). Nonmyristoylated hisactophilin is a model of the myr_{acc} state (see above); in which ionizable groups involved in the switch will exhibit $pK_{a,acc}$. In myristoylated hisactophilin, both $pK_{a,acc}$ and $pK_{a,seq}$ may contribute to the observed pH-dependence, with the observed overall behaviour depending on the magnitude of the chemical shift changes associated with each pK_a. Although the population of certain states may be low, e.g. <5%, they may still be identified by NMR if they undergo relatively large chemical shift changes. This is similar to the observation of "invisible" states with low

population in NMR relaxation dispersion analyses (Neudecker*, et al.*, 2009). The magnitudes of the chemical shift changes caused by changes in charge of ionizable groups involved in switching are likely to be larger in general for the myr_{seq} state if the ionizable group is more buried than in myr_{acc} state where it is more exposed to solvent. Thus, the ionization of important histidines around a $pK_{a,seq}$ of ~6 can still be observed even though the pH is ~1 unit below the pK_{switch} because the myr_{seq} state is sufficiently populated and exhibits sufficiently large chemical shift changes to allow for observation by NMR.

An apparent pK_a of ~6 is observed for a large proportion of amides distributed throughout the protein (Fig. 2.S5A). It should be noted that this is not observed for all amides and many amides exhibit no change in apparent pK_a; these amides tend to be at the periphery of the protein structure, and farthest from the myristoyl group (Fig. 2.S6A). The magnitudes of the chemical shift changes associated with an apparent pK_a of ~6 are largest for amides on one side of the protein structure (Fig. 2.4F) and suggest possible histidine residues that control the switch (see main text). It should be noted that the magnitude and direction of the chemical shift changes is not in general consistent with a shift towards random coil (e.g. H75, H91, or I85 Figs 2.4D,E and 2.S5B) and a similar apparent pK_a is observed for the methyl of the myristoyl group and methyl of I85 (Figs 2.S7A, B).

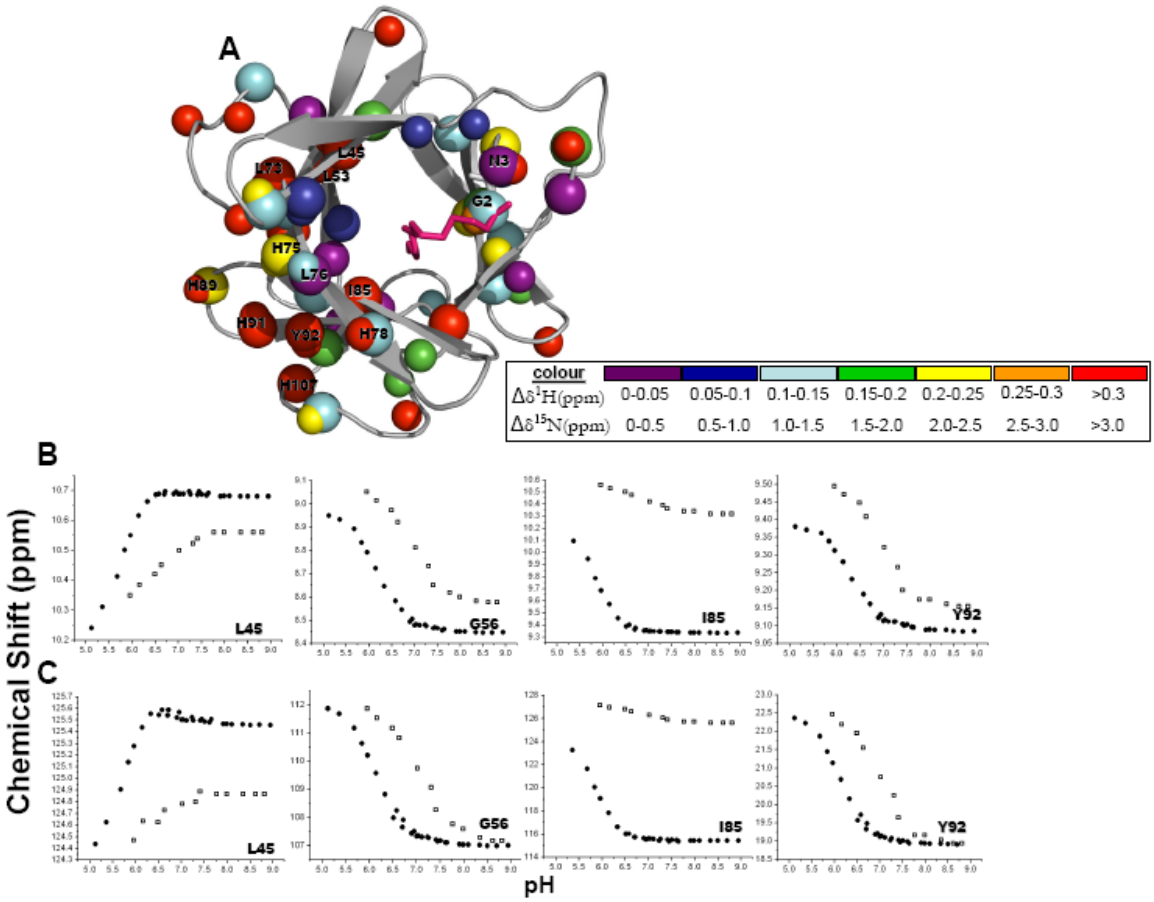

Fig. 2.S5. NH resonances monitored by ^{1}H-^{15}N HSQC that exhibit an apparent pK_{app} value of ~6 in myristoylated hisactophilin. (A) Ribbon diagram of myristoylated hisactophilin showing all ^{15}N and ^{1}H resonances that have a pK_{app} ~6 as spheres, with the myristoyl group (pink) shown in the myr$_{seq}$ conformation. Backbone ^{1}H resonances (small spheres) are colored in a rainbow gradient according to their absolute Δδ values upon myristoylation as: 0-0.05, purple; 0.05-0.1, blue; 0.1-0.15, cyan; 0.15-0.2, green; 0.2-0.25, yellow; 0.25-0.3, orange; >0.3, red. Backbone ^{15}N resonances (large spheres) are colored in a rainbow gradient according to absolute Δδ values as: 0-0.5, purple; 0.5-1.0, blue; 1.0-1.5, cyan; 1.5-2.0, green; 2.0-2.5, yellow; 2.5-3.0, orange; >3.0, red. (B) Representative plots of δ vs. pH for backbone ^{1}H resonances for myristoylated (filled circle) and nonmyristoylated (open square) hisactophilin that show a decrease in pK_{app} from ~7 to ~6 upon myristoylation as also seen for H75 and H91 (Figs 4D, E, main text). Panels are labeled with single residue code and amino acid number. The backbone amide ^{1}H resonances exhibiting pK_{app} ~6 in myristoylated hisactophilin include: G2, K7, H12, F34, V36, K42, V43, G49, L53, S54, G56, L67, H68, H71, F74, H75, H78, I85, H89, H91, Y92, H107, D110 and I118. (C) Representative plots of δ vs. pH plots for backbone ^{15}N resonances for myristoylated (filled circle) and nonmyristoylated (open square) hisactophilin that show a decrease in pK_{app} from ~7 to ~6 upon myristoylation as also seen for H75 and H91 (Figs 2.4D,E, main text). Panels are labeled with single residue code and amino acid number. The backbone amide ^{15}N resonances showing a pK_{app} ~6 include G2, N3, R4, A5, F6, S8, H9, F13, L14, A16, K42, V43, L45, K46, L53, Q60, V61, S64, H66, L73, F74, H75, L76, H78, I85, K86, H89, S94 and I117. The large number of nuclei exhibiting an apparent pK_a of ~6 in myristoylated hisactophilin indicate that protonation of this ionizable group in the myr$_{seq}$ conformation has effects that are felt throughout the structure, likely due to the ionizable group being in a buried hydrophobic environment and/or near positively charged groups (which also decreases its apparent pK_a value).

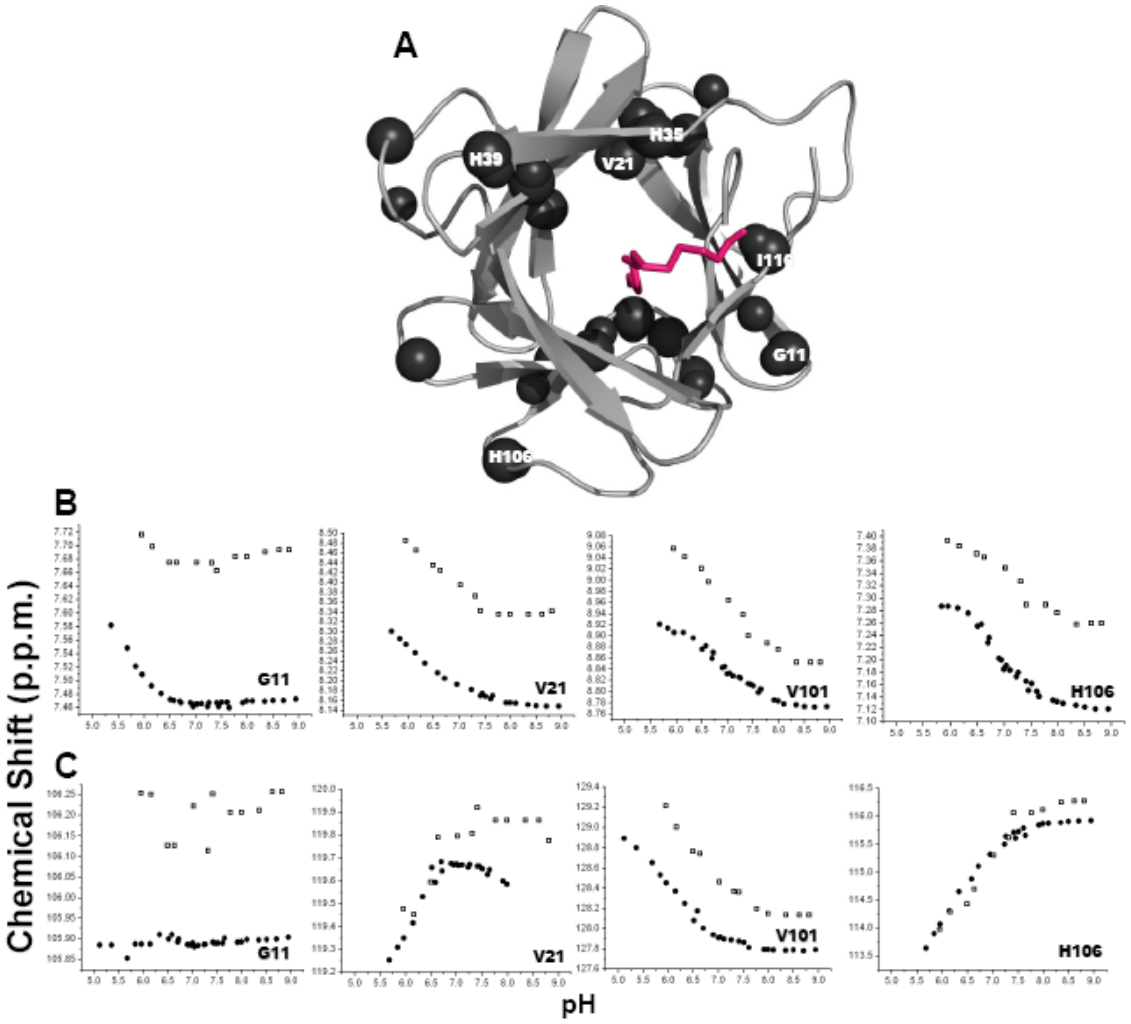

Fig. 2.S6. NH resonances monitored by ^{1}H-^{15}N HSQC that exhibit little significant changes in apparent pK_{app} values upon myristoylation. (A) Ribbon diagram of myristoylated hisactophilin illustrating all ^{15}N (large black spheres) and ^{1}H (small black spheres) that show no significant change in pK_{app} values. The myristoyl (pink) is shown in the myr_{seq} conformation. (B) Representative plots of δ vs. pH plots for backbone ^{1}H resonances that show no significant changes in pK_{app} upon myristoylation (panels are labeled with single residue code and amino acid number). The amide ^{1}H resonances that show no change include: G11, E17, A20, V21, H33, H35, H39, A44, G99, V101, S102, K104, H106, E115 and I116. (C) Representative plots of δ vs. pH plots for backbone ^{15}N resonances that show no significant changes in pK_{app} upon myristoylation (panels are labeled with single residue code and amino acid number). The amide ^{15}N resonances that show no change include: G11, A20, V21, H35, H39, A44, Y62, H68, H90, S94, G99, H100, V101, T103, H106 and I116. The nuclei that show no change are generally at the periphery of the structure.

A logical interpretation of these results is as follows: in the myr_{seq} state, the myristoyl group is buried in the hydrophobic core (Figs 2.4A, B) and histidines controlling the switch have relatively low apparent $pK_{a,seq}$ values (e.g. one is at ~6). The low values may result from a hydrophobic environment and/or proximity of positively charged groups. Upon protonation of the buried histidines many amides throughout the protein show chemical shift changes as a consequence of highly cooperative perturbations arising from the generation of buried positively charged groups. The magnitude of the changes in chemical shift caused by changes in charge of ionizable groups involved in switching are likely to be larger in general in myr_{seq} if the ionisable group is more buried than in myr_{acc} where it is more exposed and effects are shielded by the solvent.

Estimation of exchange rates by NMR lineshape analysis. NMR lineshape analysis has been used to study the dynamics of many different groups in proteins that undergo exchange processes such as ring flipping of aromatic residues (Wagner and Wuthrich, 1978), global protein folding/unfolding rates (Wang and Verkhivker, 2003), and cis-trans isomerization (Duggan and Craik, 1997). The dynamics of the myristoyl switch can be characterized by k_{out}, the rate constant for changing from the myr_{seq} to the myr_{acc} state, and k_{in}, the rate constant for changing from the myr_{acc} to myr_{seq} state (Duggan and Craik, 1997, Huang and Oas, 1995). In order to estimate the values of these rate constants, we analyzed exchange effects manifested in the lineshape of the myristoyl methyl group by measuring 1D ^{1}H spectra as a function of temperature (Fig. 2.S7C). These analyses reveal that at 25°C the myristoyl group exhibits minimal line broadening, indicating that that exchange between myr_{seq} and myr_{acc} is fast on the NMR time scale. In contrast, at 1°C pronounced line broadening is observed, indicating that exchange has slowed, becoming intermediate on the

NMR time scale. From simulation of the lineshapes, at 1°C, k_{in} and k_{out} are estimated as ~400s^{-1} and ~3600s^{-1}, respectively. At 25°C, due to less line broadening, the simulated lineshapes are less sensitive to the values of k_{in} and k_{out}, for which lower limits are estimated as ~55000s^{-1} and ~120000s^{-1}, respectively.

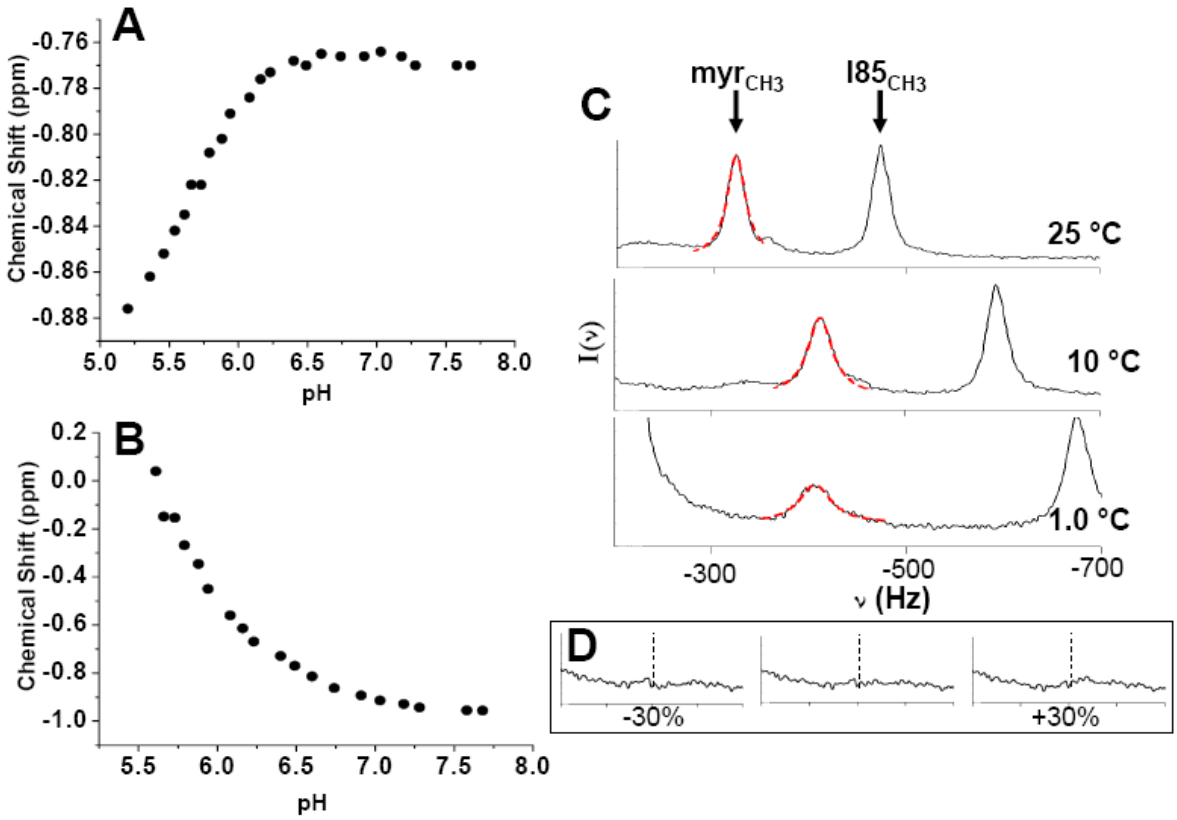

Fig. 2.S7. ^{1}H NMR lineshape analysis of I85 and myristoyl methyl groups in hisactophilin. 1D ^{1}H NMR-monitored pH titration for (A) $I85_{\delta CH3}$ and (B) myristoyl terminal CH_3 groups. Measured chemical shift values, δ, at different pHs are shown by filled circles. (C) Lineshape analysis of dynamics of the myristoyl methyl group as a function of temperature at pH 6.1. Measured NMR spectra are shown as continuous black lines and simulated spectra for the myristoyl terminal -CH_3 group are shown as red lines. Lineshapes were simulated as described previously (Duggan and Craik, 1997). Limiting values of ν and linewidth for myr_{seq} and myr_{acc} in the simulation were estimated from spectra obtained at pH 7.7 and 5.8, respectively. The values of k_{in} and k_{out} used for the simulated peaks at 1, 10 and 25 °C are: 400s^{-1} and 3600s^{-1}, 7850s^{-1} and 25000s^{-1}, and 55000s^{-1} and 120000s^{-1}, respectively. (D) Plots of residuals (i.e. experimental – simulated lineshape data) for different values of k_{in} and k_{out} at 1°C. Centre plot shows residual for reported values of k_{in} and k_{out}, left plot shows residual when k_{in} and k_{out} are both set 30% lower than reported values and right plot shows residual when k_{in} and k_{out} are both set 30% higher than reported values. This gives an estimate of effects of changes in the rate constants on the simulated spectra.

Discussion

Myristoylation increases protein stability. Despite the relatively common occurrence of protein myristoylation, there is remarkably little information available concerning its effects on protein folding. Here we show that myristoylation significantly increases the stability of hisactophilin for both the myr_{seq} and the myr_{acc} states. The relatively smaller increase in stability for myr_{acc} suggests that there are some residual stabilizing interactions and/or burial of the myristoyl group at low pH. Much larger stabilization is observed for the myr_{seq} state when the myristoyl group is buried in the hydrophobic core at high pH. It is well established that, in general, increasing the burial of hydrophobic groups increases protein stability (Kuhlman and Baker, 2004). It appears that burial of myristoyl groups may also commonly stabilize other proteins in an analogous fashion. For example, protein melting temperatures are increased upon myristoylation of HIV-1 matrix protein p17 (Wu*, et al.*, 2004), GCAP1 (Orban*, et al.*, 2010, Dell'orco*, et al.*) and calcineurin (Kennedy*, et al.*, 1996). Increased stability upon myristoylation is also implicated by structural data for recoverin, which is well ordered when the myristoyl is sequestered inside the protein but shows increased disorder when the myristoyl is exposed to solvent (Ames*, et al.*, 1997); this is also observed for GCAP1. It is noteworthy that all of the aforementioned proteins are structurally unrelated to hisactophilin. Recoverin, GCAP1 and calcineurin are highly helical, but the myristoyl group also inserts into the major hydrophobic core of these proteins. Thus, myristoylation may frequently contribute to increasing protein stability via hydrophobic burial in protein cores made by various structural elements.

Myristoylation increases global protein folding and unfolding. Quite unexpectedly, despite increasing protein stability, myristoylation of hisactophilin also increases protein dynamics. This is evident in the markedly increased rates of global folding and unfolding. These increased dynamics may be linked to and promote the rapid interconversion between myr_{seq} and myr_{acc} states, which is revealed by the apparent 2-state transitions in denaturant (Fig. 2.1A) and averaged resonances in NMR experiments (Fig. 2.S7). The increased dynamics with increased stability may initially seem counter-intuitive; however, there is precedence for similar effects from Φ-values involving hydrophobic amino acids in other proteins. The global kinetic and thermodynamic data for hisactophilin reveal that myristoylation has a larger stabilizing effect on the transition state of folding relative to the ground (native and denatured) states, manifested as a nonclassical Φ-value. Such Φ-values, while not common, have been reported in numerous experimental (Lopez-Hernandez and Serrano, 1996, Riddle*, et al.*, 1999, Villegas*, et al.*, 1998) and theoretical studies (Zarrine-Afsar*, et al.*, 2008). In various wild-type proteins, removal of hydrophobic groups (analogous to removal of the myristoyl moiety) has analogous effects of decreasing stability and decreasing folding and unfolding rates e.g. I34A in src SH3 (Riddle*, et al.*, 1999); V21T in CheY (Lopez-Hernandez and Serrano, 1996); I23V in ADA2h (Villegas*, et al.*, 1998); in other proteins the rates are decreased but stability is increased or changes little (Northey*, et al.*, 2002). Similar effects also occur in designed proteins where stability, and folding and unfolding rates are all increased when the hydrophobicity of the protein core is increased (comparable to addition of the myristoyl group). For example, this is observed in src SH3 best 4 and best 5 (Ventura*, et al.*, 2002), src SH3 A39V/V55I (Northey*, et al.*, 2002) and acylphosphatase with a redesigned hydrophobic core (Kuhlman and Baker, 2004). More

dramatic increases (several orders of magnitude) in folding and unfolding rates resulted from redesigning the hydrophobic core of Rop, with slight decreases in stability (Munson*, et al.*, 1997). Together these results suggest that hydrophobic groups, including myristoyl, can accelerate global protein dynamics. This may be important for facilitating folding in general and for facilitating conformational changes associated with function.

Complex energy changes upon myristoylation and mechanisms for increased dynamics. We propose that the mechanism for the increased stability and dynamics in myristoylated hisactophilin involves: 1) destabilization of the denatured state due to increased exposure of the hydrophobic myristoyl group; 2) strain in the native myr_{seq} state upon burial of the myristoyl group in the protein core; and 3) non-native interactions and/or relief of strain in the transition state (Fig. 2.3). This mechanism is based on and includes elements of different mechanisms proposed previously to explain non-classical Φ-values including: 1) denatured state effects (Cho and Raleigh, 2006); 2) over-packing of hydrophobic groups and strain in the native state with relief of strain in the transition state (Ventura*, et al.*, 2002); and 3) non-native interactions of hydrophobic groups in the transition state (Zarrine-Afsar*, et al.*, 2008). In general, folding rates are favoured by classical hydrophobic burial effects (Zarrine-Afsar*, et al.*, 2008, Cho*, et al.*, 2004), which would also apply to burial of the myristoyl group in going from the unfolded to the transition state. The effects of hydrophobic groups on unfolding tend to be less pronounced, perhaps due to a different mechanism involving rate limiting disruption of tight native packing (Zarrine-Afsar*, et al.*, 2008). However, this may not be the case for the myristoyl group in hisactophilin since it appears not to be tightly packed, as suggested by the rapid interconversion between

myr_{seq} and myr_{acc} states. The increased dynamics in myristoylated hisactophilin suggest over-packing and strain in the folded state. This strain may be relieved in the transition state in which, based on the Tanford β_T ($\beta_T = m_f/m_{eq}$) (Fersht, 1999) of ~0.7, there is ~30% exposure of hydrophobic surface. In addition, there may be some non-native interactions in the transition state. Nonspecific non-native interactions have been proposed for mutations of solvent exposed Tyr to Phe mutations in SH3, where the increased hydrophobicity of F accelerates both folding and unfolding rates with little effect on stability (Viguera*, et al.*, 2002). There is also evidence for position-specific non-native interactions of hydrophobic groups increasing rates for Fyn SH3 (Zarrine-Afsar*, et al.*, 2008). Considering that a myristoyl group is relatively long and flexible compared to natural hydrophobic amino acids, it has high potential in general for making nonspecific and/or specific non-native interactions in the transition state and thereby facilitating structural transitions.

Decreased folding frustration upon myristoylation. The speed at which a protein folds is often explained in terms of its energy landscape: proteins with smooth landscapes tend to fold quickly, while those with rugged or frustrated landscapes tend to fold slowly and populate partly folded intermediate states (Gosavi*, et al.*, 2006). A key finding here is that myristoylation decreases frustration in the energy landscape of hisactophilin. This is supported by the increased folding and unfolding rates, and good fits of equilibrium and kinetic data to a 2-state transition, with no detectable population of partly folded intermediates (Figs 2.1 and 2.2, Tables 2.S1 and 2.S2). In contrast, previous studies on nonmyristoylated hisactophilin showed population of a folding intermediate, evidenced by rollover and double exponential folding kinetics (Liu*, et al.*, 2002). This suggests that the

myristoyl group makes specific non-native interactions that compete with other non-native interactions that favour intermediate formation. Similarly, specific non-native interactions by certain hydrophobic residues in SH3 were found to accelerate folding and unfolding, while other hydrophobic residues had the opposite effect (Zarrine-Afsar*, et al.*, 2008). The much faster folding of R15 compared the R16 and R17 α-spectrins may also be related to key transition state interactions of residues in the cores of these proteins, with the core of R15 notably containing more hydrophobic residues (Wensley*, et al.*). In general, non-native interactions may act to favour or disfavour folding (Morton*, et al.*, 2007). Folding simulations have identified frustration in the folding pathway of β-trefoil proteins, including nonmyristoylated hisactophilin and interleukin-1β, manifested as formation of intermediates and backtracking during folding (Gosavi*, et al.*, 2006, Chavez*, et al.*, 2006, Capraro*, et al.*, 2008). In interleukin-1β, the frustration is particularly pronounced due to non-native interactions made by a hydrophobic loop (not found in hisactophilin) which is required for receptor binding. The authors concluded that the flux through multiple pathways on the β-trefoil folding landscapes may differ as a result of different functional requirements of the various trefoil proteins. It is very interesting that the naturally occurring hydrophobic myristoyl group on hisactophilin has a critical role in function and does not hinder but rather dramatically enhances folding.

Switching facilitated by hydrophobic interactions and regulated by ligand binding. The increased dynamics in hisactophilin upon myristoylation may illustrate a general mechanism whereby hydrophobic groups facilitate conformational

changes and switching. Another striking example is the switching of a repacked hydrophobic core mutant of Rop, which folds and unfolds 2 and 4 orders of magnitude faster, respectively, than the wild-type protein (Munson*, et al.*, 1997), and exhibits a novel switching between active and inactive folded states (Gambin*, et al.*, 2009). Also, non-classical Φ-values are indicative of increased dynamics (Kuhlman and Baker, 2004) and have been observed in various proteins that undergo switches, such as CheY (Sharma and Rajarathnam, 2000) and ADA2h (Villegas*, et al.*, 1998). The residues exhibiting non-classical Φ-values are often hydrophobic, again implicating a key role for hydrophobic groups in facilitating conformational dynamics. Thus, the presence of strain and/or non-native effects seen in the global dynamics and Φ-values may be linked to switching in these proteins as well.

Another noteworthy finding here is that the thermodynamic and ligand (H^+) binding characteristics of the myristoyl switch in hisactophilin are nicely tuned to enable high sensitivity signalling. The dynamic range and detection limit for switching controlled by ligand binding is determined by the thermodynamics of switching (i.e. the equilibrium constant between the two switching states) (Vallee-Belisle*, et al.*, 2009, Ababou*, et al.*, 2001, Marvin and Hellinga, 2001). In hisactophilin, the ΔG_{switch} of 2.03 kcal·mol^{-1} centred around a pK_{switch} of 6.95 allows for a large signal (i.e. change in populations of the myr_{acc} and myr_{seq} states) upon H^+ binding/release (Vallee-Belisle*, et al.*, 2009). These characteristics measured *in vitro* provide an explanation for *in vivo* observations of large changes in membrane binding by hisactophilin with changes in cellular pH (Hanakam*, et al.*, 1996). Switching from myr_{seq} to myr_{acc} in hisactophilin is accompanied by the binding of ~1.5 protons, due to an increase in the apparent pK_a of ionizable groups. It is not possible from the available data to precisely define the number and identity of the ionizable groups that control switching.

However, fitting of the pH-dependence of the switch energetics (Fig. 2.S2, and SI Results) combined with the pH-dependence of NMR chemical shifts (Figs 2.4D-F and 2.S5, and SI Results) suggest that a small number of ionizable groups make a major contribution to switching. The lower apparent pK_a in the sequestered state, which disfavours proton binding, may be a consequence of various effects, in particular increased hydrophobic environment of the ionizable groups or their closer proximity to other positively charged groups (Fig. 2.4F). An analogous switching mechanism applies to recoverin, where the binding of 2 Ca^{2+} ions also results in altered interactions of hydrophobic groups and myristoyl switching to the accessible state (Ames*, et al.*, 1997). Similar mechanisms may also occur in the maltose binding protein (Marvin and Hellinga, 2001) and N-terminal domain of calmodulin (Ababou*, et al.*, 2001), where hydrophobic moieties tune a switch through alteration of ligand (maltose and Ca^{2+}, respectively) binding affinity. Thus, the results presented here reveal a general mechanism of switching based on cooperativity between hydrophobic groups and ligand binding.

Conclusions. We have shown here that myristoylation can simultaneously favour protein stability, folding, and function. Increases in stability and folding rates resulting from myristoylation may be advantageous for generating and maintaining proteins *in vivo*, while increases in global dynamics upon myristoylation may facilitate switching and regulation of function. It will be of great interest to determine how general these effects are for myristoylation and for other post-translational modifications, for which there is currently very little quantitative data (Shental-Bechor and Levy, 2008). Myristoyl and other lipid modification-based switches in a wide range of proteins can be modulated by binding of

various ligands, including H^+, Ca^{2+}, GTP and even regulatory proteins, which favour extrusion of the lipid group from a binding pocket within the protein (Resh, 2006). Changing intracellular pH is a common mechanism for regulating protein function, and often acts in cooperation with other binding interactions (Nuccitelli, 1982). Regulation of the interactions of various hydrophobic moieties via ligand binding is not yet well understood in terms of mechanisms and energetics, although it occurs in many types of switching proteins, such as recoverin, maltose binding protein, calmodulin, calbindin (Stratton*, et al.*, 2008) and the low density lipoprotein receptor (Yamamoto*, et al.*, 2008), and is of tremendous biological significance. The methodology for analyzing the energetics of switching presented herein is general and can be used to gain valuable insights into many other switches.

Preamble

At the time when the research in chapter 2 was published there were other studies that were attempting to quantify the thermodynamic switching in DNA and apply them to other systems using an alternative method to the equations used in chapter 2 (Vallee-Belisle*, et al.*, 2009). Similarly, the equations used to study the pH-dependent energetics of myristoyl switching are also applicable to other switching systems. However, in chapter 2, our analysis was presented specifically for hisactophilin and the pH myristoyl switch. Therefore, in order to show the applicability of our model to other switching systems, the equations used in chapter 2 are derived using a general notation that allow the thermodynamic analysis of other ligand-binding-induced switching system. Then, using data from the literature, our model is applied to other switching systems.

The analysis presented in chapter 3 illustrates the the general applicability of our thermodynamic model and elaborates further on the nature of the thermodynamics that facilitate switching in many systems. Results presented in chapter 3 on the LLL hisactophilin also show that myristoyl switching can be tuned through hydrophobic mutations. The content of chapter 3 represents the main body of the communication published as:

Smith, MTJ., MacKenzie, DWS., Meiering, EM. (2011) Dissecting the molecular determinants of ligand binding-induced macromolecular switching using thermodynamic cycles. *Protein Engineering Design and Selection.* 24 (1-2), pp. 213-17

The work has been reproduced here in accordance with journal publication policy (also see letter of permissions section). Results presented in this chapter were obtained by Martin Smith except for some measurements of stability on the LLL hisactophilin mutant, which were carried out by Duncan MacKenzie. The research was designed to expand the methodologies in chapter 2 using thermodynamic cycles and apply them to ligand-induced switching systems in general. This research also presents the preliminary mutagenesis results that are elaborated upon further in chapter 4.

Chapter 3 – Dissecting the Molecular Determinants of Ligand-Induced Switching as Determined by Thermodynamic Cycles.

Introduction

Ligand binding is a widespread mechanism for regulating the switching of macromolecules between distinct functional states (Vallee-Belisle*, et al.*, 2009, Schaeffer*, et al.*, 2008). Owing to the cooperative nature of structural transitions in proteins and nucleic acids, the molecular mechanisms governing switching are complex and details of the energetics are poorly understood. Here we describe a general methodology for dissecting the coupling energetics between specific group(s) in a macromolecule and ligand binding-induced switching using thermodynamic stability or binding data. Thermodynamic cycles are a well-established approach for analyzing the energetics of interactions within or between macromolecules (Fersht*, et al.*, 1992, Fersht, 1999, Horovitz and Fersht, 1990). The methodology described herein is based on combining thermodynamic cycles to quantitate changes in stability of a macromolecule upon alteration (e.g. deletion of a post-translational modification, or mutation(s)) with cycles to measure the effects of ligand binding (Fersht, 1999). In the following sections, we describe first the theoretical basis of the methodology, and then illustrate the versatility of the method through application to data for proteins studied in our own laboratory and to data reported in the literature for other macromolecular switches that have not been analyzed previously by this method.

Methodology

The combined thermodynamic cycles for folding of the original (wild-type) and variant (*e.g.* covalently modified or mutated) macromolecule, with and without bound ligand, can be considered as a thermodynamic cube, as illustrated in Fig 3.1.

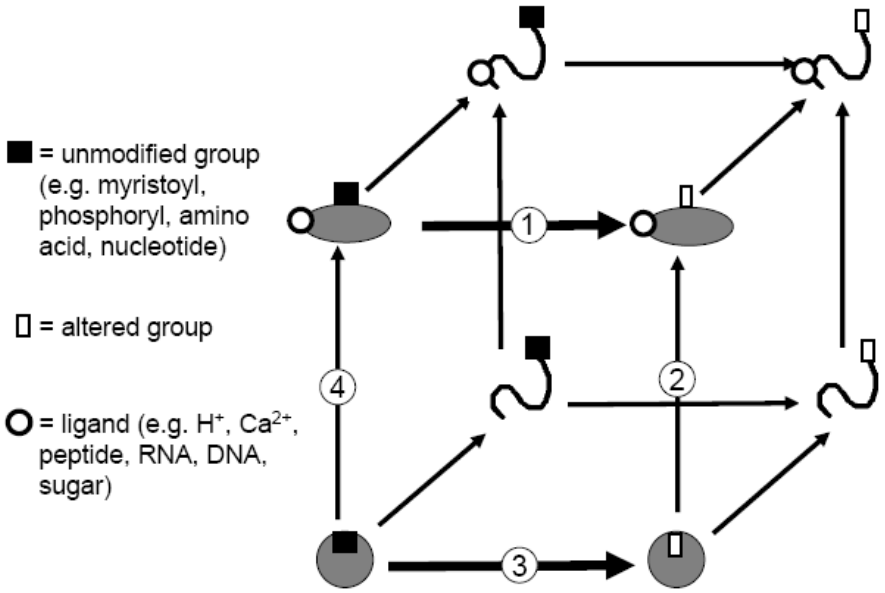

$$\Delta G_{switch} = \underset{①}{\Delta G_{F(WT\rightarrow Alt)bound}} - \underset{③}{\Delta G_{F(WT\rightarrow Alt)free}} = \underset{②}{\Delta G_{F,Alt(free\rightarrow bound)}} - \underset{④}{\Delta G_{F,WT(free\rightarrow bound)}}$$

Fig. 3.1. Thermodynamic cycle for calculating ΔG_{switch}. Each arrow defines a change in free-energy, ΔG, associated with the corresponding transition between two states. The direction of the arrow defines the initial and final states. The front face (grey circles/ovals corresponding to the two switch states) and back face (random coil) of the thermodynamic cube represent the folded and unfolded states, respectively. The top and bottom faces represent the ligand-bound and ligand-free states, respectively. Assuming $\Delta G_{U,WT(free\rightarrow bound)} = \Delta G_{U,Alt(free\rightarrow bound)}$, i.e. modification has no effect on the ligand-dependence of the free energy of the unfolded state and so these terms cancel out. The unmodified group (■) may be myristoyl (Smith, *et al.*, 2010), phosphoryl (Nelson, *et al.*, 2010), amino acid(s) (Marvin and Hellinga, 2001), nucleotide(s) (Vallee-Belisle, *et al.*, 2009, Jenison, *et al.*, 1994), or glycosyl (Shental-Bechor and Levy, 2009). The altered group (□) may be residues that have been modified in some manner (e.g. nonmyristoylated, nonphosphorylated, mutated or truncated). Ligands (○) may include Ca^{2+} (Ames, *et al.*, 1995), H+ (Hanakam, *et al.*, 1996), peptides (McCarney, *et al.*, 2005), proteins (Remy, *et al.*, 1999) or nucleotides (Vallee-Belisle, *et al.*, 2009). In cases where data is available on the concentration dependence of ligand binding more information can be extracted (Smith, *et al.*, 2010).

The coupling energy between the altered group(s) and ligand binding, ΔG_{switch}, corresponds to the difference in energy between the top and bottom faces of the cube. In general, ΔG_{switch} will be the sum of many energetic terms arising from interactions propagating through the macromolecule, such as electrostatic interactions, hydrogen bonding, van der Waals interactions, ligand-independent reorganization, and solvation, as described previously (Fersht*, et al.*, 1992, Horovitz*, et al.*, 1991, Serrano*, et al.*, 1990). Depending on the nature of the alteration made to the macromolecule, these terms may simplify to a true interaction energy. Evaluation of the switch energy is analogous to analyzing enzyme-substrate interactions and intramolecular interactions upon respective alteration of groups in either the enzyme or substrate, or using multiple mutations. Many previous studies have focussed on modifying groups that interact directly with the ligand in a binding site; here we focus more on distal modifications whose effects are indirect, propagating through the macromolecule.

ΔG_{switch} can be determined experimentally from measurements of the free energy of unfolding, $\Delta G_{U\text{-}F}$ (= G_U - G_F, where U and F represent the unfolded and folded states, respectively) as follows. The difference in free energy of unfolding of the wild-type and altered macromolecule, $\Delta\Delta G_{U\text{-}F(WT \rightarrow Alt)}$, can be defined as:

$$\Delta\Delta G_{U-F(WT \rightarrow Alt)} = \Delta G_{U-F,WT} - \Delta G_{U-F,Alt} \qquad [3.1]$$

where the subscripts *WT*, *Alt* and *(WT→Alt)* represent terms for the unmodified group in the wild-type, altered group or the change associated with alteration of the specific group, respectively (*e.g.* removal of a covalent modification such as an acyl or phosphoryl group, or

mutation of amino acid residue(s)). The apparent coupling energy between the altered group(s) and ligand binding, ΔG_{switch}, may be defined as the change in $\Delta\Delta G_{U\text{-}F(WT\rightarrow Alt)}$ from the ligand-free to fully ligand-bound state:

$$\Delta G_{switch} = \Delta\Delta G_{U-F(WT\rightarrow Alt)bound} - \Delta\Delta G_{U-F(WT\rightarrow Alt)free} \quad [3.2]$$

where the subscripts *free* and *bound* represent the terms associated with the folded ligand-free and fully ligand-bound switch states. If the altered group makes interactions that affect ligand binding-induced switching, then $\Delta\Delta G_{U\text{-}F(WT\rightarrow Alt)}$ will usually be different for the ligand-bound and ligand-free states, *i.e.* there will be a measurable coupling energy and ΔG_{switch} will be nonzero. Conversely, if there is no coupling, then $\Delta\Delta G_{U\text{-}F(WT\rightarrow Alt)}$ will be independent of ligand binding and ΔG_{switch} will be zero. Thus, measurements of ΔG_{switch} can be used to identify the interactions that control ligand-induced switching. Eq. 3.1 can be substituted into eq. 3.2 to give:

$$\Delta G_{switch} = \Delta G_{U-F,WT,bound} - \Delta G_{U-F,Alt,bound} - \left(\Delta G_{U-F,WT,free} - \Delta G_{U-F,Alt,free}\right) \quad [3.3]$$

illustrating the link between ΔG_{switch} and the thermodynamic stability of the wild-type and altered form of the macromolecule. Eq. 3.3 for ΔG_{switch} can be rewritten in terms of the free energies of the folded, unfolded, ligand-bound and ligand-free forms of the macromolecule:

$$\Delta G_{switch} = \left(G_{F,Alt,bound} - G_{F,Alt,free}\right) - \left(G_{F,WT,bound} - G_{F,WT,free}\right) + \left(G_{U,WT,bound} - G_{U,WT,free}\right) - \left(G_{U,Alt,bound} - G_{U,Alt,free}\right) \quad [3.4]$$

Assuming that the change in the free energy of the unfolded state upon ligand binding is not altered by the modification (i.e. $\Delta G_{U,WT(free\rightarrow bound)} = G_{U,WT,bound} - G_{U,WT,free} = \Delta G_{U,Alt(free\rightarrow bound)} = G_{U,Alt,bound} - G_{U,Alt,free}$), which is likely to hold if the modification is distant from the ligand binding site (Smith*, et al.*, 2010), equation [3.4] simplifies to:

$$\Delta G_{switch} = \Delta G_{F(WT\rightarrow Alt)bound} - \Delta G_{F(WT\rightarrow Alt)free} = \Delta G_{F,Alt(free\rightarrow bound)} - \Delta G_{F,WT(free\rightarrow bound)} \qquad [3.5]$$

where ΔG_F refers the free energies in the folded state of the protein (Fig. 3.1). Thus ΔG_{switch} can be interpreted as the coupling energies between ligand binding and the altered group. We note that, owing to the symmetry of the thermodynamic cycle in Fig. 3.1, ΔG_{switch} may alternatively be calculated from the ratio of the ligand association constants, K_a, of the wild-type and altered macromolecules, provided that these are measured under conditions where the two forms of the macromolecule are predominantly folded. If this is not the case, then the measured apparent K_a values, and consequently ΔG_{switch}, will include contributions from changes in folding equilibria (*e.g.* Zn^{2+} binding-induced switching of the antenna finger protein, see Table 3).

The next section describes examples of these coupling energies between individual residues or groups of residues and ligand-induced switching, as determined from chemical or thermal denaturation data and/or values of K_a. The systems studied and the calculated switch energetics are summarized in Table 3. Although the coupling energy is comprised of several energetic terms, ΔG_{switch} itself represents a neat interpretation of contributions from a residue in a macromolecule to ligand-induced switching. The magnitude of ΔG_{switch} can be a measure

of the extent of the coupling energetics of the altered group to ligand-binding induced switching (*e.g.* the involvement of the myristoyl group in various myristoyl switching mechanisms (Table 3, see below)). A negative value of ΔG_{switch} indicates that the unaltered group couples ligand binding to switching in a favourable manner, while a positive value suggests an unfavourable coupling of ligand binding to switching (*e.g.* the involvement of the C-terminal residues in the troponin C Ca^{2+} switch, Table 3, see below).

Results and Discussion

We first illustrate application of eq. 3.5 to determine ΔG_{switch} using data obtained in our own laboratory on myristoyl switching induced by H^+-binding. In hisactophilin, increased H^+ binding with decreasing pH results in switching of an N-terminal covalently linked myristoyl moiety from a sequestered state in the hydrophobic core of the protein to a state in which the myristoyl has increased accessibility for membrane binding (Hanakam*, et al.*, 1996). Based on stability measurements by chemical denaturation at limiting low (H^+ bound) and high (H^+ free) pH for myristoylated (wild-type) and nonmyristoylated (altered) hisactophilin, the ΔG_{switch} between the myristoyl group and H^+ binding is -2.03 kcal·mol^{-1} (Smith*, et al.*, 2010) (Fig. 3.2). We further investigated the role of hydrophobic core residues in the switching network by making analogous measurements for a hisactophilin triple mutant (F6L + I85L + I93L), LLL-hisactophilin, which has increased symmetry in the protein hydrophobic core.

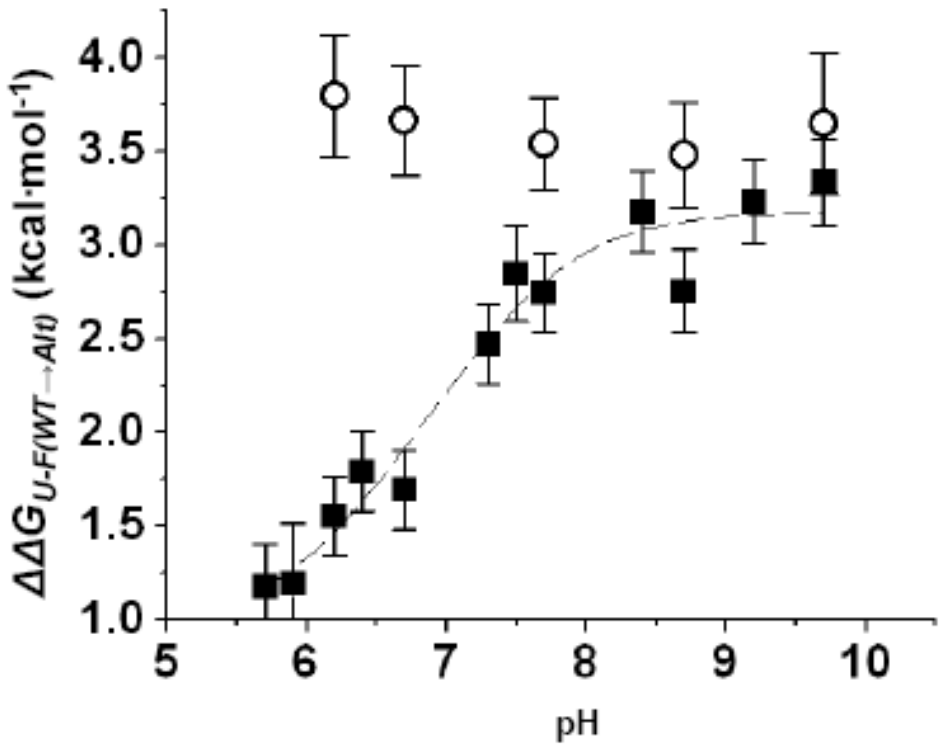

Fig. 3.2. $\Delta\Delta G_{U\text{-}F(WT\rightarrow Alt)}$ vs. pH for wild-type hisactophilin (■) and LLL-hisactophilin (○). The dashed line represents a fit of $\Delta\Delta G_{U\text{-}F(WT\rightarrow Alt)}$ between two conformational states as described elsewhere (Cho*, et al.*, 2004, Smith*, et al.*, 2010). Fitted values are included to illustrate the pH-dependent nature of the myristoyl switch in hisactophilin.

NMR studies showed that the amides of F6, I85 and I93 are close to the myristoyl group (Smith*, et al.*, 2010). Strikingly, $\Delta\Delta G_{U\text{-}F(WT\rightarrow Alt)}$ for LLL-hisactophilin remains essentially constant at the high pH value for wild-type hisactophilin (Fig. 3.2). The corresponding ΔG_{switch} of ~0 kcal/mol indicates abolition of the pH-dependence of $\Delta\Delta G_{U\text{-}F(WT\rightarrow Alt)}$ for LLL-hisactophilin. Thus, the myristoyl group appears to remain sequestered in the LLL-hisactophilin core, likely due to disruption of the signalling pathway mediated by hydrophobic residues between the H^+ binding residues and the myristoyl binding site (Friel,

et al., 2009). This suggests that asymmetry in hisactophilin may be important for facilitating functional switching; similarly, asymmetry has been implicated in the function of other trefoil proteins (Brych*, et al.*, 2004). These results for hisactophilin not only give insight into the molecular determinants of myristoyl switching, but also illustrate how switches may be analyzed and rationally altered by mutation.

The myristoyl switches for recoverin, neuronal calcium sensor-1 (NCS-1), and GCAP-1 are controlled by Ca^{2+} rather than H^{+} binding. For these proteins, the magnitude of ΔG_{switch} between the myristoyl group and Ca^{2+} binding calculated from stability and binding data vary dramatically, ranging from -10.9 kcal/mol for recoverin to ~0 kcal/mol in GCAP-1 (Ames*, et al.*, 1995, Lim*, et al.*, 2009)(Table 3). It has been proposed that the myristoyl switch in recoverin involves full extrusion of the myristoyl group from the hydrophobic core of the protein into solvent, whereas in GCAP-1 the myristoyl group may undergo only a dynamic without a structural change and remain buried (Hwang and Koch, 2002). Thus, the magnitude of ΔG_{switch} for recoverin and GCAP-1 may be related to the extent of conformational change occurring upon switching. For NCS-1, the ΔG_{switch} between Ca^{2+} binding and the myristoyl group is 1.88 kcal/mol (Muralidhar*, et al.*, 2005) (Table 3.1). It is interesting that the magnitudes of ΔG_{switch} for hisactophilin and NCS-1 fall between those for recoverin and GCAP-1. While the structures of the myristoyl-accessible states for NCS-1, GCAP-1 and hisactophilin are currently unknown, the energetics suggest that the myristoyl switches in these two proteins involve more subtle conformational changes than in recoverin. This provides a testable hypothesis that values of ΔG_{switch} may be correlated with the extent of conformational change involving the myristoyl group that occurs upon switching.

Table 3.1. ΔG_{switch} values in switching systems

Macromolecule	**Modification**	**Ligand**[ξ]	ΔG_{switch} *(kcal/mol)*	**Data Used**	**Ref.**
Hisactophilin	myrG[§]→G	H^+	-2.03	chemical denaturation	(Smith, *et al.*, 2010)
LLL-Hisactophilin[‡]	myrG[§]→G	H^+	~0	chemical denaturation	this work
NCS-1	myrG[§]→G	Ca^{2+}	1.88	chemical denaturation	(Muralidhar, *et al.*, 2005)
Recoverin	myrG[§]→G	Ca^{2+}	-10.9	binding data[†]	(Ames, *et al.*, 1995)
GCAP-1	myrG[§]→G	Ca^{2+}	~0	binding data[*]	(Lim, *et al.*, 2009)
ChTnC 1-85[‡]	N-term Δ1-12	Ca^{2+}	0.70	thermal denaturation / binding data	(Fredricksen and Swenson, 1996)
ChTnC 1-105[‡]	N-term Δ1-12	Ca^{2+}	-3.90		
Ste2p	N205A	WT α-factor	0.65	binding data	(Naider, *et al.*, 2007)
		A_1A_2 α-factor[˚]	-1.00		
Ste2p	Y266A	WT α-factor	1.13		
		A_1A_2 α-factor[˚]	-1.29		
Antenna Finger	AntF-H1[††]	Zn^{2+}	1.41	chemical denaturation	(Hori and Sugiura, 2004)
Calmodulin	L39F	Ca^{2+}	1.50	binding data[‡‡]	(Ababou, *et al.*, 2001)
Maltose Binding Protein	I329A	maltose	0.48	binding data[‡‡]	(Marvin and Hellinga, 2001)
	I329W		-1.85		
Theophylline (TPL) binding RNA aptamer	TCT8-4→ mTCT8-4[**]	TPL	1.06	binding data[‡‡]	(Jenison, *et al.*, 1994)

(table notes on following page)

[ξ]Since we use the limiting cases of ligand-free and fully ligand bound states to define ΔG_{switch}, energetic terms for one or multiple bound ligands implicitly included in ΔG_{switch}. If appropriate data are available (as for recoverin), the contributions of distinct ligand binding sites can be combined or considered separately.
[§]myrG→G indicates removal of an N-teminal myristoyl moiety that was covalently linked via an amide linkage to G.
[‡]The thermodynamic cube analysis presented can be built into extra dimensions by performing this analysis on additional mutations (Horovitz and Fersht, 1990).
[†]ΔG_{switch} was determined using the allosteric model presented in this paper for the binding of calcium to recoverin.
[*]Authors noted that K_d was not affected by whether or not GCAP-1 was myristoylated, thus ΔG_{switch} must be equal to 0.
[°]The A_1A_2 mutant α-factor is one example within a series of other alanine mutants that were presented in this reference.
[††]AntF-H1 has R10E, H21R, F22R, L14R mutations in Helix 1, which is thought to participate in metal binding and the conformational change.
[‡‡]ΔG_{switch} was calculated by $\Delta G_{switch} = -R \cdot T \cdot \ln(K_d'/K_d)$ where $'$ refers to the modified group.
[**]m refers to a truncation mutant presented in the cited reference. When compared to mTCT8-4, TCT8-4 contains a 5' A to G mutation and an additional A. In addition, at the 3' end, TCT8-4 has a C to U mutation followed by an additional C and A.

Analyses of ΔG_{switch} for other switching proteins regulated by binding of various ligands are also included in Table 3, including Ca^{2+}-binding troponin C (ChTnC), Zn^{2+}-binding antenna finger protein (ZAF), and Ste2p, a G-protein coupled receptor that undergoes a conformational switch upon binding to a peptide ligand known as α-factors. Thermal stability data were obtained at different calcium concentrations for two types of ChTnC, a wild-type and a variant with 12 C-terminal residues removed (i.e. ChTnC 1-105 and ChTnC 1-85). Each protein was then individually altered with the deletion of 12 N-terminal residues (N-term Δ12). ΔG_{switch} between Ca^{2+} binding and the N-terminal residues for the full-length protein is -3.90 kcal/mol (Fredricksen and Swenson, 1996). Interestingly, the value of ΔG_{switch} changes dramatically to 0.70 kcal/mol upon deletion of the N-terminal residues with the C-terminal deletion variant. This suggests that interactions between the C- and N-terminus facilitate the Ca^{2+}-switch in ChTnC. We note that the ΔG_{switch} values for ChTnC obtained from chemical denaturation data match those determined from K_a values

which were measured under strongly folding conditions. The results for ChTnC provide insight into how different segments of a protein may contribute to switching. Studies on Ste2p illustrate the contributions of individual residues to switching. In this case, the single residue substitutions, Y266A and N205A, yield ΔG_{switch} values of 1.13 and 0.651 kcal/mol, respectively, when the α-factor peptide ligand binds (Naider*, et al.*, 2007). The ΔG_{switch} values are markedly changed for a mutant α-factor in which two alanine mutations have been introduced (-1.29 and -1.00 kcal/mol for Y266A and N205A, see Table 3). As for hisactophilin, this is another example of how switch energetics can be highly sensitive to mutational changes. An interesting trend is that hydrophobic groups often appear to play significant roles in mediating switching, not only in myristoylated proteins and Ste2p, but also in calmodulin (Ababou*, et al.*, 2001) and maltose binding protein (Marvin and Hellinga, 2001). Thus, hydrophobic residues may often facilitate conformational changes involved in switching (Smith*, et al.*, 2010).

In conclusion, we would like to point out that, although we have described examples of dissecting switch energetics in proteins, the method is generally applicable to other macromolecules as well. For example, it may be applied to analyze switches in nucleic acids, such as RNA ribo-switches induced by small molecule binding (Jenison*, et al.*, 1994), conformational switches induced by oligonucleotide binding to DNA-based fluorescent sensors (Vallee-Belisle*, et al.*, 2009) and polymers (Tonge and Tighe, 2001).

Preamble

The conclusions made from the research conducted in chapter 2 provide a quantitative understanding of the thermodynamic and kinetic effects of myristoylation on the folding and switching of proteins. These studies provided indications that the myristoyl group was making important native and nonnative interactions with hisactophilin, which included strain, interactions in the transition state and denatured state effects. However, the exact interactions that give rise to the thermodynamic and kinetic effects were still unknown. Therefore, research presented in chapter 4 describes experiments to map the residue specific native and nonnative interactions that were identified in the thermodynamic and kinetic analyses in Chapter 2. The research was a collaborative effort of experiments/simulations performed in the Meiering lab, and simulation performed in the lab of Dr. Yaakov Levy.

Based upon the experimental results presented in chapter 2 and current efforts to simulate nonnative efects, simulations designed and conducted by the Levy group provide a model to examine the nature of the native and nonnative interactions between the myristoyl group and the rest of hisactophilin. Experiments presented in chapter 4 elaborate further on the nature of the interactions of the myristoyl group with specific residues of hisactophilin and are compared to the simulations on hisactophilin. The experiments provide further information about the nature of the effects of myristoylation on strain in the native state and nonnative effects that occur in the denatured and transition state. The content represents the main body and supplementary information that will be published as:

Dalit Shental-Bechor*, **Martin T.J. Smith***, Duncan W.S. MacKenzie, Aron Broom, Amir Marcovitz, Fadila Ghashut, Chris Go, Fernando Bralha, Elizabeth M. Meiering[+] and Yaakov Levy[+](2012) Nonnative interactions regulate folding and switching of myristoylated protein. *Proc. Natl. Acad. Sci,* published online, doi: 10.1073/pnas.1201803109.
(* these authors contributed equally, [+] co-corresponding authors)

This work has been reproduced here in accordance with the journal publication policy (also see letter of permission section). In this research Experimental data in this chapter was acquired by Martin Smith (i.e. mutant design, NH/D characterization and thermodynamic characterization) except for some of the some of the stability and folding measurements, which were performed by Duncan MacKenzie. Aron Broom (Meiering lab) contributed the atomistic molecular dynamics simulations, and Dalit Shental-Bechor (Levy lab) contributed coarse-grained simulations. For context and clarity, the simulations and experiments are presented together, supplementary materials and methods section and supplementary figures have been placed into the main body of text with the original naming. The order of sections has been modified from the original publication.

Chapter 4 – Nonnative Interactions Regulate Folding and Switching of Myristoylated Proteins.

Introduction

Protein folding is governed by various physicochemical forces that bias the native state, which for many proteins is also the functional state, over the many alternative nonnative states. The network of native interactions has been found in many cases to be sufficient to capture the folding mechanism and kinetics of proteins (Onuchic and Wolynes, 2004, Baker, 2000). The discrimination between native and nonnative interactions is the foundation of the principle of minimal frustration (Bryngelson*, et al.*, 1995, Leopold*, et al.*, 1992) and explains the power of native topology-based models in studying folding biophysics (Clementi*, et al.*, 2000, Simler*, et al.*, 2006, Levy*, et al.*, 2005, Turjanski*, et al.*, 2008, Zhang and Chan, 2009). The dominant role of native interactions is manifested by the funnel-shaped energy landscape for folding that suggests folding is robust and an efficient process. The information stored in the native topology may, however, be tuned by various factors such as confining the protein in a small space (Takagi*, et al.*, 2003), crowding agents (Cheung*, et al.*, 2005), or conjugating the protein to other biomolecules (e.g., oligosaccharides (Shental-Bechor and Levy, 2008), or fatty acyl chains, such as myristoyl (Smith*, et al.*, 2010)). In addition to manipulating folding characteristics by modifications or environmental conditions, nonnative interactions that are by definition in conflict with the native state, may decorate the folding funnel (Sutto*, et al.*, 2007, Capaldi*, et al.*, 2002, Friel*, et al.*, 2003) by increasing energetic frustration (Shea*, et al.*, 1999) between interactions and therefore its roughness. The degree of roughness, which affects the trapping of the protein in

nonnative states, depends on the particular sequence of the protein and can be tuned by mutations.

Investigations of several proteins have reported evidence for nonnative interactions that assist, rather than hinder, folding (Zarrine-Afsar*, et al.*, 2008, Viguera*, et al.*, 2002, Li*, et al.*, 1999, Di Nardo*, et al.*, 2004, Plotkin, 2001, Clementi and Plotkin, 2004, Zhang and Chan, 2010, Chan*, et al.*, 2011), and more importantly they may also support function (Ferreiro*, et al.*, 2011, Chavez*, et al.*, 2006, Smith*, et al.*, 2010) by assisting conformational changes. Residues in functional sites in proteins have been implicated in causing geometric frustration (Capraro*, et al.*, 2008) or increasing localized energetic frustration (Ferreiro*, et al.*, 2011). Nonnative interactions that result with localized frustration can transiently be formed, for example between hydrophobic residues (Zarrine-Afsar*, et al.*, 2008) or between oppositely charged residues (Chen*, et al.*, 2008, Weinkam*, et al.*, 2009, Shan*, et al.*, 2009, Azia and Levy, 2009). This is akin to frustration in RNA folding that arises from negatively charged groups (Thirumalai and Hyeon, 2005). Formation of nonnative interactions may affect folding in various ways. For example, nonnative interactions in the unfolded state may affect its entropy and therefore the overall stability of the protein. Also, nonnative interactions in the transition state that support the critical nucleus may speed up the folding process.

In the current study, we investigate the effect of myristoylation on protein folding and in particular the involvement of nonnative interactions. Myristoylation is a common modification, occurring in ~0.5-0.8% of eukaryotic proteins, where a saturated C14 fatty acyl chain is covalently linked to the N-terminal glycine in a protein (Resh, 2006). In many proteins, the myristoyl interconverts between a sequestered state, where it is located in a

hydrophobic binding pocket in the protein, and an accessible state, where it is available to bind to membrane or other proteins. Often this interconversion, or switching, is reversible and controlled by ligand (H^+, Ca^{2+}, GTP, regulatory protein) binding. Myristoyl switching is associated with diverse and vital regulated signalling pathways in cells (Resh, 2006).

We investigate here the effect of myristoylation on the folding kinetics and thermodynamics of the β-trefoil protein, hisactophilin, a small (118 residues) protein from *D. discoideum* (Fig 4.1A). The function of hisactophilin is to reversibly recruit actin filaments to membranes during chemotaxis and osmotic stress. Previous experimental studies revealed that increasing hisactophilin charge with decreasing pH favours actin and membrane binding but decreases protein stability and folding kinetics (Liu*, et al.*, 2001, Liu*, et al.*, 2002). The myristoyl increases hisactophilin stability with an apparent pKa of 6.95, as it switches between a "sequestered" state at high pH where the myristoyl is buried in the protein core (Fig 4.1A), and an "accessible" state at low pH for membrane binding (Smith*, et al.*, 2010). Concomitantly, the myristoyl markedly accelerates both folding and unfolding kinetics, and undergoes rapid native-state switching, implicating the long and flexible hydrophobic myristoyl chain in creating strain in the native state and forming non-native interactions during folding and switching. Here we report an integrated approach combining various computational and experimental methods to analyze myristyolated hisactophilin, including characterization of hydrophobic mutations distributed in the primary and tertiary structure of the protein (Fig 4.1B). Variants include a triple myristoyl binding pocket mutant in which pH-dependent switching is abolished (F6L/I85L/I93L) (Smith*, et al.*, 2011), and single mutations that alter stereochemistry (I85L) or truncate side chains inside (V36A and L76A)

or outside (I118A) the binding pocket. The results provide new insight into the role of non-native interactions on folding as well as the atomistic mechanism of myristoyl switching.

Materials and Methods

Coarse-grained molecular dynamics simulations. We used simplified coarse-grained models in which each residue is represented by a single bead centered at the alpha carbon. The model is described in detail in (Clementi*, et al.*, 2000). This is a topology-based model and the energy function is based on the structure of the native state of the protein. Each native interaction (either residue-residue or residue-myristoyl) is modeled using a Lennard-Jones term $E_{ij}^{\text{Native contact}}=\varepsilon[5(A_{ij}/r_{ij})^{12} - 6(A_{ij}/r_{ij})^{10}]$, where A_{ij} is the optimal distance in Å between beads *i* and *j* and r_{ij} is the distance (in Ångstroms) between beads *i* and *j* in a given conformation along the trajectory. ε is the strength of the native interaction. The nonnative interactions are all the possible interactions between hydrophobic beads in the protein (including the myristoyl group), which are not in contact in the native structure and are not close in sequence ($i<j$-3). In this work, we followed the procedure introduced by Chan and coworkers (Zarrine-Afsar*, et al.*, 2008). In short, an attractive potential between each pair of hydrophobic residues was added (pairs were defined as was described above) in addition to the repulsive interactions between pairs that are not in contact in the native state. Any nonnative hydrophobic interaction is therefore modeled as $E_{HP} = -K_{HP}\kappa_i\kappa_j \exp[-(r_{ij} - 5)^2 / 2]$, where κ_i and κ_j is the hydrophobicity strength of beads *i and j* that represents an amino acid or a carbon of the myristoyl group and its value ranges from 0 to 1. K_{HP} is the overall (i.e. native and nonnative) strength of the hydrophobic forces

that was selected to be 0.8. In the present study, alanine, valine, leucine, isoleucine, methionine, tryptophan, phenylalanine, and tyrosine were considered to be hydrophobic. The nonnative electrostatic interactions were modeled using the Debye-Huckel potential (for details see (Azia and Levy, 2009)). These interactions were defined between each pair of charged residues (lysine, arginine, aspartic and glutamic acids). In this model, called His0, histidine residues had neutral charge and mimic high pH. Modeling low pH was achieved by adding a positive charge to all the histidine residues (called His1 model). When nonnative electrostatic interactions were modeled, the nonnative hydrophobic interactions were included as well.

Structure of non-myr and myr-hisactophilin. We did some refinements on the model structure that was provided from the NMR measurements. We ran long all-atom MD simulations of the myristoylated protein and clustered the conformations that were generated during the simulation to find the representative conformation to be treated as the native structure. We used this conformation as the conformation to construct the native topology-based model. In the coarse-grained simulations, the protein was represented only by its Cα atoms and the myristoyl was represented by 6 beads (each represents two aliphatic carbons of the myristoyl chain). We used this conformation of the myristoylated protein to model the non-myr variant. To this end, we removed all the contacts of the myristoyl beads except for the virtual bonds that connect the beads to each other.

All-atom molecular dynamics. All-atom molecular dynamics were performed using the AMBER simulation package (Case*, et al.*, 2010). The TIP3P water model was used and

all hydrogens were constrained to have rigid bonds, with a 2 fs timestep being used. The initial wild-type model was built from the NMR structure (PDB 1HCD), and the two binding pocket mutants (I85L, F6L/I85/LI93L) were initially constructed using PyMol (Delano Scientific). AMBER parameters for the myristoyl group were determined using the RED RESP charge fitting server (Vanquelef*, et al.*, 2011) package, to be consistent with the AMBER03 force field used for the remainder of the protein (Duan*, et al.*, 2003). The models were initially refined by conjugate gradient energy minimization until no further decreases in energy found, and then equilibrated in an NPT ensemble (Langevin thermostat, Berdnensen barostat) for 20 ns. Final production was done for 80 ns, with snapshots taken every 20 ps, and analyzed using VMD (Humphrey*, et al.*, 1996).

Protein purification. F6L/I85L/I93L and I85L mutant plasmids were created in-lab using the HiYieldTM Plasmid Miniprep Kit site-directed mutagenesis (United Bioinformatica Inc., Canada). Site-directed mutagenesis for V36A, L76A and I118A mutants was performed by GenScript Inc. (Piscataway, USA). Plasmids were sequenced to confirm their identity (Appendix 3). Myristoylated WT and mutant forms of hisactophilin were purified as described previously in chapter 2 and checked by mass spectrometry (Meissner, 2007). However, during hisactophilin expression in *E.coli*, the V36A, L76A and I118A were grown at 25˚C instead of 37˚C. Induction times varied between 8 and 16 hours for mutants grown at 25˚C.

Equilibrium, folding and unfolding measurements. Equilibrium denaturation curves were measured as described previously in chapter 2.

NMR Experiments. ^{15}N-labeled hisactophilin was prepared by growing *E. coli* in M9 minimal media with $^{15}NH_4Cl$ (Cambridge Isotopes, MA) as the sole nitrogen source and assigned as described previously in chapter 2.

Amide exchange. Amide H/D exchange samples were prepared containing ~1 mM ^{15}N-enriched myristoylated hisactophilin in 50 mM phosphate buffer at pH 8.1 or pH 5.9 and then lyophilized. Exchange was initiated by dissolving lyophilized protein in D_2O, the sample was thermally equilibrated in the NMR spectrometer (Bruker Avance TCI 700 cryoprobe) and acquisition began after a dead time of ~22 minutes. Amide exchange decays were monitored using successive ^{15}N-^{1}H HSQC spectra using gradients for water suppression and to eliminate artefacts. A spectrum was acquired every 12 minutes over the first 72 hours and rechecked periodically thereafter for 120 days. NMR data were processed using Bruker NMRSuite. Amide exchange decay rates, k_{obs}, were monitored by integrating NH cross-peaks and fitting successive areas to a single exponential decay. Intrinsic exchange rates, k_{int}, were calculated using the SPHERE server (Zhang, 1995). Protection factors, P (= k_{obs}/k_{int}, where k_{obs} is the observed rate constant for exchange and k_{int} is the intrinsic exchange rate in a random coil), for myristoylated hisactophilin were calculated for comparison with simulated values.

Results and Discussion

Hydrophobic and electrostatic nonnative interactions are necessary to accurately simulate the folding of a myristoylated protein. We simulated the folding of hisactophilin in its nonmyristoylated form using the native topology-based model which considers only native interactions found in the high resolution structure of the protein. For hisactophilin, we observed two-state folding with a relatively high energy barrier (5.9 in kT units) (Fig 4.1C), consistent with experimentally observed, relatively slow folding (Liu*, et al.*, 2002). While the native topology-based model captures many features of the folding energy landscape, it neglects the roughness of the landscape due to nonnative interactions which surely exist to some extent. Nonnative interactions may transiently form in either the unfolded state or the transition state and influence both folding thermodynamics and kinetics. We first modeled potential nonnative interactions by the formation of non-specific interactions between hydrophobic residues (HP model). The integration of hydrophobic nonnative interactions did not change the folding energy barrier, implying that hydrophobic nonnative interactions do not participate in the folding and are likely to have a minor effect on folding of nonmyristoylated hisactophilin. A comparison of all the pairwise distances in the unfolded state indicates more compact conformations in the ensemble of the unfolded state when hydrophobic nonnative interactions are included in addition to the native interactions. In general, the hydrophobic interactions bring the first half of the chain (residues 1-60) closer to the second half (residues 60-118). In the ensembles of transition and folded states, the differences due to the hydrophobic interactions are smaller.

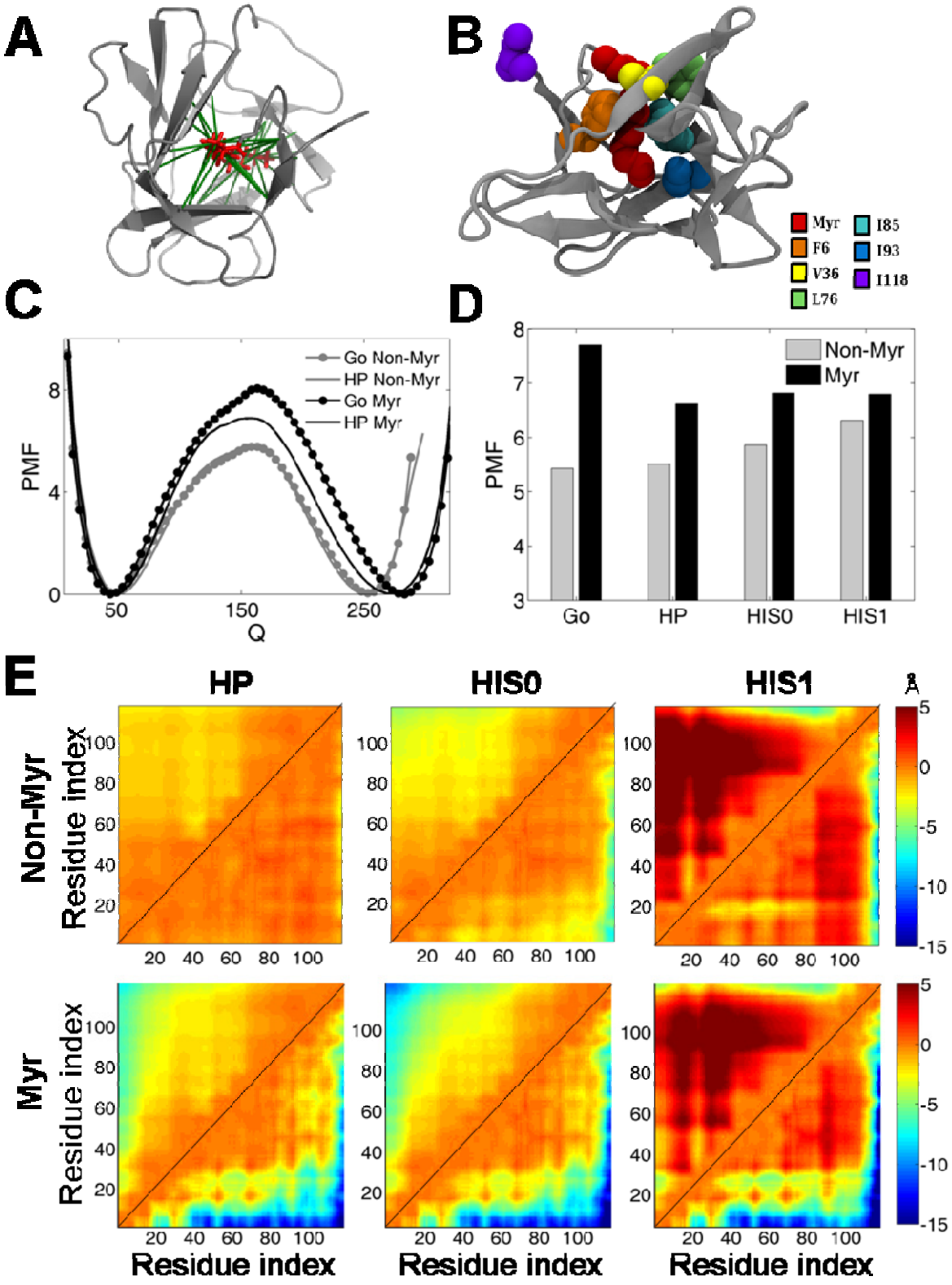

(figure legend on the following page)

Fig. 4.1. The effect of nonnative interactions on simulating the folding of nonmyristoylated and myristoylated hisactophilin. (A) Top view of myristoylated hisactophilin (grey) with native contacts (green) between the myristoyl group (red) and the protein. (B) Side view of hisactophilin with space-filling representations for mutated residues. (C) Potential of mean force vs. Q, the number of native contacts within hisactophilin., for folding of myristoylated (black) and nonmyristoylated (gray) hisactophilin calculated for four different simulation models: the native-topology based model (Go), nonnative hydrophobic model (HP), charged residue model at high pH (His0) and positively charged electrostatic model (His1). The His0 and His1 electrostatic models also include the HP model. Folding barriers are calculated at the folding temperature, T_F, which is the temperature where the protein is 50% unfolded. (D) The folding barrier for non-myr (grey) and myr (black) hisactophilin using the Go, HP, His0, and His1 models at the T_F of each system. (E) The Δ distance matrices of the transition state (lower-half) and unfolded state (upper-half) ensembles calculated relative to the corresponding ensemble obtained using the native topology-based models. Pair-wise distances between residues i and j, R_{ij} (= $\langle R_{ij}^{nonnative} \rangle$ - $\langle R_{ij}^{Go} \rangle$). Red color indicates larger distance while blue color indicates contraction due to the nonnative interactions (in Å).

In addition to nonnative interactions between hydrophobic residues, electrostatic interactions may also contribute to the roughness of the energy landscape. The effects of nonnative electrostatic interactions compared to hydrophobic interactions obviously depend on the protein sequences as well as the fact that the electrostatic interactions are long-range while the hydrophobic forces are short-range by nature. Transient interactions between hydrophobic residues and between charged residues can both increase the ruggedness of the landscape and change the folding thermodynamics and kinetics. Integration of electrostatic nonnative interactions between Asp, Glu, Lys and Arg residues together with the hydrophobic nonnative interactions (model His0) results in a more compact unfolded state compared to the unfolded state generated from the model with nonnative interactions originating from hydrophobic interactions only. The electrostatic nonnative interactions result in a higher folding barrier (an increase of ~5% in comparison to the model with hydrophobic nonnative only, Fig 4.1D). Hisactophilin contains 31 histidine residues (average pK_a value of ~6.8, (Hammond*, et al.*, 1998)) which may also participate in electrostatic nonnative interactions. When we modeled the histidine residues with positive charge (model

His1), we observed a significantly increased folding barrier (~13%) owing to the repulsion between the numerous positive charges in the protein. The repulsive interactions are reflected by the increased distances between specific areas in the protein in the unfolded and transition states. The modeling is consistent with experimentally observed large decreases in hisactophilin folding rate with decreasing pH (Liu*, et al.*, 2002, Smith*, et al.*, 2010).

We studied the effect of the myristoyl group on folding kinetics using a coarse-grained simulation. We found that myristoylated hisactophilin folds more slowly than the nonmyristoylated protein, in contradiction to the experimental result (Liu*, et al.*, 2002, Smith*, et al.*, 2010). The energy barrier at folding temperature was increased from 5.4 kT to 7.7 kT due to myristoylation (an increase of 42%, Fig 4.1C). Adding the hydrophobic nonnative interactions between the myristoyl group and the protein resulted in a dramatic acceleration of folding and a decrease in the energy barrier to 6.6 kT (Fig 4.1D). Note that the energy barrier of the myristoylated protein is higher than that of the nonmyristoylated protein (even when the hydrophobic nonnative interactions are included), because the barrier heights were estimated at the folding temperature of each system. When, however, the folding barrier heights were measured at the same temperature for all the systems, the experimentally observed accelerated folding upon myristoylation is reproduced. Integration of electrostatic nonnative interactions (at low and high pH) within the myristoylated protein did not have an additional effect on the energy barrier. From examination of the distances between residues and the change in distances upon integration of the various nonnative interactions we conclude that the major effect on the folding is in the transition state ensemble. Hydrophobic nonnative interactions position the myristoyl group 15 Å closer to the other hydrophobic residues in the protein with respect to the native topology based simulations that included

only native interactions (Fig 4.1E). The electrostatic interactions, especially at high pH, had a dual effect on the distances; the non-polar residues were still closer but the His residues were slightly farther from one another. It is possible that simulations at different ionic strength would also affect electrostatic interactions and therefore folding, as shown for folding RNA (Biyun*, et al.*, 2011)

The incorporation of the nonnative interactions (both hydrophobic and electrostatic) also influences the thermal stability of the protein as measured by the simulation. Hydrophobic nonnative interactions slightly increased the stability of the protein by 0.1%. The inclusion of the electrostatic interactions between the charged residues increased the stability by 0.8%. When we added charges to the histidine residues, the stability dropped by 3.3%. From this we conclude that the hydrophobic and electrostatic nonnative interactions contribute to the thermodynamic stability of the protein, but when too many positive charges are present in the protein stability is decreased, as has also been observed experimentally (Liu*, et al.*, 2001, Smith*, et al.*, 2010). In terms of stability, the hydrophobic nonnative interactions increased the T_F by 0.5% relative to the T_F when nonnative interactions were excluded. The electrostatic nonnative model at high pH increased the T_F by 1.1% and at low pH decreased the T_F by 2.7% (Fig. 4.S1).

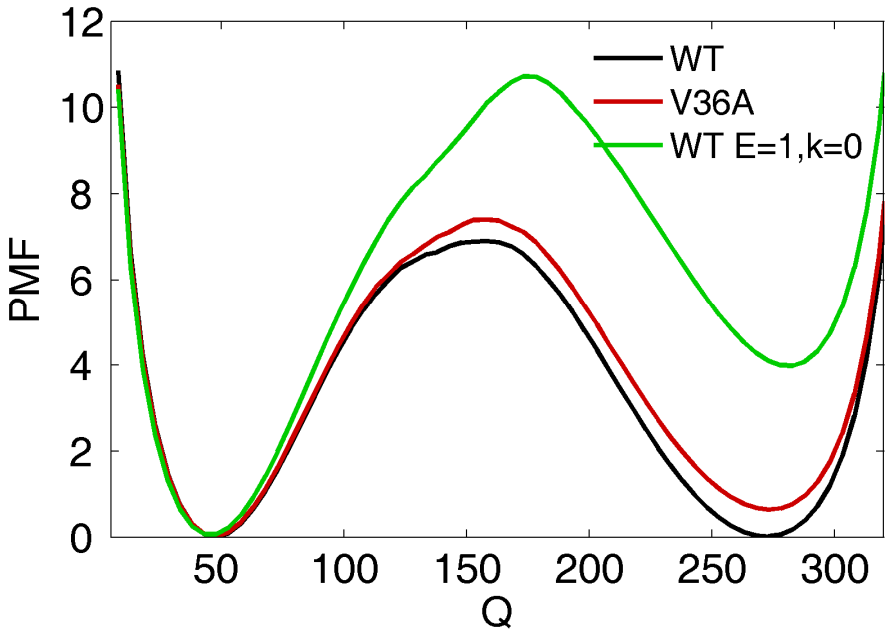

Fig. 4.S1. The free energy profiles for folding of myristoylated hisactophilin. Profiles are shown with (black) and without (green) non-native interactions between the myristoyl and the protein. All PMFs are shown at TF of WT myristoylated hisactophilin. Free energy profile for V36A is shown in red where all the nonnative hydrophobic interactions between V36 and the myristoyl group and the protein have been removed. The mutation V36A results with higher free energy barrier. The role of nonnative interactions is illustrated by the folding barrier for the system in which the myristoyl has only native interactions with the protein but no nonnative hydrophobic interactions.

To better understand the effect of the myristoylation on the kinetics and stability of the protein, we gradually changed the strength of the native and nonnative interactions between the myristoyl group and the protein. To this end, we gradually changed the value of ε and κ which correspond to the strength of native and nonnative contacts, respectively, formed at the interface between the myristoyl group and the relevant amino acids. When ε equals unity, the contacts between the myristoyl group and the protein are equivalent in their energy contribution to the rest of the contacts within the protein. On the other hand, when ε equals zero, these contacts do not make any energetic contribution. The contacts between the

myristoyl and the protein are presented in Fig 4.1A. The matrix in Fig 4.2A presents variation in the folding temperature of myristoylated hisactophilin for different values of κ and ε. In general, the T_F is increased (i.e. the protein is more thermostable) as ε and κ are increased, probably because more interactions are formed between the myristoyl and the protein and the enthalpy is larger. Calculation of the average radius of gyration for the protein, <*Rg*>, at each simulation condition shows that the <*Rg*> of the folded state is mostly affected by variations in the strength of ε and κ while the <*Rg*> of the unfolded state is robust (Fig. 4.S2). We therefore conclude that the major effect on the free energy is on the folded state. The changes in the dimensions of the folded state are in agreement with changes in the enthalpy and entropy of the folded state. The more compact folded state with increased κ and ε has correspondingly lower enthalpy and lower entropy which results in an overall decrease in the free energy of the folded state. It is notable that the strength of nonnative interactions in the simulations seems to have an effect on both the native and the transition state. The nonnative interactions in the native state may represent interactions involved in switching.

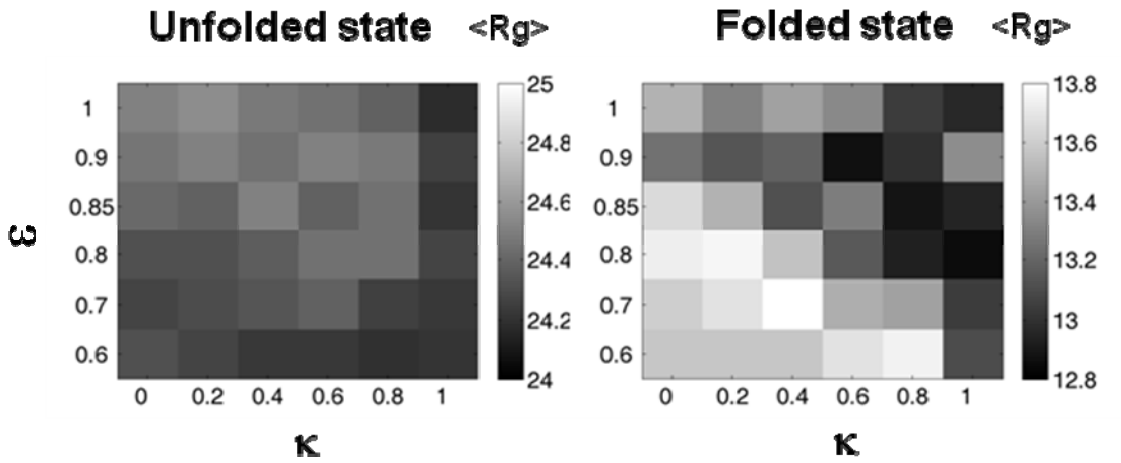

Fig. 4.S2. Compaction of the unfolded and folded states as a function of the strength of native and nonnative interactions. The compactness of the hisactophilin structure illustrated by the value of the mean radius of gyration, <*Rg*>, of the unfolded state (left) and the folded state (right) of myristoylated hisactophilin modeled with different strength of ε (native) and κ (non-native) contributions. In the calculation of <*Rg*> only the beads of the protein are considered.

Analysis of myristoyl interactions in the transition state and the native state. Fig. 4.2B presents a summary of the folding energy barrier of the myristoylated protein for differing strengths of native and nonnative interactions, each calculated at the respective folding temperature of the myristoylated protein. The matrix illustrates that the energy barrier for folding increases with the value of ε, i.e., when the myristoyl is forced to be sequestered in the protein (and interacts strongly with its pocket). When hydrophobic nonnative interactions are included, the energy barrier of folding may be decreased, in accordance with the experimental finding that the nonnative interactions play a role in accelerating folding kinetics of the myristoylated hisactophilin (Smith*, et al.*, 2010). Notably, the increase in the energy barrier is moderated when the nonnative interactions are included (κ=1) compared to when they are omitted (κ=0). The formation of the hydrophobic nonnative interactions at the folding transition state is illustrated by shorter pairwise distances between

hydrophobic residues. These distances in the transition state ensemble are generally shorter for nonnative interactions between the myristoyl and hydrophobic residues than between two hydrophobic residues (Fig. 4.2C).

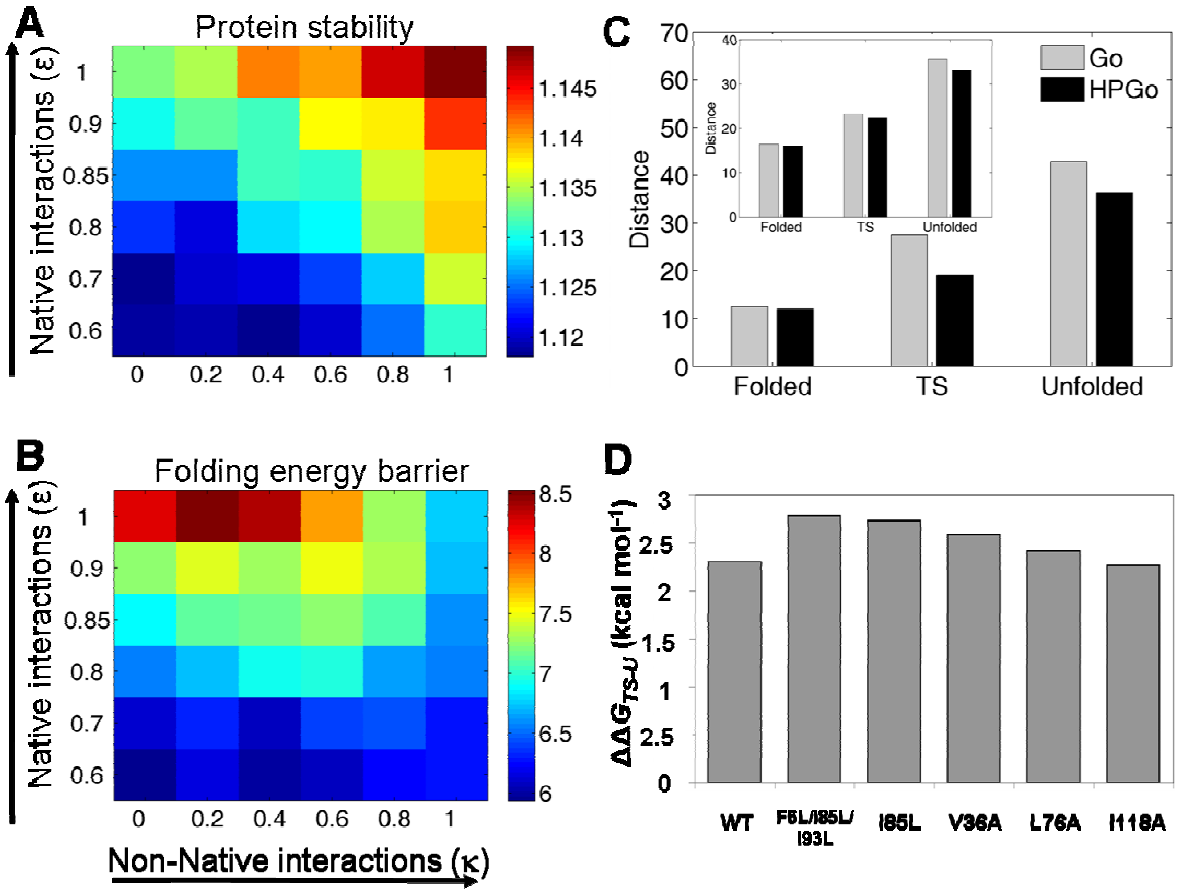

Fig. 4.2. Interplay between nonnative interactions on the folding barrier and stability. (A) The value of the folding temperature, T_F, at different strengths of native (ε) and nonnative (κ) native interactions between the myristoyl and the protein. (B) The value of the free energy barrier for folding at different strength of native and nonnative interactions of the myristoyl with the protein (at T_F). In these simulations, the ε of the native residue-residue contacts equals 1. κ = 0 corresponds to the pure native topology-based model. (C) The median of the distances of all the hydrophobic nonnative pairs between the protein and the myristoyl in the folded, unfolded, and transition state ensembles for the native topology based model (Go, grey) and the model supplemented by nonnative hydrophobic interactions (HPGo, black) hisactophilin. The inset shows the median of all hydrophobic nonnative interactions within the protein. (D) The decrease in the energy barrier for folding of WT and mutant hisactophilin upon myristoylation, $\Delta\Delta G_{TS\text{-}U}$ ($=m_{f,avg}\cdot([\text{urea}]_{\ln(kf)=0,myr}-[\text{urea}]_{\ln(kf)=0,nonmyr})$) calculated using the average denaturant dependence for ln k_f, $m_{f,avg}$, for all proteins (Fig. 4.S3).

Experimental measurement of folding kinetics for hisactophilin variants can provide information on the formation of interactions for specific groups (e.g. myristoyl and/or amino acid sidechains) during protein folding. As mentioned above, such measurements have shown that the myristoyl group greatly accelerates the folding of WT hisactophilin and this involves the formation of nonnative interactions in the transition state (Smith*, et al.*, 2010). The effects of mutation of hydrophobic residues inside and outside the myristoyl binding pocket range from slightly increasing to considerably decreasing the rate of protein folding (Fig. 4.S3). Remarkably, however, the large increase in folding rate conferred by myristoylation remains largely unchanged for all mutants (Fig. 4.2D). In other words, none of the mutated residues appear to make critical, specific interactions with the myristoyl group in the transition state ensemble. This suggests that the myristoyl group accelerates the rate of folding by making nonspecific, including nonnative, interactions in the transition state. These interactions may be highly robust to mutation and have the effect of smoothing the folding energy landscape and reducing frustration.

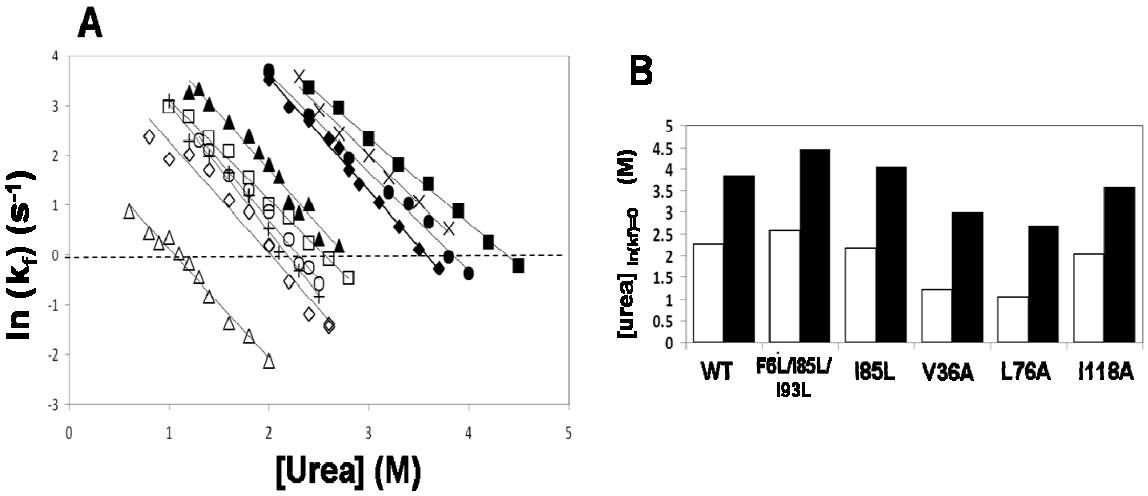

Fig. 4.S3. Observed folding rate constants versus urea concentration for variant hisactophilins. (A) Rate constants are shown for myristoylated proteins: L76A (closed triangles), WT (closed circles), I85L (Xs), I118A (closed diamonds) and F6L/I85L/I93L (closed squares); and for the corresponding nonmyristoylated proteins: L76A (open triangles), WT (open circles), I85L (crosses), I118A (open diamonds) and F6L/I85L/I93L (open squares). The dashed line illustrates where $\ln(k_f) = 0$. (B) Urea concentration where the rate constant for folding of variant hisactophilins, k_f, is $1s^{-1}$, i.e. $[\text{urea}]_{\ln(kf)=0}$ where $\ln(k_f) = 0$, for nonmyristoylated (white) and myristoylated (black) proteins. Proteins with higher values of $[\text{urea}]_{\ln(kf=0)}$ fold faster.

Energetic myristoyl switch with pH. The experimental study of hisactophilin shows a clear energetic switch between the nonmyristoylated and myristoylated forms upon changing from low to high pH (Smith*, et al.*, 2010). At low pH, in excess ligand (H^+s) the difference in stabilization upon myristoylation is much smaller than at high pH, where the absence of bound H^+ increases the stability of both the myristoylated and nonmyristoylated protein (Fig 4.3A). Also, the stability of the protein at low pH is much smaller than that in high pH. Assuming that the change in pH mostly affects the protonation state of histidine residues, we simulated the protein using the His0 and His1 models (which model the protein at high and low pH, respectively). In the simulations the myristoylated protein is more stable than the nonmyristoylated protein both at low and high pH (Fig 4.3B), similar to experiment.

However, the modulation of the stabilization with pH could not be simply observed in the simulations, but only by assuming that the strength of the interactions of the myristoyl with the protein (either native or nonnative) is indirectly affected by the pH due to the change in the protonation state of the histidine. This energetic switch is accompanied by a conformational switch: at low pH the myristoyl group is in the accessible state and at high pH it is sequestered. We observe this dual effect of energetic and structural switching when we manipulate the strength of the native or nonnative interactions between the myristoyl group and the protein. In this way, we can decrease the amount of extra stability that was achieved by adding the myristoyl, implying that changes in pH not only affect the protonation state of the histidine residues, but also change the strength of the interactions between the protein and the myristoyl. We conjecture, therefore, that the switch originates from a thermodynamic effect. In the absence of ligand (at high pH), the protein is thermodynamically stable and undergoes minor structural fluctuations, therefore the probability of the switching between the sequestered and accessible states is low (high free energy). In excess of ligand (at low pH), the protein is less stable, the probability for the switching is higher and the accessible state is more populated. This leads to a lower thermodynamic stability due to the loss of enthalpic contributions from the direct interaction of the myristoyl and the hydrophobic pocket. Thus, simulations provide evidence that the experimentally observed energetic switch is governed by the balance of native and nonnative interactions. This highlights the importance of modeling nonnative interactions for understanding the mechanism of myristoyl switching. We then analyzed the contributions of individual residues to switching, using a combination of experimental measurements and atomistic simulations for mutant proteins. In previous experiments, we found that the switch

in hisactophilin is broken in the triple myristoyl binding pocket mutant, F6L/I85L/I93L, such that the myristoyl group remains in the fully sequestered state (I) and does not switch to the accessible state (II) with decreasing pH (Smith*, et al.*, 2011) (Fig. 4.3C). We now report that the single mutation, I85L, breaks the switch in the opposite way, i.e. by weakening interactions of the myristoyl with the protein such that the mutant protein remains in the accessible state (II). It is noteworthy that this highly conservative mutation, changing only the stereochemistry of a single hydrophobic sidechain, essentially abolishes switching. We speculate that moving the branch point in the sidechain from the β to the γ carbon may create steric clashes with the myristoyl, interfering with it adopting its fully sequestered conformation, and concomitantly increasing protein dynamics such that coupling between the myristoyl binding site and sites of protonation is disrupted.

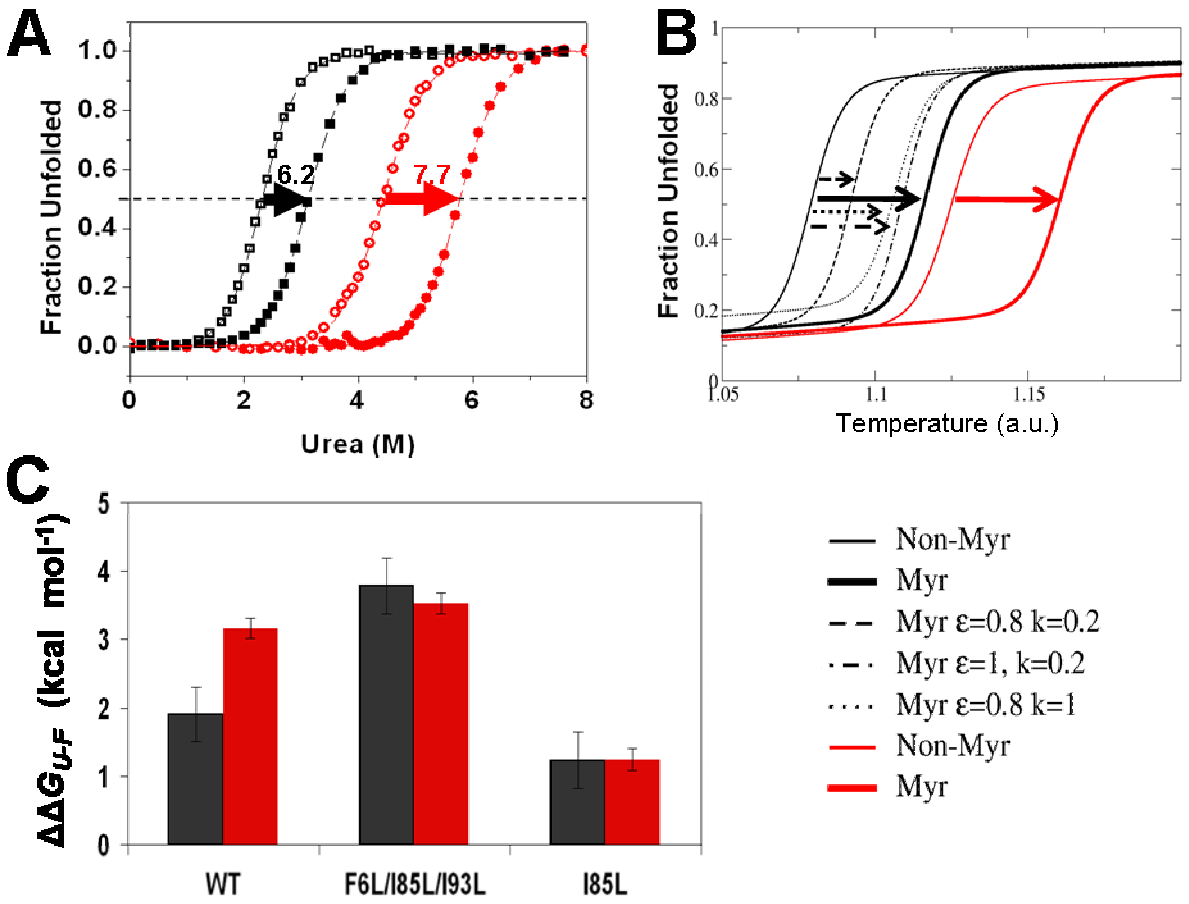

Fig. 4.3. Energetics of myristoyl switching. (A) Equilibrium urea denaturation curve measurements of stability for nonmyristoylated (open symbols) and myristoylated (closed symbols) hisactophilin at pH 6.2 (black squares) and 7.7 (red circles). Stabilization upon myristoylation, $\Delta\Delta G_{U\text{-}F}$ (= $\Delta C_{mid} \cdot m_{avg}$), calculated from the difference in the midpoint of denaturation, ΔC_{mid}, for myristoylated relative to nonmyristoylated hisactophilin multiplied by m_{avg}, the average denaturant dependence of $\Delta G_{U\text{-}F}$ for the 2 forms of hisactophilin (Smith, *et al.*, 2010). (B) Simulated fraction unfolded *vs.* temperature for myristoylated (solid bold line) and nonmyristoylated (solid line) hisactophilin at low pH (black) and high pH (red) under different strengths of ε (native) and κ (nonnative) myristoyl interactions. (C) Stabilization upon myristoylation, $\Delta\Delta G_{U\text{-}F}$, for WT, F6L/I85L/I93L and I85L hisactophilin at pH 6.2 (black) and pH 7.7 (red).

The F6L/I85L/I93L and I85L mutations have dramatically different effects on the transition state compared to the native state. Rather counter-intuitively, despite the broken switching, both F6L/I85L/I93L and I85L fold slightly faster than WT in the myristoylated form (Fig. 4.S3A). This suggests that the folding of the WT protein is slightly slowed, i.e. frustrated, by residues required for switching functionality. Nevertheless, as mentioned above, the energetics of the transition state relative to the unfolded state is robust (Fig 4.2D). In contrast, the energetics of the native state and protein function are dramatically affected by the mutations (Fig 4.3C). This suggests that I85L introduces too much strain into the native state to allow for switching, while F6L/I85L/I93L causes a too large reduction in strain, consistent with altered dynamics observed in atomistic simulations (see below).

Structural switch of the myristoyl between sequestered, accessible and exposed states. From our folding simulations, we identified the conditions where myristoyl switching occurs. Fig 4.4A shows a two-dimensional free energy surface for the coupling between folding of hisactophilin (depicted by $Q_{Folding}$) and switching of the myristoyl group (depicted by $Q_{Prot\text{-}Myristoyl}$) for three sets of ε and κ parameters for native and nonnative interactions of the myristoyl group. At low values of $Q_{Folding}$, the protein is unfolded and the myristoyl is highly exposed to solvent (i.e., $Q_{Prot\text{-}Myristoyl}$ is low but some sporadic interactions between the myristoyl and the protein are found). At high values of $Q_{Folding}$, the protein is folded and the myristoyl forms many more contacts with the protein as it fits in the hydrophobic pocket. When ε=0.6 and κ= 0, the enthalpic stabilization is insufficient for populating the sequestered state. However, increasing the strength of the

native and nonnative interactions (ε=0.8 and κ=0.2) results in the full insertion of the myristoyl into its pocket. The switching of the myristoyl from the exposed to the sequestered state follows the folding of the protein (Fig 4.4A). Only when the strength of the interactions of the myristoyl with the protein are sufficiently strong (close to unity, comparable to the strength of other native contact within the protein), a coupling between folding and switching emerges (i.e., the folding follows more two-state rather than three-state behaviour). In this scenario, the strong coupling between folding and switching can be reduced when the strength of nonnative interactions is increased as they may allow the protein to populate states other than the fully sequestered state while the rest of the protein is folded.

To further elucidate the switching mechanism, we analyzed the position of the tip of the myristoyl with respect to the bottom of its hydrophobic pocket; specifically, we measured the distance between the bead representing C13 and C14 of the myristoyl group and the center of mass of the beads representing the alpha carbons of three residues at the bottom of the barrel (V21, V61, V101). This analysis revealed three typical structural states of the myristoyl group relative to the protein. The two limiting states correspond to the myristoyl being fully sequestered in the protein binding pocket versus the fully exposed state of the myristoyl (states I and III in Fig 4.4). In the remaining state, the myristoyl is partially accessible to the solvent (state II) and is stabilized by nonnative interactions between the myristoyl and hydrophobic residues located at the rim of the pocket (Fig 4.4E). This intermediate state (state II in which the myristoyl forms about 8 native interactions with the protein compared to 25 in the fully sequestered state, Fig 4.4B) resembles the accessible state that was observed in experiments as pH was lowered. In this accessible state, the myristoyl group is less buried, however, there remain significant interactions between the myristoyl and

the protein, based on measurements of energetics and structural NMR data (Smith*, et al.*, 2010). In the simulations, the strength of native and nonnative interactions between the protein and the myristoyl has a major impact on the position of the myristoyl with respect to the protein. In general, we see that when the native interactions are strong ($\varepsilon \geq 0.9$), the protein is mostly in the sequestered state (state I), regardless of the strength of the hydrophobic nonnative interactions. The exposed state (state III) is common in simulations in which both the native and nonnative interactions are weak (κ and $\varepsilon < 0.6$). The partially accessible state (state II), is most common when the nonnative interactions are strong ($\kappa=1$), but native contacts between the myristoyl and the pocket are weak ($\varepsilon < 0.7$) (see Figs. 4.4A and 4.S4). We speculate that in hisactophilin the nonnative interactions between the protein and the myristoyl are strong while the native interactions are a bit weaker than the rest of the native interactions in the protein, and this combination leads to the observed intermediate position of the myristoyl group relative to the protein at low pH.

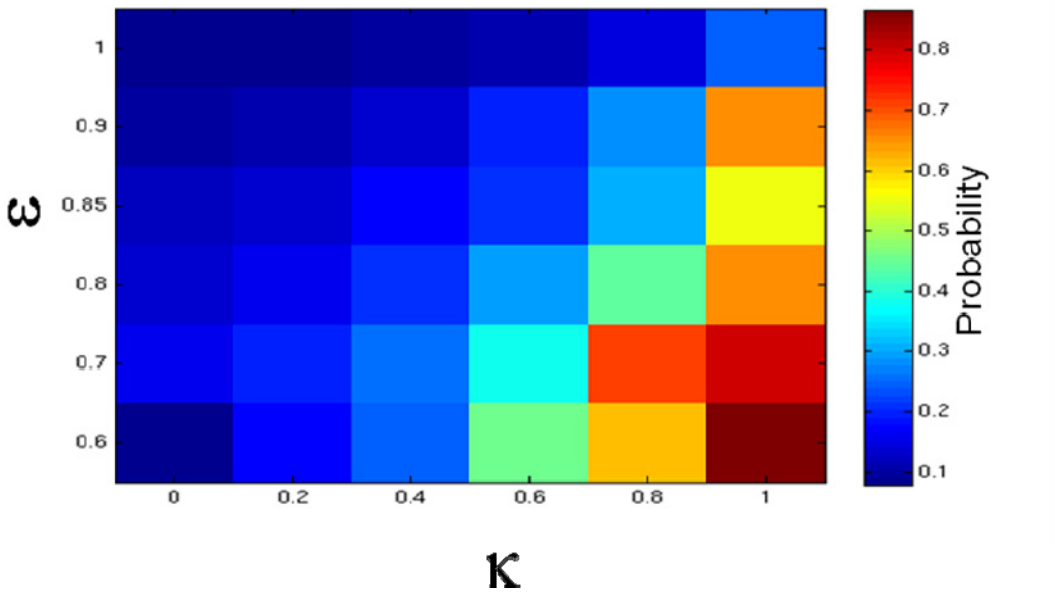

Fig. 4.S4. The probability to populate state II at different strength of native, ε, and non-native, κ, protein-myristoyl interactions.

Using molecular dynamics simulations of the folded state for WT, F6L/I85L/I93L and I85L, we assessed the extent of burial of the myristoyl group in the protein binding pocket by measuring the distance from the tip of the myristoyl to the bottom of the barrel. We also calculated the time for the position of the myristoyl group in the protein to become decorrelated, which provides a measure of myristoyl dynamics. The simulations suggest that WT accesses both the sequestered and partially accessible states (I and II). In contrast, F6L/I85L/I93L is very predominantly in a sequestered state (I), with the myristoyl inserted further into the protein than in WT and little fluctuation of the myristoyl into the accessible state (II). On the other hand, in I85L the myristoyl tends to be slightly less buried than in WT, leading to an increased population of the accessible state (II). In addition, the triple mutant transitions between states more slowly than WT based on increased autocorrelation

time for the position of the myristoyl group compared to WT, whereas the single mutant shows the opposite behaviour, transitioning more rapidly with a faster decay in autocorrelation time (Fig 4.4D). Thus, both the location and dynamics of the myristoyl group in the atomistic simulations are consistent with the experimental energetic data (Fig 4.3C) and folding simulations (Fig 4.4A-C), which taken together indicate that the myristoyl: 1) makes stronger interactions with the protein in F6L/I85L/I93L causing it to remain in the sequestered state; 2) makes weaker interactions in I85L so that it stays in the accessible state II; and 3) is poised to switch between the two states in WT.

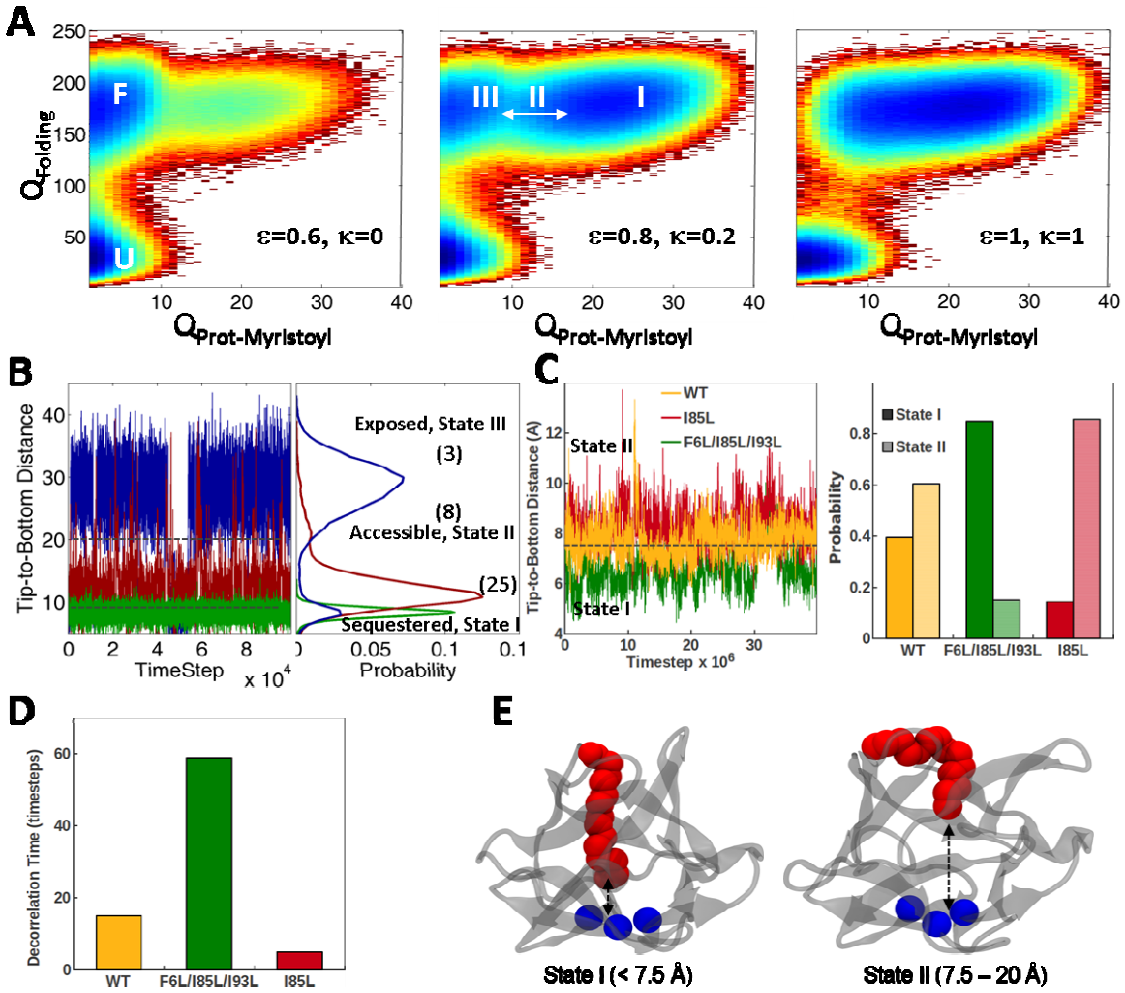

Fig. 4.4. Structural characterization of the myristoyl switching mechanism. (A) The coupling between folding and switching is shown by projecting the free energy onto two reactions coordinates: $Q_{Folding}$ (number of native contacts within hisactophilin) and $Q_{Prot\text{-}Myristoyl}$ (number of native contacts between the myristoyl and hisactophilin) for $\varepsilon = 0.6$, $\kappa = 0$; $\varepsilon = 0.8$, $\kappa = 0.2$; and $\varepsilon = 1$, $\kappa = 1$. Blue areas correspond to highly populated states and red to poorly populated ones. (B) Definition of the three states of the myristoyl relative to the bottom of the barrel: fully sequestered (state I, < 7.5 Å), accessible (state II, 7.5 – 20 Å), and exposed (state III, > 20 Å). The numbers in brackets refer to the average number of native contacts between the myristoyl and the protein in each state. (C) Analysis of atomistic molecular dynamics simulations for WT, F6L/I85L/I93L and I85L showing effects of mutations on the probability of populating states I and II analogous to increasing or decreasing the native interaction strength (F6L/I85L/I93L and I85L, respectively). (D) Decorrelation time of the tip-to-bottom distance. (E) Representative conformations of the myristoyl for states I and II that were found in atomistic simulations.

Localized stability changes associated with myristoyl switching. We obtained higher resolution insights into the energetics of switching by further analysis of simulations combined with experimental measurements of amide H/D exchange rates. Full stabilization of the protein occurs only after the myristoyl is switched from the accessible to the sequestered state (transition from state II to state I). We identified 12 residues that become significantly more ordered after the myristoyl is fully inserted into the pocket (Fig 4.5A, blue). Some of these residues are close in sequence to the myristoyl and may be expected to behave in this way, whereas others are far in sequence but close in structure. Notably, the N- and C- termini of the protein exhibit the largest increase in order when the myristoyl becomes sequestered.

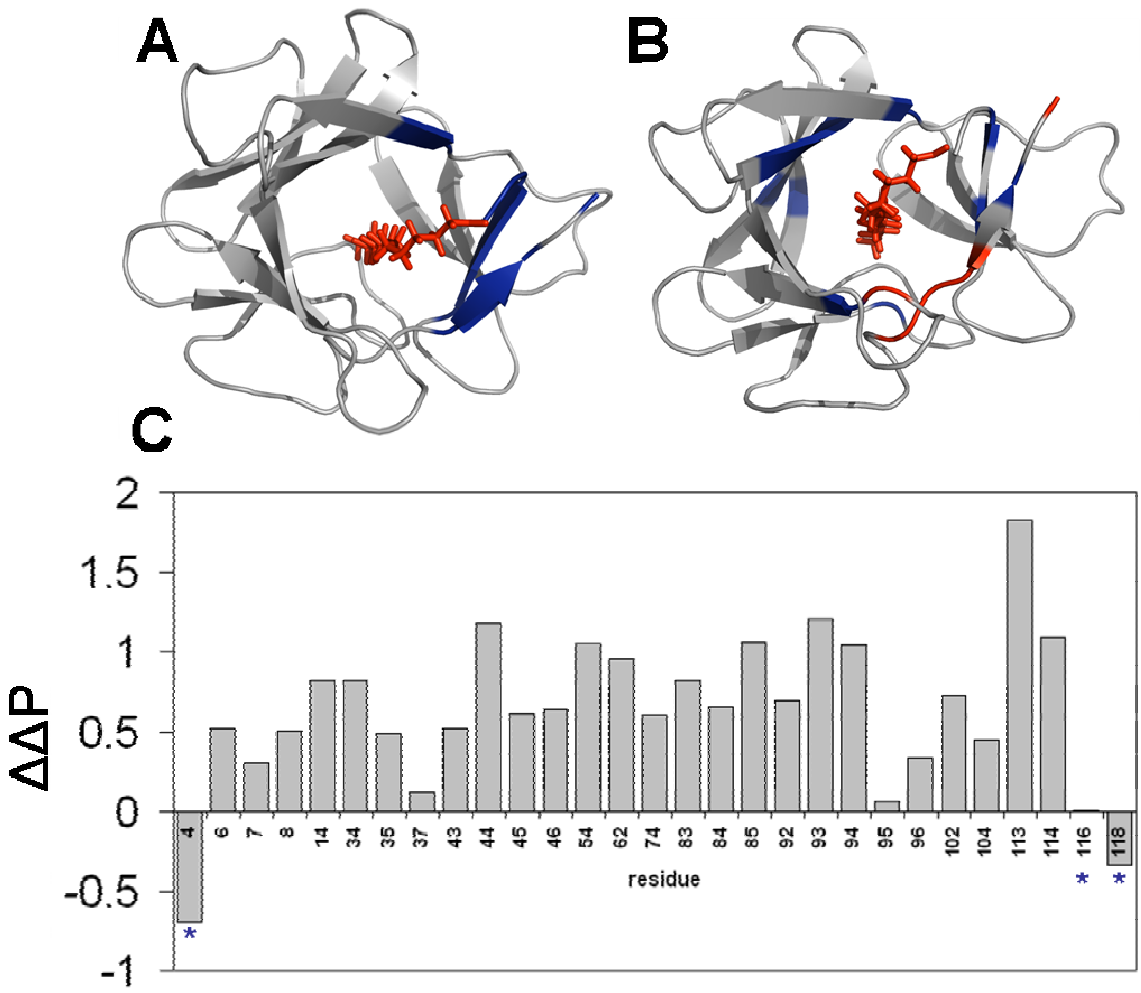

Fig. 4.5. Changes in dynamics upon myristoylation. (A) Top-view of hisactophilin with residues predicted to become ordered (blue, G2, N3, R4, A5, F6, K7, H35, V36, E114, E115, I116, I118) upon sequestering of the myristoyl group as observed by simulation. (B) Measured change in amide exchange protection factor, $\Delta P_{pH8.1}$ (= $\log(P_{myr} \cdot P_{non}^{-1})$), upon myristoylation of WT hisactophilin, measured at pH 8.1 where the myristoyl group is sequestered. Residues R4, V43, A95 and I116 show the largest increase in protection upon myristoylation and are shown in dark blue (other residues that are mildly protected are shown with lighter shades of blue) and V83, T112, F113, E114 and I118 show decreased protection and are indicated in red. The myristoyl group is shown in red stick representations and the structure has been rotated slightly to emphasize perturbed residues. (C) Change in protection upon switching, $\Delta\Delta P$ (= $\log(\Delta P_{pH8.1} \cdot \Delta P_{pH5.9}^{-1})$) for individual NH groups in hisactophilin. $\Delta\Delta P$ is a measure of the relative change in protection, and hence change in dynamics, associated with the myristoyl group switching from state II at pH 5.9 to state I at pH 8.1. Residues, at the N- and C-termini show the most pronounced decrease in dynamics upon myristoyl sequestration.

We obtained an experimental measure of changes in protein flexibility upon myristoylation using amide H/D exchange rate measurements for ~35 amides located throughout the protein structure (Fig. 4.5B and S4.5). Increased amide H/D protection factors upon myristoylation are observed for many amides throughout the protein, at both pH 5.9 where the protein is predominantly in the accessible myristoyl conformation (state II) and at pH 8.1 where the protein is predominantly in the sequestered conformation (state I) (Fig. 4.5B). This protection is consistent with myristoylation increasing the global protein stability, as has also been observed in chemical denaturation experiments (Houliston*, et al.*, 2002, Smith*, et al.*, 2010). Furthermore, the largest increases in amide protection arising from the myristoyl group from pH 5.9 to 8.1 are observed for amides close to the N- and C-termini (Fig. 4.5C). This is consistent with the increase in structure upon full insertion of the myristoyl group observed by simulation (Fig 4.5A). The amide protection factors also reveal that a small group of amides (V83, T112, F113, E114 and I118) show small decreases in protection upon myristoylation (Fig 4.5C). These residues are clustered at one side of the myristoyl binding pocket, suggesting that mobility in this region may be linked to and facilitate switching between accessible and sequestered states.

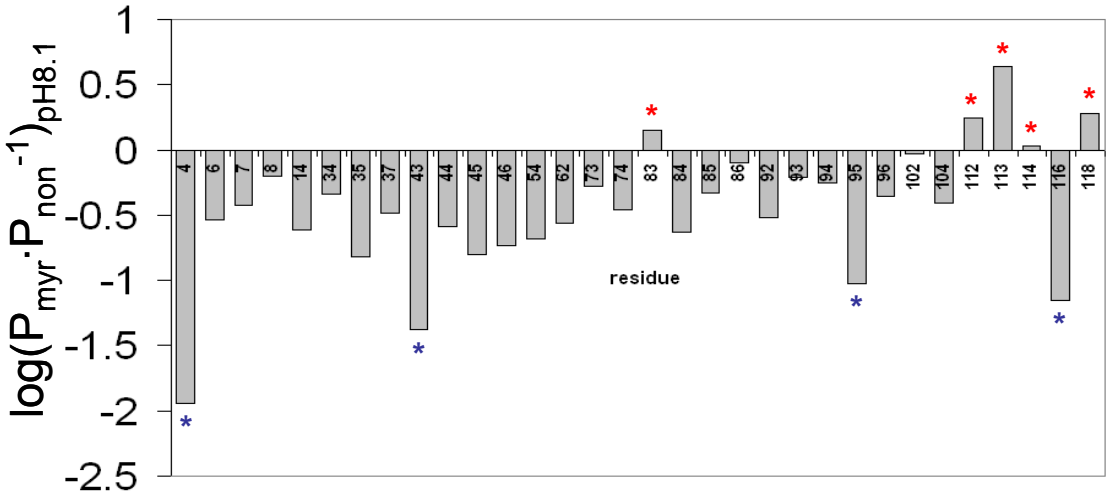

Fig. 4.S5. Amide H/D exchange protection factors in myristoylated hisactophilin relative to nonmyristoylated hisactophilin. Changes in amide protection factors, P, are plotted versus residue number. Change in protection upon myristoylation, $\Delta P_{pH8.1}$ (= $\log(P_{myr} \cdot P_{non}^{-1})$), for individual NH groups in hisactophilin at pH 8.1. The overall negative values of $\Delta P_{pH8.1}$ reflect increased global stability upon myristoylation. Residues that are relatively more protected ($\Delta P_{pH8.1}$ <0) and less protected ($\Delta P_{pH8.1}$ >0) are marked with blue and red asterisks, respectively.

Conclusions. Post-translational modifications are a common means to regulate protein function. In many cases the regulation is achieved by the modification directly modulating the biophysical properties of the protein. Our study reveals molecular details of significant changes in protein stability and kinetics caused by myristoylation. The effects of myristoylation are more pronounced than those observed for glycosylation (Shental-Bechor and Levy, 2008) and ubiquitination (Hagai and Levy, 2010) and can be simply rationalized by the close interactions of the hydrophobic myristoyl group with its binding pocket within the protein, while in the case of glycan and ubiquitin conjugates the interface with the protein is smaller and dominated by excluded-volume effects. The extensive interface the myristoyl forms with the protein may therefore change the folding enthalpy as well as the internal dynamics of the protein.

Using a range of complementary experimental and computational approaches, we characterized the pronounced effects of myristoylation on the folding thermodynamics and kinetics of hisactophilin. The effects on folding cannot be explained solely by the native interactions defined in the NMR structure of hisactophilin with the myristoyl sequestered in its binding pocket (Smith*, et al.*, 2010); additional nonnative hydrophobic and electrostatic interactions also have significant roles. The coarse-grained simulation models highlight the importance of nonnative hydrophobic interactions in reducing the free energy barrier for folding and for stabilizing the protein. The simulations reveal an intermediate state distinct from the sequestered observed by NMR and a state with fully exposed myristoyl, in which the myristoyl is partially accessible and makes stabilizing nonnative interactions with the protein. In simulations and experiments, hisactophilin has maximal global stability only after the myristoyl switches to the sequestered state. Furthermore, coarse-grained simulations and amide H/D exchange measurements reveal molecular details of switching mechanism involving changes in local stability clustered at one side of the binding pocket and including the N- and C-termini of the protein. The effects of mutating hydrophobic residues distributed around and outside the myristoyl binding pocket reveal the robust effect of myristoylation on folding kinetics, which contrasts with the relative ease of breaking native state switching. These results suggest that the long and flexible nature of the myristoyl alkyl chain may enable sampling of a relatively broad, nonspecific ensemble of hydrophobic interactions in the transition state which is much more restricted and finely tuned in the native state.

In summary, a combination of computational and experimental approaches provides new insights on how a common fatty-acyl protein modification can tune folding through both native and nonnative interactions, and how changes in stability and dynamics control

function. The effects of myristoylation in hisactophilin are similar to results for other proteins where regions of increased local stability are counterbalanced by regions of decreased local stability implicated in function regulation by ligand binding (Namanja*, et al.*, 2011, Marlow*, et al.*, 2010, Tzeng and Kalodimos, 2011). The folding energetics and mechanism for myristoylated hisactophilin support the notion that local energetic frustration and the accumulation of strain during the switching can be linked to function as observed in allosteric proteins (Ferreiro*, et al.*, 2011) and for functional and/or hydrophobic residues in other proteins (Capaldi*, et al.*, 2002, Wensley*, et al.*, 2010, Friel*, et al.*, 2009, Di Nardo*, et al.*, 2004, Baxter*, et al.*).

Chapter 5 – The Energetic Link Between Allostery and Myristoyl Switching in Hisactophilin.

Introduction

Allostery is a fundamental control mechanism that governs many protein functions. Under allosteric control a protein receives an external signal, via binding of a small molecule ligand to the protein, which is transmitted into a change in functionality (Tzeng and Kalodimos, 2011). These signals are transmitted through a coupling pathway connecting effector ligand binding to distal regions in the protein undergoing the switch (Kalodimos*, et al.*, 2002). NMR has been used to understand allostery in proteins at the atomic level (Hilser*, et al.*, 2012, McDonald*, et al.*, 2012, Cui and Karplus, 2008). New methods for the analysis are emerging to study the allosteric communication pathways in proteins (Smith*, et al.*, 2010, Boyer*, et al.*, 2010, Das*, et al.*, 2006, Selvaratnam*, et al.*, 2012). In particular, recent NMR studies have stimulated new debate about the exact mechanisms that regulate allosteric communication pathways (Namanja*, et al.*, 2011, Marlow*, et al.*, 2010, Kalodimos*, et al.*, 2004). Therefore, further study is required to understand the fine tuning of energetics and dynamics that govern allosteric communication pathways in proteins. NH/D exchange is a method that has been widely used to characterize folding and switching in proteins (Marlatt and Shaw, 2007, LeMaster*, et al.*, 2005, Polshakov*, et al.*, 2006, Meiering*, et al.*, 1993). It can also provide high resolution site-specific information on long range coupling in proteins (Boyer*, et al.*, 2010). A general method is developed here that uses thermodynamic cycle analysis of amide NH/D exchange to map the local energetics involved in regulating

allosteric communication pathways of myristoyl switching proteins. The thermodynamic model developed to characterize the site-specific switch energetics has also been applied to other myristoyl switching proteins.

Myristoyl switches represent a regulated protein function whereby ligand binding signals are communicated through the protein to elicit a conformational or energetic switch at distal sites (Ames*, et al.*, 1997, Smith*, et al.*, 2010). Myristoyl switching typically involves conversion between a myristoyl-sequestered state, myr_{seq}, where the myristoyl group is located in a hydrophobic binding pocket within the protein, and a myristoyl-accessible state, myr_{acc}, where the myristoyl group has increased accessibility for binding to membranes or other proteins (Chapters 2 - 4 and (Ames*, et al.*, 1997)). Switching may be associated with relatively large or subtle structural and/or dynamic changes in the myristoylated protein. Switching can be regulated by binding of various ligands (e.g. H^+, Ca^{2+}, GTP, or regulatory protein) (McLaughlin and Aderem, 1995, Ames*, et al.*, 1995, Resh, 2004, Orban*, et al.*, 2010, Hanakam*, et al.*, 1996). The pH-dependent myristoyl switch in hisactophilin is involved in controlling cytoskeletal changes during cellular movement and osmotic stress (Pintsch*, et al.*, 2002, Hanakam*, et al.*, 1996, Ponte*, et al.*, 2000). Hisactophilin has been used as a model system to study protein folding and myristoyl switching using a combination of thermodynamic cycle analysis, kinetic folding/unfolding and NH/D exchange measurements (Chapter 2 - 4 and Hammond*, et al.*, 1998, Liu*, et al.*, 2001, Wong*, et al.*, 2004, Liu*, et al.*, 2002, Houliston*, et al.*, 2002, Smith*, et al.*, 2010, Smith*, et al.*, 2011).

NH/D exchange is a powerful tool that provides site-specific information on protein folding, stability and dynamics (Hvidt and Nielsen, 1966, Englander*, et al.*, 1972, Englander

and Kallenbach, 1983). The exchange of amide protons with solvent deuterons can be described by the two-step model:

$$closed^{H} \underset{k_{op}}{\overset{k_{cl}}{\rightleftarrows}} open^{H} \xrightarrow{k_{\text{int}}} exchanged^{D} \qquad [5.1]$$

where closed^{H} and open^{H} refer to the protonated form of the closed (i.e. protected) and open (i.e. exchange competent) states, respectively, exchanged^{D} refers to the deuterium exchanged state. k_{op}, k_{cl} and k_{int} refer to the rate constants of opening, closing and intrinsic exchange in a random coil peptide, respectively. Under conditions that favour the folded state of a protein, k_{obs}, the observed rate constant of exchange is:

$$k_{obs} = \frac{k_{op} \cdot k_{\text{int}}}{k_{cl} + k_{\text{int}}} \qquad [5.2]$$

When $k_{cl} << k_{int}$, NH/D exchange occurs via the EX1 mechanism and $k_{obs} = k_{op}$. Under EX2 conditions $k_{cl} >> k_{int}$ and k_{obs} becomes proportional to K_{op} (= $k_{op} \cdot k_{cl}^{-1}$), the equilibrium constant of opening and k_{int}, thus becoming:

$$k_{obs} = \left(K_{op}\right) \cdot k_{\text{int}} \qquad [5.3]$$

and the observed site-specific stability of a given amide group, ΔG_{ex}, can be expressed as:

$$\Delta G_{ex} = - R \cdot T \cdot \ln(k_{obs} \cdot k_{int}^{-1}) \quad [5.4]$$

where R is the universal gas constant and T represents the temperature in Kelvin. The slowest exchanging amides undergo exchange only through global unfolding of the protein and make up the global core. ΔG_{ex} for these global exchangers should be equivalent to the Gibbs free energy of unfolding, $\Delta G_{U\text{-}F,}$ for amides exchanging under EX2 conditions via global unfolding. Information about the enthalpy of opening, ΔH_{ex} (=ΔH_{op} + ΔH_{int}), can be obtained through measurements of k_{obs} as a function of temperature through the following equation (LeMaster*, et al.*, 2005):

$$\frac{d\left(\ln\left(K_{op}\right)\right)}{d\left(\frac{1}{T}\right)} = \frac{-\Delta H_{ex}}{R} \quad [5.5]$$

where K_{op} is the equilibrium constant for opening. The intrinsic enthalpy of exchange in random coil peptides, ΔH_{int}, has been estimated as 17 kcal·mol^{-1} (Englander*, et al.*, 1972). Here, the kinetics of NH/D exchange are reported for myristoylated hisactophilin as a function of pH and temperature. A general methodology is developed here based on the kinetics of exchange at different pHs to determine site-specific coupling energetics of myristoyl switching in hisactophilin. Site-specific information is compared to the global switch energetics, ΔG_{switch}, in several mutants. Changes in ΔH_{ex} upon myristoylation, $\Delta\Delta H_{ex}$, are compared with changes in ΔG_{ex} upon myristoylation, $\Delta\Delta G_{ex}$, and provide further information about the site-specific thermodynamics.

Materials and Methods

Protein purification. Myristoylated hisactophilin was expressed and purified as described previously (Chapter 2 Materials and Methods).

Equilibrium, folding and unfolding measurements. Equilibrium denaturation curves were measured as described previously (Chapter 2 and (Wong*, et al.*, 2004)). Stock protein solution was prepared by dissolving lyophilized hisactophilin to a concentration of 2 $mg \cdot mL^{-1}$ in 500 mM potassium phosphate buffer at pH 6.8. Protein stock was diluted ten-fold in water and stock urea to the desired final concentration of urea. Samples were equilibrated at the appropriate temperature in a water bath for at least ten half-lives as measured for kinetic folding/unfolding transitions at 25˚C. Samples were monitored by fluorescence using a Fluorolog3-22 spectrofluorometer (Horiba-Jobin-Yvon Spex Inc.) as described previously with excitation and emission wavelengths of 277 nm and 306 nm, respectively (Wong*, et al.*, 2004, Liu*, et al.*, 2002).

Amide exchange. Myristoylated hisactophilin amide H/D exchange samples were prepared containing ~1 mM ^{15}N-enriched myristoylated hisactophilin in 50 mM phosphate buffer at pH 6.8; or pH 8.1 and then lyophilized. The temperature-dependence of exchange was determined at pH 6.8 at 17˚C, 25˚C and 37˚C. Exchange was initiated by dissolving lyophilized protein in thermally pre-equilibrated D_2O. The sample was then thermally equilibrated in the NMR spectrometer (Bruker Avance 700 with TCI cryoprobe) and

acquisition began after a dead time of ~22 minutes. Exchange decay rate constants, k_{obs}, were determined by integrating amide NH cross-peaks and fitting successive peak volumes to a single exponential decay as described previously (Houliston*, et al.*, 2002). Values of k_{obs} for each amide groups in the nonmyristoylated form of hisactophilin were previously determined in the pH range 5.9 – 9.7 previously (Houliston*, et al.*, 2002). Intrinsic exchange rates, k_{int}, were calculated using the SPHERE server (Zhang, 1995).

Results and Discussion

Local coupling energies. A method for double mutant energetic analysis was adapted to analyze the global energetics involved in ligand-binding-induced myristoyl switching using stability measurements (Chapter 3). In this approach a coupling energy between the myristoyl group and the ligand binding site is determined. The overall coupling energy, ΔG_{switch}, is calculated between the myristoyl group and ligand-binding sites is calculated as:

$$\Delta G_{switch} = \Delta\Delta G_{U-F(myr \rightarrow nonmyr)\,free} - \Delta\Delta G_{U-F(myr \rightarrow nonmyr)bound} \qquad [5.6]$$

where $\Delta\Delta G_{U\text{-}F(myr \rightarrow nonmyr)bound}$ and $\Delta\Delta G_{U\text{-}F(myr \rightarrow nonmyr)free}$ represent the change in stability upon myristoylation in the ligand-bound and ligand-free states, respectively, as determined by equilibrium stability measurements. For the hisactophilin pH-dependent myristoyl switch, the ligand is H^+ and the ligand-bound and ligand-free states represent the low and high pH states, respectively. In this case, ΔG_{switch} becomes:

$$\Delta G_{switch} = \Delta\Delta G_{U-F(myr \rightarrow nonmyr)highpH} - \Delta\Delta G_{U-F(myr \rightarrow nonmyr)lowpH} = \Delta G_{U-F(myr)highpH} - \Delta G_{U-F(nonmyr)highpH} - \left(\Delta G_{U-F(myr)lowpH} - \Delta G_{U-F(nonmyr)lowpH}\right) \quad [5.7]$$

where $\Delta G_{U\text{-}F(myr)}$ and $\Delta G_{U\text{-}F(nonmyr)}$ represent the Gibbs free energy of unfolding of myristoylated and nonmyristoylated hisactophilin, respectively, at the given pH.

Under EX2 conditions this cycle can also be applied to NH/D exchange data to yield site-specific information about the myristoyl switching energetics, as shown below using pH 6.8 and pH 8.1 as limiting pH values such that:

$$\Delta G_{switch,NH} = \Delta G_{ex(myr)pH8.1} - \Delta G_{ex(nonmyr)pH8.1} - \left(\Delta G_{ex(myr)pH6.8} - \Delta G_{ex(nonmyr)pH6.8}\right) \quad [5.8]$$

can determine site-specific coupling energies between the myristoyl group and sites of protonation, measured at individual backbone amide groups in hisactophilin. These pH were chosen to maximize the magnitude of $\Delta G_{switch,NH}$, but remain under EX2 conditions. Note that this pH range does not encompass the entire pH-dependence of the myristoyl switch, however, occurrence of EX1 mechanism increases in nonmyristoylated hisactophilin at lower and higher pH values (Houliston*, et al.*, 2002). Site-specific coupling energies are analogous to the overall ΔG_{switch}, determined by global chemical denaturation (see Chapter 3 and Materials and Methods in Chapter 4), however, for $\Delta G_{switch,NH}$ each amide provides a site-specific probe into the strength of coupling at each site in the protein to the myristoyl group. It should be emphasized that significant deviation away from the EX2 exchange mechanism will give meaningless coupling energies.

Decreased NH/D exchange is observed upon myristoylation. The kinetics of NH/D exchange for nonmyristoylated hisactophilin have been extensively studied previously ((Liu*, et al.*, 2002, Houliston*, et al.*, 2002, Houliston, 2004) and the results are summarized in Figures 5.1A and 5.1C). Chemical shift assignments have been made previously for myristoylated hisactophilin (chapter 2) and transferred to other pHs using ^{1}H-^{15}N HSQC monitored pH titrations. The chemicals shift assignments at various pHs were used to measure the NH/D exchange for ~45 of the slowest exchanging amides in myristoylated hisactophilin at pH 6.8 and 8.1. The observable amides show increased protection upon myristoylation as may be expected due to the increase in global stability. At pH 8.1 the majority of amides show decreased NH/D exchange rates upon myristoylation (Chapter 4) based upon the increase in global stability at pH 8.1 (Fig. 2.1A). The slowest exchanging amides that make up the slow exchanging core of nonmyristoylated hisactophilin are generally maintained as the slow exchanging core upon myristoylation; however, there are a few residues that shift away from global exchange. For example, at pH 6.8, Y62 and E114 appear to have slightly reduced $\Delta G_{ex,}$ in myristoylated hisactophilin. Additional residues, including Y62, I85, K86, I93, S94, F113 and E114, show decreased ΔG_{ex} at pH 8.1. This may be indicative of a more prominent role of local fluctuations that are facilitated by the fast dynamics of the myristoyl group at increased pH.

The values of ΔG_{ex} for myristoylated and nonmyristoylated hisactophilin are in general agreement with $\Delta G_{U\text{-}F}$ at pH 8.1. This suggests that both forms of hisactophilin exchange predominantly via the EX2 mechanism at this pH. There are, however, several amides that show faster exchange in myristoylated hisactophilin at pH 8.1 (chapter 4). At pH 6.8 NH/D exchange becomes faster in both myristoylated and nonmyristoylated hisactophilin

when compared to k_{obs} at pH 8.1, respectively. This is expected because both forms of the protein have markedly decreased global stability at lower pH. As may be predicted from the increase in $\Delta\Delta G_{U\text{-}F}$ from pH 6.8 to pH 8.1 (Fig. 2.1A), indicating increased stability, the exchange rates are slower for myristoylated hisactophilin and show increased ΔG_{ex}. ΔG_{ex} for the slowest exchanging residues in myristoylated hisactophilin agree with $\Delta G_{U\text{-}F}$ at pH 6.8, which provides evidence that myristoylated hisactophilin exchanges via the EX2 mechanism at pH 6.8. At lower pH increased exchange via the EX1 mechanism is observed for pH 5.9 and pH values 8.7 – 9.7. Myristoylated hisactophilin is expected to have increased EX2 exchange because global folding rates (i.e. the slowest closing rates in the protein) are increased by >50 times. While a switch to EX1 would alter the exact value of $\Delta G_{switch,NH}$ the characterization results would still hold qualitatively and be informative of the allosteric communication pathway in hisactophilin.

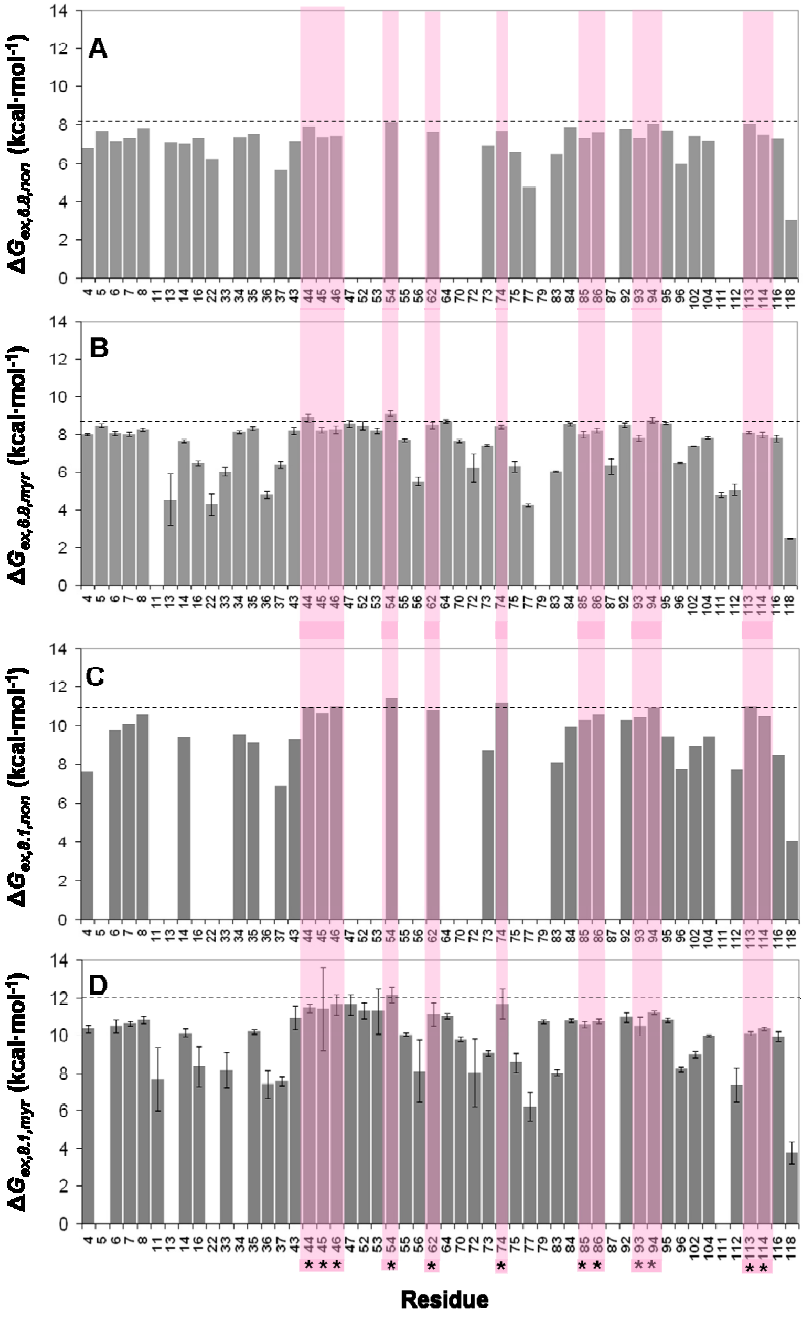

Fig. 5.1. Values of ΔG_{ex} for myristoylated and nonmyristoylated hisactophilin at pH 6.8 and 8.1. Exchange rates are reported for: (A) Nonmyristoylated hisactophilin at pH 6.8, (B) Myristoylated hisactophilin at pH 6.8, (C) Nonmyristoylated hisactophilin at pH 8.1, and (D) Myristoylated hisactophilin at pH 8.1. Dashed lines represent range estimate of global stability, $\Delta G_{U\text{-}F}$, in D_2O at the reported pH. Stabilities have been estimated by applying a general stabilization of 1.5 kcal·mol^{-1} for the stabilization of hisactophilin in D_2O relative to H_2O (Houliston *et al.*, 2002). Stars and pink bars highlight residues that were reported to exchange via global unfolding in nonmyristoylated hisactophilin. Exchange rates for nonmyristoylated hisactophilin at pH 6.8 were determined previously and corrected for temperature differences (Houliston, *et al.*, 2002). Exchange rates for nonmyristoylated hisactophilin at pH 8.1 were interpolated using exchange data acquired at pH 7.8 and 8.7 assuming a linear proportionality between these pH values.

Allosteric communication pathway in hisactophilin identified by pH-dependence of exchange. $\Delta G_{switch,NH}$ were calculated using eq. 5.8 for amides throughout hisactophilin. The site-specific coupling energies for each site are mapped onto the structure of myristoylated hisactophilin, yielding a putative coupling network between the H^+ binding site(s) and the myristoyl group (Figure 5.1B). The values of $\Delta G_{switch,NH}$ observed for hisactophilin show a dispersion of values that range from -0.9 to 1.3 kcal·mol^{-1} (Fig. 5.2A). A few residues within hisactophilin have $\Delta G_{switch,NH} > 0$ kcal·mol^{-1} (Fig.5.2B, blue). The most strongly coupled residues, R4 and I116, are comparable to ΔG_{switch} (as expected for EX2 exchange) and localized together at the N- and C-terminus of hisactophilin. Sites with $\Delta G_{switch,NH} > 0$ kcal·mol^{-1} are destabilized upon ligand (H^+) binding, at low pH, suggesting this region of the protein facilitates switching though enhanced local opening events that favour the myristoyl group to become accessible.

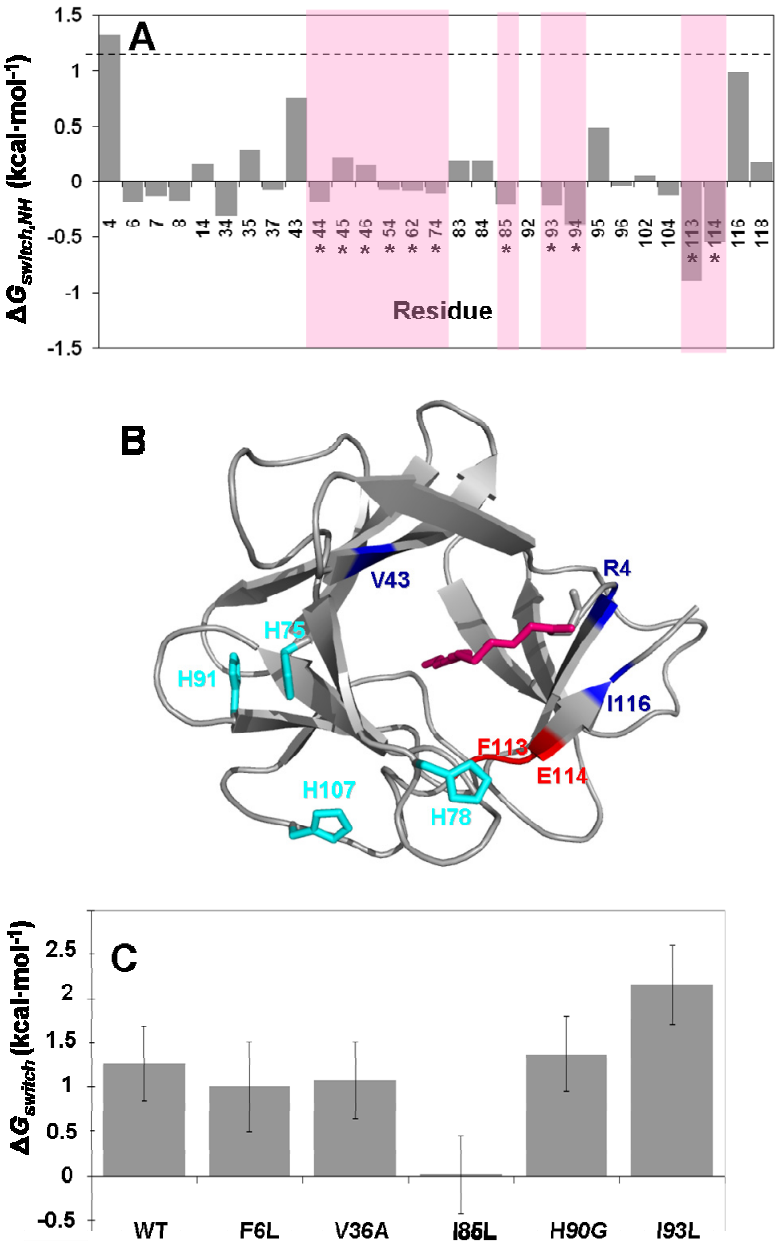

Fig. 5.2. Local coupling in myristoylated hisactophilin. (A) Bar chart illustrating local coupling energies, $\Delta G_{switch,NH}$, between site(s) of protonation and the myristoyl group for individual amides from pH 6.8 – 8.1. The dashed line shows the approximate values of ΔG_{switch} expected over this pH range based upon measurements of global stability by chemical denaturation curves. Stars and pink bars highlight residues that were reported to exchange via global unfolding in nonmyristoylated hisactophilin. (B) Top view of myristoylated hisactophilin (backbone grey ribbon, modeled from PDB 1HCD) with the strongly coupled residues colored. NHs with $\Delta G_{switch,NH} < 0$ kcal·mol^{-1} are colored red and those with $\Delta G_{switch,NH} > 0.75$ kcal·mol^{-1} are colored blue. Histidines implicated in switching (H75, H78, H91 and H107, cyan sticks)(Smith, *et al.*, 2011) are shown on the structure and the myristoyl group (pink sticks) is represented in the myr_{seq} state (Smith, *et al.*, 2011). (C) Estimated ΔG_{switch} for mutant hisactophilins for pH 6.2 – 7.8 (Shental-Bechor, *et al.*, in press). Error bars represent standard uncertainty of obtained from the fitting of denaturation curves.

In contrast, F113 and E114 clustered around H78 in the tertiary structure have $\Delta G_{switch,NH} < 0$ kcal·mol^{-1} (Fig. 5.2B, red). Sites with negative local coupling energies have increased local stability upon ligand binding. Speculating, it is possible that residues around H78 become more structured and interact with the myristoyl group and stabilize alternate conformations, such as the myr_{acc} state. Taken together, NH/D exchange coupling data provide evidence supporting a coupled allosteric communication pathway that includes widespread areas of decreased local stability with specific areas of increased stability to bring about myristoyl switching. The highly localized nature of the energetically-coupled allosteric communication pathway and the disagreement with global ΔG_{switch} perturbations indicate that further investigations are required.

To test the allosteric communication pathway, several mutations (F6L, V36A, I85L, H90G and I93L) were introduced around the structure of hisactophilin and the global switch energetics in the mutants compared to WT. It was hypothesized that if a mutation significantly perturbs the communication pathway it will have a larger effect on the overall ΔG_{switch}. The F6L and V36A mutations of residues do not alter ΔG_{switch}, i.e. such that the differences are larger than the experimental error (Fig 5.1C). In the current structural model the side chain of F6 packs near the amides of R4 and I116. However, the F6L mutation has little effect on the ΔG_{switch}. In contrast, the I85L and I93L mutations do result in changes in ΔG_{switch} values that are larger than the experimental uncertainties. The ΔG_{switch} measured for the I93L mutation has a larger ΔG_{switch} than WT (Fig. 5.1C). As suggested in the thermodynamic cycle, it is possible that the increased ΔG_{switch} in I93L is caused by an increase in pK_a differences observed for histidines in the myr_{seq} and myr_{acc} states (Smith*, et al.*, 2011). Likewise, the opposite effect of I85L on ΔG_{switch} would suggest that switching is

broken (Smith, *et al.*, 2011, Shental-Bechor, *et al.*, in press). These two residues do not pack next to amides that exhibited strong $\Delta G_{switch,NH}$ values. Therefore, the original hypothesis that strongly coupled residues would have a larger effect on the ΔG_{switch} was incorrect. Rather, it appears that mutating the side chains of residues near the terminal methyl of the myristoyl group show the largest changes in ΔG_{switch}. Another possibility may be that the pH switch has been shifted to a different pH range. These subtle Ile to Leu mutations which elicit the largest response highlight the finely tuned nature of the allosteric communication pathway. This is interesting because it suggests that the global allosteric communication pathway can be altered by changing local energetic interactions. Although there is no NH/D data available for regions surrounding H90, the unaltered ΔG_{switch} for the H90G mutation suggests that this region of the protein is not involved in switching. Thus, mutagenesis shows that even slightly altering residues close to the terminal methyl group of the myristoyl group can have dramatic effects on the global energetics of myristoyl switching and that this does not coincide with the local coupling within hisactophilin.

Applying the $\Delta G_{switch,NH}$ model to other myristoyl switching systems to identify allosteric communication pathways. Recoverin and GCAP1 are examples of Ca^{2+}-binding myristoyl switching systems. The myristoyl switch in recoverin has been characterized extensively (Ames, *et al.*, 1997). Briefly, upon binding two Ca^{2+} the myristoyl group undergoes a large conformational switch from the myr_{seq} state to the fully exposed state, myr_{exp}, where the myristoyl group is fully exposed to the solvent. Previous analysis suggests that this large conformational change in recoverin is associated with a large ΔG_{switch}

~ 10 kcal·mol^{-1} (Smith, *et al.*, 2011). Alternatively, GCAP1 undergoes a myristoyl switch between states with altered dynamics. This myristoyl switch in GCAP1, which does not involve a conformational change, exhibits a ΔG_{switch} of ~ 0 kcal·mol^{-1} (Chapter 3, (Smith, *et al.*, 2011) and references therein). A literature search yielded previously published mass-spectrometry-monitored NH/D exchange kinetics for recoverin (Neubert, *et al.*, 1997) and GCAP1 (Orban, *et al.*, 2010) to which the current thermodynamic analysis is applied providing two other systems that differ greatly in their degree of conformational change. It is important to note that NH/D exchange data obtained by mass spectrometry is acquired for small segments of protein ranging from ~ 3 to 20 residues. This may complicate the interpretation of NH/D exchange data, nevertheless, a qualitative comparison to hisactophilin can provide some insight into the general nature of the allosteric communication pathway involved in myristoyl switching.

Using data from the study by Neubert *et al.*, $\Delta G_{switch,NH}$ values have been calculated for recoverin that range from 0.157 – 5.30 kcal·mol^{-1}. In contrast to hisactophilin all $\Delta G_{switch,NH}$ values are greater than 0 kcal·mol^{-1}. Values for $\Delta G_{switch,NH}$ have been mapped onto the myr$_{seq}$ (Fig. 5.3A) and myr$_{exp}$ (5.3B) structure of recoverin using the same colour scheme used for hisactophilin (Fig. 5.2B). The communication pathway consisting of regions in recoverin is more widespread throughout the protein structure. The strongly coupled residues (Fig. 5.3, red) in recoverin show an extensive path between important Ca^{2+} binding sites and the myristoyl group. $\Delta G_{switch,NH}$ values for recoverin are larger and more widespread than those found in hisactophilin and agree qualitatively with the reported ΔG_{switch} that that was larger for recoverin than hisactophilin (Smith, *et al.*, 2011). The more extensive communication pathway found in recoverin (i.e. when compared to hisactophilin)

may be important in efficiently linking calcium binding to the larger conformational change involved in the recoverin Ca^{2+}-myristoyl switch.

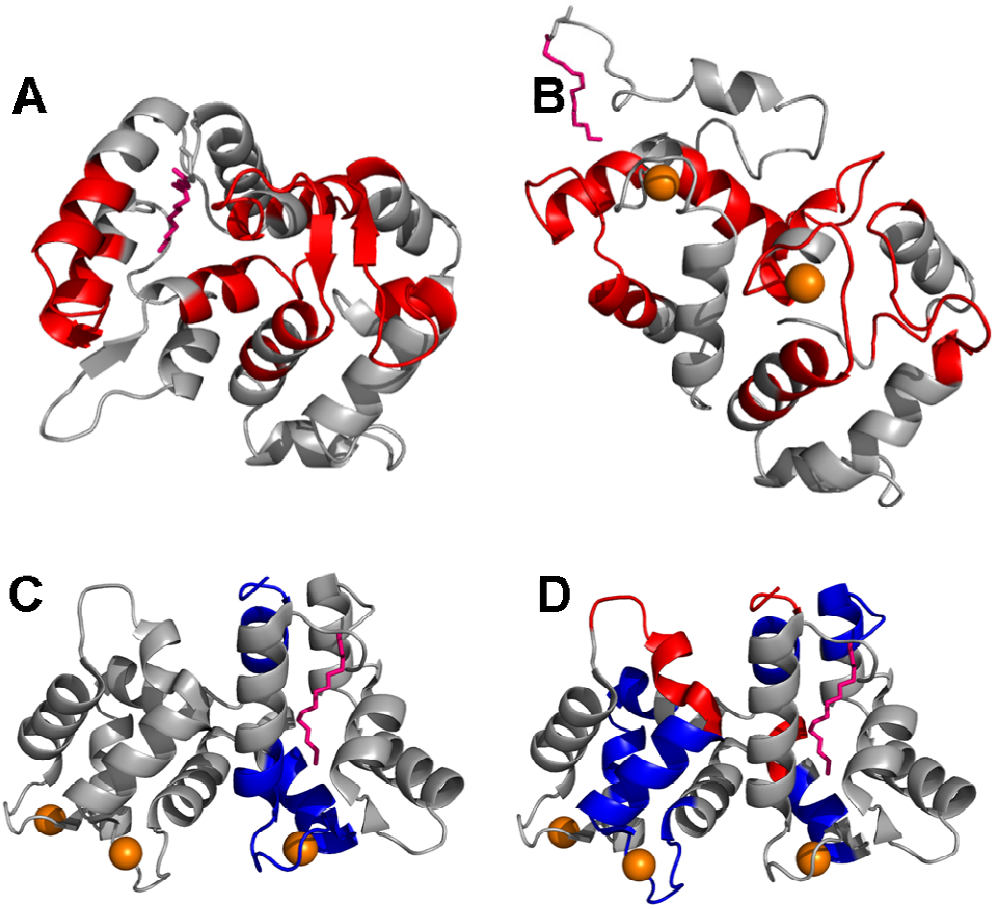

Fig. 5.3. Local coupling in recoverin and GCAP1. (A) ${}^{i}\Delta G_{switch,local}$ values mapped onto the structure of (A) myr_{seq} state of recoverin (PDB 1iku), (B) myr_{exp} state of recoverin (PDB 1jsa), (C) the fast phase of GCAP1 (PDB 2r2i), and (D) the slow phase of GCAP1 (PDB 2r2i). The ribbon backbone and myristoyl group for each protein have been coloured using the same scheme as in Fig. 5.1. The structures of recoverin in panel A and B represent the best pairwise alignment (Z = 9.4, r.m.s.d = 2.8Å) using the Dali server (Hasegawa and Holm, 2009).

The kinetics of NH/D exchange in GCAP1 provides a different myristoyl switching system for comparison to hisactophilin and recoverin. Orban *et al.* report a fast and slow phase for NH/D exchange in GCAP1. $\Delta G_{switch,NH}$ values were calculated for both the fast phase (Fig. 5.3C) and slow phase (Fig. 5.3D) and mapped onto the structure of GCAP1 using the same colour scheme used for hisactophilin (Fig. 5.2B) and recoverin (Fig. 5.3A and 5.3B). Unlike either hisactophilin or recoverin, both the fast and slow phase in GCAP1 exhibited regions of positive and negative $\Delta G_{switch,NH}$ values ranging from -0.72 – 0.48kcal·mol^{-1} and -2.31 – 2.54kcal·mol^{-1}, respectively. Neither the fast or slow phase of GCAP1 show a connected allosteric communication as was observable in recoverin or hisactophilin. This is interesting because it may also agree with the myristoyl switch mechanism in GCAP1 described by Orban *et al.* that does not involve a conformational change (Orban*, et al.*, 2010). The alternating regions of positive and negative site-specific coupling in GCAP1 may interrupt the communication pathway and prevent any significant conformational change. If the communication pathway in GCAP1 was interrupted it may explain why the reported ΔG_{switch} for GCAP1 is approximately 0 kcal·mol^{-1} (Smith*, et al.*, 2011). Thus, applying the new analysis of NH/D exchange data for recoverin, GCAP1 and hisactophilin to calculate $\Delta G_{switch,NH}$ may suggest that the extent of conformational change involved in the myristoyl switch is linked to the strength and continuity of the allosteric communication pathway linking ligand-binding sites to the myristoyl group. The lack of a connected network in hisactophilin may also give clues into the degree of conformational change involved in the myristoyl switch. Alternatively, a strongly coupled allosteric communication pathway may not be required in hisactophilin because it is much smaller than either recoverin or GCAP1.

Global stability measurements as a function of temperature. The equilibrium stabilities of myristoylated hisactophilin was measured by fluorescence-monitored urea denaturation curves in the temperatures range of 280.15K – 330.15K (Fig. 5.4A). The data can be well fit by a reversible 2-state folding transition between folded (F) and unfolded (U) states of the protein, which gives the Gibbs free energy of unfolding, $\Delta G_{U\text{-}F}$ (= $G_U - G_F$) (see Chapter 2 SI Methods). $\Delta G_{U\text{-}F}$ is plotted *vs.* temperature for myristoylated hisactophilin and may be used to estimate the $\Delta G_{U\text{-}F}$ of myristoylated hisactophilin in D_2O (Fig. 5.4B). The lack of observable 3-state behaviour in the equilibrium curves at room temperature is consistent with a rapid interchange between the two folded states, myr_{seq} and myr_{acc}. Decreased m_1-values at lower temperatures may represent the initial distinction between the interconversion of the myr_{seq} and myr_{acc} folding transitions (Fig. 5.4C). Slowed exchange between the myr_{seq} and myr_{acc} states was confirmed by NMR lineshape analysis (Chapter 2 and Fig. 2.S7C). Note that previous measurements of temperature-dependence of global stability for nonmyristoylated hisactophilin showed the opposite trend, i.e. increasing m value with decreasing temperature, as has also been observed with other proteins, and is caused by the temperature-dependence of denaturant binding to proteins (Wong*, et al.*, 2004). However, since the folding transitions still appear two-state, the temperature-dependence of the measured global stability is analyzed further.

The shape of the $\Delta G_{U\text{-}F}$ vs. T plot shows that myristoylated hisactophilin is most stable near room temperature. The data can be fit using the Gibbs-Hemholtz equation:

$$\Delta G^{o}_{U-F} = \Delta H^{o}_{U-F}\left(T^{o}\right) - T\Delta S^{o}_{U-F}\left(T^{o}\right) + \Delta C_{p,U-F}\left(T - T^{o} - T \cdot \ln\left\{T / T^{o}\right\}\right) \qquad [5.9]$$

where $\Delta G^{\circ}_{U\text{-}F}$, $\Delta H^{\circ}_{U\text{-}F}$, and $\Delta S^{\circ}_{U\text{-}F}$ represent the changes in Gibbs free energy, enthalpy and entropy at the reference temperature, T° (= 293.15K), which was chosen to match previous analyses of nonmyristoylated hisactophilin (Wong, *et al.*, 2004). $\Delta C_{p,U\text{-}F}$ represents the change in heat capacity of unfolding at constant pressure. The best-fit value of $\Delta C_{p,U\text{-}F}$ obtained for myristoylated hisactophilin is 2.52 ± 0.14 kcal·mol^{-1}·K^{-1}, which is close to previously reported $\Delta C_{p,U\text{-}F}$ for nonmyristoylated hisactophilin of 2.26 ± 0.26 kcal·mol^{-1}·K^{-1} (Wong, *et al.*, 2004). Fitting of data for myristoylated hisactophilin to equation 5.9 gave $\Delta H^{\circ}_{U\text{-}F}$ and $\Delta S^{\circ}_{U\text{-}F}$ of -2.85 ± 1.39 kcal·mol^{-1} and -0.040 ± 0.006 kcal·mol^{-1}·K^{-1}, respectively. Comparison with data collected previously for nonmyristoylated hisactophilin gives an estimated change in enthalpy upon myristoylation, $\Delta\Delta H^{\circ}_{U\text{-}F}$ (= $\Delta H^{\circ}_{U\text{-}F,myr} - \Delta H^{\circ}_{U\text{-}F,nonmyr}$), and the change in entropy, $\Delta\Delta S^{\circ}_{U\text{-}F}$ (= $\Delta S^{\circ}_{U\text{-}F,myr} - \Delta S^{\circ}_{U\text{-}F,nonmyr}$), of -3.72 ± 2.98 kcal·mol^{-1} and -0.0198 ± 0.01 kcal·mol^{-1}·K^{-1}, respectively. The negative $\Delta\Delta H^{\circ}_{U\text{-}F}$ values indicate that myristoylation results in unfavourable enthalpic interactions in hisactophilin. This is consistent with results presented in chapter 2 that indicate myristoylation increases strain in the native state. Changes in enthalpy and entropy upon myristoylation measured by global stabilities will be compared to the site-specific information obtained by NH/D exchange.

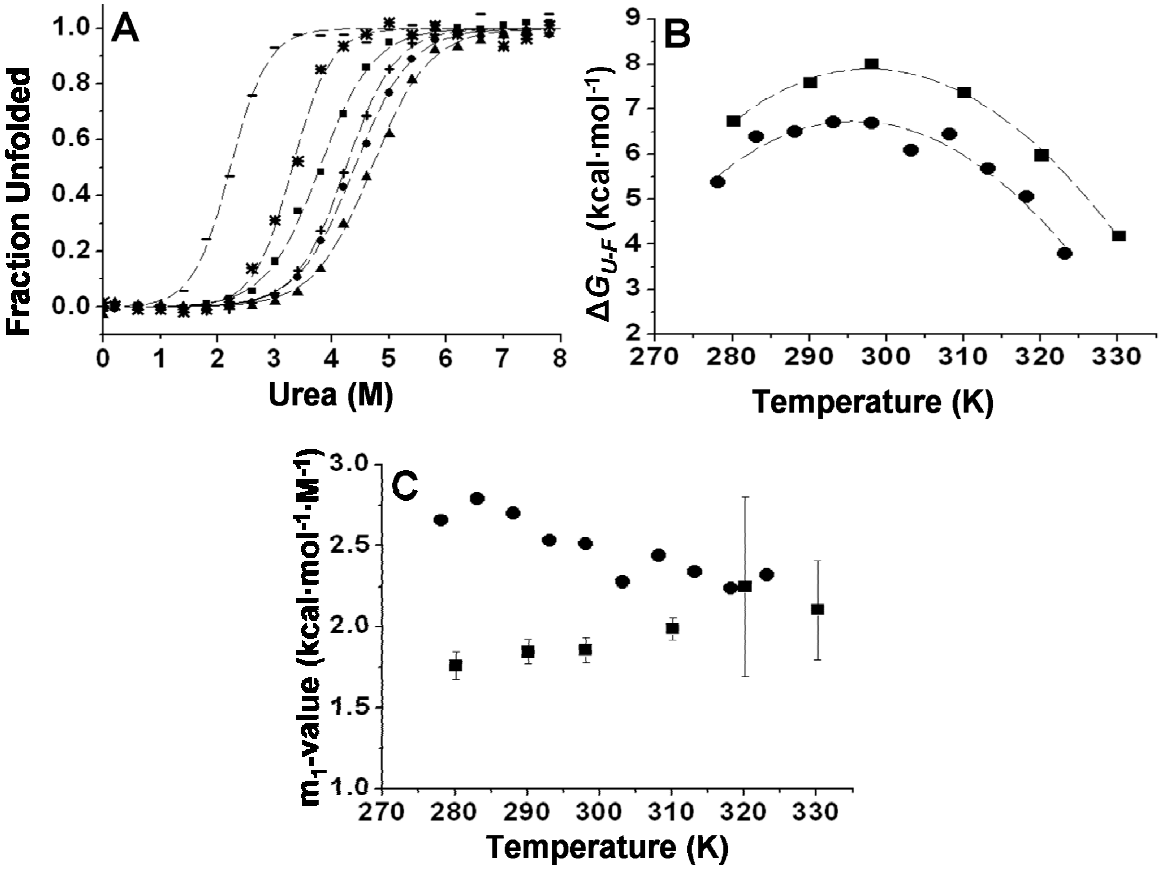

Fig. 5.4. Temperature dependence of global stability measurements for myristoylated and nonmyristoylated hisactophilin. (A) Preliminary denaturation curves showing the fraction of unfolded protein *vs.* increasing urea concentrations for myristoylated hisactophilin acquired at: 280.15K (■), 290.15K (+), 298.15K (▲), 310.15K (●), 320.15K (*) and 330.15K (—). Data has been plotted and fit to the BEM model using the Origin software package (see chapter 2). (B) $\Delta G_{U\text{-}F}$ vs. temperature for myristoylated (■) and nonmyristoylated (●) hisactophilin. Stabilities have been calculated for myristoylated hisactophilin using an average m_1-value measured for myristoylated hisactophilin from pH studies (Chapter 2) and the C_{mid} at each temperature, respectively. Data for nonmyristoylated hisactophilin were acquired previously (Wong*, et al.*, 2004). The dashed line represents the data fit to Eq. 5.9 with T° = 293.15K. (C) m_1-values over the measured temperature range for myristoylated (■) and nonmyristoylated (●) hisactophilin. The reported error estimates represent the standard error provided by the Origin fitting software. The large errors in the m_1-values for myristoylated hisactophilin at 320.15K and 330.15K may occur because of poorly defined folded baselines.

Altered site-specific energetics in hisactophilin identified by temperature dependence of exchange. The kinetics of NH/D exchange for nonmyristoylated hisactophilin have been measured previously at pH 6.8 over the temperature range 274.15K – 313K (Houliston, 2004). The ΔG_{ex} for nonmyristoylated hisactophilin at pH 6.8 and 290.15K, 301.65K and 313K are reported for comparison to myristoylated hisactophilin over a similar temperature range (Fig. 5.5A, 5.5B and 5.5C, respectively). Again, for myristoylated hisactophilin, the ΔG_{ex} for the slowest exchanging amides are in agreement with estimated $\Delta G_{U\text{-}F}$ in D_2O, $\Delta G_{U\text{-}F,D2O}$. This provides evidence that amides exchange via the EX2 mechanism. Eyring plots for each amide have been constructed and give a linear relationship when $\ln(k_{obs} \cdot T^{-1})$ *vs.* $1/T$ is plotted. From these plots ΔH_{ex} for each amide is determined from the slope of the line (Fig. 5.4D and (Houliston, 2004)). For nonmyristoylated hisactophilin, the values of ΔH_{ex} range from 9.81 kcal·mol^{-1} - 41.7 kcal·mol^{-1}. There is an inverse correlation between ΔH_{ex} and k_{obs} such that amides with larger k_{obs} (i.e. faster exchange) tend to have smaller ΔH_{ex}. This is similar to results found for other proteins (Clarke and Itzhaki, 1998, Kuhlman and Raleigh, 1998). This occurs because more enthalpic interactions are broken when amides undergo large structural openings. The slowest exchanging amides in nonmyristoylated hisactophilin have the largest values of ΔH_{ex} as expected for amides undergoing global unfolding.

NH/D exchange has now been measured for myristoylated hisactophilin at pH 6.8 over the temperature range 290.15K – 310.15K (Fig. 5.6A-C). The ΔG_{ex} for the slowest exchanging amides in myristoylated hisactophilin are in general agreement with the estimated $\Delta G_{U\text{-}F,D2O}$ measured for myristoylated hisactophilin at the different temperatures. The fact that $\Delta G_{U\text{-}F,D2O}$ is similar to ΔG_{ex} for the slowest exchanging residues provides

evidence that exchange occurs via the EX2 mechanism between 290.15K and 310.15K. ΔH_{ex} measured for amides in myristoylated hisactophilin range from 5.51 kcal·mol^{-1} to 42.07 kcal·mol^{-1} (Fig. 5.6D).

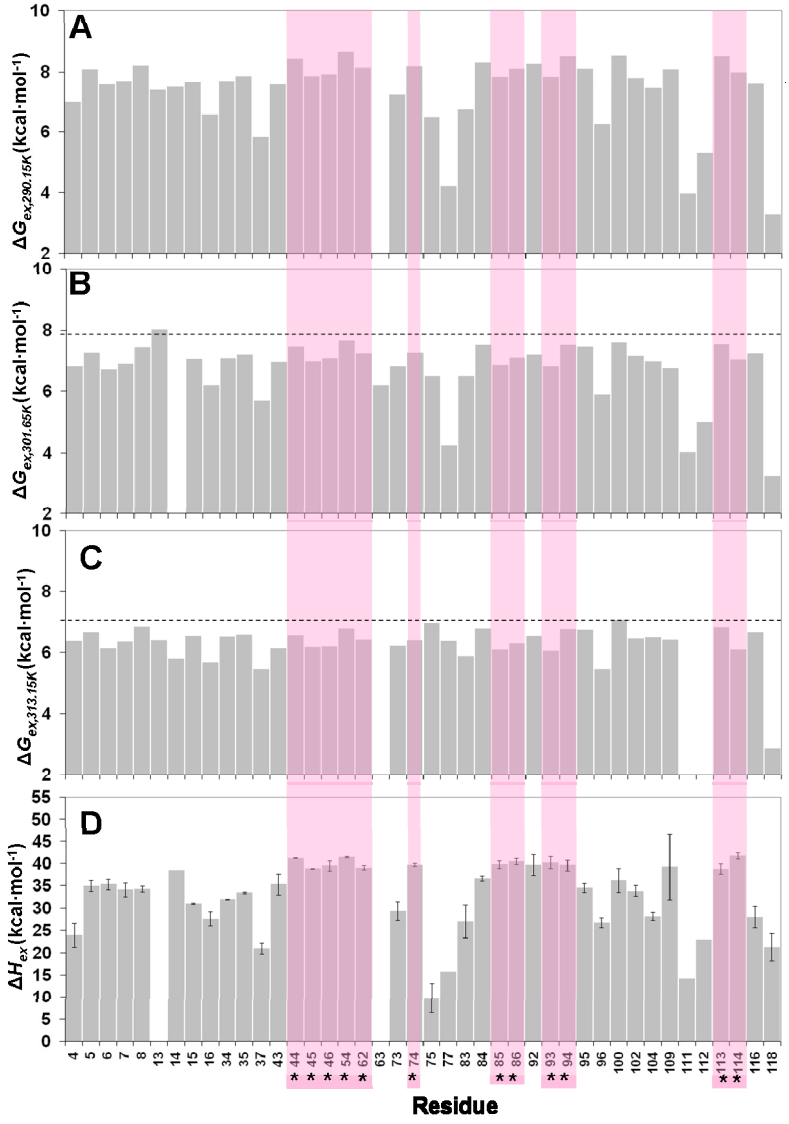

Fig. 5.5. Thermodynamics of NH/D exchange for nonmyristoylated hisactophilin at different temperatures. Observed NH/D exchange rates for myristoylated hisactophilin at pH 6.8 and (A) 290.15˚C, (B) 301.65K, and (C) 313K. (D) ΔH_{ex} values obtained for nonmyristoylated hisactophilin using linear regression analysis of Eyring plots. Data for nonmyristoylated hisactophilin was obtained previously (Houliston, 2004). Dashed lines represent range estimate for global stability, $\Delta G_{U\text{-}F}$, in D_2O at the reported pH. Stabilities have been estimated by applying a general stabilization of 1.5 kcal·mol^{-1} caused by dissolving hisactophilin in D_2O. Stars and pink bars highlight residues that were reported to exchange via global unfolding in nonmyristoylated hisactophilin. Error estimates are estimated from propagated standard error obtained from the Origin software used for fitting.

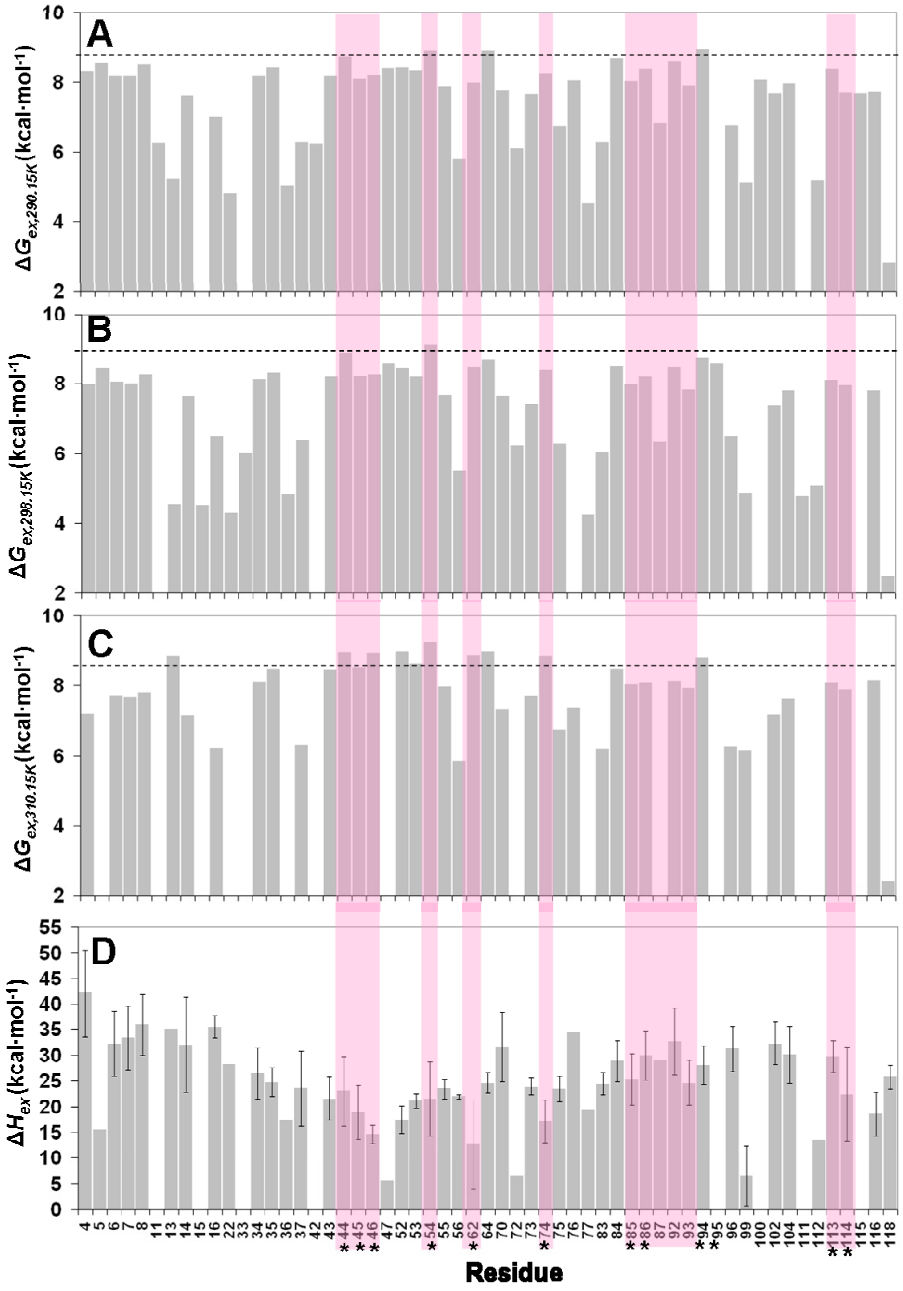

Fig. 5.6. Thermodynamics of NH/D exchange for myristoylated hisactophilin at different temperatures. Observed NH/D exchange rates for myristoylated hisactophilin at pH 6.8 and (A) 290.15˚C, (B) 298.15K, and (C) 310.15K. (D) ΔH_{ex} values obtained for myristoylated hisactophilin using linear regression analysis of Eyring plots. Dashed lines represent range estimate for global stability, $\Delta G_{U\text{-}F}$, in D_2O at the reported pH. Stabilities have been estimated by applying a general stabilization of 1.5 kcal·mol^{-1} caused by dissolving hisactophilin in D_2O. Stars and pink bars highlight residues that were reported to exchange via global unfolding in nonmyristoylated hisactophilin. Error estimates are estimated from propagated standard error obtained from the Origin software used for fitting.

$\Delta\Delta G_{ex}$ have been plotted to provide site-specific information about the effects of myristoylation on stability (Fig. 5.7A). Regions of increased stability and regions of decreased stability are observed upon myristoylation. Several of the slowest exchanging residues agree with estimated $\Delta\Delta G_{U\text{-}F,D2O}$ providing further evidence that amides are exchanging via the EX2 mechanism. However, several of the residues that were reported to exchange by global unfolding in nonmyristoylated hisactophilin (i.e. I85, K86, I93, F113 and E114) show smaller than expected increases in site-specific stability. This may occur because myristoylation facilitates local openings near these residues that have some contribution to the NH/D exchange. Furthermore, other residues (i.e. H75, E77, V83, S102 and I118) show decreases in stability upon myristoylation. It is interesting that many amides in hisactophilin have increased contributions of local opening in the observed exchange. These residues may represent regions of hisactophilin of large increases in local dynamics that facilitate the myristoyl group becoming accessible through local openings. The $\Delta\Delta G_{ex}$ upon myristoylation has been mapped onto the structure of myristoylated hisactophilin (Fig. 5.7D). It is interesting that the few residues that show $\Delta\Delta G_{ex} < 0$ kcal·mol^{-1} upon myristoylation pack near the sidechains of histidines that have been implicated in myristoyl switching (Smith*, et al.*, 2010). This could suggest that protonation of important histidines facilitate switching in these regions. Thus, upon myristoylation certain regions of hisactophilin have lower than expected $\Delta\Delta G_{ex}$ values, which suggest that the myristoyl group causes increased local dynamics.

$\Delta\Delta H_{ex}$ values have also been determined to provide additional site-specific information on the enthalpic interactions made by the myristoyl group (Fig. 5.7B). The

majority of amides in hisactophilin show decreases in enthalpy of opening upon myristoylation. The slowest exchanging amides that make up the global core generally show the largest decreases in enthalpy upon myristoylation. This agrees qualitatively with the $\Delta\Delta H^{\circ}_{U\text{-}F}$ calculated using global stabilities. This would suggest that the myristoyl group makes significant interactions with the slow exchanging core of hisactophilin. To provide further information about the distribution of these interactions $\Delta\Delta H_{ex}$ have been mapped onto the structure of hisactophilin (Fig. 5.7E). The distribution of $\Delta\Delta H_{ex}$ shows that amides with larger decreases in enthalpy upon myristoylation also tend to be destabilized. Changes in entropy upon myristoylation, $-T\Delta\Delta S_{ex,298.15K}$ (= $\Delta\Delta G_{ex,298.15K} - \Delta\Delta H_{ex}$), have been calculated at the reference temperature, T° (=298.15K) (Fig. 5.7C). A large decrease in enthalpy associated with an increase in stability would suggest that the myristoyl group makes favourable entropic interactions (Fig. 5.7C). Generally, this may suggest a site-specific enthalpy-entropy trade off that occurs upon myristoylation as seen for experiments where other modifications have been made to rubredoxin (LeMaster*, et al.*, 2005). It is interesting that the residues Y62, F74, I85, I93, F113 and E114 have the largest increases in entropy upon myristoylation because they are also the residues that appear to have increased exchange. Therefore, the entropically driven increased stability may be contributed by the by the myristoyl group dynamics. An observed increase in entropy upon myristoylation could also suggest that the allosteric communication linked to the myristoyl group in hisactophilin may arise from increased local entropy and decreased enthalpic interactions. Entropy driven communication pathways have been suggested for calmodulin and CAP proteins (Marlow*, et al.*, 2010, Kalodimos*, et al.*, 2004). Therefore, NH/D exchange as a function of temperature

has provided new information on the nature of the interactions that the myristoyl group makes with hisactophilin.

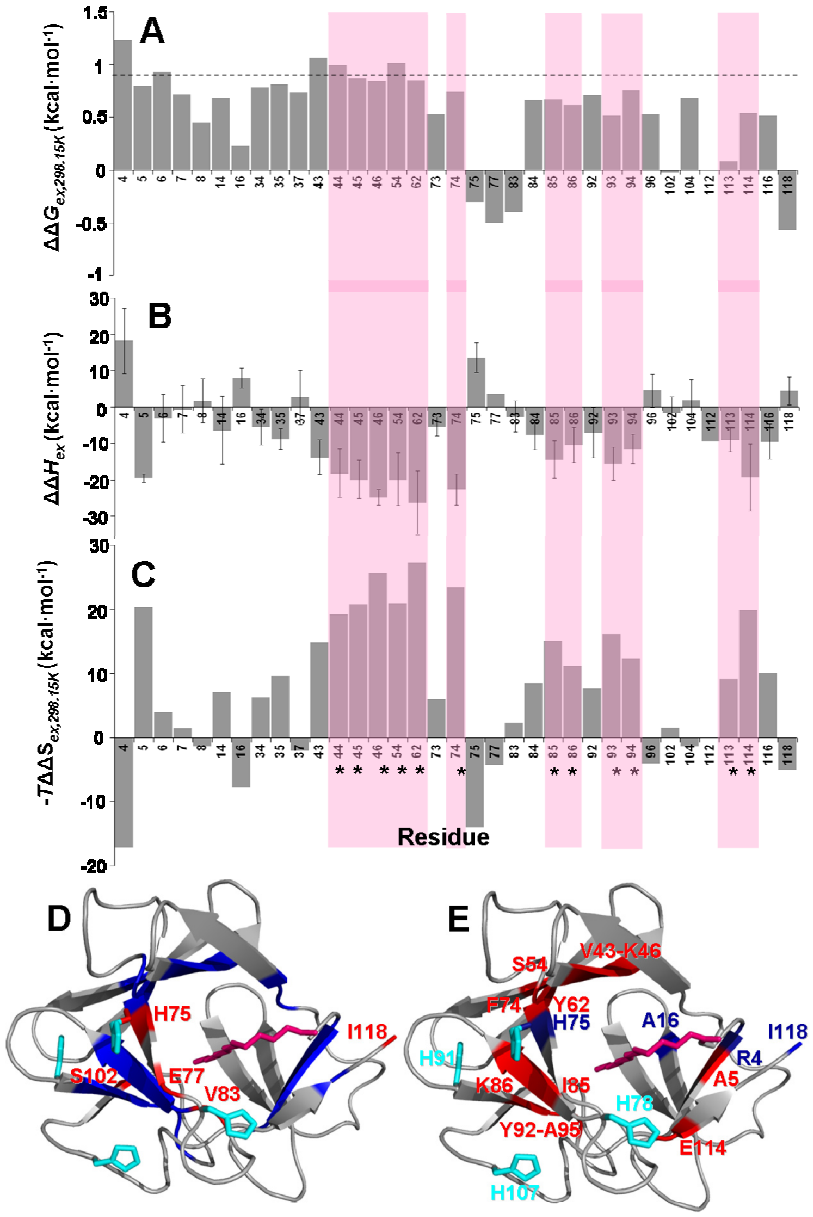

Fig. 5.7. Comparison of site-specific stabilities and enthalpies. (A) Changes in site-specific stability, $\Delta\Delta G_{ex}$, for comparable amide NHs at pH 6.8 and 298.15K. Dashed lines represent an estimated $\Delta G_{U\text{-}F}$ in D_2O for myristoylated hisactophilin. Stars and pink bars highlight residues that were reported to exchange via global unfolding in nonmyristoylated hisactophilin. Uncertainty estimates are estimated from propagated standard error obtained from the Origin software used for fitting. (B) Change in site-specific enthalpy, $\Delta\Delta H_{ex}$, for comparable amide NHs at pH 6.8. Data reported for nonmyristoylated hisactophilin was obtained previously ((Houliston, *et al.*, 2002) and (Houliston, 2004)). NHs with $\Delta\Delta H_{ex} > 0$ kcal·mol^{-1} show increased enthalpy of exchange upon myristoylation while $\Delta\Delta H_{ex} < 0$ kcal·mol^{-1} show decreased stability upon myristoylation. (C) Calculated changes in entropy upon myristoylation, $-T\Delta\Delta S_{ex,298.15K}$ (= $\Delta\Delta G_{ex,298.15K}$ - $\Delta\Delta H_{ex}$). (D) Top view of myristoylated hisactophilin (grey ribbon backbone, pink myristoyl group) with $\Delta\Delta G_{ex}$ for stabilized (blue) and destabilized (red) upon myristoylation at pH 6.8 mapped onto the structure. (E) Top view of myristoylated hisactophilin (backbone grey ribbon, pink myristoyl group) colored with residues that have significantly decreased enthalpy (red) and increased (blue) $\Delta\Delta H_{ex}$ upon myristoylation.

Conclusions. The site-specific ΔG_{ex} values have been reported for myristoylated hisactophilin as a function of temperatures and pH. Some residues show increased contributions of local exchange upon myristoylation, which illustrates that local fluctuations of the myristoyl group may influence the exchange pattern. A new method is reported based upon using ΔG_{ex} at different pH to characterize the allosteric communication pathway in ligand-binding-induced switching systems. Applying this method to hisactophilin revealed localized sites that are allosterically coupled to the myristoyl group. Another small patch of residues that are oppositely coupled were found close to the sidechain of H78. Interestingly, F113 and E114 may also have the most significant contributions of local exchange introduced upon myristoylation. Mutations that were introduced into hisactophilin showed that the global switch energetics of hisactophilin could be altered by single mutations, but, they were not coincident with regions of local coupling detected by this analysis. The highly localized nature of the energetically-coupled allosteric communication pathway and the disagreement with global ΔG_{switch} perturbations indicate that further investigations are required. Perhaps applying this analysis over a larger pH range (while remaining under the EX2 regime) would provide more insight into the connection between local and global switch energetics.

Using the newly developed methodology with data from the literature on recoverin and GCAP1 illustrated that the extent and continuity of the allosteric communication pathway may be associated with the degree of conformational change upon ligand binding. Therefore, utilizing thermodynamic cycles in conjunction with NH/D exchange data has provided site-specific information about the nature of the coupling pathway.

Additional NH/D exchange studies as a function of temperature revealed widespread increased stability for many of the amides in hisactophilin that agree with the increased global stability observed upon myristoylation. Myristoylation caused changes in stability throughout the protein that arose from an enthalpy-entropy trade off. Regions with decreased local stability were also identified that coincided with important histidines, thus providing more site-specific information about the myristoyl switch mechanism in hisactophilin. Taken together, NH/D exchange data have revealed molecular details of the allosteric communication pathway in hisactophilin and provided new insight into the nature of the enthalpic and entropic interactions that govern this allostery.

Chapter 6 – General Conclusions and Future Work.

General Conclusions

Throughout the previous chapters the biophysical characterization of myristoylated hisactophilin has been presented and compared to previous analyses of nonmyristoylated hisactophilin focussed on 4 main goals. The main goals of this thesis were 1) characterize the thermodynamic and kinetic effects of myristoylation on all native and nonnative states found within the folding pathway of hisactophilin, 2) understand the effects of myristoylation on folding in the context of existing folding models, 3) obtain structural information that describes the conformation of the myristoyl group in the different states involved the myristoyl switch, and 4) gain insight into the energetic and dynamic processes that govern the myristoyl switching function. We may now draw some general conclusions about the research related to these goals.

Myristoylation has a significant effect on protein folding. The combination of multiple techniques has yielded critical information about the effects of myristoylation on protein folding. The N-terminal myristoyl group has been shown to aid the folding of hisactophilin. Myristoylation increases the stability of hisactophilin at all pH values, ranging from ~1kcal·mol^{-1} at low pH to ~3.11kcal·mol^{-1} at high pH (chapter 2). NH/D exchange studies provide molecular details of the increased stability (chapter 4). The majority of the observed amide groups in myristoylated hisactophilin show increased protection upon myristoylation. The slowest exchanging amides formed the globally exchanging core of myristoylated hisactophilin and the observed protection factors are in agreement with

denaturation studies. The overall pattern in the amides that exchange through global unfolding has a similar pattern to those in nonmyristoylated hisactophilin with the additional observance of increased local exchange in several core residues. Therefore equilibrium denaturation studies and NH/D exchange provide important insight into the stabilizing effects of myristoylation on proteins. Kinetic studies build upon these results to provide important information about the unfolded and transition states.

The kinetic folding and unfolding of hisactophilin are both accelerated upon myristoylation (chapter 2). Increased folding rates for myristoylated hisactophilin are expected because the protein is stabilized upon myristoylation. However, increased unfolding rates seem somewhat counterintuitive because an increase in stability is generally not associated with an increase in the unfolding rate. Here, stabilization is observed because the folding rate is increased much more than the unfolding rate. The increased unfolding rates may also facilitate functional switching in hisactophilin by increasing the global dynamics of the protein, thereby making switching more efficient.

The effects of myristoylation seem to fit with the addition of a large hydrophobic group into the core of a protein. While these results represent one of the first in-depth quantitative characterizations of the stability of a myristoylated protein, other proteins also show increased thermal stability upon myristoylation (chapter 2). This suggests that the stabilizing effects of myristoylation are general. An increase in the folding and unfolding rate upon myristoylation suggests destabilization of the unfolded state, formation of stabilizing interactions in the transition state, or strain in the native state. These nonnative effects are observed for hydrophobic mutations and proteins with redesigned cores. Therefore, the

myristoyl group makes important native and nonnative interactions with the rest of the protein that increase stability and aid folding.

Nonnative interactions can help as well as hinder protein folding. Generally, studies in the past have focussed upon the formation of nonnative interactions that introduce intermediates that interfere with folding. The research presented in this thesis illustrate that the nonnative interactions formed by the myristoyl group facilitate the folding of hisactophilin. This is itself an important step forward as it provides evidence that there may be important nonnative interactions that facilitate folding and function in other proteins. Building upon this notion, our collaborations with Yaakov Levy's group have further defined the nonnative interactions in hisactophilin using a combined computational and experimental approach. These studies suggest that myristoylation has an effect on both the native and nonnative states on proteins; whereas, the native and nonnative effects of other protein modifications such as ubiquitination and glycosylation seem to arise mainly from interactions with the solvent (chapter 4). This can be explained because the myristoyl group packs in the core of hisactophilin while glycosyl and ubiquitin groups pack outside their host protein. Interestingly, our experiments have shown that the stabilization of the transition state upon myristoylation is the same in all of the mutants studied. That is to say the nonnative interactions probed by these mutations that accelerate hisactophilin folding that appear to be nonspecific. Thus, the interactions made by the myristoyl group in the transition state are robust, such that they are not affected when specific mutations are introduced. This builds upon previous studies that have shown both important specific and nonspecific hydrophobic nonnative interactions in proteins.

Myristoylation facilitates fast conformational switching in proteins. The difference in stabilization at limiting pH was modelled to give a ΔG_{switch} and suggested that the conformational change between the sequestered and accessible states exhibits a coupling energy of ~2kcal·mol^{-1} and is governed to the binding of a ~2 protons to key histidines. The nomenclature used to describe this coupling was extending to other systems and showed that the ΔG_{switch} is a good way to characterize the energetic coupling ligand-binding-induced macromolecular switching (chapter 3). The stabilization of hisactophilin upon myristoylation was further modelled using a new equation based upon the work of Raleigh and co-workers (chapter 2, supplementary). This equation allowed the switch energy to be fit as a function of ligand concentration and supported the idea that a small number of histidines governed the pH myristoyl switch. Thus, the equilibrium studies have provided an important step in modelling ligand-binding-induced conformational switching.

Initial characterization revealed that myristoyl switching is fast on an NMR timescale (chapter 2, supplementary). This fast switching the sequestered and accessible states is implicated in the function of hisactophilin, where in *D. discoideum* hisactophilin is implicated in the need for fast rearrangement during the reorganization of the cytoskeleton in chemotaxis and osmoprotection mechanisms.

Mutational studies of both the LLL mutant (i.e. F6L/I85L/I93L) and the even more subtle I85L mutant hisactophilin showed that ΔG_{switch} can be altered (chapters 2 and 5). This suggests that there are finely balanced interactions arising from the myristoyl group within the core of hisactophilin that govern efficient switching. These crucial interactions are reminiscent of the research presented by Plaxco *et al*. that show switching can be tuned in a

number of systems (Plaxco*, et al.*, 2010). Conclusions about myristoylation are supported by results in other proteins with redesigned cores, such as Rop, where function has been altered (Wensley*, et al.*, 2010). Therefore, myristoylation provides a physiological example where subtle changes in the core can have a significant effect on function. They also provide further evidence that the physiological function can be controlled through protein engineering techniques.

The conclusions drawn from this research have provided new insight into the effects of myristoylation on the folding and function of the β-trefoil, hisactophilin. The goal to understand the thermodynamic and kinetic effects of myristoylation has been provided by equilibrium and kinetic folding experiments. Together, equilibrium and kinetics have highlighted some the native and nonnative interactions that the myristoyl group makes with hisactophilin in all states along the folding pathway. Comparison of the results obtained for hisactophilin with other modified proteins has helped to place the effects of myristoylation within the context of current folding models in the field. Thus, we were able to meet the goal of understanding the effects of myristoylation on folding in the context of existing folding models. Site-specific energetic and structural information obtained by NMR and NH/D exchange helped to meet the goal of obtaining structural information about the sequestered, accessible and (to some degree) the exposed myristoyl states. Further NMR analysis allowed us to gain insight into the dynamic processes that govern the transition between these switching states. Where there was previously a void of relevant information on the effects of myristoylation, the successful completion of the main goals of this thesis begins to fill that void with the information needed to move forward. This work provides a good foundation to

design future work that will investigate the biophysical characteristics of myristoylation in the broader context of cellular processes such as membrane and actin binding.

Future Work

Studying the exposed myristoyl state. The studies in this thesis have characterized the folding and switching of hisactophilin to the sequestered and accessible states. Another physiologically relevant state of myristoylated hisactophilin that would be interesting to pursue experimentally is the fully exposed myristoyl state. Though simulations have provided initial detail for the transition to the fully exposed myristoyl state, the energetics governing the exposed state of hisactophilin has not been studied empirically. In the exposed state the myristoyl group is fully exposed to solvent and has minimal interactions with the protein. Presumably, the extrusion of the large hydrophobic myristoyl group into solution is unfavourable and therefore would be populated for a short time before becoming fully membrane-bound. Recent works have successfully used lipid bicelles to stabilize and study the structures of the exposed myristoyl group where it is inserted into the membrane of the bicelle (Liu*, et al.*, 2009, Liu*, et al.*, 2010). As such, studies of myristoylated hisactophilin bound to bicelles have been initiated. Preliminary results show that myristoylated hisactophilin will bind to reversibly to bicelles as a function of pH. However, in these studies the addition of bicelles reduced the quality of the spectra such that the NMR spectrum becomes unreadable. However, future studies may be successful if hisactophilin is bound to smaller bicelles. Bicelle binding studies could be augmented by isothermal titration

calorimetry studies that give thermodynamic binding parameters to support any structural findings.

Characterizing dynamic motions of the myristoyl switching. The dynamic processes involved in switching between conformational states are extremely important for understanding how proteins function (chapter 5). NH/D exchange studies performed on myristoylated hisactophilin have already provided site-specific information on the energetic and dynamic processes that occur upon myristoylation. However, these processes may occur on timescale ranging from seconds to nanoseconds. For hisactophilin, pH-myristoyl switch dynamics were observed to be fast (chapter 2). That is, line broadening observed at low temperature in the upfield terminal myristoyl methyl peak showed that the myristoyl group was in fast exchange at pH 6.1 (chapter 2 supplementary). Interestingly, preliminary HSQCs monitored *vs.* temperature at pH 6.1 indicate amide peaks for I85 and H91 show similar line broadening at low temperatures. The terminal methyl group, H91 and I85 are in close proximity to each other and may be involved in correlated myristoyl switching motions (chapter 2). While these measurements are preliminary, line broadening observed in spatially close regions of the protein may indicate coordinated fast opening events involved in myristoyl switching that are important for protein function. With indications of cooperative opening events it would be interesting to fully characterize the dynamic processes that occur in pH-dependent myristoyl switching. Processes on the second, millisecond, microsecond and faster timescale can be studied further using techniques such as ZZ-exchange (Farrow*, et al.*, 1994), NH/D exchange (Krishna*, et al.*, 2004), CPMG techniques (Vallurupalli*, et al.*, 2009) or model-free analysis (Lipari and Szabo, 1981, Schneider*, et al.*, 1992). Thus,

combining the different timescale observations in hisactophilin would allow us to create a better model for coordinated switching between conformational states in hisactophilin and perhaps other protein systems.

Letters of Permission

Dear Martin Smith,

Permission is granted for your use of the articles as described in your message below. Please cite the full journal references.

1. Smith, MTJ., Meissner, J., Esmonde, S., Wong, HJ., Meiering, EM. (2010) Energetics and mechanisms of folding and flipping the myristoyl switch in the beta-trefoil protein, hisactophilin. Proc. Natl. Acad. Sci. 107(49), pp. 20952-7

and

2. Dalit Shental-Bechor*, Martin T.J. Smith*, Duncan W.S. MacKenzie, Aron Broom, Amir Marcovitz, Fadila Ghashut, Chris Go, Fernando Bralha, Elizabeth M. Meiering and Yaakov Levy (2012) Nonnative interactions regulate folding and switching of myristoylated protein. Proc. Natl. Acad. Sci (in press) available through electronic publication on July 31, 2012
(* these authors contributed equally)

I've included the written permission above even though you are correct in that you do not need permission to reuse your work in your thesis: Authors need not obtain permission for the following uses of material they have published in PNAS: (1) to use their original figures or tables in their future works; (2) to make copies of their papers for their classroom teaching; or (3) to include their papers as part of their dissertations (or thesis). Of course, citation to the original source should be included (full journal references).

I should also note that since the second article has published online but not in print yet, it is no longer in press. You can cite the DOI number instead of the issue/pages: doi: 10.1073/pnas.1201803109

Please feel free to contact us with any additional questions you might have.

Thank you!

Best regards,
Kelly Gerrity for
Diane Sullenberger
Executive Editor
PNAS

Dear Martin Smith

RE: Martin T.J. Smith, Duncan W.S. MacKenzie, and Elizabeth M. Meiering. Dissecting the molecular determinants of ligand-binding-induced macromolecular switching using thermodynamic cycles. Protein Engineering, Design and Selection (2011) 24(1-2): 213-217

Thank you for your email requesting permission to reprint the above material. Our permission is granted without fee to reproduce the material.

Use of the OUP Material is restricted to: Inclusion in the forthcoming PhD thesis, Martin Smith, Determining the native and nonnative effects of myristoylation on the folding and switching of hisactophilin, to be submitted in print, and an e-thesis (NB: the © line must appear on the same page as the OUP material) to the University of Waterloo in 2012. Territory: World Language: English This permission is limited to this particular use and does not allow you to use it elsewhere or in any other format other than specified above.

Please include a credit line in your publication citing full details of the Oxford University Press publication which is the source of the material and by permission of Oxford University Press/ on behalf of the sponsoring society if this is a society journal.

If the credit line or acknowledgement in our publication indicates that material including any illustrations/figures etc was drawn or modified from an earlier source it will be necessary for you to also clear permission with the original publisher. If this permission has not been obtained, please note that this material cannot be included in your publication/photocopies.

Please do not hesitate to contact me if I can be of any further assistance.

Yours sincerely

Emma Thornton
Permissions Assistant
Academic Rights & Journals
Tel. +44 (0)1865 353672
E-mail: emma.thornton@oup.com

References

Dill, K. A. Dominant forces in protein folding (1990) *Biochemistry* **29,** 7133-7141.

Daggett, V., Li, A., Itzhaki, L. S., Otzen, D. E. & Fersht, A. R. Structure of the transition state for folding of a protein derived from experiment and simulation (1996) *J Mol Biol* **257,** 430-40.

Fersht, A. R., Matouschek, A., Sancho, J., Serrano, L. & Vuilleumier, S. Pathway of protein folding (1992) *Faraday Discuss***,** 183-93.

Daggett, V. & Fersht, A. R. Protein folding and unfolding at atomic resolution (2002) *Cell* **108,** 573-582.

Bowler, B. E. Residual structure in unfolded proteins (2012) *Curr Opin Struct Biol* **22,** 4-13.

Yoo, T. Y., Adhikari, A., Xia, Z., Huynh, T., Freed, K. F., Zhou, R. & Sosnick, T. R. The Folding Transition State of Protein L Is Extensive with Nonnative Interactions (and Not Small and Polarized) (2012) *J Mol Biol*.

Zarrine-Afsar, A., Wallin, S., Neculai, A. M., Neudecker, P., Howell, P. L., Davidson, A. R. & Chan, H. S. Theoretical and experimental demonstration of the importance of specific nonnative interactions in protein folding (2008) *Proc Natl Acad Sci U S A* **105,** 9999-10004.

Onuchic, J. N. & Wolynes, P. G. Theory of protein folding (2004) *Curr Opin Struct Biol* **14,** 70-75.

Fersht, A. (1999) *Structure and Mechanism in Protein Science: A Guide to Enzyme Catalysis and Protein Folding* (W. H. Freeman New York).

Baker, D. A surprising simplicity to protein folding (2000) *Nature* **405,** 39-42.

Sutto, L., Latzer, J., Hegler, J. A., Ferreiro, D. U. & Wolynes, P. G. Consequences of localized frustration for the folding mechanism of the IM7 protein (2007) *Proc Natl Acad Sci USA* **104,** 19825-19830.

Capaldi, A. P., Kleanthous, C. & Radford, S. E. Im7 folding mechanism: misfolding on a path to the native state (2002) *Nat Struct Biol* **9,** 209-16.

Bryngelson, J. D., Onuchic, J. N., Socci, N. D. & Wolynes, P. G. Funnels, Pathways, and the Energy Landscape of Protein-Folding - a Synthesis (1995) *Proteins-Structure Function and Genetics* **21,** 167-195.

Ferreiro, D. U., Hegler, J. A., Komives, E. A. & Wolynes, P. G. On the role of frustration in the energy landscapes of allosteric proteins (2011) *Proc Natl Acad Sci U S A* **108,** 3499-503.

Gosavi, S., Whitford, P. C., Jennings, P. A. & Onuchic, J. N. Extracting function from a beta-trefoil folding motif (2008) *Proc Natl Acad Sci U S A* **105,** 10384-9.

Gianni, S., Guydosh, N. R., Khan, F., Caldas, T. D., Mayor, U., White, G. W., DeMarco, M. L., Daggett, V. & Fersht, A. R. Unifying features in protein-folding mechanisms (2003) *Proc Natl Acad Sci U S A* **100,** 13286-91.

Jackson, S. E., elMasry, N. & Fersht, A. R. Structure of the hydrophobic core in the transition state for folding of chymotrypsin inhibitor 2: a critical test of the protein engineering method of analysis (1993) *Biochemistry* **32,** 11270-8.

Jackson, S. E., Moracci, M., elMasry, N., Johnson, C. M. & Fersht, A. R. Effect of cavity-creating mutations in the hydrophobic core of chymotrypsin inhibitor 2 (1993) *Biochemistry* **32,** 11259-69.
Daggett, V. & Fersht, A. R. Is there a unifying mechanism for protein folding? (2003) *Trends in Biochemical Sciences* **28,** 18-25.
Viguera, A. R., Vega, C. & Serrano, L. Unspecific hydrophobic stabilization of folding transition states (2002) *Proc Natl Acad Sci U S A* **99,** 5349-54.
Resh, M. D. Fatty acylation of proteins: new insights into membrane targeting of myristoylated and palmitoylated proteins (1999) *Biochim Biophys Acta* **1451,** 1-16.
Gordon, J. I., Duronio, R. J., Rudnick, D. A., Adams, S. P. & Gokel, G. W. Protein N-myristoylation (1991) *J Biol Chem* **266,** 8647-50.
Raju, R. V., Magnuson, B. A. & Sharma, R. K. Mammalian myristoyl CoA: protein N-myristoyltransferase (1995) *Mol Cell Biochem* **149-150,** 191-202.
Taniguchi, H. & Manenti, S. Interaction of myristoylated alanine-rich protein kinase C substrate (MARCKS) with membrane phospholipids (1993) *J Biol Chem* **268,** 9960-3.
McLaughlin, S. & Aderem, A. The myristoyl-electrostatic switch: a modulator of reversible protein-membrane interactions (1995) *Trends in Biochemical Sciences* **20,** 272-6.
Blenis, J. & Resh, M. D. Subcellular localization specified by protein acylation and phosphorylation (1993) *Current Opinion in Cell Biology* **5,** 984-9.
Arbuzova, A., Schmitz, A. A. & Vergeres, G. Cross-talk unfolded: MARCKS proteins (2002) *Biochem J* **362,** 1-12.
Zozulya, S. & Stryer, L. Calcium-myristoyl protein switch (1992) *Proc Natl Acad Sci U S A* **89,** 11569-73.
Ames, J. B., Tanaka, T., Ikura, M. & Stryer, L. Nuclear magnetic resonance evidence for Ca(2+)-induced extrusion of the myristoyl group of recoverin (1995) *J Biol Chem* **270,** 30909-13.
Ames, J. B., Porumb, T., Tanaka, T., Ikura, M. & Stryer, L. Amino-terminal myristoylation induces cooperative calcium binding to recoverin (1995) *J Biol Chem* **270,** 4526-33.
Tanaka, T., Ames, J. B., Harvey, T. S., Stryer, L. & Ikura, M. Sequestration of the membrane-targeting myristoyl group of recoverin in the calcium-free state (1995) *Nature* **376,** 444-7.
Valentine, K. G., Mesleh, M. F., Opella, S. J., Ikura, M. & Ames, J. B. Structure, topology, and dynamics of myristoylated recoverin bound to phospholipid bilayers (2003) *Biochemistry* **42,** 6333-40.
Resh, M. D. A myristoyl switch regulates membrane binding of HIV-1 Gag (2004) *Proc Natl Acad Sci U S A* **101,** 417-8.
Tang, C., Loeliger, E., Luncsford, P., Kinde, I., Beckett, D. & Summers, M. F. Entropic switch regulates myristate exposure in the HIV-1 matrix protein (2004) *Proc Natl Acad Sci U S A* **101,** 517-22.
Ponting, C. P. & Russell, R. B. Identification of distant homologues of fibroblast growth factors suggests a common ancestor for all beta-trefoil proteins (2000) *J Mol Biol* **302,** 1041-7.
Pollard, T. D., Almo, S., Quirk, S., Vinson, V. & Lattman, E. E. Structure of actin binding proteins: insights about function at atomic resolution (1994) *Annu Rev Cell Biol* **10,** 207-49.

Adams, J. C. Roles of fascin in cell adhesion and motility (2004) *Current Opinion in Cell Biology* **16,** 590-6.
Edwards, R. A. & Bryan, J. Fascins, a family of actin bundling proteins (1995) *Cell Motil Cytoskeleton* **32,** 1-9.
Kureishy, N., Sapountzi, V., Prag, S., Anilkumar, N. & Adams, J. C. Fascins, and their roles in cell structure and function (2002) *BioEssays* **24,** 350-61.
Adams, J. C. Fascin protrusions in cell interactions (2004) *Trends Cardiovasc Med* **14,** 221-6.
Adams, J. C. & Schwartz, M. A. Stimulation of fascin spikes by thrombospondin-1 is mediated by the GTPases Rac and Cdc42 (2000) *J Cell Biol* **150,** 807-22.
Hanakam, F., Albrecht, R., Eckerskorn, C., Matzner, M. & Gerisch, G. Myristoylated and non-myristoylated forms of the pH sensor protein hisactophilin II: intracellular shuttling to plasma membrane and nucleus monitored in real time by a fusion with green fluorescent protein (1996) *Embo J* **15,** 2935-43.
Scheel, J., Ziegelbauer, K., Kupke, T., Humbel, B. M., Noegel, A. A., Gerisch, G. & Schleicher, M. Hisactophilin, a histidine-rich actin-binding protein from Dictyostelium discoideum (1989) *J Biol Chem* **264,** 2832-9.
Behrisch, A., Dietrich, C., Noegel, A. A., Schleicher, M. & Sackmann, E. The actin-binding protein hisactophilin binds in vitro to partially charged membranes and mediates actin coupling to membranes (1995) *Biochemistry* **34,** 15182-90.
Hanakam, F., Eckerskorn, C., Lottspeich, F., Muller-Taubenberger, A., Schafer, W. & Gerish, G. The pH-sensitive actin-binding protein hisactophilin of Dictyostelium exists in two isoforms which both are myristoylated and distributed between plasma membrane and cytoplasm (1995) *J Biol Chem* **270,** 596-602.
Pintsch, T., Zischka, H. & Schuster, S. C. Hisactophilin is involved in osmoprotection in Dictyostelium (2002) *BMC Biochem* **3,** 10.
Hanakam, F. & Gerisch, G. Monitoring intracellular shutting of histidine-rich pH sensor proteins tagged with green fluorescent protein (1999) *Methods Enzymol* **302,** 51-8.
Stoeckelhuber, M., Noegel, A. A., Eckerskorn, C., Kohler, J., Rieger, D. & Schleicher, M. Structure/function studies on the pH-dependent actin-binding protein hisactophilin in Dictyostelium mutants (1996) *J Cell Sci* **109 (Pt 7),** 1825-35.
Habazettl, J., Gondol, D., Wiltscheck, R., Otlewski, J., Schleicher, M. & Holak, T. A. Structure of hisactophilin is similar to interleukin-1 beta and fibroblast growth factor (1992) *Nature* **359,** 855-8.
Hammond, M. S., Houliston, R. S. & Meiering, E. M. Two-dimensional 1H and 15N NMR titration studies of hisactophilin (1998) *Biochem Cell Biol* **76,** 294-301.
Meissner, J. (2007) in *Chemistry* (University of Waterloo, Waterloo), Vol. Master's.
Liu, C., Chu, D., Wideman, R. D., Houliston, R. S., Wong, H. J. & Meiering, E. M. Thermodynamics of denaturation of hisactophilin, a beta-trefoil protein (2001) *Biochemistry* **40,** 3817-27.
Wong, H. J., Stathopulos, P. B., Bonner, J. M., Sawyer, M. & Meiering, E. M. Non-linear effects of temperature and urea on the thermodynamics and kinetics of folding and unfolding of hisactophilin (2004) *J Mol Biol* **344,** 1089-107.
Resh, M. Trafficking and signaling by fatty-acylated and prenylated proteins (2006) *Nat Chem Biol* **2,** 584-590.

Orban, T., Bereta, G., Miyagi, M., Wang, B., Chance, M. R., Sousa, M. C. & Palczewski, K. Conformational changes in guanylate cyclase-activating protein 1 induced by Ca^{2+} and N-terminal fatty acid acylation (2010) *Structure* **18,** 116-26.

Ames, J. B., Ishima, R., Tanaka, T., Gordon, J. I., Stryer, L. & Ikura, M. Molecular mechanics of calcium-myristoyl switches (1997) *Nature* **389,** 198-202.

Kahn, R. A., Randazzo, P., Serafini, T., Weiss, O., Rulka, C., Clark, J., Amherdt, M., Roller, P., Orci, L. & Rothman, J. E. The amino terminus of ADP-ribosylation factor (ARF) is a critical determinant of ARF activities and is a potent and specific inhibitor of protein transport (1992) *J Biol Chem* **267,** 13039-46.

Lim, S., Peshenko, I., Dizhoor, A. & Ames, J. B. Effects of Ca2+, Mg2+, and myristoylation on guanylyl cyclase activating protein 1 structure and stability (2009) *Biochemistry* **48,** 850-62.

Randazzo, P. A., Terui, T., Sturch, S., Fales, H. M., Ferrige, A. G. & Kahn, R. A. The myristoylated amino terminus of ADP-ribosylation factor 1 is a phospholipid- and GTP-sensitive switch (1995) *J Biol Chem* **270,** 14809-15.

Hanakam, F., Gerisch, G., Lotz, S., Alt, T. & Seelig, A. Binding of hisactophilin I and II to lipid membranes is controlled by a pH-dependent myristoyl-histidine switch (1996) *Biochemistry* **35,** 11036-44.

Pace, C. N. Determination and analysis of urea and guanidine hydrochloride denaturation curves (1986) *Methods Enzymol* **131,** 266-80.

Duronio, R. J., Jackson-Machelski, E., Heuckeroth, R. O., Olins, P. O., Devine, C. S., Yonemoto, W., Slice, L. W., Taylor, S. S. & Gordon, J. I. Protein N-myristoylation in *Escherichia coli*: reconstitution of a eukaryotic protein modification in bacteria (1990) *Proc Natl Acad Sci U S A* **87,** 1506-10.

Liu, C., Gaspar, J. A., Wong, H. J. & Meiering, E. M. Conserved and nonconserved features of the folding pathway of hisactophilin, a beta-trefoil protein (2002) *Protein Sci* **11,** 669-79.

Houliston, R. S., Liu, C., Singh, L. M. & Meiering, E. M. pH and urea dependence of amide hydrogen-deuterium exchange rates in the beta-trefoil protein hisactophilin (2002) *Biochemistry* **41,** 1182-94.

Wuthrich, K. (1986) *NMR of proteins and nucleic acids* (Wiley, New York).

Duggan, B. M. & Craik, D. J. Conformational dynamics of thyroid hormones by variable temperature nuclear magnetic resonance: the role of side chain rotations and cisoid/transoid interconversions (1997) *J Med Chem* **40,** 2259-65.

Cho, J. H., Sato, S. & Raleigh, D. P. Thermodynamics and kinetics of non-native interactions in protein folding: a single point mutant significantly stabilizes the N-terminal domain of L9 by modulating non-native interactions in the denatured state (2004) *J Mol Biol* **338,** 827-37.

Li, L., Mirny, L. A. & Shakhnovich, E. I. Kinetics, thermodynamics and evolution of non-native interactions in a protein folding nucleus (2000) *Nat Struct Biol* **7,** 336-42.

Tanford, C. The hydrophobic effect and the organization of living matter (1978) *Science* **200,** 1012-8.

Kuhlman, B. & Baker, D. Exploring folding free energy landscapes using computational protein design (2004) *Curr Opin Struct Biol* **14,** 89-95.

Wu, Z., Alexandratos, J., Ericksen, B., Lubkowski, J., Gallo, R. C. & Lu, W. Total chemical synthesis of N-myristoylated HIV-1 matrix protein p17: structural and mechanistic implications of p17 myristoylation (2004) *Proc Natl Acad Sci U S A* **101,** 11587-92.

Dell'orco, D., Behnen, P., Linse, S. & Koch, K. W. Calcium binding, structural stability and guanylate cyclase activation in GCAP1 variants associated with human cone dystrophy (2010) *Cell Mol Life Sci*.

Kennedy, M. T., Brockman, H. & Rusnak, F. Contributions of myristoylation to calcineurin structure/function (1996) *J Biol Chem* **271,** 26517-21.

Lopez-Hernandez, E. & Serrano, L. Structure of the transition state for folding of the 129 aa protein CheY resembles that of a smaller protein, CI-2 (1996) *Fold Des* **1,** 43-55.

Riddle, D. S., Grantcharova, V. P., Santiago, J. V., Alm, E., Ruczinski, I. & Baker, D. Experiment and theory highlight role of native state topology in SH3 folding (1999) *Nat Struct Biol* **6,** 1016-24.

Villegas, V., Martinez, J. C., Aviles, F. X. & Serrano, L. Structure of the transition state in the folding process of human procarboxypeptidase A2 activation domain (1998) *J Mol Biol* **283,** 1027-36.

Northey, J. G., Maxwell, K. L. & Davidson, A. R. Protein folding kinetics beyond the phi value: using multiple amino acid substitutions to investigate the structure of the SH3 domain folding transition state (2002) *J Mol Biol* **320,** 389-402.

Ventura, S., Vega, M. C., Lacroix, E., Angrand, I., Spagnolo, L. & Serrano, L. Conformational strain in the hydrophobic core and its implications for protein folding and design (2002) *Nat Struct Biol* **9,** 485-93.

Munson, M., Anderson, K. S. & Regan, L. Speeding up protein folding: mutations that increase the rate at which Rop folds and unfolds by over four orders of magnitude (1997) *Fold Des* **2,** 77-87.

Cho, J. H. & Raleigh, D. P. Denatured state effects and the origin of nonclassical phi values in protein folding (2006) *J Am Chem Soc* **128,** 16492-3.

Gosavi, S., Chavez, L. L., Jennings, P. A. & Onuchic, J. N. Topological frustration and the folding of interleukin-1 beta (2006) *J Mol Biol* **357,** 986-96.

Wensley, B. G., Batey, S., Bone, F. A., Chan, Z. M., Tumelty, N. R., Steward, A., Kwa, L. G., Borgia, A. & Clarke, J. Experimental evidence for a frustrated energy landscape in a three-helix-bundle protein family (2010) *Nature* **463,** 685-8.

Morton, V. L., Friel, C. T., Allen, L. R., Paci, E. & Radford, S. E. The effect of increasing the stability of non-native interactions on the folding landscape of the bacterial immunity protein Im9 (2007) *J Mol Biol* **371,** 554-68.

Chavez, L. L., Gosavi, S., Jennings, P. A. & Onuchic, J. N. Multiple routes lead to the native state in the energy landscape of the beta-trefoil family (2006) *Proc Natl Acad Sci U S A* **103,** 10254-8.

Capraro, D. T., Roy, M., Onuchic, J. N. & Jennings, P. A. Backtracking on the folding landscape of the beta-trefoil protein interleukin-1beta? (2008) *Proc Natl Acad Sci U S A* **105,** 14844-8.

Gambin, Y., Schug, A., Lemke, E. A., Lavinder, J. J., Ferreon, A. C., Magliery, T. J., Onuchic, J. N. & Deniz, A. A. Direct single-molecule observation of a protein living in two opposed native structures (2009) *Proc Natl Acad Sci U S A* **106,** 10153-8.

Sharma, D. & Rajarathnam, K. 13C NMR chemical shifts can predict disulfide bond formation (2000) *J Biomol NMR* **18,** 165-71.
Vallee-Belisle, A., Ricci, F. & Plaxco, K. W. Thermodynamic basis for the optimization of binding-induced biomolecular switches and structure-switching biosensors (2009) *Proc Natl Acad Sci U S A* **106,** 13802-7.
Ababou, A., Shenvi, R. A. & Desjarlais, J. R. Long-range effects on calcium binding and conformational change in the N-domain of calmodulin (2001) *Biochemistry* **40,** 12719-26.
Marvin, J. S. & Hellinga, H. W. Manipulation of ligand binding affinity by exploitation of conformational coupling (2001) *Nat Struct Biol* **8,** 795-8.
Shental-Bechor, D. & Levy, Y. Effect of glycosylation on protein folding: a close look at thermodynamic stabilization (2008) *Proc Natl Acad Sci U S A* **105,** 8256-61.
Nuccitelli, R., Deamer, D.W. (1982) *Intracellular pH: Its Measurement, Regulation, and Utilization in Cellular Functions* (Alan R. Liss, Inc, New York).
Stratton, M. M., Mitrea, D. M. & Loh, S. N. A Ca^{2+}-sensing molecular switch based on alternate frame protein folding (2008) *ACS Chem Biol* **3,** 723-32.
Yamamoto, T., Chen, H. C., Guigard, E., Kay, C. M. & Ryan, R. O. Molecular studies of pH-dependent ligand interactions with the low-density lipoprotein receptor (2008) *Biochemistry* **47,** 11647-52.
Horovitz, A. & Fersht, A. R. Strategy for analysing the co-operativity of intramolecular interactions in peptides and proteins (1990) *J Mol Biol* **214,** 613-7.
Tanford, C. Protein denaturation (1968) *Adv Protein Chem* **23,** 121-282.
Pettersen, E. F., Goddard, T. D., Huang, C. C., Couch, G. S., Greenblatt, D. M., Meng, E. C. & Ferrin, T. E. UCSF Chimera--a visualization system for exploratory research and analysis (2004) *J Comput Chem* **25,** 1605-12.
Humphrey, W., Dalke, A. & Schulten, K. VMD: visual molecular dynamics (1996) *J Mol Graph* **14,** 33-8, 27-8.
Phillips, J. C., Braun, R., Wang, W., Gumbart, J., Tajkhorshid, E., Villa, E., Chipot, C., Skeel, R. D., Kale, L. & Schulten, K. Scalable molecular dynamics with NAMD (2005) *J Comput Chem* **26,** 1781-802.
Cavanagh, J. (2007) *Protein NMR spectroscopy : principles and practice* (Amsterdam ; Boston : Academic Press.
Korzhnev, D. M., Salvatella, X., Vendruscolo, M., Di Nardo, A. A., Davidson, A. R., Dobson, C. M. & Kay, L. E. Low-populated folding intermediates of Fyn SH3 characterized by relaxation dispersion NMR (2004) *Nature* **430,** 586-90.
Neudecker, P., Lundstrom, P. & Kay, L. E. Relaxation dispersion NMR spectroscopy as a tool for detailed studies of protein folding (2009) *Biophys J* **96,** 2045-54.
Wagner, G. & Wuthrich, K. Dynamic model of globular protein conformations based on NMR studies in solution (1978) *Nature* **275,** 247-8.
Wang, J. & Verkhivker, G. M. Energy landscape theory, funnels, specificity, and optimal criterion of biomolecular binding (2003) *Phys Rev Lett* **90,** 188101.
Huang, G. S. & Oas, T. G. Submillisecond folding of monomeric lambda repressor (1995) *Proc Natl Acad Sci U S A* **92,** 6878-82.

Schaeffer, R. D., Fersht, A. & Daggett, V. Combining experiment and simulation in protein folding: closing the gap for small model systems (2008) *Curr Opin Struct Biol* **18,** 4-9.

Smith, M. T., Meissner, J., Esmonde, S., Wong, H. J. & Meiering, E. M. Energetics and mechanisms of folding and flipping the myristoyl switch in the {beta}-trefoil protein, hisactophilin (2010) *Proc Natl Acad Sci U S A* **107,** 20952-7.

Nelson, M. L., Kang, H. S., Lee, G. M., Blaszczak, A. G., Lau, D. K., McIntosh, L. P. & Graves, B. J. Ras signaling requires dynamic properties of Ets1 for phosphorylation-enhanced binding to coactivator CBP (2010) *Proc Natl Acad Sci U S A* **107,** 10026-31.

Jenison, R. D., Gill, S. C., Pardi, A. & Polisky, B. High-resolution molecular discrimination by RNA (1994) *Science* **263,** 1425-9.

Shental-Bechor, D. & Levy, Y. Folding of glycoproteins: toward understanding the biophysics of the glycosylation code (2009) *Curr Opin Struct Biol* **19,** 524-33.

McCarney, E. R., Kohn, J. E. & Plaxco, K. W. Is there or isn't there? The case for (and against) residual structure in chemically denatured proteins (2005) *Crit Rev Biochem Mol Biol* **40,** 181-9.

Remy, I., Wilson, I. A. & Michnick, S. W. Erythropoietin receptor activation by a ligand-induced conformation change (1999) *Science* **283,** 990-3.

Smith, M. T. J., Meissner, J., Esmonde, S., Wong, H. J. & Meiering, E. M. Energetics and mechanisms of folding and flipping the myristoyl switch in the beta-trefoil protein, hisactophilin (2010) *Proc Natl Acad Sci USA* **107,** 20952-20957.

Horovitz, A., Serrano, L. & Fersht, A. R. COSMIC analysis of the major alpha-helix of barnase during folding (1991) *J Mol Biol* **219,** 5-9.

Serrano, L., Horovitz, A., Avron, B., Bycroft, M. & Fersht, A. R. Estimating the contribution of engineered surface electrostatic interactions to protein stability by using double-mutant cycles (1990) *Biochemistry* **29,** 9343-52.

Friel, C. T., Smith, D. A., Vendruscolo, M., Gsponer, J. & Radford, S. E. The mechanism of folding of Im7 reveals competition between functional and kinetic evolutionary constraints (2009) *Nat Struct Mol Biol* **16,** 318-24.

Brych, S. R., Dubey, V. K., Bienkiewicz, E., Lee, J., Logan, T. M. & Blaber, M. Symmetric primary and tertiary structure mutations within a symmetric superfold: a solution, not a constraint, to achieve a foldable polypeptide (2004) *J Mol Biol* **344,** 769-80.

Hwang, J. Y. & Koch, K. W. Calcium- and myristoyl-dependent properties of guanylate cyclase-activating protein-1 and protein-2 (2002) *Biochemistry* **41,** 13021-8.

Muralidhar, D., Jobby, M. K., Krishnan, K., Annapurna, V., Chary, K. V., Jeromin, A. & Sharma, Y. Equilibrium unfolding of neuronal calcium sensor-1: N-terminal myristoylation influences unfolding and reduces protein stiffening in the presence of calcium (2005) *J Biol Chem* **280,** 15569-78.

Fredricksen, R. S. & Swenson, C. A. Relationship between stability and function for isolated domains of troponin C (1996) *Biochemistry* **35,** 14012-26.

Naider, F., Becker, J. M., Lee, Y. H. & Horovitz, A. Double-mutant cycle scanning of the interaction of a peptide ligand and its G protein-coupled receptor (2007) *Biochemistry* **46,** 3476-81.

Hori, Y. & Sugiura, Y. Effects of Zn(II) binding and apoprotein structural stability on the conformation change of designed antennafinger proteins (2004) *Biochemistry* **43,** 3068-74.
Tonge, S. R. & Tighe, B. J. Responsive hydrophobically associating polymers: a review of structure and properties (2001) *Adv Drug Deliv Rev* **53,** 109-22.
Leopold, P. E., Montal, M. & Onuchic, J. N. Protein folding funnels: A kinetic approach to the sequence-structure relationship (1992) *Proc Natl Acad Sci USA* **89,** 8721-8725.
Clementi, C., Nymeyer, H. & Onuchic, J. N. Toplogical and energetical factors: What determines the structural details of the transition state ensemble and "En-route" intermediate for protein folding? An investigation of small globular proteins (2000) *Journal of Molecular Biology* **298,** 937-953.
Simler, B. R., Levy, Y., Onuchic, J. N. & Matthews, C. R. The folding energy landscape of the dimerization domain of Escherichia coli Trp repressor: a joint experimental and theoretical investigation (2006) *J Mol Biol* **363,** 262-78.
Levy, Y., Cho, S. S., Shen, T., Onuchic, J. N. & Wolynes, P. G. Symmetry and frustration in protein energy landscapes: A near degeneracy resolves the Rop dimer-folding mystery (2005) *Proc Natl Acad Sci USA* **102,** 2373-2378.
Turjanski, A. G., Gutkind, J. S., Best, R. B. & Hummer, G. Binding-induced folding of a natively unstructured transcription factor (2008) *Plos Computational Biology* **4,** -.
Zhang, Z. & Chan, H. S. Native topology of the designed protein Top7 is not conducive to cooperative folding (2009) *Biophys J* **96,** L25-7.
Takagi, F., Koga, N. & Takada, S. How protein thermodynamics and folding mechanisms are altered by the chaperonin cage: Molecular simulations (2003) *Proc Natl Acad Sci* **100,** 11367-11372.
Cheung, M. S., Klimov, D. & Thirumalai, D. Molecular crowding enhances native state stability and refolding rates of globular proteins (2005) *Proc Natl Acad Sci* **102,** 4753-4758.
Friel, C. T., Capaldi, A. P. & Radford, S. E. Structural analysis of the rate-limiting transition states in the folding of Im7 and Im9: similarities and differences in the folding of homologous proteins (2003) *J Mol Biol* **326,** 293-305.
Shea, J.-E., Onuchic, J. N. & III, C. L. B. Exploring the origins of topological frustration: Design of a minimally frustrated model of fragment B of protein A (1999) *Proc Natl Acad Sci USA* **96,** 12512-12517.
Li, X., Romero, P., Rani, M., Dunker, A. K. & Obradovic, Z. Predicting Protein Disorder for N-, C-, and Internal Regions (1999) *Genome Inform Ser Workshop Genome Inform* **10,** 30-40.
Di Nardo, A. A., Korzhnev, D. M., Stogios, P. J., Zarrine-Afsar, A., Kay, L. E. & Davidson, A. R. Dramatic acceleration of protein folding by stabilization of a nonnative backbone conformation (2004) *Proc Natl Acad Sci U S A* **101,** 7954-9.
Plotkin, S. S. Speeding protein folding beyond the G(o) model: how a little frustration sometimes helps (2001) *Proteins* **45,** 337-45.
Clementi, C. & Plotkin, S. The effects of nonnative interactions on protein folding rates: Theory and simulation (2004) *Protein Science* **13,** 1750-1766.

Zhang, Z. & Chan, H. S. Competition between native topology and nonnative interactions in simple and complex folding kinetics of natural and designed proteins (2010) *Proc Natl Acad Sci U S A* **107,** 2920-5.
Chan, H. S., Zhang, Z., Wallin, S. & Liu, Z. Cooperativity, local-nonlocal coupling, and nonnative interactions: principles of protein folding from coarse-grained models (2011) *Annual Review of Physical Chemistry* **62,** 301-26.
Chen, Y., Ding, F., Nie, H., Serohijos, A. W., Sharma, S., Wilcox, K. C., Yin, S. & Dokholyan, N. V. Protein folding: then and now (2008) *Arch Biochem Biophys* **469,** 4-19.
Weinkam, P., Pletneva, E. V., Gray, H. B., Winkler, J. R. & Wolynes, P. G. Electrostatic effects on funneled landscapes and structural diversity in denatured protein ensembles (2009) *Proc Natl Acad Sci U S A* **106,** 1796-801.
Shan, B., Eliezer, D. & Raleigh, D. The Unfolded State of the C-terminal Domain of the Ribosomal Protein L9 Contains Both Native and Non-Native Structure (2009) *Biochemistry*.
Azia, A. & Levy, Y. Nonnative Electrostatic Interactions Can Modulate Protein Folding: Molecular Dynamics with a Grain of Salt (2009) *J Mol Biol*.
Thirumalai, D. & Hyeon, C. RNA and protein folding: common themes and variations (2005) *Biochemistry* **44,** 4957-70.
Smith, M. T., Mackenzie, D. W. & Meiering, E. M. Dissecting the molecular determinants of ligand-binding-induced macromolecular switching using thermodynamic cycles (2011) *Protein Eng Des Sel* **24,** 213-7.
Case, D. A., Darden, T. A., Cheatham, I., T. E., Simmerling, C. L., Wang, J., Duke, R. E., Luo, R., Walker, R. C., Zhang, W., Merz, K. M.*, et al.* AMBER 11 (2010) *University of California, San Francisco*.
Vanquelef, E., Simon, S., Marquant, G., Garcia, E., Klimerak, G., Delepine, J. C., Cieplak, P. & Dupradeau, F. Y. RED Server: a web service for deriving RESP and ESP charges and building force field libraries for new molecules and molecular fragments (2011) *Nucleic Acids Research* **39,** W511-W517.
Duan, Y., Wu, C., Chowdhury, S., Lee, M. C., Xiong, G. M., Zhang, W., Yang, R., Cieplak, P., Luo, R., Lee, T.*, et al.* A point-charge force field for molecular mechanics simulations of proteins based on condensed-phase quantum mechanical calculations (2003) *Journal of Computational Chemistry* **24,** 1999-2012.
Zhang, Y.-Z. (1995) in *Structural Biology and Molecular Biophysics* (University of Pennsylvania Philadephia), Vol. PhD.
Biyun, S., Cho, S. S. & Thirumalai, D. Folding of human telomerase RNA pseudoknot using ion-jump and temperature-quench simulations (2011) *J Am Chem Soc* **133,** 20634-43.
Hagai, T. & Levy, Y. Ubiquitin not only serves as a tag but also assists degradation by inducing protein unfolding (2010) *Proc Natl Acad Sci USA* **107,** 2001-2006.
Namanja, A. T., Wang, X. J., Xu, B., Mercedes-Camacho, A. Y., Wilson, B. D., Wilson, K. A., Etzkorn, F. A. & Peng, J. W. Toward flexibility-activity relationships by NMR spectroscopy: dynamics of Pin1 ligands (2011) *J Am Chem Soc* **132,** 5607-9.
Marlow, M. S., Dogan, J., Frederick, K. K., Valentine, K. G. & Wand, A. J. The role of conformational entropy in molecular recognition by calmodulin (2010) *Nat Chem Biol* **6,** 352-8.

Tzeng, S. R. & Kalodimos, C. G. Protein dynamics and allostery: an NMR view (2011) *Curr Opin Struct Biol* **21,** 62-7.
Baxter, E. L., Jennings, P. A. & Onuchic, J. N. Strand swapping regulates the iron-sulfur cluster in the diabetes drug target mitoNEET *Proc Natl Acad Sci U S A* **109,** 1955-60.
Kalodimos, C. G., Boelens, R. & Kaptein, R. A residue-specific view of the association and dissociation pathway in protein--DNA recognition (2002) *Nat Struct Biol* **9,** 193-7.
Hilser, V. J., Wrabl, J. O. & Motlagh, H. N. Structural and energetic basis of allostery (2012) *Annu Rev Biophys* **41,** 585-609.
McDonald, L. R., Boyer, J. A. & Lee, A. L. Segmental Motions, Not a Two-State Concerted Switch, Underlie Allostery in CheY (2012) *Structure*.
Cui, Q. & Karplus, M. Allostery and cooperativity revisited (2008) *Protein Sci* **17,** 1295-307.
Boyer, J. A., Clay, C. J., Luce, K. S., Edgell, M. H. & Lee, A. L. Detection of native-state nonadditivity in double mutant cycles via hydrogen exchange (2010) *J Am Chem Soc* **132,** 8010-9.
Das, R., Abu-Abed, M. & Melacini, G. Mapping allostery through equilibrium perturbation NMR spectroscopy (2006) *J Am Chem Soc* **128,** 8406-7.
Selvaratnam, R., Chowdhury, S., VanSchouwen, B. & Melacini, G. Mapping allostery through the covariance analysis of NMR chemical shifts (2012) *Proc Natl Acad Sci U S A* **108,** 6133-8.
Kalodimos, C. G., Biris, N., Bonvin, A. M., Levandoski, M. M., Guennuegues, M., Boelens, R. & Kaptein, R. Structure and flexibility adaptation in nonspecific and specific protein-DNA complexes (2004) *Science* **305,** 386-9.
Marlatt, N. M. & Shaw, G. S. Amide exchange shows calcium-induced conformational changes are transmitted to the dimer interface of S100B (2007) *Biochemistry* **46,** 7478-87.
LeMaster, D. M., Tang, J., Paredes, D. I. & Hernandez, G. Enhanced thermal stability achieved without increased conformational rigidity at physiological temperatures: spatial propagation of differential flexibility in rubredoxin hybrids (2005) *Proteins* **61,** 608-16.
Polshakov, V. I., Birdsall, B. & Feeney, J. Effects of co-operative ligand binding on protein amide NH hydrogen exchange (2006) *J Mol Biol* **356,** 886-903.
Meiering, E. M., Bycroft, M., Lubienski, M. J. & Fersht, A. R. Structure and dynamics of barnase complexed with 3'-GMP studied by NMR spectroscopy (1993) *Biochemistry* **32,** 10975-87.
Ponte, E., Rivero, F., Fechheimer, M., Noegel, A. & Bozzaro, S. Severe developmental defects in Dictyostelium null mutants for actin-binding proteins (2000) *Mech Dev* **91,** 153-61.
Smith, M. T. J., MacKenzie, D. W. S. & Meiering, E. M. Dissecting the molecular determinants of ligand-binding-induced macromolecular switching using thermodynamic cycles (2011) *Protein Engineering Design & Selection* **24,** 213-217.
Hvidt, A. & Nielsen, S. O. Hydrogen exchange in proteins (1966) *Adv Protein Chem* **21,** 287-386.
Englander, S. W., Downer, N. W. & Teitelbaum, H. Hydrogen exchange (1972) *Annu Rev Biochem* **41,** 903-24.

Englander, S. W. & Kallenbach, N. R. Hydrogen exchange and structural dynamics of proteins and nucleic acids (1983) *Q Rev Biophys* **16,** 521-655.
Houliston, R. S. (2004) in *Chemistry* (University of Guelph, Guelph), Vol. Ph.D, pp. 143.
Shental-Bechor, D., Smith, M. T. J., MacKenzie, D. W. S., Broom, A., Marcovitz, A., Ghashut, F., Go, C., Bralha, F., Meiering, E. M. & Levy, Y. Nonnative interactions regulate folding and switching of myristoylated protein (in press) *Proceedings of the National Academy of Sciences of the United States of America*
Neubert, T. A., Walsh, K. A., Hurley, J. B. & Johnson, R. S. Monitoring calcium-induced conformational changes in recoverin by electrospray mass spectrometry (1997) *Protein Sci* **6,** 843-50.
Hasegawa, H. & Holm, L. Advances and pitfalls of protein structural alignment (2009) *Curr Opin Struct Biol* **19,** 341-8.
Clarke, J. & Itzhaki, L. S. Hydrogen exchange and protein folding (1998) *Curr Opin Struct Biol* **8,** 112-8.
Kuhlman, B. & Raleigh, D. P. Global analysis of the thermal and chemical denaturation of the N-terminal domain of the ribosomal protein L9 in H2O and D2O. Determination of the thermodynamic parameters, deltaH(o), deltaS(o), and deltaC(o)p and evaluation of solvent isotope effects (1998) *Protein Sci* **7,** 2405-12.
Kalodimos, C. G., Biris, N., Bonvin, A. M. J. J., Levandoski, M. M., Guennuegues, M., Boelens, R. & Kaptein, R. Structure and flexibility adaptation in nonspecific and specific protein-DNA complexes (2004) *Science* **305,** 386-389.
Liu, Y., Kahn, R. A. & Prestegard, J. H. Structure and membrane interaction of myristoylated ARF1 (2009) *Structure* **17,** 79-87.
Liu, Y., Kahn, R. A. & Prestegard, J. H. Dynamic structure of membrane-anchored Arf*GTP (2010) *Nat Struct Mol Biol* **17,** 876-81.
Farrow, N. A., Zhang, O., Forman-Kay, J. D. & Kay, L. E. A heteronuclear correlation experiment for simultaneous determination of 15N longitudinal decay and chemical exchange rates of systems in slow equilibrium (1994) *J Biomol NMR* **4,** 727-34.
Krishna, M. M., Hoang, L., Lin, Y. & Englander, S. W. Hydrogen exchange methods to study protein folding (2004) *Methods* **34,** 51-64.
Vallurupalli, P., Hansen, D. F., Lundstrom, P. & Kay, L. E. CPMG relaxation dispersion NMR experiments measuring glycine 1H alpha and 13C alpha chemical shifts in the 'invisible' excited states of proteins (2009) *J Biomol NMR* **45,** 45-55.
Lipari, G. & Szabo, A. Nuclear magnetic resonance relaxation in nucleic acid fragments: models for internal motion (1981) *Biochemistry* **20,** 6250-6.
Schneider, D. M., Dellwo, M. J. & Wand, A. J. Fast internal main-chain dynamics of human ubiquitin (1992) *Biochemistry* **31,** 3645-52.
Koletzko, B., Sauerwald, T. & Demmelmair, H. Safety of stable isotope use (1997) *Eur J Pediatr* **156** Suppl 1**,** S12-7.

Appendix 1 – Mass Spectrometry to Verify Myristoylation

Nonmyristoylated Hisactophilin

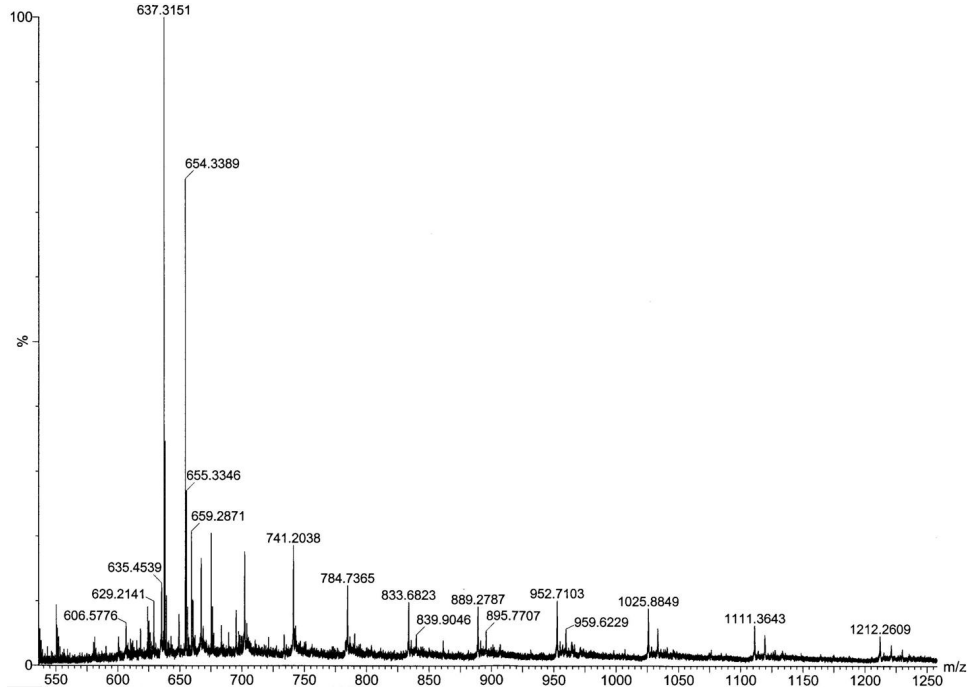

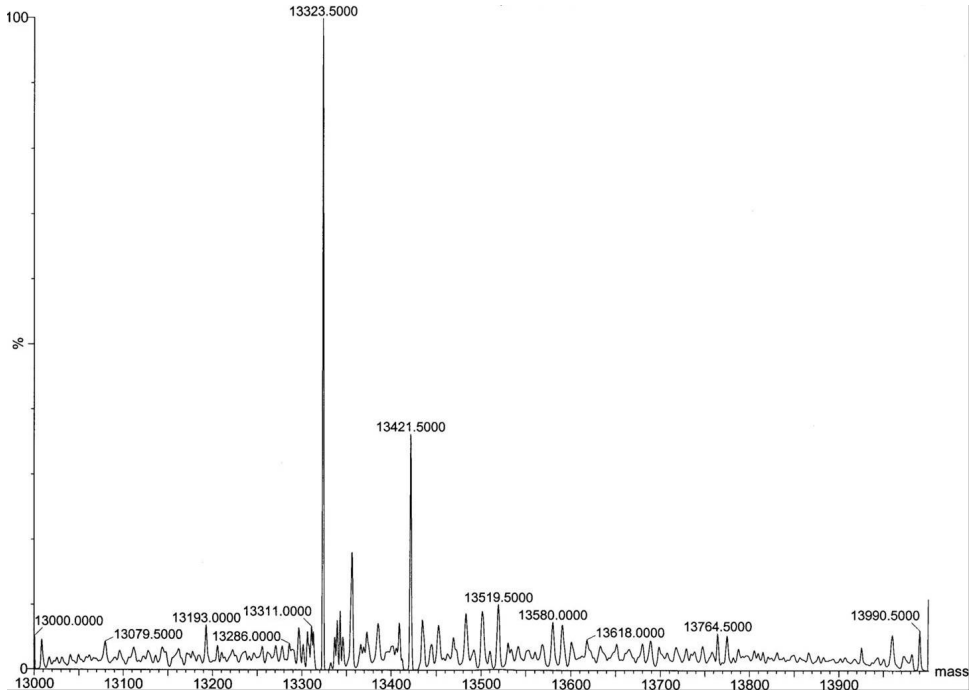

Myristoylated Hisactophilin

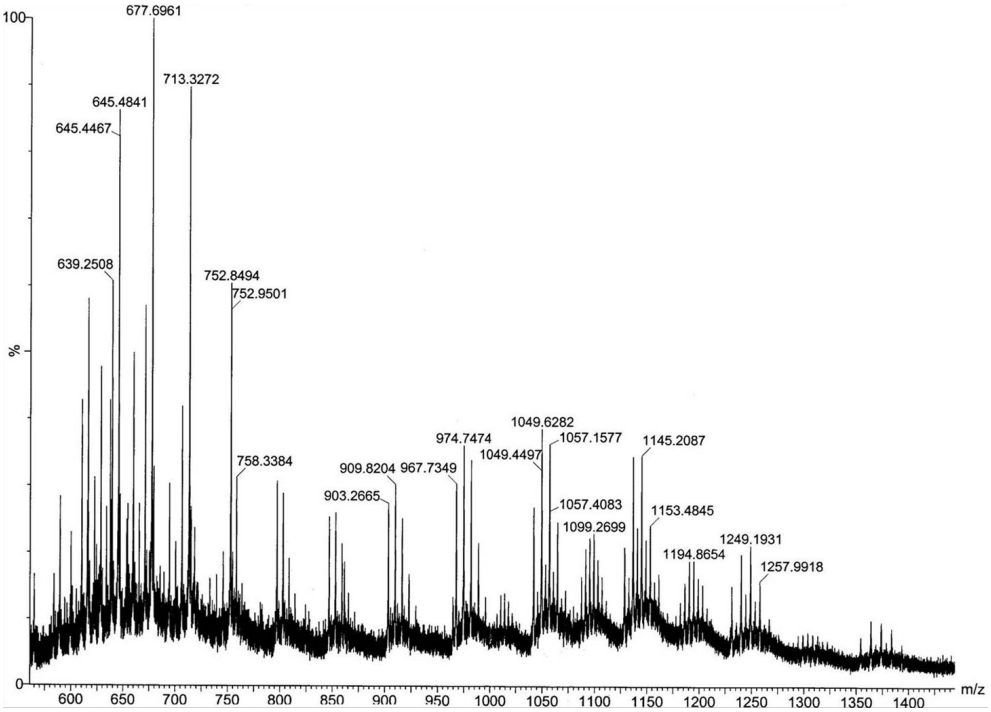

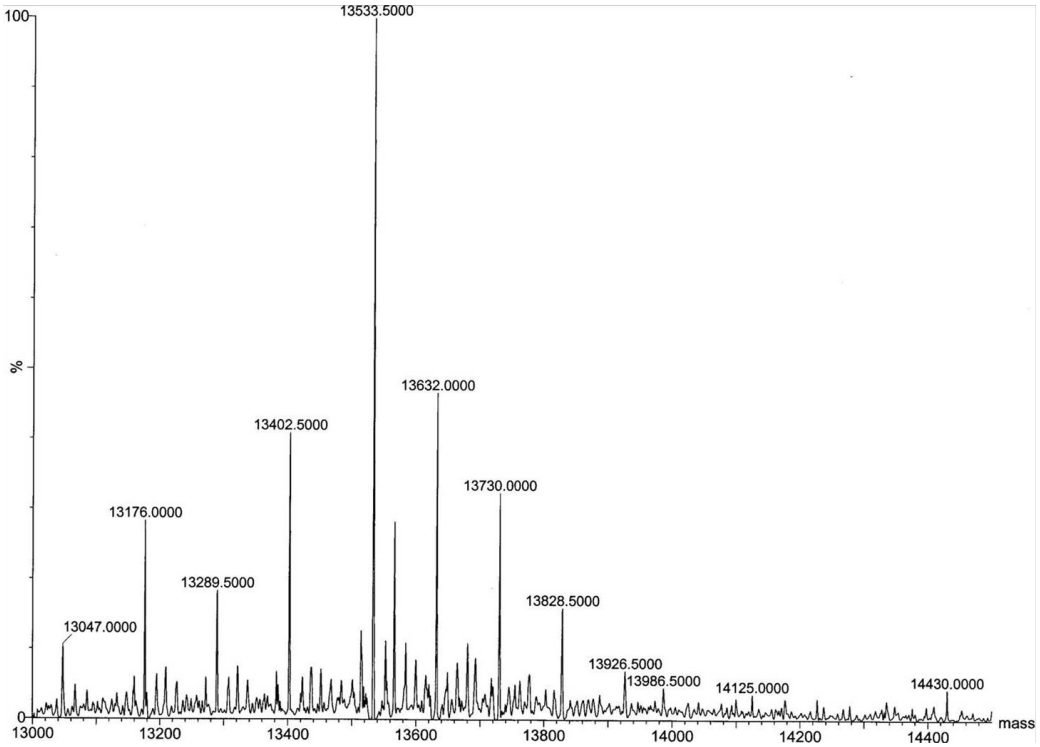

Expected mass: myristoylated = 13534.5Da; nonmyristoylated = 13324.5Da

Appendix 2 – Pulse Programs for NMR

A2.1 – ^{1}H-^{15}N HSQC Pulse Program

```
;invifpf3gpsi
;avance-version
;2D H-1/X correlation via double inept transfer
;   using sensitivity improvement
;phase sensitive using Echo/Antiecho-TPPI gradient
selection
;with decoupling during acquisition
;using f3 - channel
;using flip-back pulse
;A.G. Palmer III, J. Cavanagh, P.E. Wright & M. Rance,
J. Magn.
;   Reson. 93, 151-170 (1991)
;L.E. Kay, P. Keifer & T. Saarinen, J. Am. Chem. Soc.
114,
;   10663-5 (1992)
;J. Schleucher, M. Schwendinger, M. Sattler, P. Schmidt,
O. Schedletzky,
;   S.J. Glaser, O.W. Sorensen & C. Griesinger, J. Biomol.
NMR 4,
;   301-306 (1994)
;S. Grzesiek & A. Bax, J. Am. Chem. Soc. 115, 12593-
12594 (1993)

define list<gradient> EA=<EA>

;$Id: Grad1.incl,v 1.7 2002/06/12 09:04:22 ber Exp $
# 20 "C:/Bruker/XWIN-
NMR/exp/stan/nmr/lists/pp/invifpf3gpsi" 2

# 1 "C:/Bruker/XWIN-
NMR/exp/stan/nmr/lists/pp/Delay.incl" 1
;Delay.incl  -  include file for commonly used delays
;
;version 00/02/07

;general delays

define delay DELTA
define delay DELTA1
define delay DELTA2
define delay DELTA3
define delay DELTA4
define delay DELTA5
define delay DELTA6
define delay DELTA7
define delay DELTA8

define delay TAU
define delay TAU1
define delay TAU2
define delay TAU3
define delay TAU4
define delay TAU5
;delays for centering pulses

define delay CEN_HN1
define delay CEN_HN2
define delay CEN_HN3
define delay CEN_HC1
define delay CEN_HC2
define delay CEN_HC3
define delay CEN_HC4
define delay CEN_HP1
define delay CEN_HP2
define delay CEN_CN1
define delay CEN_CN2
define delay CEN_CN3
define delay CEN_CN4
define delay CEN_CP1
define delay CEN_CP2

;loop counters

define loopcounter COUNTER
define loopcounter SCALEF
define loopcounter FACTOR1
define loopcounter FACTOR2
define loopcounter FACTOR3

;$Id: Delay.incl,v 1.11 2002/06/12 09:04:22 ber Exp $
# 21 "C:/Bruker/XWIN-
NMR/exp/stan/nmr/lists/pp/invifpf3gpsi" 2

"p2=p1*2"

"p22=p21*2"

"d0=3u"

"d11=30m"

"d26=1s/(cnst4*4)"

"DELTA=p16+d16+p2+d0*2"
"DELTA1=p16+d16+8u"

"CEN_HN1=(p21-p1)/2"
"CEN_HN2=(p22-p2)/2"

"l3=(td1/2)"
```

```
1 ze
  d11 pl16:f3
2 d1 do:f3
  6m
3 d11
  18m
4 (p1 ph1)
  d26 pl3:f3
  (CEN_HN2 p2 ph2) (p22 ph6):f3
  d26 setnmr2|0 setnmr0|34|32|33
  (p1 ph2)
  4u pl0:f1
  (p11:sp1 ph1:r):f1
  4u
  p16:gp1
  d16 pl1:f1
  (p21 ph3):f3
  d0
  p2 ph7
  d0
  p16:gp2*EA
  d16
  (p22 ph4):f3
  DELTA
  (CEN_HN1 p1 ph1) (p21 ph4):f3
  d24
  (CEN_HN2 p2 ph1) (p22 ph1):f3
  d24
  (CEN_HN1 p1 ph2) (p21 ph5):f3
  d26
  (CEN_HN2 p2 ph1) (p22 ph1):f3
  d26
  (p1 ph1)
  DELTA1
  (p2 ph1)
  4u
  p16:gp3
  d16 pl16:f3
  4u setnmr2^0 setnmr0^34^32^33
  go=2 ph31 cpd3:f3
  d1 do:f3 wr #0 if #0 zd
  3m ip5 igrad EA
  3m ip5
  lo to 3 times 2
  d11 id0
  3m ip3
  3m ip3
  3m ip6
  3m ip6
  3m ip31
  3m ip31
  lo to 4 times l3
exit
```

```
ph1=0
ph2=1
ph3=0 2
ph4=0 0 2 2
ph5=1 1 3 3
ph6=0
ph7=0 0 2 2
ph31=2 0 0 2

;pl0 : 120dB
;pl1 : f1 channel - power level for pulse (default)
;pl3 : f3 channel - power level for pulse (default)
;pl16: f3 channel - power level for CPD/BB decoupling
;sp1: f1 channel - shaped pulse  90 degree
;p1 : f1 channel -  90 degree high power pulse
;p2 : f1 channel - 180 degree high power pulse
;p11: f1 channel -  90 degree shaped pulse
;p16: homospoil/gradient pulse                    [1 msec]
;p21: f3 channel -  90 degree high power pulse
;p22: f3 channel - 180 degree high power pulse
;d0 : incremented delay (2D)                      [3 usec]
;d1 : relaxation delay; 1-5 * T1
;d11: delay for disk I/O                          [30 msec]
;d16: delay for homospoil/gradient recovery
;d24: 1/(4J)YH for YH
;     1/(8J)YH for all multiplicities
;d26: 1/(4J(YH))
;cnst4: = J(YH)
;l3: loop for phase sensitive 2D using  E/A method : l3 =
td1/2
;in0: 1/(2 * SW(X)) = DW(X)
;nd0: 2
;NS: 1 * n
;DS: >= 16
;td1: number of experiments
;MC2: echo-antiecho
;cpd3: decoupling according to sequence defined by
cpdprg3
;pcpd3: f3 channel - 90 degree pulse for decoupling
sequence

;use gradient ratio:            gp 1 : gp 2 : gp 3
; 50 :   80 : 20.1       for C-13
; 50 :   80 :  8.1       for N-15

;for z-only gradients:
;gpz1: 50%
;gpz2: 80%
;gpz3: 20.1% for C-13, 8.1% for N-15

;use gradient files:
;gpnam1: SINE.100
;gpnam2: SINE.100
;gpnam3: SINE.100
```

A2.2 – ^{15}N-edited 3D TOCSY Pulse Program

```
;dipsiif3gpsi3d
;avance-version (00/10/05)
;TOCSY-HSQC
;3D sequence with
;   homonuclear Hartman-Hahn transfer using DIPSI2
sequence
;      for mixing
;   H-1/X correlation via double inept transfer
;      using sensitivity improvement
;phase sensitive (t1)
;phase sensitive using Echo/Antiecho-TPPI gradient
selection (t2)
;using trim pulses in inept transfer
;using f3 - channel
;A.G. Palmer III, J. Cavanagh, P.E. Wright & M. Rance,
J. Magn.
;   Reson. 93, 151-170 (1991)
;L.E. Kay, P. Keifer & T. Saarinen, J. Am. Chem. Soc.
114,
;   10663-5 (1992)
;J. Schleucher, M. Schwendinger, M. Sattler, P. Schmidt,
O. Schedletzky,
;   S.J. Glaser, O.W. Sorensen & C. Griesinger, J. Biomol.
NMR 4,
;   301-306 (1994)

define list<gradient> EA=<EA>

;version 00/02/07

;general delays

define delay DELTA
define delay DELTA1
define delay DELTA2
define delay DELTA3
define delay DELTA4
define delay DELTA5
define delay DELTA6
define delay DELTA7
define delay DELTA8

define delay TAU
define delay TAU1
define delay TAU2
define delay TAU3
define delay TAU4
define delay TAU5

;delays for centering pulses

define delay CEN_HN1
define delay CEN_HN2
define delay CEN_HN3
define delay CEN_HC1
define delay CEN_HC2
define delay CEN_HC3
define delay CEN_HC4
define delay CEN_HP1
define delay CEN_HP2
define delay CEN_CN1
define delay CEN_CN2
define delay CEN_CN3
define delay CEN_CN4
define delay CEN_CP1
define delay CEN_CP2

;loop counters

define loopcounter COUNTER
define loopcounter SCALEF
define loopcounter FACTOR1
define loopcounter FACTOR2
define loopcounter FACTOR3

;$Id: Delay.incl,v 1.11 2002/06/12 09:04:22 ber Exp $
# 25 "C:/Bruker/XWIN-
NMR/exp/stan/nmr/lists/pp/dipsiif3gpsi3d" 2

"p2=p1*2"
"p22=p21*2"
"d0=3u"
"d10=3u"
"d11=30m"
"d12=20u"
"d13=4u"
"d26=1s/(cnst4*4)"

"DELTA=p16+d16+p2+d10*2"
"DELTA1=d13+p16+d16+4u"
"DELTA2=p22+d0*2"

"CEN_HN1=(p21-p1)/2"
"CEN_HN2=(p22-p2)/2"

"FACTOR1=(d9/(p6*115.112))/2+0.5"
"l1=FACTOR1*2"

aqseq 321

# 1 "mc_line 61 file C:/Bruker/XWIN-
NMR/exp/stan/nmr/lists/pp/dipsiif3gpsi3d expanding
definition part of mc command before ze"
; dimension 3 aq-mode (F2) Echo-Antiecho (F1) States-
TPPI  F2->F1
define delay MCWRK
define delay MCREST
define loopcounter ST1CNT
"ST1CNT = td1 / (2)"
define loopcounter ST2CNT
"ST2CNT = td2 / (2)"
"MCWRK = 0.090909*d11"
"MCREST = d11 - d11"
```

```
# 61 "C:/Bruker/XWIN-
NMR/exp/stan/nmr/lists/pp/dipsiif3gpsi3d"
1 ze
# 1 "mc_line 61 file C:/Bruker/XWIN-
NMR/exp/stan/nmr/lists/pp/dipsiif3gpsi3d expanding
definition of mc command after ze"
# 62 "C:/Bruker/XWIN-
NMR/exp/stan/nmr/lists/pp/dipsiif3gpsi3d"
  d11 pl16:f3
# 1 "mc_line 63 file C:/Bruker/XWIN-
NMR/exp/stan/nmr/lists/pp/dipsiif3gpsi3d expanding start
label for mc command"
2 MCWRK  * 2 do:f3
LBLSTS2, MCWRK  * 4
LBLF2, MCWRK  * 4
LBLSTS1, MCWRK
LBLF1, MCREST
# 64 "C:/Bruker/XWIN-
NMR/exp/stan/nmr/lists/pp/dipsiif3gpsi3d"
3 d12 pl9:f1
  d1 cw:f1 ph29
  4u do:f1
  d12 pl1:f1

  (p1 ph8)
   DELTA2 pl3:f3
  (p2 ph9)
  d0
  (p22 ph1):f3
  d0
  (p1 ph10)
  d20 pl10:f1

;begin DIPSI2
7 p6*3.556 ph23
  p6*4.556 ph25
  p6*3.222 ph23
  p6*3.167 ph25
  p6*0.333 ph23
  p6*2.722 ph25
  p6*4.167 ph23
  p6*2.944 ph25
  p6*4.111 ph23

  p6*3.556 ph25
  p6*4.556 ph23
  p6*3.222 ph25
  p6*3.167 ph23
  p6*0.333 ph25
  p6*2.722 ph23
  p6*4.167 ph25
  p6*2.944 ph23
  p6*4.111 ph25

  p6*3.556 ph25
  p6*4.556 ph23
  p6*3.222 ph25
  p6*3.167 ph23
  p6*0.333 ph25
  p6*2.722 ph23
  p6*4.167 ph25
  p6*2.944 ph23
  p6*4.111 ph25

  p6*3.556 ph23
  p6*4.556 ph25
  p6*3.222 ph23
  p6*3.167 ph25
  p6*0.333 ph23
  p6*2.722 ph25
  p6*4.167 ph23
  p6*2.944 ph25
  p6*4.111 ph23
  lo to 7 times l1
                                                                ;end
DIPSI2

  d21 pl1:f1
  (p1 ph11)

  d26
  (CEN_HN2 p2 ph1) (p22 ph6):f3
  d26 setnmr2|0 setnmr0|34|32|33
  p28 ph1
  d13
  (p1 ph2)
  3u
  p16:gp1
  d16
  (p21 ph3):f3
  d10
  p2 ph7
  d10
  p16:gp2*EA
  d16
  (p22 ph4):f3
  DELTA
  (CEN_HN1 p1 ph1) (p21 ph4):f3
  d24
  (CEN_HN2 p2 ph1) (p22 ph1):f3
  d24
  (CEN_HN1 p1 ph2) (p21 ph5):f3
  d26
  (CEN_HN2 p2 ph1) (p22 ph1):f3
  d26
  (p1 ph1)
  DELTA1
  (p2 ph1)
  d13
  p16:gp3
  d16 pl16:f3
  4u setnmr2^0 setnmr0^34^32^33
  go=2 ph31 cpd3:f3
# 1 "mc_line 159 file C:/Bruker/XWIN-
NMR/exp/stan/nmr/lists/pp/dipsiif3gpsi3d expanding mc
command in line"
  MCWRK  do:f3 wr #0 if #0 zd igrad EA  MCWRK
ip5*2
```

```
  lo to LBLSTS2 times 2
  MCWRK id10 MCWRK ip3*2 MCWRK ip6*2
MCWRK ip31*2
  lo to LBLF2 times ST2CNT
  MCWRK rd10 MCWRK ip8 MCWRK ip9 MCWRK
ip29
  lo to LBLSTS1 times 2
  MCWRK id0
  lo to LBLF1 times ST1CNT
# 162 "C:/Bruker/XWIN-
NMR/exp/stan/nmr/lists/pp/dipsiif3gpsi3d"
exit

ph1=0
ph2=1
ph3=0 2
ph4=0 0 2 2
ph5=1 1 3 3
ph6=0
ph7=0 0 2 2
ph8=0 0 0 0 2 2 2 2
ph9=1 1 1 1 3 3 3 3
ph10=2 2 2 2 2 2 2 2 2 2 2 2 2 2 2 2
    0 0 0 0 0 0 0 0 0 0 0 0 0 0 0 0
ph11=0 0 0 0 0 0 0 0 2 2 2 2 2 2 2 2
ph23=1
ph25=3
ph29=0
ph31=0 2 2 0 2 0 0 2 2 0 0 2 0 2 2 0
    2 0 0 2 0 2 2 0 0 2 2 0 2 0 0 2
;pl0 : 120dB
;pl1 : f1 channel - power level for pulse (default)
;pl3 : f3 channel - power level for pulse (default)
;pl9 : f1 channel - power level for presaturation
;pl10: f1 channel - power level for TOCSY-spinlock
;pl16: f3 channel - power level for CPD/BB decoupling
;p1 : f1 channel -  90 degree high power pulse
;p2 : f1 channel - 180 degree high power pulse
;p6 : f1 channel -  90 degree low power pulse
;p16: homospoil/gradient pulse                  [1 msec]
;p21: f3 channel -  90 degree high power pulse
;p22: f3 channel - 180 degree high power pulse
;p28: f1 channel - trim pulse                   [1 msec]
;d0 : incremented delay (F1 in 3D)              [3 usec]
;d1 : relaxation delay; 1-5 * T1
;d9 : TOCSY mixing time
;d10: incremented delay (F2 in 3D)              [3 usec]
;d11: delay for disk I/O                        [30 msec]
;d12: delay for power switching                 [20 usec]
;d13: short delay                               [4 usec]
;d16: delay for homospoil/gradient recovery
;d20: first z-filter delay                      [10 usec]
;d21: second z-filter delay                     [10 usec]
;d24: 1/(4J)YH for YH
;     1/(8J)YH for all multiplicities
;d26: 1/(4J(YH))
;cnst4: = J(YH)
;l1: loop for DIPSI cycle: ((p6*115.112) * l1) = mixing
time
;in0: 1/(2 * SW(H)) = DW(H)
;nd0: 2
;in10: 1/(2 * SW(X)) = DW(X)
;nd10: 2
;NS: 8 * n
;DS: >= 16
;td1: number of experiments
;td2: number of experiments in F2
;FnMODE: States-TPPI (or TPPI) in F1
;FnMODE: echo-antiecho in F2
;cpd3: decoupling according to sequence defined by
cpdprg3
;pcpd3: f3 channel - 90 degree pulse for decoupling
sequence
;use gradient ratio:    gp 1 : gp 2 : gp 3
;                    50 :   80 :  8.1        for N-15
;                    50 :   80 : 20.1      for C-13
;for z-only gradients:
;gpz1: 50%
;gpz2: 80%
;gpz3: 8.1% for N-15, 20.1% for C-13

;use gradient files:
;gpnam1: SINE.100
;gpnam2: SINE.100
;gpnam3: SINE.100

;set pl9 to 120dB when presaturation is not required
;   use 70 - 80dB to reduce radiation damping

;$Id: dipsiif3gpsi3d,v 1.7.2.1 2001/09/11 10:14:36 ber
Exp$
```

A2.3 – ^{15}N-edited 3D NOESY Pulse Program

```
# 1 "C:/Bruker/XWIN-
NMR/exp/stan/nmr/lists/pp/noesiifpf3gpsi3d"
;noesiifpf3gpsi3d
;avance-version (00/10/05)
;NOESY-HSQC
;3D sequence with
;   homonuclear correlation via dipolar coupling
;   dipolar coupling may be due to noe or chemical
exchange
;   H-1/X correlation via double inept transfer
;      using sensitivity improvement
;phase sensitive (t1)
;phase sensitive using Echo/Antiecho-TPPI gradient
selection (t2)
;with decoupling during acquisition
;using flip-back pulse
;using f3 - channel
;
;O. Zhang, L.E. Kay, J.P. Olivier & J.D. Forman-Kay,
;   J. Biomol. NMR 4, 845 - 858 (1994)
;A.G. Palmer III, J. Cavanagh, P.E. Wright & M. Rance,
J. Magn.
;   Reson. 93, 151-170 (1991)
;L.E. Kay, P. Keifer & T. Saarinen, J. Am. Chem. Soc.
114,
;   10663-5 (1992)
;J. Schleucher, M. Schwendinger, M. Sattler, P. Schmidt,
O. Schedletzky,
;   S.J. Glaser, O.W. Sorensen & C. Griesinger, J. Biomol.
NMR 4,
;   301-306 (1994)

;avance-version (02/05/31)

define list<gradient> EA=<EA>

;$Id: Grad1.incl,v 1.7 2002/06/12 09:04:22 ber Exp $
# 30 "C:/Bruker/XWIN-
NMR/exp/stan/nmr/lists/pp/noesiifpf3gpsi3d" 2

# 1 "C:/Bruker/XWIN-
NMR/exp/stan/nmr/lists/pp/Delay.incl" 1
;Delay.incl  -  include file for commonly used delays
;
;version 00/02/07

;general delays

define delay DELTA
define delay DELTA1
define delay DELTA2
define delay DELTA3
define delay DELTA4
define delay DELTA5
define delay DELTA6
define delay DELTA7
define delay DELTA8
define delay TAU
define delay TAU1
define delay TAU2
define delay TAU3
define delay TAU4
define delay TAU5

;delays for centering pulses

define delay CEN_HN1
define delay CEN_HN2
define delay CEN_HN3
define delay CEN_HC1
define delay CEN_HC2
define delay CEN_HC3
define delay CEN_HC4
define delay CEN_HP1
define delay CEN_HP2
define delay CEN_CN1
define delay CEN_CN2
define delay CEN_CN3
define delay CEN_CN4
define delay CEN_CP1
define delay CEN_CP2

;loop counters

define loopcounter COUNTER
define loopcounter SCALEF
define loopcounter FACTOR1
define loopcounter FACTOR2
define loopcounter FACTOR3

;$Id: Delay.incl,v 1.11 2002/06/12 09:04:22 ber Exp $
# 31 "C:/Bruker/XWIN-
NMR/exp/stan/nmr/lists/pp/noesiifpf3gpsi3d" 2

"p2=p1*2"

"p22=p21*2"

"d0=3u"

"d10=3u"

"d11=30m"

"d12=20u"

"d13=4u"

"d26=1s/(cnst4*4)"

"DELTA=p16+d16+p2+d10*2"
"DELTA1=d13+p19+d16+4u"
"DELTA2=p22+d0*2"
```

```
"DELTA3=d24-p16-4u"
"DELTA4=d26-p16-d16"

"TAU=d8-p16-d16"

"CEN_HN1=(p21-p1)/2"
"CEN_HN2=(p22-p2)/2"

aqseq 321

# 1 "mc_line 67 file C:/Bruker/XWIN-
NMR/exp/stan/nmr/lists/pp/noesiifpf3gpsi3d expanding
definition part of mc command before ze"
; dimension 3 aq-mode (F2) Echo-Antiecho (F1) States-
TPPI  F2->F1
define delay MCWRK
define delay MCREST
define loopcounter ST1CNT
"ST1CNT = td1 / (2)"
define loopcounter ST2CNT
"ST2CNT = td2 / (2)"
"MCWRK = 0.100000*d11"
"MCREST = d11 - d11"
# 67 "C:/Bruker/XWIN-
NMR/exp/stan/nmr/lists/pp/noesiifpf3gpsi3d"
1 ze
# 1 "mc_line 67 file C:/Bruker/XWIN-
NMR/exp/stan/nmr/lists/pp/noesiifpf3gpsi3d expanding
definition of mc command after ze"
# 68 "C:/Bruker/XWIN-
NMR/exp/stan/nmr/lists/pp/noesiifpf3gpsi3d"
  d11 pl16:f3
# 1 "mc_line 69 file C:/Bruker/XWIN-
NMR/exp/stan/nmr/lists/pp/noesiifpf3gpsi3d expanding
start label for mc command"
2 MCWRK  * 2 do:f3
LBLSTS2, MCWRK  * 4
LBLF2, MCWRK  * 3
LBLSTS1, MCWRK
LBLF1, MCREST
# 70 "C:/Bruker/XWIN-
NMR/exp/stan/nmr/lists/pp/noesiifpf3gpsi3d"
3 d12
  d1
  (p1 ph8)
  DELTA2 pl3:f3
  (p2 ph9)
  d0
  (CEN_CN2 p22 ph1):f3
  d0
  (p1 ph10)
  TAU setnmr2|0 setnmr0|34|32|33
  p16:gp1
  d16
  (p1 ph11)
  d26
  (CEN_HN2 p2 ph1) (p22 ph6):f3
  d26
  (p1 ph2)
  4u pl0:f1
  (p11:sp1 ph12):f1
  4u
  p16:gp2
  d16

  (p21 ph3):f3
  d10
  p2 ph7
  d10
  p16:gp3*EA
  d16
  (p22 ph4):f3
  DELTA
  (CEN_HN1 p1 ph1) (p21 ph4):f3
  4u
  p16:gp4
  DELTA3
  (CEN_HN2 p2 ph1) (p22 ph1):f3
  DELTA4
  p16:gp4
  d16
  (CEN_HN1 p1 ph2) (p21 ph5):f3
  4u
  p16:gp5
  DELTA3
  (CEN_HN2 p2 ph1) (p22 ph1):f3
  DELTA4
  p16:gp5
  d16
  (p1 ph1)
  DELTA1
  (p2 ph1)
  d13
  p19:gp6
  d16 pl16:f3
  4u setnmr2^0 setnmr0^34^32^33
  go=2 ph31 cpd3:f3
# 1 "mc_line 126 file C:/Bruker/XWIN-
NMR/exp/stan/nmr/lists/pp/noesiifpf3gpsi3d expanding
mc command in line"
  MCWRK  do:f3 wr #0 if #0 zd igrad EA  MCWRK
ip5*2
  lo to LBLSTS2 times 2
  MCWRK id10  MCWRK  ip3*2  MCWRK  ip6*2
MCWRK  ip31*2
  lo to LBLF2 times ST2CNT
  MCWRK rd10  MCWRK  ip8  MCWRK  ip9
  lo to LBLSTS1 times 2
  MCWRK id0
  lo to LBLF1 times ST1CNT
# 129 "C:/Bruker/XWIN-
NMR/exp/stan/nmr/lists/pp/noesiifpf3gpsi3d"
exit

ph1=0
ph2=1
ph3=0 2
```

```
ph4=0 0 2 2
ph5=1 1 3 3
ph6=0
ph7=0 0 2 2
ph8=0 0 0 0 2 2 2 2
ph9=1 1 1 1 3 3 3 3
ph10=0 0 0 0 0 0 0 0 0 0 0 0 0 0 0 0
    2 2 2 2 2 2 2 2 2 2 2 2 2 2 2 2
ph11=0 0 0 0 0 0 0 0 2 2 2 2 2 2 2 2
ph12=2 2 2 2 2 2 2 2 0 0 0 0 0 0 0 0
ph31=0 2 2 0 2 0 0 2 2 0 0 2 0 2 2 0
    2 0 0 2 0 2 2 0 0 2 2 0 2 0 0 2

;pl0 : 120dB
;pl1 : f1 channel - power level for pulse (default)
;pl3 : f3 channel - power level for pulse (default)
;pl16: f3 channel - power level for CPD/BB decoupling
;sp1 : f1 channel - shaped pulse  90 degree
;p1 : f1 channel -  90 degree high power pulse
;p2 : f1 channel - 180 degree high power pulse
;p11: f1 channel -  90 degree shaped pulse
;p16: homospoil/gradient pulse                      [1 msec]
;p21: f3 channel -  90 degree high power pulse
;p22: f3 channel - 180 degree high power pulse
;d0 : incremented delay (F1 in 3D)                  [3 usec]
;d1 : relaxation delay; 1-5 * T1
;d8 : mixing time
;d10: incremented delay (F2 in 3D)                  [3 usec]
;d11: delay for disk I/O                            [30 msec]
;d12: delay for power switching                     [20 usec]
;d13: short delay                                   [4 usec]
;d16: delay for homospoil/gradient recovery
;p19: homospoil/gradient pulse                      [300 usec]
;d24: 1/(4J)YH for YH
;     1/(8J)YH for all multiplicities
;d26: 1/(4J(YH))
;cnst4: = J(YH)
;in0: 1/(2 * SW(H)) = DW(H)
;nd0: 2
;in10: 1/(2 * SW(X)) = DW(X)
;nd10: 2
;NS: 8 * n
;DS: >= 16
;td1: number of experiments in F1
;td2: number of experiments in F2
;FnMODE: States-TPPI (or TPPI) in F1
;FnMODE: echo-antiecho in F2
;cpd3: decoupling according to sequence defined by
cpdprg3
;pcpd3: f3 channel - 90 degree pulse for decoupling
sequence

;use gradient ratio:            gp 1 : gp 2 : gp 3 :  gp 4 : gp 5
: gp 6
;                                 30 :  -50 :   80 :    11 :    5 :
8.1*x

;   with x = p16/p19

;for z-only gradients:
;gpz1: 30%
;gpz2: -50%
;gpz3: 80%
;gpz4: 11%
;gpz5: 5%
;gpz6: 27% (8.1% *p16(=1 ms)/p19(=300 us))

;use gradient files:
;gpnam1: SINE.100
;gpnam2: SINE.100
;gpnam3: SINE.100
;gpnam4: SINE.100
;gpnam5: SINE.100
;gpnam6: SINE.50

;$Id: noesiifpf3gpsi3d,v 1.4 2000/10/06 09:09:32 ber Exp
```

Appendix 3 – Mutant Verification by DNA Sequencing

I85L

Expected Sequence

atgggtaaca gagcattcaa atcacatcac ggtcactttt
taagcgctga aggcgaagct gtaaagactc accacggtca
tcatgatcat cacacccatt tccacgttga aaaccatggt
ggtaaagttg cattaaagac ccattgcggt aaataccttt
caattggtga tcataaacaa gtttacctct cacaccactt
acacggtgac cactcactct tccacttaga acatcatggc
ggtaaagtct cactgaaagg tcatcaccac cactacattt
ccgctgatca tcatggtcat gtttcaacca aagaacacca
cgatcacgac accacctttg aagaaattat tatttaa

NOTE: Mutated bases are shown in red.

Mobix Sequencing Results (Mobix, McMaster University, Hamilton)

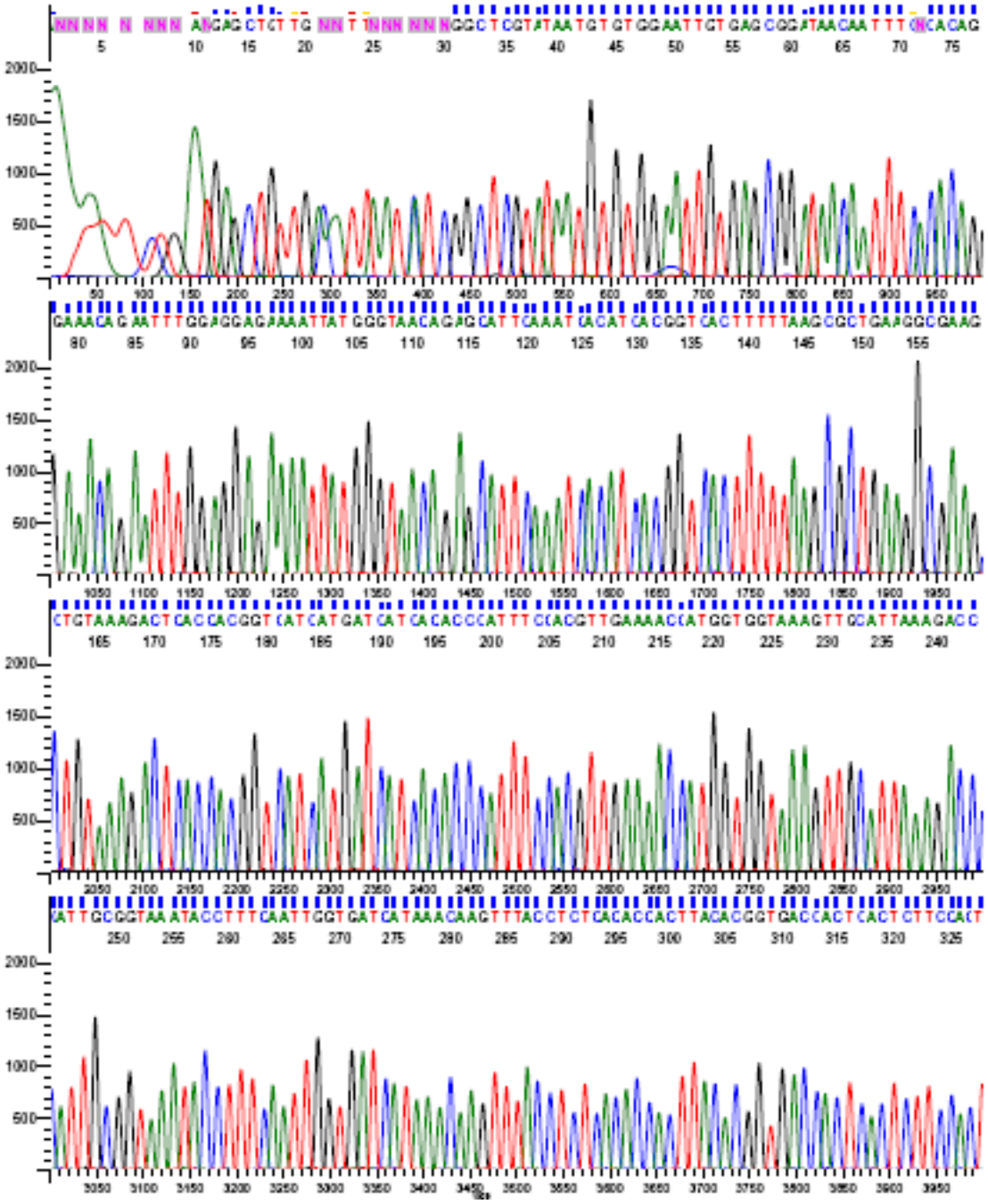

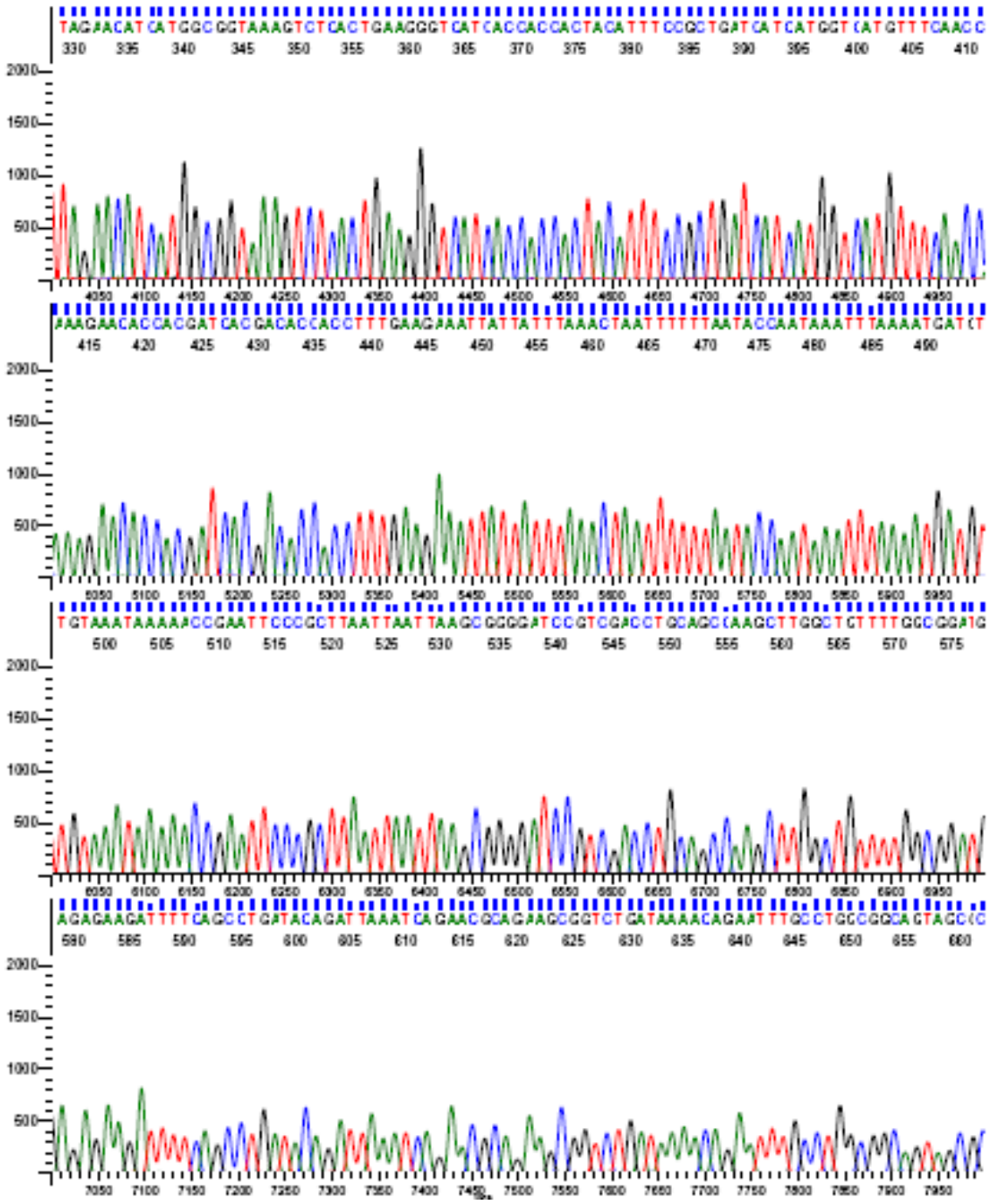

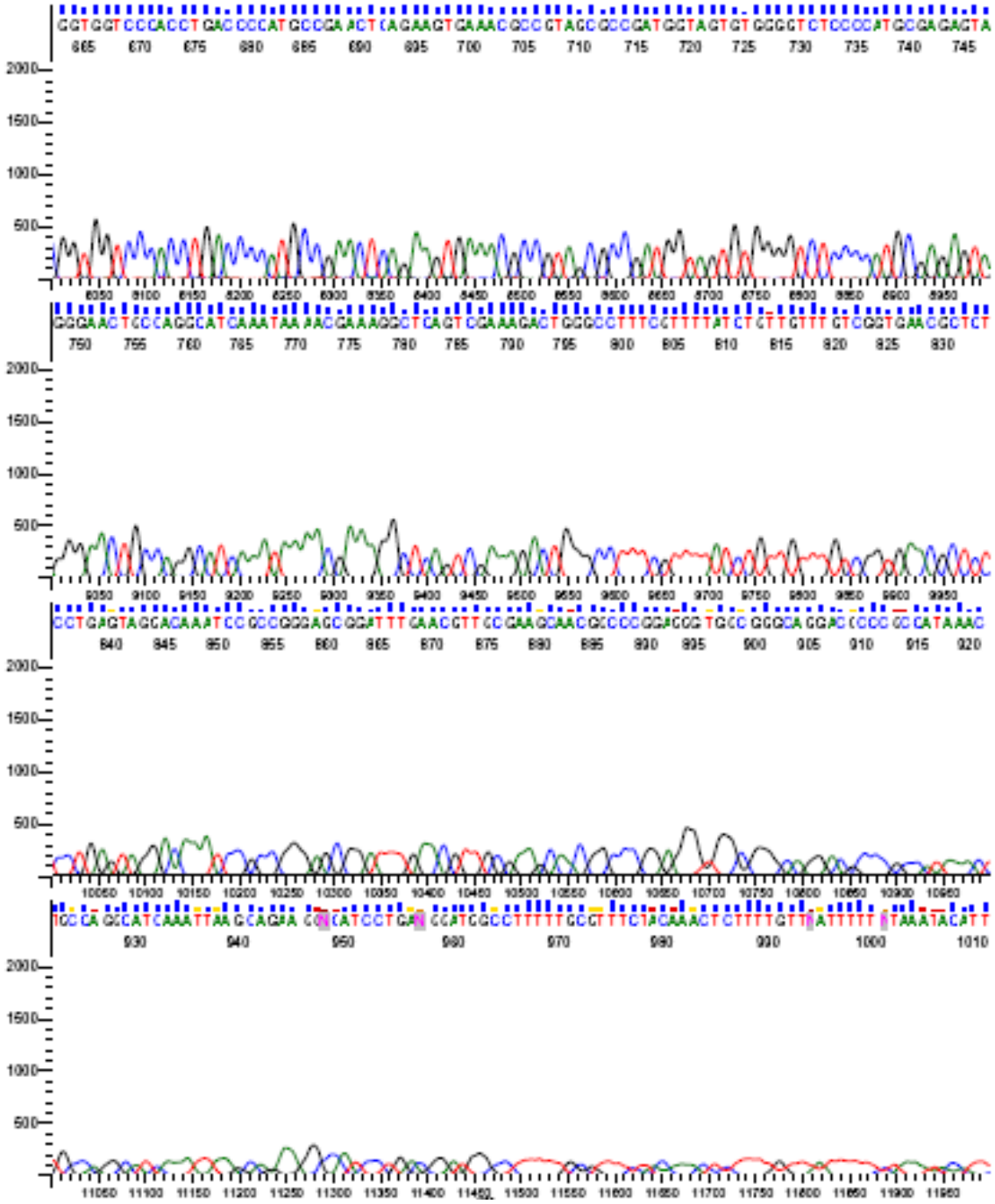

F6L/I85L/I93L

Expected Sequence

atgggtaaca gagcactgaa atcacatcac ggtcactttt
taagcgctga aggcgaagct gtaaagactc accacggtca
tcatgatcat cacacccatt tccacgttga aaaccatggt
ggtaaagttg cattaaagac ccattgcggt aaataccttt
caattggtga tcataaacaa gtttacctct cacaccactt
acacggtgac cactcactct tccacttaga acatcatggc
ggtaaagtct cactgaaagg tcatcaccac cactacctgt
ccgctgatca tcatggtcat gtttcaacca aagaacacca
cgatcacgac accacctttg aagaaattat tatttaa

NOTE: Mutated bases are shown in red.

Mobix Sequencing Results (Mobix, McMaster University, Hamilton)

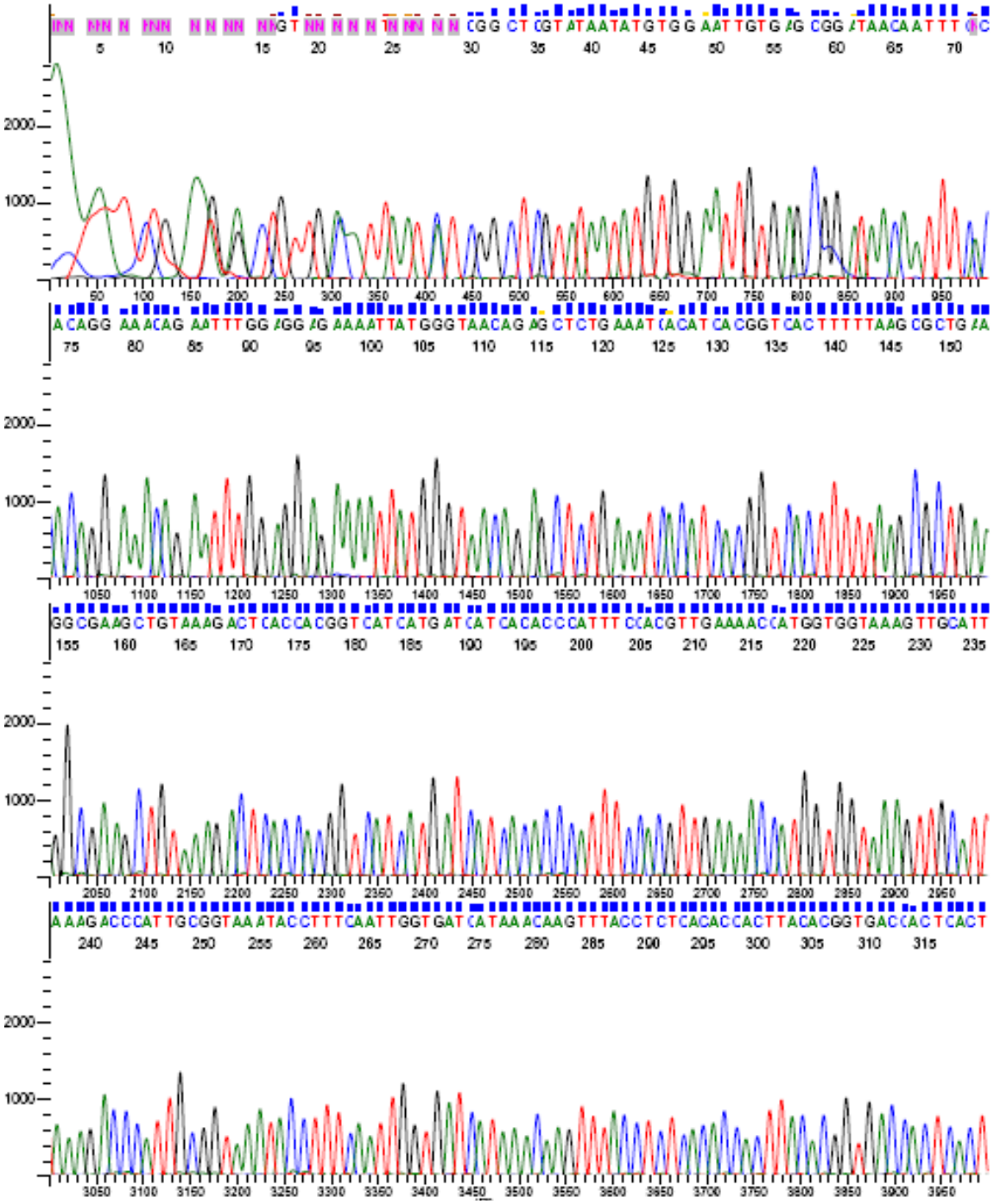

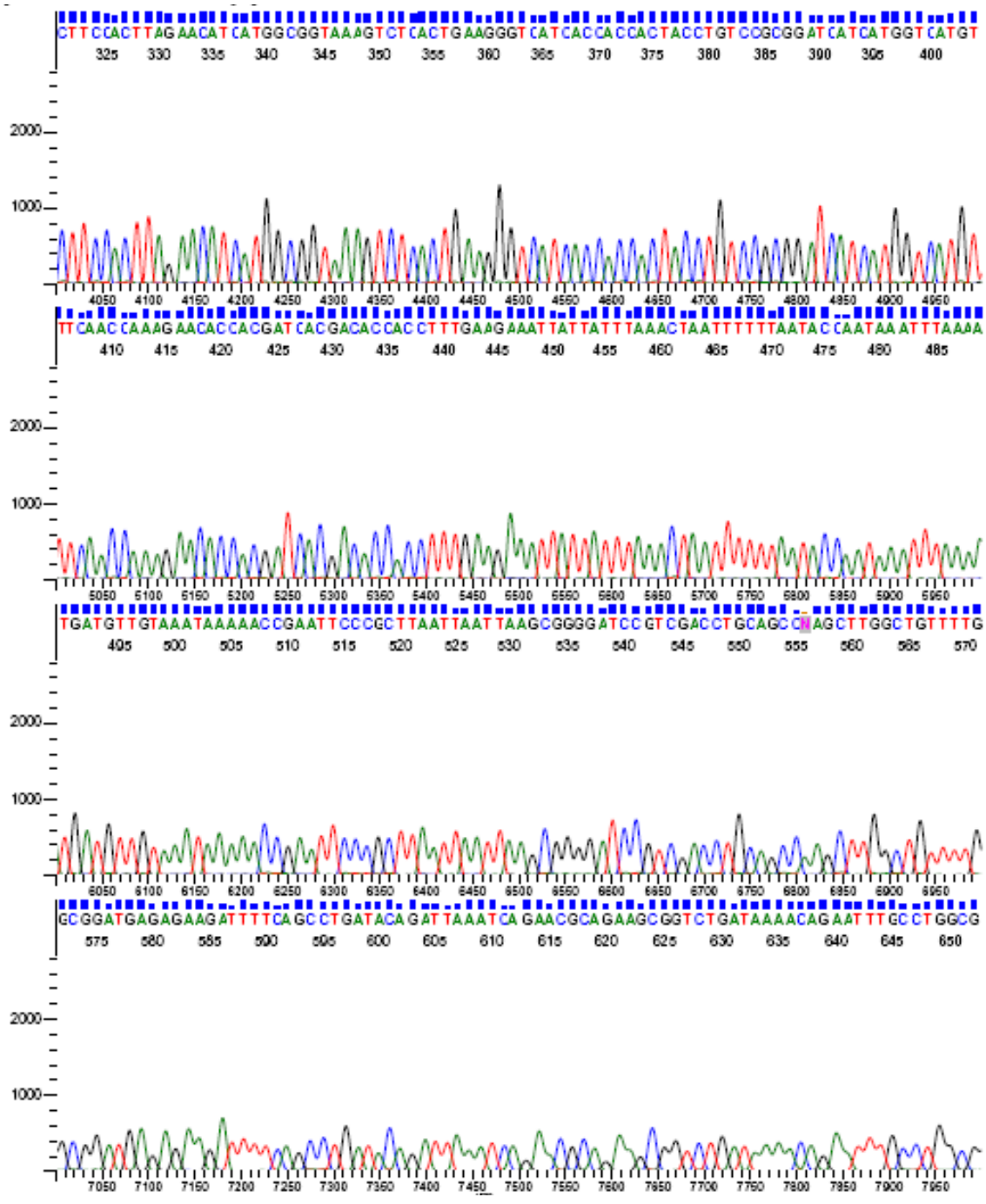

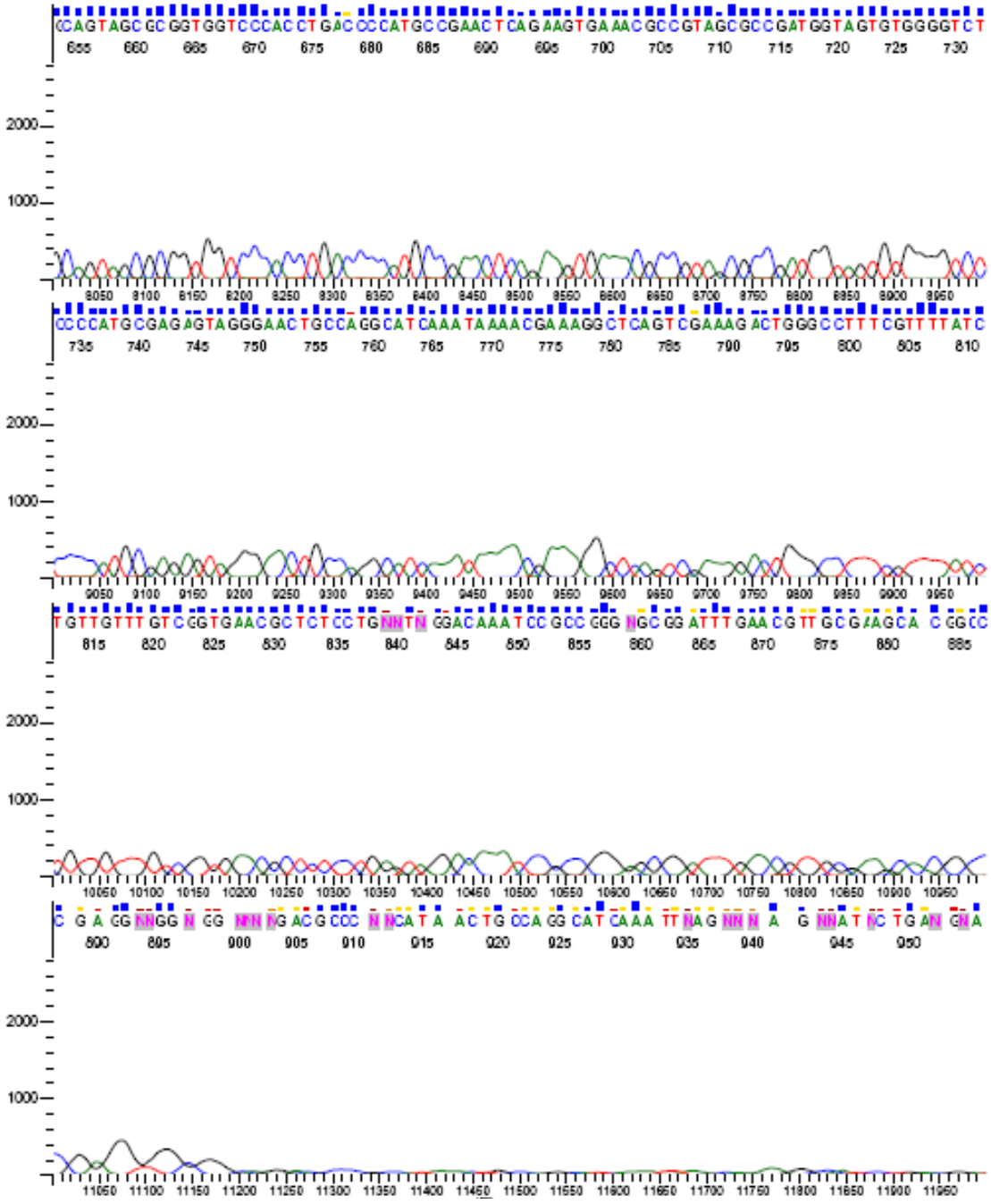

V36A

Expected Sequence

atgggtaaca gagcattcaa atcacatcac ggtcactttt
taagcgctga aggcgaagct gtaaagactc accacggtca
tcatgatcat cacacccatt tccacgcgga aaaccatggt
ggtaaagttg cattaaagac ccattgcggt aaatacctttt
caattggtga tcataaacaa gtttacctct cacaccactt
acacggtgac cactcactct tccacttaga acatcatggc
ggtaaagtct caatcaaagg tcatcaccac cactacattt
ccgctgatca tcatggtcat gtttcaacca aagaacacca
cgatcacgac accacctttg aagaaattat tatttaa

Note: Mutated bases are shown in red.

GenScript Sequence Construct (GenScript USA Inc., NJ)

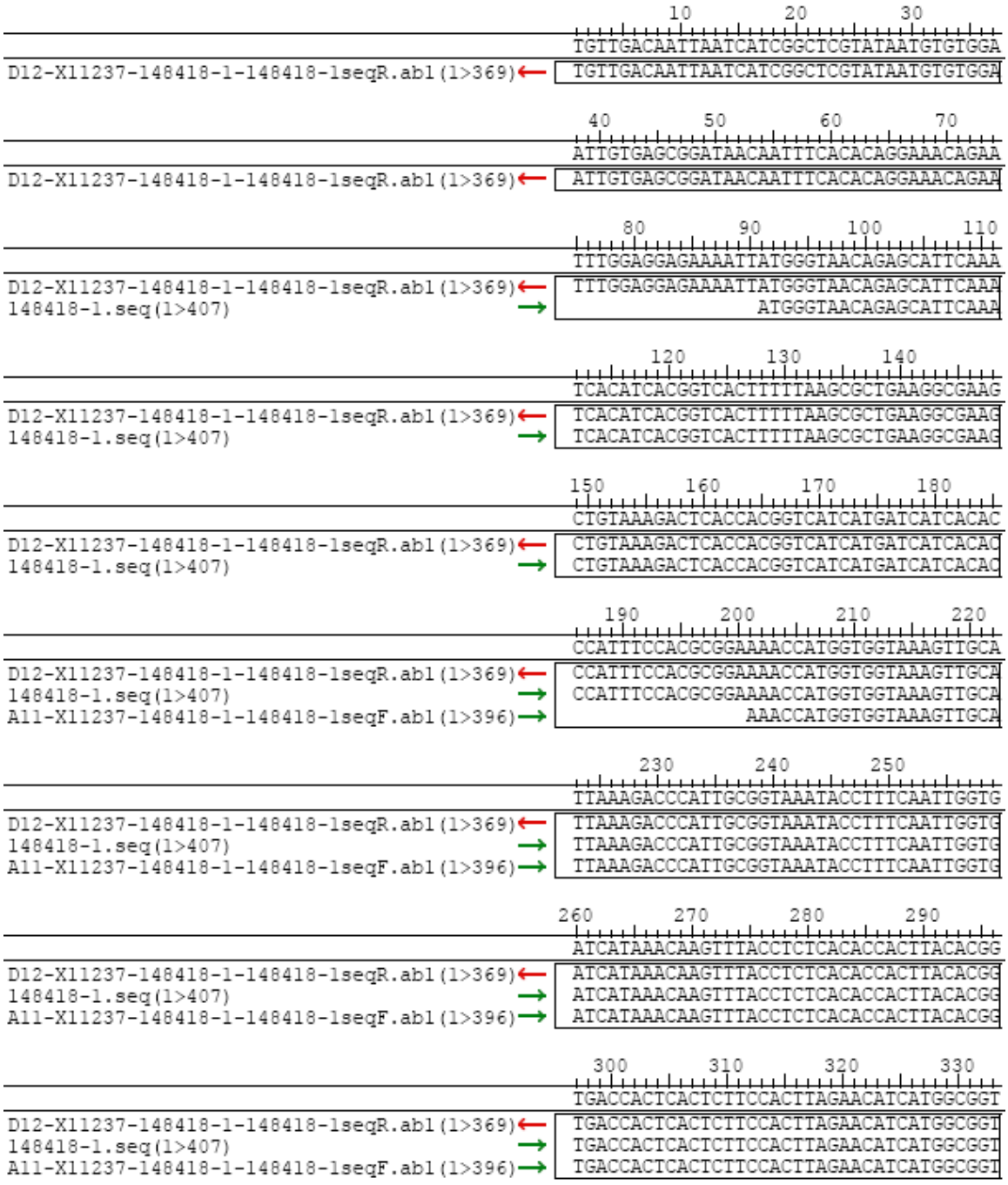

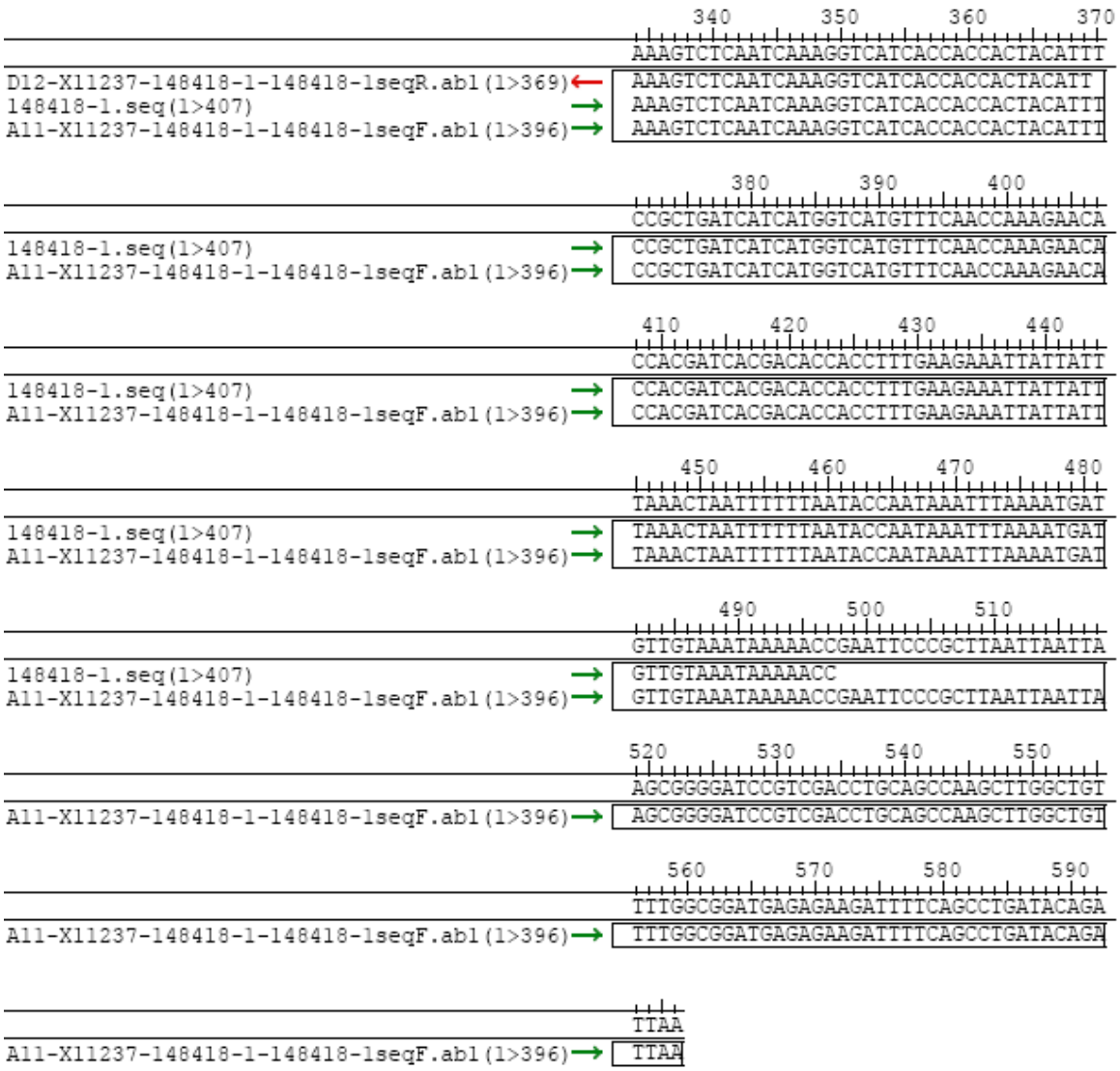
340 350 360 370
AAAGTCTCAATCAAAGGTCATCACCACCACTACATTT
D12-X11237-148418-1-148418-1seqR.abl(1>369)
148418-1.seq(1>407)
A11-X11237-148418-1-148418-1seqF.abl(1>396)
AAAGTCTCAATCAAAGGTCATCACCACCACTACATT
AAAGTCTCAATCAAAGGTCATCACCACCACTACATTT
AAAGTCTCAATCAAAGGTCATCACCACCACTACATTT
380 390 400
CCGCTGATCATCATGGTCATGTTTCAACCAAAGAACA
148418-1.seq(1>407)
A11-X11237-148418-1-148418-1seqF.abl(1>396)
CCGCTGATCATCATGGTCATGTTTCAACCAAAGAACA
CCGCTGATCATCATGGTCATGTTTCAACCAAAGAACA
410 420 430 440
CCACGATCACGACACCACCTTTGAAGAAATTATTATT
148418-1.seq(1>407)
A11-X11237-148418-1-148418-1seqF.abl(1>396)
CCACGATCACGACACCACCTTTGAAGAAATTATTATT
CCACGATCACGACACCACCTTTGAAGAAATTATTATT
450 460 470 480
TAAACTAATTTTTTAATACCAATAAATTTAAAATGAT
148418-1.seq(1>407)
A11-X11237-148418-1-148418-1seqF.abl(1>396)
TAAACTAATTTTTTAATACCAATAAATTTAAAATGAT
TAAACTAATTTTTTAATACCAATAAATTTAAAATGAT
490 500 510
GTTGTAAATAAAAACCGAATTCCCGCTTAATTAATTA
148418-1.seq(1>407)
A11-X11237-148418-1-148418-1seqF.abl(1>396)
GTTGTAAATAAAAACC
GTTGTAAATAAAAACCGAATTCCCGCTTAATTAATTA
520 530 540 550
AGCGGGGATCCGTCGACCTGCAGCCAAGCTTGGCTGT
A11-X11237-148418-1-148418-1seqF.abl(1>396)
AGCGGGGATCCGTCGACCTGCAGCCAAGCTTGGCTGT
560 570 580 590
TTTGGCGGATGAGAGAAGATTTTCAGCCTGATACAGA
A11-X11237-148418-1-148418-1seqF.abl(1>396)
TTTGGCGGATGAGAGAAGATTTTCAGCCTGATACAGA
TTAA
A11-X11237-148418-1-148418-1seqF.abl(1>396)
TTAA

L76A

Expected Sequence

atgggtaaca gagcattcaa atcacatcac ggtcactttt
taagcgctga aggcgaagct gtaaagactc accacggtca
tcatgatcat cacacccatt tccacgttga aaaccatggt
ggtaaagttg cattaaagac ccattgcggt aaatacctttt
caattggtga tcataaacaa gtttacctct cacaccactt
acacggtgac cactcactct tccacgcgga acatcatggc
ggtaaagtct caatcaaagg tcatcaccac cactacattt
ccgctgatca tcatggtcat gtttcaacca aagaacacca
cgatcacgac accacctttg aagaaattat tatttaa

Note: Mutated residues are shown in red.

GenScript Sequencing Construct (GenScript USA Inc., NJ)

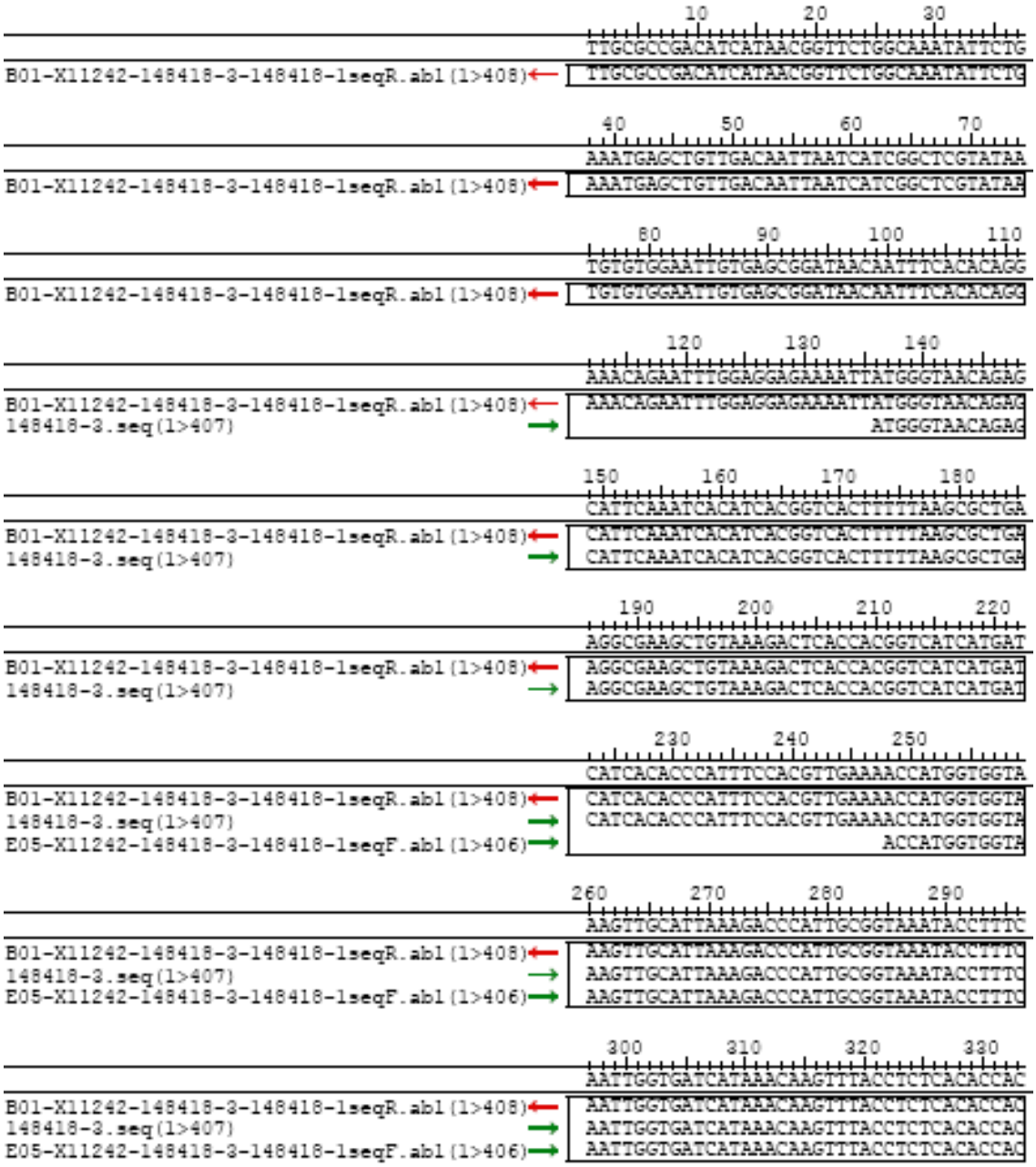

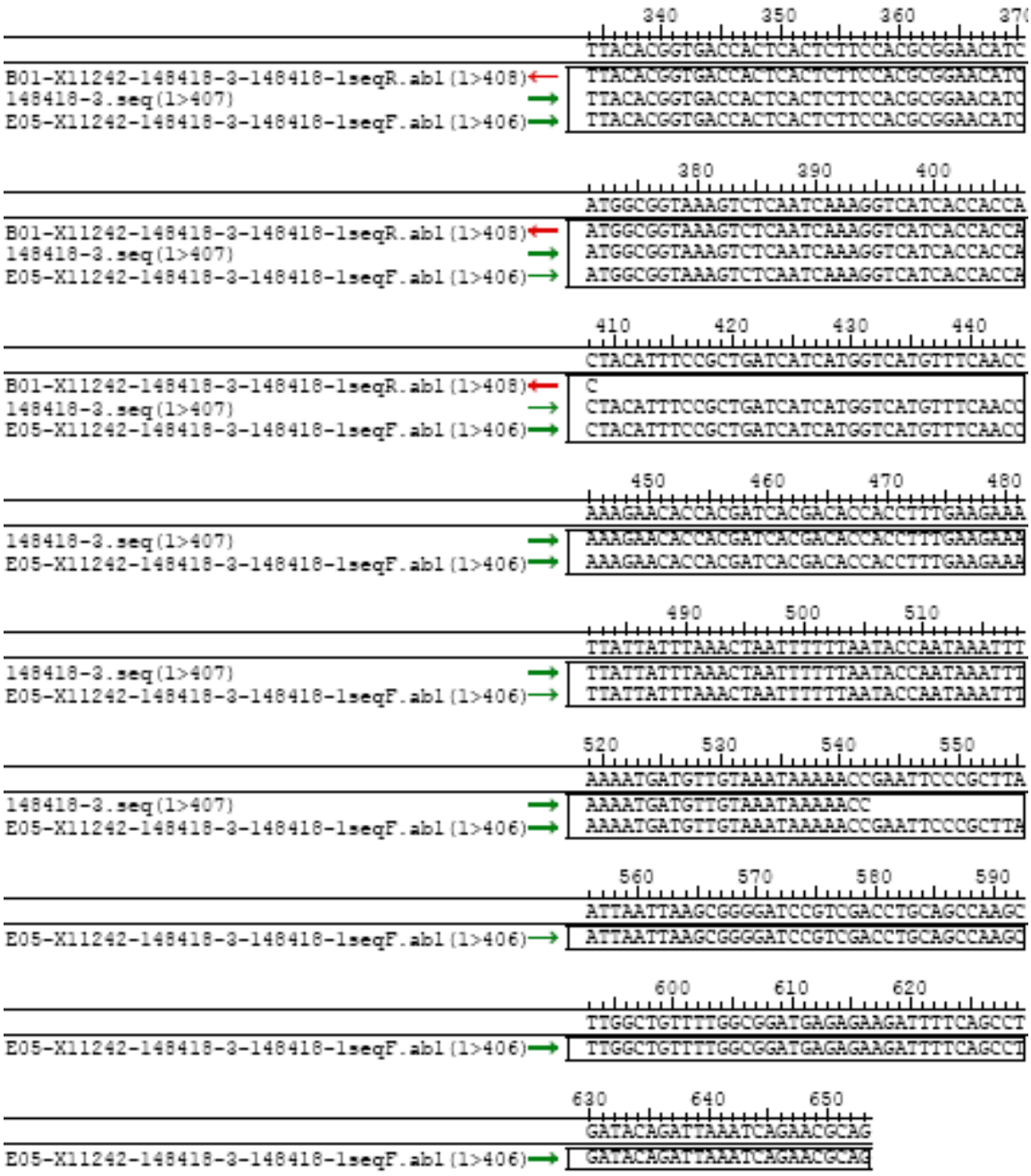
340 350 360
TTACACGGTGACCACTCACTCTTCCACGCGGAACATC
B01-X11242-148418-3-148418-1seqR.abl(1>408)
148418-3.seq(1>407)
E05-X11242-148418-3-148418-1seqF.abl(1>406)
380 390 400
ATGGCGGTAAAGTCTCAATCAAAGGTCATCACCACCA
410 420 430 440
CTACATTTCCGCTGATCATCATGGTCATGTTTCAACC
450 460 470 480
AAAGAACACCACGATCACGACACCACCTTTGAAGAAA
490 500 510
TTATTATTTAAACTAATTTTTTAATACCAATAAATTT
520 530 540 550
AAAATGATGTTGTAAATAAAAACCGAATTCCCGCTTA
560 570 580 590
ATTAATTAAGCGGGGATCCGTCGACCTGCAGCCAAGC
600 610 620
TTGGCTGTTTTGGCGGATGAGAGAAGATTTTCAGCCT
630 640 650
GATACAGATTAAATCAGAACGCAG

I118A

Expected Sequence

atgggtaaca gagcattcaa atcacatcac ggtcactttt
taagcgctga aggcgaagct gtaaagactc accacggtca
tcatgatcat cacacccatt tccacgttga aaaccatggt
ggtaaagttg cattaaagac ccattgcggt aaatacctttt
caattggtga tcataaacaa gtttacctct cacaccactt
acacggtgac cactcactct tccacttaga acatcatggc
ggtaaagtct caatcaaagg tcatcaccac cactacattt
ccgctgatca tcatggtcat gtttcaacca aagaacacca
cgatcacgac accacctttg aagaaattat tgcgtaa

Note: Mutated bases are shown in red.

GenScript Sequencing Construct (GenScript USA Inc., NJ)

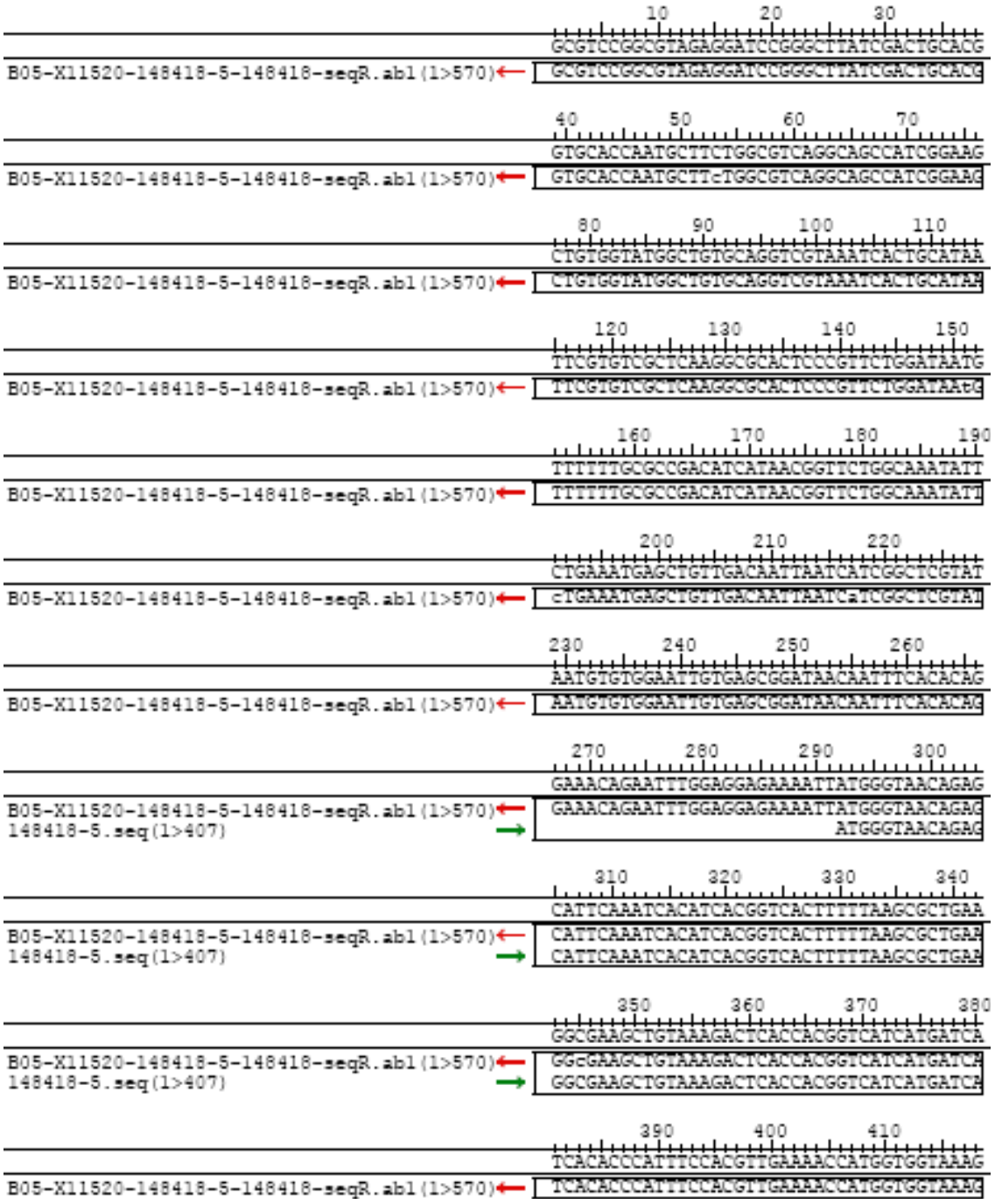

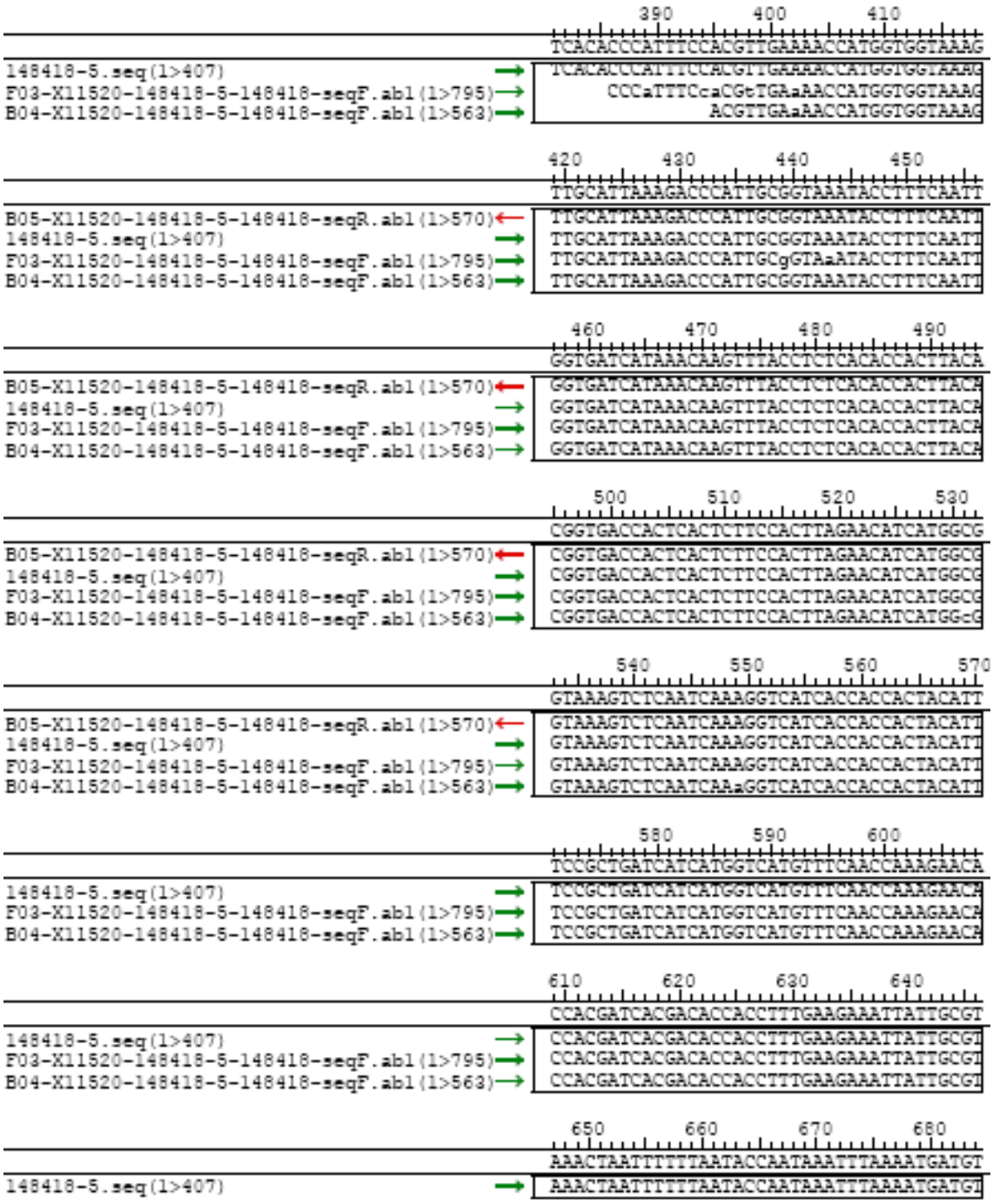
390 400 410
TCACACCCATTTCCACGTTGAAAACCATGGTGGTAAAG
148418-5.seq(1>407)
F03-X11520-148418-5-148418-seqF.ab1(1>795)
B04-X11520-148418-5-148418-seqF.ab1(1>563)
420 430 440 450
TTGCATTAAAGACCCATTGCGGTAAATACCTTTCAATT
B05-X11520-148418-5-148418-seqR.ab1(1>570)
148418-5.seq(1>407)
F03-X11520-148418-5-148418-seqF.ab1(1>795)
B04-X11520-148418-5-148418-seqF.ab1(1>563)
460 470 480 490
GGTGATCATAAACAAGTTTACCTCTCACACCACTTACA
B05-X11520-148418-5-148418-seqR.ab1(1>570)
148418-5.seq(1>407)
F03-X11520-148418-5-148418-seqF.ab1(1>795)
B04-X11520-148418-5-148418-seqF.ab1(1>563)
500 510 520 530
CGGTGACCACTCACTCTTCCACTTAGAACATCATGGCG
B05-X11520-148418-5-148418-seqR.ab1(1>570)
148418-5.seq(1>407)
F03-X11520-148418-5-148418-seqF.ab1(1>795)
B04-X11520-148418-5-148418-seqF.ab1(1>563)
540 550 560 570
GTAAAGTCTCAATCAAAGGTCATCACCACCACTACATT
B05-X11520-148418-5-148418-seqR.ab1(1>570)
148418-5.seq(1>407)
F03-X11520-148418-5-148418-seqF.ab1(1>795)
B04-X11520-148418-5-148418-seqF.ab1(1>563)
580 590 600
TCCGCTGATCATCATGGTCATGTTTCAACCAAAGAACA
148418-5.seq(1>407)
F03-X11520-148418-5-148418-seqF.ab1(1>795)
B04-X11520-148418-5-148418-seqF.ab1(1>563)
610 620 630 640
CCACGATCACGACACCACCTTTGAAGAAATTATTGCGT
148418-5.seq(1>407)
F03-X11520-148418-5-148418-seqF.ab1(1>795)
B04-X11520-148418-5-148418-seqF.ab1(1>563)
650 660 670 680
AAACTAATTTTTTAATACCAATAAATTTAAAATGATGT
148418-5.seq(1>407)

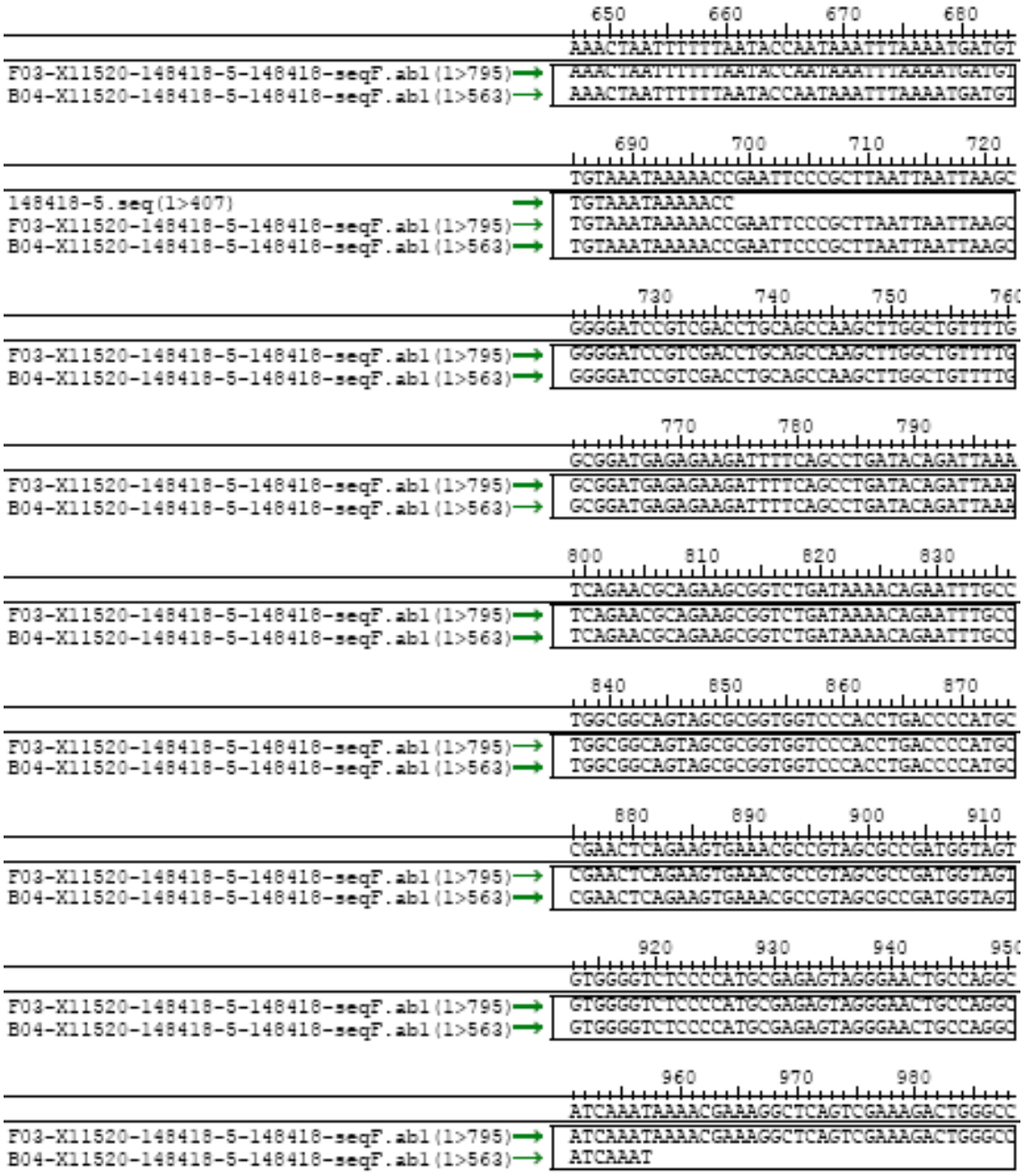
650 660 670 680
AAACTAATTTTTTAATACCAATAAATTTAAAATGATGT
F03-X11520-148418-5-148418-seqF.abl(1>795)
B04-X11520-148418-5-148418-seqF.abl(1>563)
690 700 710 720
TGTAAATAAAAACCGAATTCCCGCTTAATTAATTAAGC
148418-5.seq(1>407)
F03-X11520-148418-5-148418-seqF.abl(1>795)
B04-X11520-148418-5-148418-seqF.abl(1>563)
730 740 750
GGGGATCCGTCGACCTGCAGCCAAGCTTGGCTGTTTTG
F03-X11520-148418-5-148418-seqF.abl(1>795)
B04-X11520-148418-5-148418-seqF.abl(1>563)
770 780 790
GCGGATGAGAGAAGATTTTCAGCCTGATACAGATTAAA
F03-X11520-148418-5-148418-seqF.abl(1>795)
B04-X11520-148418-5-148418-seqF.abl(1>563)
800 810 820 830
TCAGAACGCAGAAGCGGTCTGATAAAACAGAATTTGCC
F03-X11520-148418-5-148418-seqF.abl(1>795)
B04-X11520-148418-5-148418-seqF.abl(1>563)
840 850 860 870
TGGCGGCAGTAGCGCGGTGGTCCCACCTGACCCCATGC
F03-X11520-148418-5-148418-seqF.abl(1>795)
B04-X11520-148418-5-148418-seqF.abl(1>563)
880 890 900 910
CGAACTCAGAAGTGAAACGCCGTAGCGCCGATGGTAGT
F03-X11520-148418-5-148418-seqF.abl(1>795)
B04-X11520-148418-5-148418-seqF.abl(1>563)
920 930 940
GTGGGGTCTCCCCATGCGAGAGTAGGGAACTGCCAGGC
F03-X11520-148418-5-148418-seqF.abl(1>795)
B04-X11520-148418-5-148418-seqF.abl(1>563)
960 970 980
ATCAAATAAAACGAAAGGCTCAGTCGAAAGACTGGGCC
F03-X11520-148418-5-148418-seqF.abl(1>795)
B04-X11520-148418-5-148418-seqF.abl(1>563)
ATCAAAT

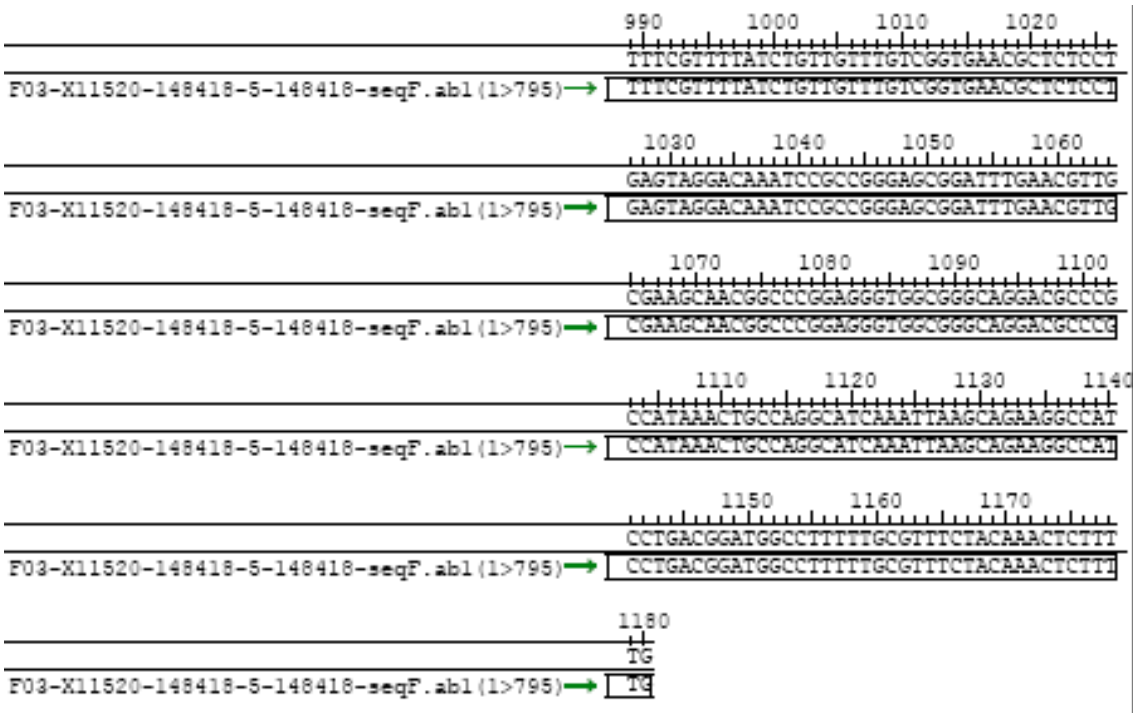
990
1000
1010
1020
TTTCGTTTTATCTGTTGTTTGTCGGTGAACGCTCTCCT
F03-X11520-148418-5-148418-seqF.abl(1>795)
1030
1040
1050
1060
GAGTAGGACAAATCCGCCGGGAGCGGATTTGAACGTTG
F03-X11520-148418-5-148418-seqF.abl(1>795)
1070
1080
1090
1100
CGAAGCAACGGCCCGGAGGGTGGCGGGCAGGACGCCCG
F03-X11520-148418-5-148418-seqF.abl(1>795)
1110
1120
1130
1140
CCATAAACTGCCAGGCATCAAATTAAGCAGAAGGCCAT
F03-X11520-148418-5-148418-seqF.abl(1>795)
1150
1160
1170
CCTGACGGATGGCCTTTTTGCGTTTCTACAAACTCTTT
F03-X11520-148418-5-148418-seqF.abl(1>795)
1180
TG
F03-X11520-148418-5-148418-seqF.abl(1>795)

Appendix 3 – Safety Precautions

NMR monitored experiments are performed using protein that has been isotopically labelled with ^{15}N and D (i.e. ^{2}H). These isotopes are generally considered safe at concentrations used during research. However, some studies indicate that at high levels ^{2}H can have adverse effects on the human body (Koletzko, et al., 1997). Therefore, when using these reagents in the laboratory the use of gloves, eye-protection and lab coat should be used to limit exposure. Disposal of these reagents is not considered dangerous. Furthermore, the study of proteins using NMR requires the use of high magnetic fields. This can pose a risk to individuals with pacemakers and other artificial surgical implants. The magnetic field is generally considered safe for the rest of the population. Having said this, metal objects not removed from the researcher may impose safety risks if they are allowed to interact with the magnetic field (i.e. choking hazard if worn around the neck, or suffocation if they cause the magnet to quench).